



Xylem and phloem functioning of
Populus tremula trees under drought, and
elevated CO₂ concentration and temperature

ir. Michiel Hubeau

Promoter

Prof. Dr. ir. Kathy Steppe
Faculty of Bioscience Engineering
Laboratory of Plant Ecology, Ghent University

Members of the examination board

Prof. Dr. Bernard De Baets (chairman)
Faculty of Bioscience Engineering
KERMIT, Ghent University

Prof. Dr. ir. Pieter De Frenne (secretary)
Faculty of Bioscience Engineering
Forest & Nature Lab, Ghent University

Prof. Dr. ir. Christian Vanhove
Faculty of Engineering and Architecture
INFINITY, Ghent University

Prof. Dr. ir. Stefaan Vandenberghe
Faculty of Engineering and Architecture
MEDISIP, Ghent University

Prof. Dr. Ivan Nijs
Faculty of Science
Centre of Excellence PLECO, University of Antwerp

Prof. Dr. Daniel Epron
Tree and Ecosystem-level Integrative Ecology and Ecophysiology
University of Lorraine

Dean

Prof. Dr. ir. Marc Van Meirvenne

Rector

Prof. Dr. ir. Rik Van de Walle

Dutch translation of the title: Het functioneren van xyleem en floëem in *Populus tremula* bomen onder droogte en verhoogde CO₂-concentratie en temperatuur

Cover: *Populus tremula* leaves inside a cuvette used during plant-PET scanning. LED lights were used to illuminate the leaves.

Hubeau, M. (2018) Xylem and phloem functioning of *Populus tremula* trees under drought, and elevated CO₂ concentration and temperature. PhD thesis, Ghent University, Belgium

ISBN 978-94-6357-089-3

The author and the promoter give the authorisation to consult and to copy parts of this work for personal use only. Every other use is subject to the copyright laws. Permission to reproduce any material contained in this work should be obtained from the author.

ir. Michiel Hubeau

**XYLEM AND PHLOEM FUNCTIONING
OF *POPULUS TREMULA* TREES UNDER DROUGHT, AND
ELEVATED CO₂ CONCENTRATION AND TEMPERATURE**

Thesis submitted in fulfilment of the requirements for
the degree of Doctor (PhD) of Applied Biological Science

PREFACE

Het is af, wat een heerlijk gevoel. Het heeft de nodige energie en opofferingen gevergd om uiteindelijk mijn doctoraat wat sneller dan gepland klaar te krijgen. Maar als fietsersbenen beginnen te tintelen is daar nog maar weinig aan te doen. De voorbije jaren, maar zeker ook deze laatste vermoeiende maanden heb ik meer dan ooit gemerkt dat het dan heel belangrijk is dat je omringd wordt door de “juiste” personen. Vandaar dat dit voorwoord een belangrijk deel van het werk is. Dank ook aan het Vlaams Agentschap Innoveren & Ondernemen (VLAIO) en het Fonds Wetenschappelijk Onderzoek (FWO) om dit onderzoek mogelijk te maken.

Beginnen kan ik moeilijk anders dan met Kathy. Wat een energie en enthousiasme kan er in één persoon zitten. Ik had haar amper resultaten van mijn thesis gepresenteerd, maar met mijn enthousiasme voor plantenonderzoek was Kathy blijkbaar al meteen overtuigd dat ze me aan een doctoraat wilde laten starten. Meteen kreeg ik zoveel vertrouwen en dat is eigenlijk niet meer veranderd en was altijd een grote energiebron voor mij. Zelfs als er al eens wat misliep, en ja, dat kwam wel eens voor, ging het niet over wiens schuld het was, maar zochten we meteen naar de beste oplossing. De laatste maanden van het doctoraat, wanneer we mijn tekst waren aan het afwerken, voelde het schrijfwerk echt aan als teamwork. Ik ben heel dankbaar de tijd en energie die Kathy in mijn doctoraat heeft willen steken, want het heeft ervoor gezorgd dat ik uiteindelijk

best wel fier ben op het werk dat voorligt. Dus, een zeer grote dankjewel en hopelijk worden er nog veel wetenschappers door jou geënthousiasmeerd.

De hartelijkheid en collegialiteit op ons labo heb ik altijd geweldig gevonden. Ik hoop maar dat ik me in een volgende werkomgeving even op men gemak kan voelen. Op amper vier jaar evolueer je hier van groentje naar de oudere garde. Begonnen als een onderzoekertje in Maurits zijn meetcampagnes, die nog steeds een super herinnering zijn, tot uiteindelijk toch het gevoel hebben dat je de fakkel wat kan doorgeven. Van de toenmalige oudere garde heb ik veel kunnen opsteken. Veerle, de floëemexpert, Ingvar, de hitte-expert, Lidewei de akoestische expert, jullie gaven meteen het goede voorbeeld. Bart, wie nood had aan ontspanning kon bij u terecht, pingpongen, talloze koekjes maken, eentje gaan drinken (zolang het zonder eten was) en toch nog zo een goed doctoraat schrijven, wat een voorbeeld. Merci voor de mentale steun en handige tips op het einde, jij kon je duidelijk nog goed inbeelden hoe die eindsprint verloopt. Fran, Hans, Selwyn, Sarah, de J's, maar ik zal jullie beleefdheidshalve met volle naam noemen, Jens, Jeroen, Jonathan, Jonas en Jonas, sfeer en gezelligheid op het labo is verzekerd! Roberto, thanks for bringing in some Spanish happiness. Wouter, al zat er een muur tussen ons in, ik apprecieerde toch het bijna-bureaugenootschap. Merci ook aan de bureaugenoten; Prof. Hans, bedankt voor je aangename rust en goedlachsheid. Hannes is zowat de meest sympathieke en vriendelijke vendelzwaaijer, minstens van Vlaanderen. Niels was er al bij in Australië en heeft ondertussen zijn doctoraat ook ingediend, compagnon-de-route. Linus, samen zijn we in Antwerpen aan onze studies begonnen en ik vond het oprecht plezant dat je uw weg naar dit labo ook hebt gevonden. Wie weet wordt de verleiding voor frieten nu wel wat kleiner als je niet meer met die frietenverslaafde naar de resto gaat.

Frinus en Jens, aan jullie mag ik toch een beetje de fakkel doorgeven. Jens, sta me toe me nog eens te verontschuldigen voor mijn eerder chaotische werkwijze. Ondanks onze verschillen in aanpak hebben we altijd super kunnen samenwerken. Ik ben er rotsvast van overtuigd dat je het ^{11}C onderzoek weer een stap verder gaat brengen, niet opgeven en veel succes. Frinus, als ik nog eens terug op bezoek kom verwacht ik minstens 2 extra serretjes, gebouwd in de sneeuw, geïnstalleerd in een hittegolf. Bedankt voor de vele malen dat jullie me

uit de nood hielpen en altijd meteen klaarstonden om te helpen. Ook de mentale (en Fran ook nutritionele) steun op het werk en de pendelritjes werden zeer gewaardeerd. Linus, hou me op de hoogte van alle vrienden die Fran nog zal maken op de trein.

De personen die ongetwijfeld nog het minst van al gemist kunnen worden op het labo zijn de “ATePeërs”: Ann, Pui Yi, Guy, Dirk, Erik, Thomas, Geert en Philip. Erik, als je ooit nood hebt aan wat discussiëren, over wat dan ook, laat het maar weten en dan houden we nog eens een sessie. Geert en Philip, jullie zijn beiden crèmen van gasten en leveren daarnaast nog eens onberispelijk werk. Harde werkers, altijd goed gezind en hoekstenen van het labo. Zoals ik al aan Frinus zei, ik kijk al uit naar de volgende serretjes, waar jullie jullie constructieskills nog eens kunnen laten botvieren. Pui Yi, bedankt voor de guitige gezelligheid en piekfijne organisatie van labo-uitstappen. Ann, vanaf de eerste moment dat we collega's waren kon ik niets verkeerd doen. Mezelf 's morgens op de stoel in het secretariaat plaveien als ik nog even niet wilde beginnen werken of een administratief vraagje had, daar kon ik elke keer van genieten. Ik ga je oprecht missen.

Buiten het eigen labo zijn er veel mensen die me hebben geholpen dit onderzoek te kunnen waarmaken. Bene en Chris, de eerste keer dat ik op Infinity kwam dacht ik dat wij, als plantwetenschappers, wat raar zouden bekeken worden op een labo waar preklinisch onderzoek verricht wordt. Dat bleek al meteen volledig onterecht en zelfs het tegendeel was waar. Met veel appreciatie voor ons werk werden we ontvangen en uit jullie nieuwsgierigheid bleek duidelijk jullie interesse. Bedankt voor jullie immer grote vriendelijkheid en bereidwilligheid tot hulp. Jan, de dagen die jij moest kloppen om toch nog voor of na een klinische productie er eentje voor ons te maken waren zeker geen 9 to 5. Merci voor je flexibiliteit en engagement. Bedankt Jan voor de tijd die je hebt gestoken in het maken van de CT-beelden en Olivier voor het maken van zeer knappe anatomische coupes en allebei voor het steeds zeer snel tijd willen maken voor vragen van mij.

Buiten het werk waren de steun en toeverlaat van familie en vrienden zeer belangrijk. Bollie en Sieglinde, 100 km stappen, de 1000 km van KOTK, maar zeker ook de vele keren dat we voor de minste reden het nodig vonden om dit te

vieren met een etentje of drankje, Jippie! Alle vrienden die me hielpen de gedachten wat te verzetten, mijn fietsenergie hielpen kwijt te raken en zich met interesse afvroegen wat ik nu precies onderzocht, het was me steeds een plezier. Mijn gezin en familie zorgden voor de ideale rustpunten doorheen dit doctoraat. Bedankt voor alle goede raad. Al werd die rust de laatste jaren wel wat verstoord door de “nieuwe aanwinsten”, maar wat een lieve schattigaards. Aan mijn ouders een enorm dikke merci om er altijd onvoorwaardelijk te zijn. Jullie hebben me altijd mijn weg laten zoeken, maar evengoed wanneer nodig richting gegeven. Mijn tweede thuis, ten huize Van Camp, hoe tevreden kan ik zijn met zo een liefdevolle en trotse schoonfamilie. Stiekem denk ik dat er ergens met fierheid wordt meegekeken



Janne, Jannie, Lovie, Sjmovie, ik had je in het lijstje van de voormalige collega's kunnen zetten, maar dat zou misschien toch wat raar geweest zijn, jij verdient uiteraard een alinea, eigenlijk een heel boek, al zou ik niet weten waar te beginnen. Ten eerste, bedankt om mijn opperste saaiheid van de laatste maanden te tolereren, of toch zeker te gedogen. Maar als ik iets heb geleerd is dat werk niet alles is, nee, dat ben jij. Geen idee waar ik zou staan zonder u, maar ik ben heel blij dat ik met dat niet moet inbeelden. We gaan dan wel enkele maanden van huis zijn, maar eigenlijk toch niet, soms durven melige liedjesteksten nu eenmaal 100 % waar te zijn: *home is wherever I'm with you*

Veel leesplezier en hopelijk vinden jullie het onderzoek even interessant als ikzelf.

Michiel

PREFACE	I
LIST OF ABBREVIATIONS AND SYMBOLS	IX
SUMMARY	XV
SAMENVATTING	XXI
CHAPTER 1 INTRODUCTION AND THESIS OUTLINE	1
INTRODUCTION	3
<i>A changing world: welcome to the Anthropocene</i>	3
<i>Biomes are expected to shift in response to climate change</i>	5
<i>Trees have evolved to face variable conditions during their lifetime, but also to face climate change?</i>	8
<i>Water, water, water</i>	10
<i>Physiological responses to elevated [CO₂] and temperature</i>	13
<i>Transport of photoassimilates in the phloem</i>	16
<i>Better understanding of tree response to climate change through ecophysiology</i>	19
THESIS OUTLINE	20
CHAPTER 2 GROWTH RESPONSES OF <i>POPULUS TREMULA</i> TREES TO DROUGHT UNDER CHANGING CLIMATE REGIMES: MITIGATION OR AMELIORATION?	27
INTRODUCTION	30
MATERIALS AND METHODS	33
<i>Plant material and growth conditions</i>	33
<i>Data acquisition</i>	34
<i>Microclimatic treatments</i>	35
<i>Microclimatic calculations</i>	36
<i>Tree measurements</i>	37
<i>Data analysis</i>	40
RESULTS	41
<i>Microclimatic conditions</i>	41
<i>Tree measurements</i>	44
DISCUSSION	52
<i>Interactions between microclimate and sap flow</i>	52
<i>Impact of climate change conditions on tree growth</i>	55
<i>Whole-tree ecophysiology to better understand the mechanisms underlying tree response to climate change</i>	58
CONCLUSION	59
SUPPLEMENTAL MATERIAL	61
CHAPTER 3 WILL <i>POPULUS TREMULA</i> TREES BE MORE VULNERABLE TO DROUGHT-INDUCED CAVITATION UNDER CLIMATE CHANGE REGIMES?	63

INTRODUCTION	66
MATERIALS AND METHODS	69
<i>Sampling procedure and measurements</i>	69
<i>Acoustic vulnerability to drought-induced cavitation</i>	72
<i>Volumetric water content and hydraulic capacitance</i>	73
<i>X-ray micro-computed tomography</i>	74
<i>Data analysis</i>	75
RESULTS	76
<i>Native state of cavitation</i>	76
<i>Vulnerability to drought-induced cavitation</i>	79
DISCUSSION	83
<i>Native state of cavitation in P. tremula stems</i>	83
<i>Trees are most vulnerable to drought-induced cavitation when well-watered and grown in elevated temperature and [CO₂]</i>	84
<i>Will other physiological changes, related to elevated [CO₂], guard trees against a higher cavitation vulnerability?</i>	87
CONCLUSION	89
CHAPTER 4 PLANT-PET SCANS: <i>IN VIVO</i> MAPPING OF XYLEM AND PHLOEM FUNCTIONING	91
PET SCANNERS ARE READY TO BRIDGE THE GAP BETWEEN MEDICAL AND PLANT SCIENCES	94
WATER AND SUGAR AS THE ALPHA AND OMEGA OF PLANTS	94
MEASUREMENTS OF WATER AND SUGAR FLOW WITH PET	96
¹¹ C HAS ALREADY PROVEN ITS IMPORTANCE IN PLANT SCIENCES	101
COMBINING IMAGING TECHNIQUES TO SEE THE WHOLE PICTURE	103
OPPORTUNITIES IN PLANT RESEARCH REMAIN TO BE SEISED	104
CONCLUDING REMARKS AND FUTURE PERSPECTIVES	106
CHAPTER 5 ¹¹C-AUTORADIOGRAPHS TO IMAGE PHLOEM LOADING	109
INTRODUCTION	112
INTRODUCTION TO AUTORADIOGRAPHY	115
MATERIALS AND METHODS	117
<i>Plant material</i>	117
<i>Exposure to gaseous ¹¹CO₂</i>	119
<i>Autoradiography</i>	121
<i>Vein anatomy</i>	122
RESULTS	123
DISCUSSION	126
<i>Carbon export requirement when imaging ¹¹C distribution during phloem loading</i>	126
<i>¹¹C-autoradiography as valuable tool to define loading strategies in leaves</i>	127
<i>Phloem loading in tropical tree species</i>	128
<i>¹¹C- versus ¹⁴C-autoradiography</i>	130

CONCLUSION	131
CHAPTER 6 PLANT-PET REVEALS PHLOEM VULNERABILITY TO DROUGHT IN <i>POPULUS TREMULA</i> UNDER CHANGING CLIMATE REGIMES	133
INTRODUCTION	136
TRACING THE FLOW OF PHOTOASSIMILATES IN PLANTS WITH ^{11}C	137
COMPARTMENTAL MODELLING TO COMPUTE PHLOEM CHARACTERISTICS	139
MATERIALS AND METHODS	142
<i>Plant material and experimental design</i>	142
<i>Leaf cuvette fitting the PET scanner</i>	143
<i>Production of $^{11}\text{CO}_2$</i>	145
<i>PET scanner</i>	146
RESULTS	147
DISCUSSION	149
<i>Elevated CO_2 changes phloem velocity and its response to drought</i>	149
<i>Leakage-retrieval, carbon storage and respirational carbon loss</i>	152
<i>Effect of drought on phloem functioning under elevated $[\text{CO}_2]$</i>	153
<i>Opportunities to improve our understanding of phloem functioning</i>	154
CONCLUSION	156
CHAPTER 7 GENERAL DISCUSSION AND OUTLOOK	159
RESEARCH JUSTIFICATION	161
INDIRECT MEASUREMENTS OF CELL CHARACTERISTIC ADJUSTMENTS	162
VULNERABILITY TO DROUGHT AND CAVITATION	162
PHLOEM LOADING AND CLIMATE CHANGE	164
PLANT-PET SCANS: INNOVATIVE METHOD TO MEASURE PHLOEM CHARACTERISTICS	165
CLIMATE CHANGE RESEARCH IN TREATMENT CHAMBERS	168
THE OUTLOOK OF CLIMATE CHANGE ON <i>POPULUS TREMULA</i> AND OTHER TREES	169
REFERENCES	173
CURRICULUM VITAE	207

LIST OF ABBREVIATIONS AND SYMBOLS

^{11}C	Carbon-11 (short-lived isotope)
$^{11}\text{CO}_2$	Short-lived radioactive carbon dioxide
$^{14}\text{CO}_2$	Long-lived radioactive carbon dioxide
^{13}C	Carbon-13 (stable isotope)
^{13}N	Nitrogen-13 (short-lived isotope)
^{14}C	Carbon-14 (long-lived isotope)
^{15}O	Oxygen-15 (short-lived isotope)
^{18}F	Fluorine-18 (short-lived isotope)
^{18}FDG	Fluorodeoxyglucose (short-lived molecule)
$^{99\text{m}}\text{Tc}$	Technetium-99m (short-lived isotope)
2-D	Two-dimensional
3-D	Three-dimensional
4-D	Three-dimensional
a	Net leakage-retrieval exchange parameter
a.u.	Arbitrary units
AE	Acoustic emissions
AE_{100}	Endpoint of vulnerability curve
ANOVA	Analysis of variance
ATP	Adenosine triphosphate
b	Storage exchange parameter
BB	Branch bag cuvette
c	Respirational loss exchange parameter
C	Hydraulic capacitance
$T_{C_i}^x$	Amount of tracer in compartment x of ROI i
$T_{C_{total}}$	Total amount of carbon tracer in input ROI
CAM	Crassulacean acid metabolism
$[\text{CO}_2]$	Concentration of carbon dioxide
CT	X-ray computed tomography
D	Stem diameter
d	Thickness of stem storage compartment
DC	Desorption curve

DOY	Day of the year
e^-	Electron
e_a	Actual vapour pressure
e_s	Saturated vapour pressure
ET_0/E_p	Potential evapotranspiration
FACE	Free-air CO ₂ enrichment
FOV	Field of view
g_s	Stomatal conductance
h	Height
H ⁺	Proton
Herb	Herbaceous
HSM	Hydraulic safety margin
K_c	Crop coefficient per tree
$K_{c,LA}$	Crop coefficient per unit leaf area
K_{sh}	Thermal conductance of sheath surrounding the heater
l	Length
LA	Leaf area
LED	Light-emitting diode
LGSO	Lu _{0.4} Gd _{1.6} SiO ₅ :Ce
LP	Large plexiglas cuvette
LVDT	linear variable displacement transducers
LYSO	Lu _{1.9} Y _{0.1} SiO ₅ :Ce
M	Mesophyll
MRI	Magnetic resonance imaging
N	Number of measurements
NADPH	Nicotinamide adenine dinucleotide phosphate
NSC	Non-structural carbohydrates
[O ₂]	Concentration of oxygen
P	P-value (probability value)
PAR/ R_{PAR}	Photosynthetic active radiation
PET	Positron emission tomography
PGA	3-phosphoglycerate
P_{in}	Heating power (in stem heat balance)
PS	Potting soil

R^2	Coefficient of determination
RH/H_R	Relative humidity
R_n	Net radiation
RuBisCO	Ribulose-1,5-bisphosphate carboxylase/oxygenase
RuBP	Ribulose-1,5-biphosphate
RW	Rockwool
RWC	Relative water content
ROI	Region of interest
SE	Standard error/Sieve element
SECCC	Sieve element-companion cell complex
SF	Sap flow
SHB	Stem heat balance
SP	Small plexiglas cuvette
SPAC	Soil-plant-atmosphere continuum
SPECT	Single photon emission computed tomography
T	Temperature
t	Time
$t_{1/2}$	Half-life time
T_a	Air temperature
T_A	Treatment ambient conditions
T_{AD}	Treatment ambient conditions with soil-drought
T_{ASD}	Treatment ambient conditions with semi soil-drought
T_{AW}	Treatment ambient conditions with well-watered soil
T_D	Treatment with soil-drought
T_{dew}	Dewpoint temperature
T_E	Treatment elevated conditions
T_{ED}	Treatment elevated conditions with soil-drought
T_{EW}	Treatment elevated conditions
T_r	Tree
T_W	Treatment with well-watered soil
u	Wind speed
V	Stem volume
v	Phloem velocity
VC	Vulnerability curve

VPD/ Δe	Vapour pressure deficit expressed in kPa
VPD _{mol}	Vapour pressure deficit expressed in mol mol ⁻¹
VWC	Volumetric water content
<i>W</i>	Stem water content
WUE	Water-use efficiency
β^+	Positron
δ	Vapour pressure curve
ΔT	Temperature increase in xylem sap
ε	Bulk elastic modulus
ε_0	Proportionality factor for bulk elastic modulus
Γ	Turgor threshold for stem growth
γ	Psychrometric constant
γ -ray	Gamma-ray
ν_e	Electron neutrino
ρ_b	Basic density of wood
ρ_w	Density of water
Φ	Cell wall extensibility
Ψ	Water potential
Ψ_{12}	Water potential at which 12 % of conductivity is lost
Ψ_{50}	Water potential at which 50 % of conductivity is lost
Ψ_{88}	Water potential at which 88 % of conductivity is lost
Ψ_{100}	Water potential at which 100 % of conductivity is lost
Ψ_{\min}	Minimum measured water potential
Ψ_l	Leaf water potential
Ψ_p	Pressure water potential
Ψ_s	Osmotic water potential
Ψ_w	Total water potential
Ψ_x	Xylem water potential

S

SUMMARY

Over the past decades, effects of climate change have become increasingly clear. The atmospheric CO₂ concentration ([CO₂]) keeps on rising, temperature records are broken over and over again, and extreme dry and wet periods are becoming more frequent. Trees and forests are affected by climatic changes, in positive but also negative ways. Enrichment of CO₂ in the atmosphere typically results in higher uptake of CO₂ and reduced transpirational losses in trees. Elevated air temperatures and more frequent soil droughts, also known as “hotter droughts”, will have negative impacts on tree functioning and put additional stress on trees and forests. Recent studies have shown that water use efficiency increased under the increasing [CO₂] levels measured the past 50 years, but without a corresponding increase in tree growth. In addition, massive tree die-off events have increased in frequency. Still, it remains unclear and poorly understood how projected further climatic changes will impact current trees and forests because of the ambiguous effects the different changing climatic factors have. To improve our knowledge of tree response to climate change, we investigated xylem and phloem functioning in a widespread and ecologically important tree species of temperate and boreal forests in Eurasia, *Populus tremula* L. or common aspen, under elevated [CO₂] and air temperature, in combination with ample soil water or soil-drought.

Young, one-year-old *P. tremula* were grown for four months in treatments chambers under ambient (T_A: ambient air temperature and [CO₂] of 480 ppm) or elevated (T_E: ambient air temperature +3°C and [CO₂] of 707 ppm) conditions. In each treatment chamber, half of the trees were subjected to ample soil water (T_W: relative soil water content of 42 %), and the remainder to soil-drought (T_D: relative soil water content of 28 %). Stem diameter variations and sap flow rates were measured continuously with plant sensors. As expected, CO₂ fertilisation caused faster stem growth and larger leaf area development, with lower average stomatal conductance, but surprisingly, trees grown under elevated [CO₂] and soil-drought (T_{ED}) grew better than those grown with ample soil water (T_{EW}). T_{EW} trees showed lowest diel stem shrinkage as well as diel stem expansions. This led us to speculate that the lack of any stress (ample water and carbon) made the living stem cells stiffer, reducing their elasticity and extensibility. Furthermore, these trees showed a riskier behaviour towards the microclimate with sap flow rates increasing more rapidly in response to drier atmospheric conditions.

To investigate how vulnerable xylem was to drought, stems from the different treatments were subjected to bench-top dehydration to determine vulnerability to drought-induced cavitation with vulnerability and desorption curves, after checking equality of the native state of cavitation. Trees that were grown for two months under soil-drought (T_D) were able to withstand more negative water potentials before entering perilous levels of cavitation compared to well-watered trees (T_W) and within the same water regime, the elevated treatment (T_E) seemed slightly more vulnerable to drought-induced cavitation than their ambient counterparts (T_A). From the desorption curves we deduced that T_{EW} trees had a low hydraulic capacitance over a large range of less negative water potential. This confirmed the putative stiffer cells determined from stem diameter variation patterns and could explain the small margin between safe and perilous levels of cavitation, and the resulting higher vulnerability of T_{EW} trees to cavitation.

In this PhD, phloem loading and transport were analysed with novel methods. Phloem cells are highly sensitive to perturbations, which explains why only limited data of direct measurements of phloem dynamics exist. We chose to perform analyses with the short-lived (half-life of 20.4 min) carbon isotope, ^{11}C , which is a positron emitter and can image carbon *in vivo* and non-invasively. The past use of ^{11}C in positron emission tomography (PET) on plants was extensively reviewed to understand the advantages, challenges and potentials to use this innovative technology for phloem research and xylem-phloem interactions.

Depending on the species, phloem loading can be passive or active. We determined phloem loading strategies with ^{11}C -autoradiography on seven contrasting species: one temperate tree species, *Populus tremula* L. (common aspen), four tropical tree species, *Erythrophleum suaveolens* (Guill. & Perr.) Brenan, *E. ivorense* A. Chev. (both tali), *E. africanum* (Benth.) Harms (African blackwood), and *Maesopsis eminii* Engl. (umbrella tree), and two herbaceous crop species, *Solanum lycopersicum* L. (tomato), and *S. tuberosum* L. (potato). ^{11}C -autoradiography was validated with the species with known loading strategies and for the tropical tree species *M. eminii*, measurements corrected for positron range pointed to active loading, although this is a loading strategy more commonly found in herbaceous species. Because the phloem loading strategy is an important determinant for the sugar concentration inside the leaf and of the

phloem sap, climate change could potentially favour one of both strategies. Therefore, ^{11}C shows to be a powerful tool to be used in future combined studies on phloem loading and transport in the face of climate change, because autoradiographic and plant-PET measurements can then be combined.

To assess the impact of climate change on phloem transport, we used a combination of $^{11}\text{CO}_2$ labelling in a small-animal PET scanner and compartmental modelling. *Populus tremula* trees that were grown for 5 months in ambient (T_A : 404 ppm) or elevated (T_E : 659 ppm) [CO_2] were measured in their native well-watered state and after being subjected to a period of sudden drought. In the native state, T_E trees showed a phloem velocity 50 % higher than T_A trees, but after drought, phloem transport in T_E trees ceased completely, while in T_A trees phloem velocity reduced by only 60 %. These results indicated that despite the stimulation of phloem transport during well-watered conditions in elevated [CO_2], phloem is more vulnerable to drought in T_E trees. This could be related to the higher vulnerability of xylem to drought, which would reduce water availability to drive phloem flow. Alternatively, the putative role of sugars in cavitation protection or repair could be impeded because of a more rapid phloem failure, leading to a higher vulnerability to drought-induced cavitation.

In the context of climate change, we might have revealed a dangerous trend that the lack of stress (high [CO_2] and ample water) in a plastic and adaptive species apparently resulted in trees with decreased drought resilience. It should be further investigated whether this is a general response or species-dependent. Climate change is expected to cause more drought periods, but also more wet periods. For *P. tremula*, wet growing conditions under climate change conditions could give rise to vulnerable generations in the forest. Species with a low plastic potential will be more likely to succumb under the high pace of climate change, but this plastic species appeared to be not well acclimated. To better understand how tree species will respond to climate change, which processes and mechanisms lie behind, and how xylem-phloem interactions are impacted more ecophysiological research is warranted and plant-PET could play an important role as method to discover more of the secrets of phloem and xylem functioning.

S

SAMENVATTING

De laatste decennia worden de effecten van klimaatsverandering steeds duidelijker. De CO₂-concentratie ([CO₂]) in de atmosfeer blijft stijgen, temperatuurrecords worden keer op keer gebroken en extreem droge en natte periodes komen vaker voor. Bomen en bossen worden zowel positief als negatief beïnvloed door klimaatsverandering. In het algemeen leiden hogere CO₂-concentraties in de atmosfeer tot hogere koolstofopname en lagere transpiratieverliezen in bomen. Verhoogde luchttemperatuur en frequenter optredende bodemdroogte, zogenaamde “warmere droogtes”, zullen dan weer een negatieve impact hebben op het functioneren van bomen en extra stress in bomen en bossen veroorzaken. Recent onderzoek toont aan dat de efficiëntie van het waterverbruik in bomen de voorbije 50 jaar gestegen is onder invloed van stijgende [CO₂] niveaus, maar dit heeft niet tot hogere groeicijfers geleid. Bovendien is het aantal gevallen van grootschalige boomsterfte toegenomen. Toch blijft het onduidelijk en weinig begrepen hoe de voorspelde veranderingen van het klimaat bomen en bossen verder zullen beïnvloeden door de niet eenduidige effecten die de verschillende klimaatfactoren hebben. Om tot een beter begrip van de boomrespons op klimaatsverandering te komen, onderzochten we het functioneren van xyleem en floëem in een wijdverspreide en ecologisch belangrijke soort in gematigde en boreale bossen in Eurazië, *Populus tremula* L. of ratelpopulier, onder verhoogde [CO₂] en luchttemperatuur, in combinatie met een goed bewaterde of droge bodem.

Jonge, eenjarige *P. tremula* groeiden gedurende vier maanden in behandelingskamers in huidige (T_A: omgevingsluchttemperatuur en [CO₂] van 480 ppm) of verhoogde (T_E: omgevingsluchttemperatuur +3°C en [CO₂] van 707 ppm) omstandigheden. In elke behandelingskamer groeide de helft van de bomen in goed bewaterde bodems (T_W: relatief bodemvochtgehalte van 42 %) en de overige in droge bodems (T_D: relatief bodemvochtgehalte van 28 %). Stamdiametervariaties en sapstroomdebieten werden continu gemeten met plantsensoren. Zoals verwacht heeft CO₂-bemesting gezorgd voor snellere stamgroei, een grotere bladoppervlakte en een lagere gemiddelde stomatale geleidbaarheid. Maar verrassend was dat bomen die opgroeiden onder verhoogde [CO₂] en bodemdroogte (T_{ED}) beter hebben gegroeid dan die in goed bewaterde bodems (T_{EW}). T_{EW} bomen vertoonden de laagste dagelijkse stamkrimp alsook stamuitzetting. We speculeerden dat het ontbreken van stress

(er was voldoende water en koolstof) heeft gezorgd voor stijvere cellen die de elasticiteit en rekbaarheid verminderden. Daarenboven vertoonden deze bomen een risicovoller gedrag ten aanzien van het microklimaat met sneller stijgende sapstroomdebieten onder invloed van drogere atmosferische condities.

Om uit te zoeken hoe vatbaar xyleem was voor droogte, werden stammen van de verschillende behandelingen onderworpen aan vergaande uitdroging. Hierbij hebben we de vatbaarheid voor cavitatie veroorzaakt door droogte bepaald aan de hand van vatbaarheids- en desorptiecurves, na controle dat de beginsituaties op vlak van cavitatie niet verschillend waren tussen behandelingen. Bomen die twee maanden aan bodemdroogte onderworpen werden (T_D), konden meer negatieve waterpotentialen aan vooraleer een gevaarlijk niveau van cavitatie werd geobserveerd. In gelijke bodemvochtcondities leken de bomen in verhoogde condities (T_E) een verhoogde vatbaarheid te vertonen in vergelijking met hun tegenhanger van de behandeling in huidige condities (T_A). Uit de desorptiecurves bleek dat T_{EW} bomen een lagere hydraulische capaciteit hadden over een grotere range van minder negatieve waterpotentialen. Dit was in lijn met de hypothese van stijvere cellen, gebaseerd op stamdiametervariaties en werd als verklaring naar voor geschoven voor de kleinere marge tussen veilige en gevaarlijke niveaus van cavitatie en de daarbij horende hogere vatbaarheid voor cavitatie in T_{EW} bomen.

In dit doctoraat werden floëmlading en -transport geanalyseerd met innovatieve methodes. Floëemcellen zijn uiterst gevoelig voor verstoringen wat ertoe heeft geleid dat er slechts een gelimiteerde hoeveelheid data bestaat van directe metingen van floëemdynamieken. Het kortlevende koolstofisotoop ^{11}C , met een halfwaardetijd van 20,4 minuten, dat positronen uitzendt, werd gekozen om het koolstof *in vivo* en niet-invasief te meten. Er werd een uitgebreid overzicht gemaakt van het gebruik van ^{11}C in positron emissie tomografie (PET) om de voordelen, uitdagingen en het potentieel ervan te kennen voor het onderzoek naar floëem en xyleem-floëem interacties.

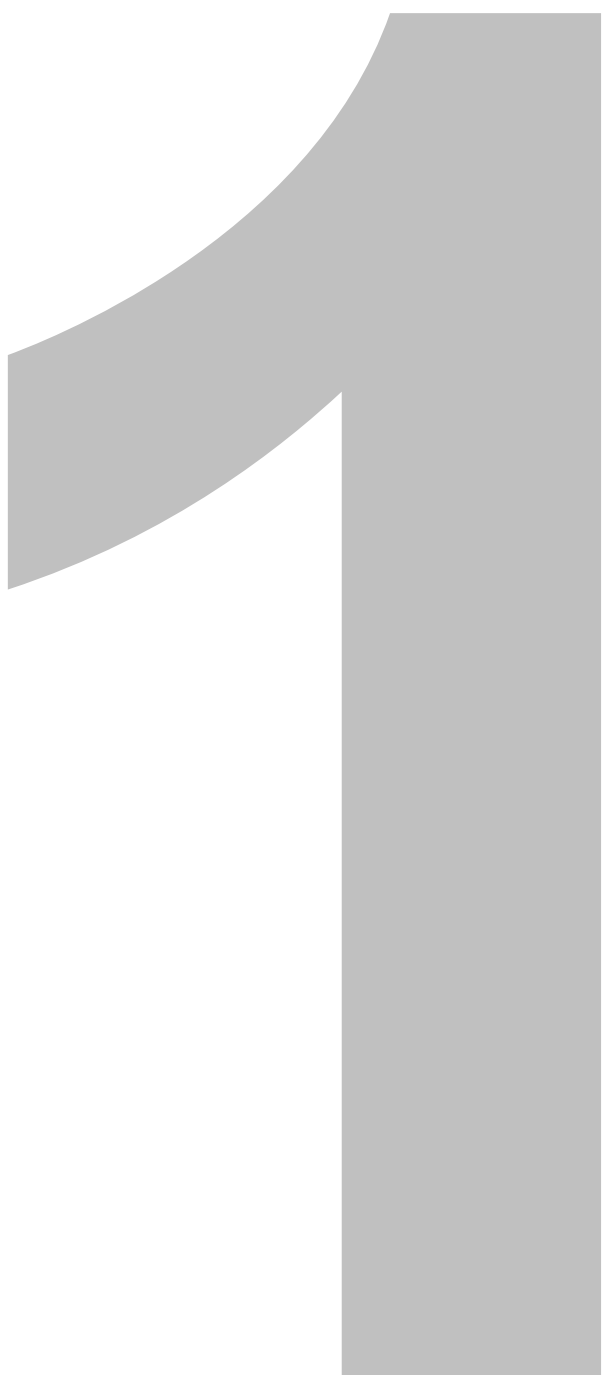
Afhankelijk van de soort kan floëmlading passief of actief zijn. Wij bepaalden met ^{11}C -autoradiografie welke floëmladingsstrategie zeven contrasterende soorten gebruikten: een gematigde boomsoort, *Populus tremula* L. (ratelpopulier), vier tropische boomsoorten, *Erythrophleum suaveolens* (Guill. & Perr.) Brenan (tali), *E. ivorense* A. Chev. (tali), *E. africanum* (Benth.) Harms,

Maesopsis eminii Engl. en twee kruidachtigen, *Solanum lycopersicum* L. (tomatenplant) en *S. tuberosum* L. (aardappelplant). ^{11}C -autoradiografie werd gevalideerd door soorten met gekende ladingsstrategieën te meten. Voor de tropische soort *M. eminii* hebben we via metingen, gecorrigeerd voor positronreisafstand, ontdekt dat het een actieve lader is, hoewel dit een strategie is die gewoonlijk in kruidachtigen waargenomen wordt. Aangezien floëemlading gevolgen heeft voor de suikerconcentratie in het blad en in het floëemsap zou klimaatsverandering één van beide kunnen bevorderen. Daarom is ^{11}C een krachtig hulpmiddel om in toekomstige studies floëemlading en -transport te meten, aangezien autoradiografie en plant-PET-metingen dan gecombineerd kunnen worden.

Om de invloed van klimaatsverandering op floëemtransport na te gaan hebben we een combinatie van $^{11}\text{CO}_2$ labelen in een PET-scanner voor kleine proefdieren en compartimentele modellering gebruikt. *P. tremula* bomen die vijf maanden in huidige (T_A : 404 ppm) of verhoogde (T_E : 659 ppm) $[\text{CO}_2]$ groeiden, werden gemeten in goed bewaterde condities en na een periode van plotse droogte. In goed bewaterde condities hadden T_E bomen een floëemsnelheid die 50 % hoger lag dan T_A bomen. Na een periode van droogte viel het floëemtransport in T_E bomen echter volledig stil, terwijl in T_A bomen de snelheid met slechts 60 % verlaagde. Deze resultaten toonden aan dat ondanks een stimulatie van het floëemtransport in goed bewaterde condities en onder verhoogde $[\text{CO}_2]$, het floëem vatbaarder is voor droogte in T_E bomen. Dit zou gerelateerd kunnen zijn met de hogere vatbaarheid van het xyleem voor droogte, wat zou kunnen leiden tot een verlaagde waterbeschikbaarheid voor de floëemstroom. Anderzijds zou de vermeende rol van suikers in cavitatiebescherming of -herstel verstoord kunnen zijn door het sneller stilvallen van het floëemtransport, wat resulteert in een hogere vatbaarheid voor droogte in het xyleem.

In een context van klimaatsverandering stelden we mogelijks een gevaarlijke trend vast waaruit blijkt dat het schijnbaar ontbreken van stress (hoge $[\text{CO}_2]$ en waterbeschikbaarheid) een soort met hoge plasticiteit minder weerbaar maakt tegen droogte. Verder onderzoek zou moeten uitwijzen of dit een soort-specifieke of algemene respons is. Klimaatsverandering wordt geacht meer droogte te veroorzaken, maar ook meer natte periodes. Voor *P. tremula* zouden

natte omstandigheden en klimaatsverandering kunnen zorgen voor kwetsbare generaties in bossen. Soorten die zich niet kunnen aanpassen hebben een grotere kans om te bezwijken door de hoge snelheid van klimaatsverandering, maar deze plastische soort blijkt zich net op een slechte manier te hebben geacclimatiseerd. Om beter te begrijpen hoe boomsoorten op toekomstige klimaatsverandering zullen reageren, welke de achterliggende processen en mechanismen zijn en hoe xyleem-floëem interacties worden beïnvloed, is meer ecofysiologisch onderzoek vereist. Plant-PET zou hierin een belangrijke rol kunnen spelen als methode om de geheimen van floëem en xyleem verder te onthullen.



CHAPTER 1

Introduction and thesis outline

Introduction

A changing world: welcome to the Anthropocene

Although climate change has been a hot topic in science for several decades, and many warnings have been sent out by the scientific world, worldwide greenhouse gas emissions keep on increasing year after year (IPCC 2014c, Boden et al. 2017, Ripple et al. 2017). Humanity's influence on the environment is causing such enormous impacts that the current era is becoming known as the Anthropocene. Due to the low responsiveness of policymakers, the world is in the process of being reshaped profoundly and rapidly (Figs 1.1 - 1.3) (IPCC 2014c, Ripple et al. 2017). For example, the year 2016 could easily fill multiple pages in the Guinness book of records (Blunden and Arndt 2017). The concentration of CO₂ molecules in the atmosphere has never been higher than the 402.9 ppm registered during 2016, for at least 800 000 years, based on ice core records (Fig. 1.1). Globally, surface temperature has never been higher than in 2016, with the previous two records set in 2014 and 2015. Averages of tropospheric temperatures and sea surface temperature in 2016 established new record values. Furthermore, the occurrence of extreme events is increasing. According to IPCC (2012), observations show a global increase in warm days and nights, in the number of warm spells, in heat wave duration, in drought severity and duration, and a changing precipitation pattern. For 2017, preliminary reports indicate that it will be the warmest year without a warming El Niño (WMO 2017), with annual global [CO₂] probably surpassing 405 ppm (Fig. 1.1) (Dlugokencky and Tans 2017). There is enough scientific base to link this to anthropogenically caused changes such as an increase in greenhouse gasses. In the Paris agreement of 2015, countries across the world pledged to keep global temperature increase under 2°C and to make efforts to limit global warming by 1.5°C. But even the +2°C scenario has been called a “fantasy” or only attainable after “heroic” efforts (Tollefson 2015). No matter how the near future looks like exactly and how policymakers act, there is a high level of confidence that the world will be hotter and CO₂-enriched (Figs 1.3 and 1.4) (IPCC 2014c). According to Climate Action Tracker, a consortium that calculates policy effects on global temperature, we are currently heading to reach a temperature increase of about

3°C by the year 2100, which is associated with an atmospheric CO₂ concentration ([CO₂]) of 700 ppm (Fig. 1.4). In this work, we set out to discover how a widespread temperate tree species responds to a temperature increase of +3°C and [CO₂] of 700 ppm, and how soil water availability influences its responses.

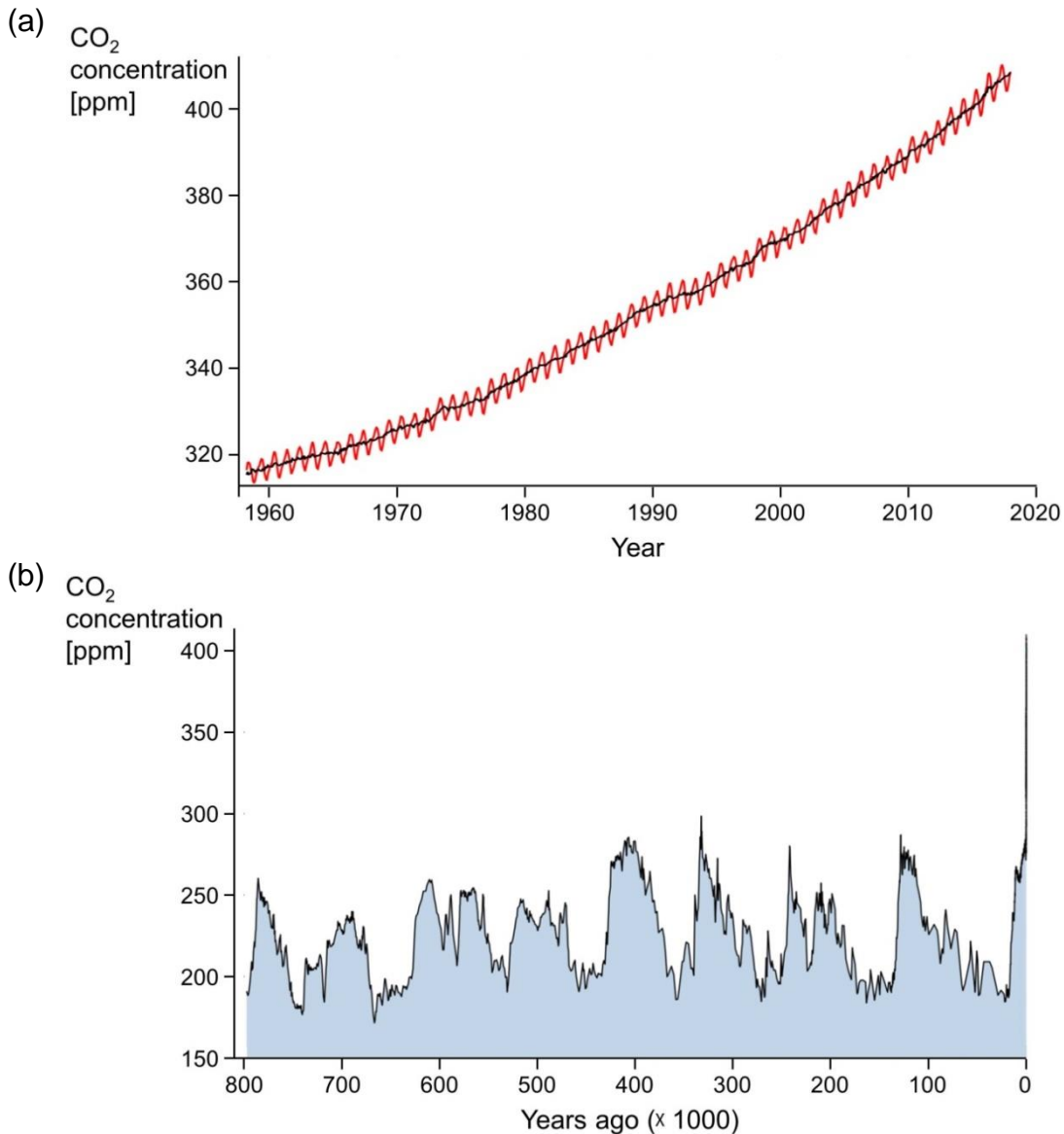


Figure 1.1 (a) Since 1958, daily measurements of atmospheric CO₂ concentration ([CO₂]) are performed at the Mauna Loa Observatory in Hawaii at high altitude, generating the so-called Keeling curve. A strong increase of the yearly concentration has been registered with yearly minimum values at the end of summer in the northern hemisphere. Adapted from Dlugokencky and Tans (2017) and Keeling et al. (1976). (b) Based on datasets of ice core measurements and recent direct measurements, a long-term reconstruction of atmospheric [CO₂] is possible. From this dataset, it is apparent that atmospheric [CO₂] is reaching record high values starting from The Industrial Revolution and caused by anthropogenic emissions. Adapted from SCRIPPS (2018) and Lüthi et al. (2008).

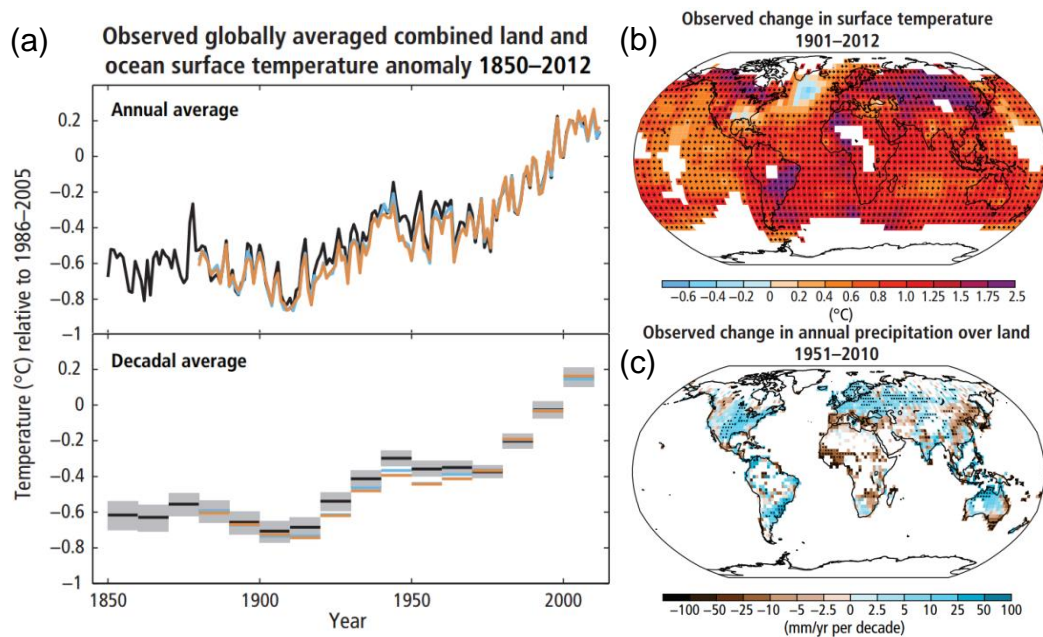


Figure 1.2 (a) Observations of the globally averaged surface temperature anomaly compared to a reference period 1886–2005, derived from different datasets (indicated by different colours), showing a clear rise in annual and decadal temperature averages. A detailed regional observed change in (b) surface temperature between 1901 and 2012 and (c) annual precipitation between 1951 and 2010. Adapted from IPCC (2014c).

Biomes are expected to shift in response to climate change

Trees and forests respond strongly to their environment. In contrast to animals, plants are not mobile and cannot shelter from harsh conditions, so they need to be able to withstand the governing conditions of their surroundings, at any time. Evolution has produced a multitude of processes, mechanisms and structures to provide plants with protective measures with the result that almost every thinkable niche is populated by one or more plant species. Climate is certainly the most important factor which defines how species are distributed across the world (Willis and Whittaker 2002, Pearson and Dawson 2003, Thuiller et al. 2005, Rohli et al. 2015). Besides climate, topography, soil-type and biotic interactions are also important determinants for niches (Pearson and Dawson 2003, Rohli et al. 2015). A changing climate can and probably will have a profound impact on the global distribution of plant species (Fig. 1.5) (Franks et al. 2014, IPCC 2014b). Although a few degrees in temperature might seem a little, it can, literally, make a world of difference.

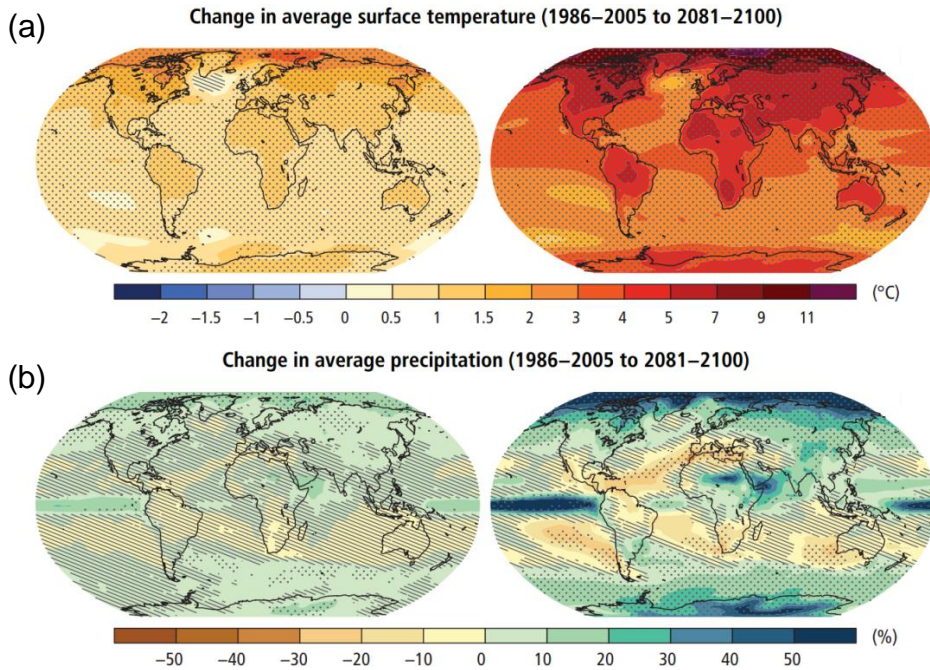


Figure 1.3 Projections of (a) changing average surface temperature, and (b) changing average precipitation by 2100 relative to 1986-2005, depending on (left) a scenario under strongly reduced emissions or (right) a scenario under the continuation of high greenhouse gas emissions. Adapted from IPCC (2014c).

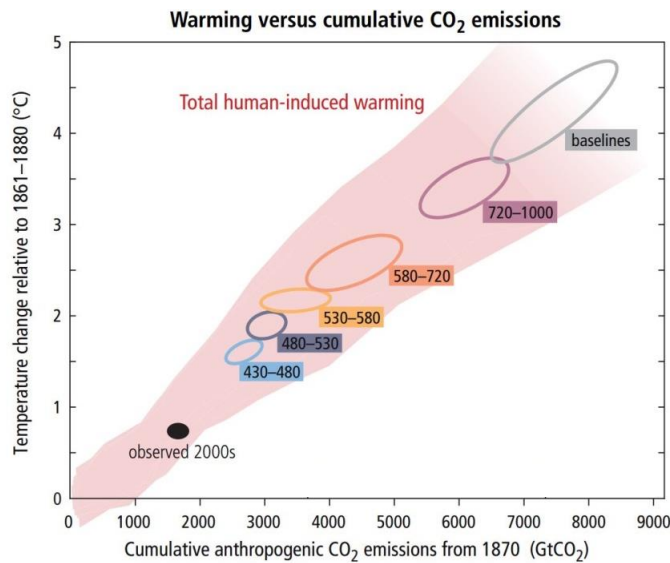


Figure 1.4 Relationship between the amount of anthropogenically emitted CO₂ and the resulting expected temperature change by 2100. Colours represent different predictive scenarios leading to other atmospheric CO₂ concentration, indicated in ppm in the coloured boxes. Baseline represents a world in which the emissions remain on the current path, the so-called business-as-usual. Coloured band represents the spread of the predictions and is less bright for predictions based on less available models. An atmospheric concentration of 700 ppm results in a temperature increase of around 3°C. Adapted from IPCC (2014c).

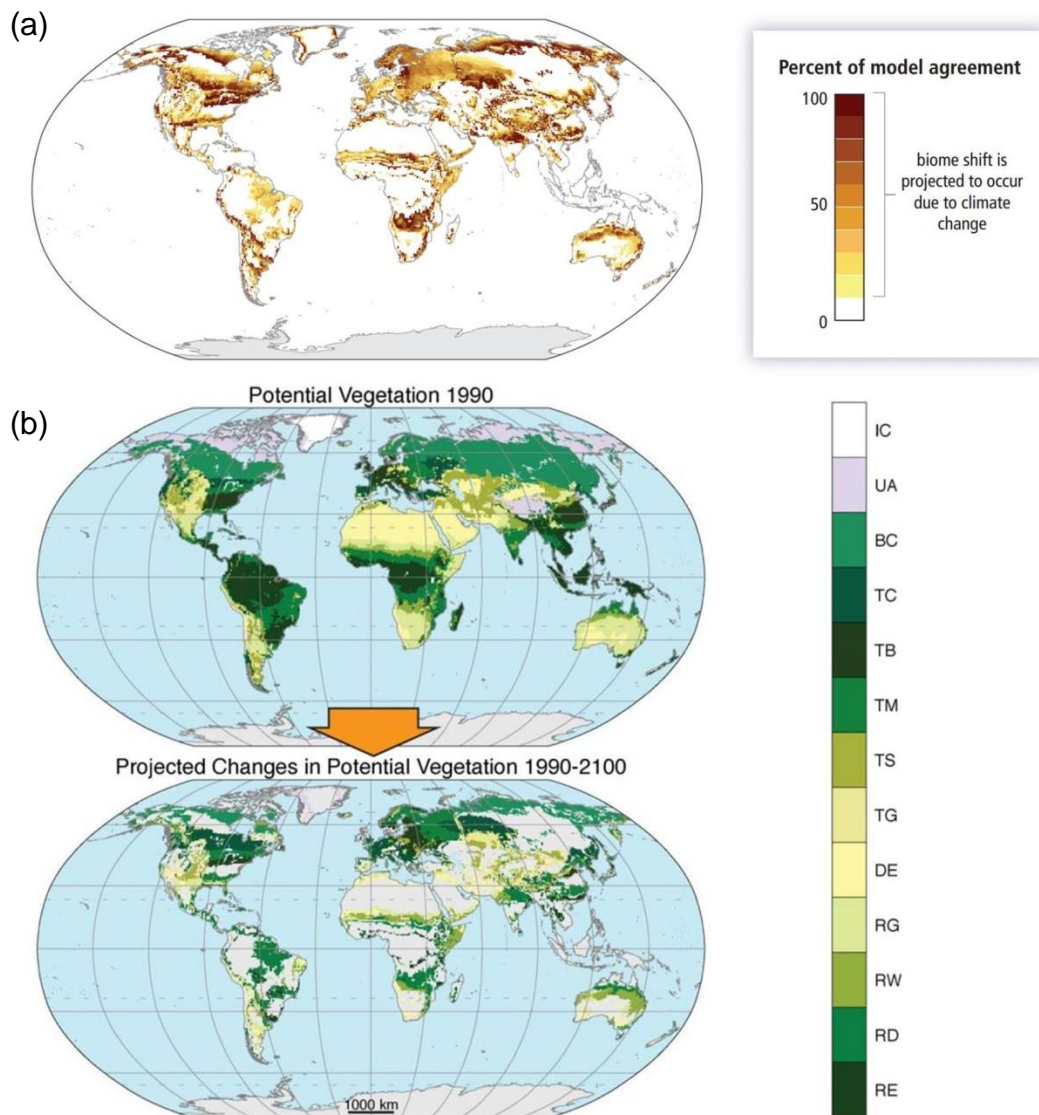


Figure 1.5 (a) Biome shift projections in which darker colour indicates a higher likelihood for a shift to occur in that region between 1990 and 2100. (b) Projections of how current vegetation will alter to other vegetation types between 1990 and 2100. Each colour represents a different vegetation type: ice (IC), tundra and alpine (UA), boreal conifer forest (BC), temperate conifer forest (TC), temperate broadleaf forest (TB), temperate mixed forest (TM), temperate shrubland (TS), temperate grassland (TG), desert (DE), tropical grassland (RG), tropical woodland (RW), tropical deciduous broadleaf forest (RD), tropical evergreen broadleaf forest (RE). Adapted from (a) IPCC (2014b) and (b) Allen et al. (2015).

An additional struggle of species that are confronted with changing environments is that the current pace of changes is unprecedented and puts a lot of pressure on their plastic responses (Hoffmann and Sgrò 2011, Corlett and Westcott 2013, Franks et al. 2014, Valladares et al. 2014, Duputié et al. 2015, Lenoir and Svenning 2015, Urban 2015, Harsch et al. 2017). The rate of change is so high that extinction is forecasted for a great deal of species (Urban 2015).

What is really problematic is that extinction of species or lower rate of success of vegetation has the risk to send a very strong positive feedback to climate change (IPCC 2014b). When trees die, or more generally, when vegetation degrades, carbon that was fixed inside these organisms will be decomposed and much of it converted into CO₂ and released into the atmosphere. This will aggravate the forcing of the greenhouse effect and thus climate change (Bonan 2008). An extra portion of climate change would put an extra portion of pressure on ecosystems and more species would succumb, entering a vicious circle. Because this is of such importance, tree mortality and forest die-off has been an active area of research (Allen et al. 2010, McDowell et al. 2011, Anderegg et al. 2012). Allen et al. (2010) compiled evidence that the number of climate change associated forest die-off events is already increasing, and they expect that this will keep on doing so. Mortality rates directly caused by drought and heat stress are projected to rise under climate change (Allen et al. 2010, Anderegg et al. 2012, Allen et al. 2015). Even if the projected hotter droughts would not directly lead to tree death, it can reduce tree resistance to pathogens and insects, which in turn can result in tree death (Allen et al. 2010, Anderegg et al. 2015, Ramsfield et al. 2016). Increased drought and heat can also directly impact insect and pathogen dynamics, and increase the probability of forest fires (IPCC 2014c, Anderegg et al. 2015, Flannigan et al. 2016, Ramsfield et al. 2016). This proves the strong link and interaction between climate and trees, and shows why improving the knowledge of how trees interact with their microclimate, the study of tree ecophysiology, is so important. This would allow us to better predict or even try to avoid certain responses of ecosystems (such as massive die-off).

Trees have evolved to face variable conditions during their lifetime, but also to face climate change?

Climatic factors that are most important for trees are temperature, light, water and carbon availability. A good illustration of this is the strong overlap between global climate types or soil types with biomes (Rohli et al. 2015). Interestingly, most facets of these factors do not unidirectionally influence plants, but plants also influence these factors in multiple ways (Bonan 2008, De Frenne et al. 2013b). For instance, an ecosystem with much vegetation and high rates of transpiration will transfer a considerable amount of water vapour in the air. But

the amount of water vapour will also have an effect on transpiration by exerting a lower pulling force on water inside the plants (Tyree and Ewers 1991). Furthermore, precipitation patterns will be influenced by the amount of water brought into the atmosphere by plants, clearly showing the many interactions and feedbacks that exist between ecosystems and the microclimate (Scheffer et al. 2005, Bonan 2008, von Arx et al. 2013). The complexity of these systems makes it very hard to predict how changes of one factor influence other factors, and how these changes are propagated throughout the entire system. This complexity can be somewhat reduced if the changes are expected to cause a transition from one known system to another known system. A well-known example in this respect is the impact that temperature increase, caused by climate change, has on the tree line in mountainous regions (Chen et al. 2011, De Frenne et al. 2013a). Under warming temperatures, trees can grow at higher altitudes, because temperatures are no longer too cold for the species to survive or thrive. Typically, entire species distributions move upward, according to Chen et al. (2011), at a mean rate of 1.22 m of altitude per year. The same shift occurs towards higher latitudes, at a rate of 1.76 km per year (Chen et al. 2011). These general response rates have large interspecific differences because of differences in plasticity to change and adapt across species (Chen et al. 2011, Franks et al. 2014, Urban 2015).

In general, trees show a relatively high degree of plasticity, because they are long-lived organisms and thus have a higher chance to encounter more variable circumstances during their lifetime (Duputié et al. 2015). However, the current changing climatic conditions are in no way comparable with naturally occurring changes. The rapidness with which changes occur will have a profound influence, as well as the magnitude of it (Hoffmann and Sgrò 2011, Urban 2015). The greater the distance tree species have to move from their “original” habitat, the higher the chances that certain factors in this new area are unsuited (Corlett and Westcott 2013, Urban 2015). For instance, the soil type can be unsuitable or a tree species might rely on an animal species to disperse its seeds, which is no longer present in its new habitat (Corlett and Westcott 2013, De Frenne et al. 2014). The lack of coevolutionary history is thought to lead to less successful systems in the face of climate change (Corlett and Westcott 2013).

Whereas in most cases, species are able to evade to a certain extent changing temperatures by moving to higher altitudes or higher latitudes, this is

not possible for an increase in $[\text{CO}_2]$. CO_2 is a quickly dispersed gas and is generally considered to occur in roughly the same concentration worldwide (Denning et al. 1995). This means that (i) if species do not cope well with a change in $[\text{CO}_2]$, they cannot shift to avoid this, and that (ii) there is no reference in the world to compare with to assess the potential influence of altered $[\text{CO}_2]$. Also, trees typically encounter climatic variability during their lifetime in terms of, amongst others, temperature, precipitation or wind, but normally not in terms of $[\text{CO}_2]$ (IPCC 2012, Franks et al. 2014). The effect of CO_2 is different compared to other climatic changes in the sense that an increase in $[\text{CO}_2]$ is shown to have neutral or positive impacts on individual plants. To understand this, it is important to explore the principles of water transport and gas exchange in plants.

Water, water, water

The importance of water for plants can hardly be overestimated. Almost all processes in plants are, one way or another, influenced by the amount of water in the plant and the pull that is exerted on this internal water (Hsiao 1973, Porporato et al. 2001, McDowell et al. 2008, Sevanto 2014). Large trees can lose hundreds of litres of water on a single day (Vertessy et al. 1997, Čermák et al. 2007). These water losses occur at the plant-atmosphere interface, the stomata of the leaves. These stomatal pores are dynamic plant cells that regulate the amount of gas exchange between the plant and the atmosphere (Leuning et al. 2004). Gas exchange is bidirectional, with water exiting the leaves to the atmosphere and CO_2 being taken up. This water loss is compensated by water uptake from the soil through the roots. Water transported throughout trees provides minerals coming from the soil, distributes important molecules, cools down the photosynthetic apparatus and generates turgidity in the living cells (Kramer and Boyer 1995, Porporato et al. 2001). Thus, water in trees is far from something static, but rather in constant movement and constantly exerting an impact on the plant. Water transport might be a dynamic feature, but it is governed by a passive process described as the cohesion-tension theory (Fig. 1.6) (Tyree and Ewers 1991, Taiz and Zeiger 2010). Compared to the plant, the atmosphere is very dry and will therefore pull strongly on water molecules in the substomatal cavity in the leaves. Under the more negative water potential of the atmosphere, water molecules will transpire, and be replaced by other water molecules that

evaporate from the mesophyll into the substomatal cavity. Because hydrogen bonds link water molecules throughout the plant, the negative water potential inside the leaves will pull the entire water column upwards, resulting in water flow throughout the plant and in water uptake by the roots, forming a continuous water movement from soil to atmosphere through what is called the soil-plant-atmosphere continuum (SPAC) (Tyree and Ewers 1991). These forces create a water potential gradient with more negative values at the top of the plant and less negative values in the roots. Looking at the SPAC, it is easy to understand that when the air gets drier (which can be both because of a lower amount of water vapour in the air, or a higher air temperature) there is a larger pressure for the plant to transpire and transport water, or when soil water availability gets lower, it gets more difficult for the plant to meet the transpirational demands.

Actually, the foregoing is a simplification of reality, because not only water running from the roots through the xylem into the leaves plays a role, but also the internally stored water in living cells plays a role in providing water to the transpiration stream (Steppe et al. 2006, Zweifel et al. 2006, Deslauriers et al. 2007, Drew and Downes 2009, De Swaef et al. 2015, Steppe et al. 2015, Vergeynst et al. 2015a). Importantly, this signifies that water in living cells is also under influence of, and responsive to, the governing water potential inside the plant. That is one of the main reasons why water is so incredibly important for plants, because the availability of water for the plant will affect the availability of water in living cells, and the pressure that is exerted on this water. The pressure on the cell water, the water potential, will influence a multitude of cell processes, as exemplified in Figure 1.7.

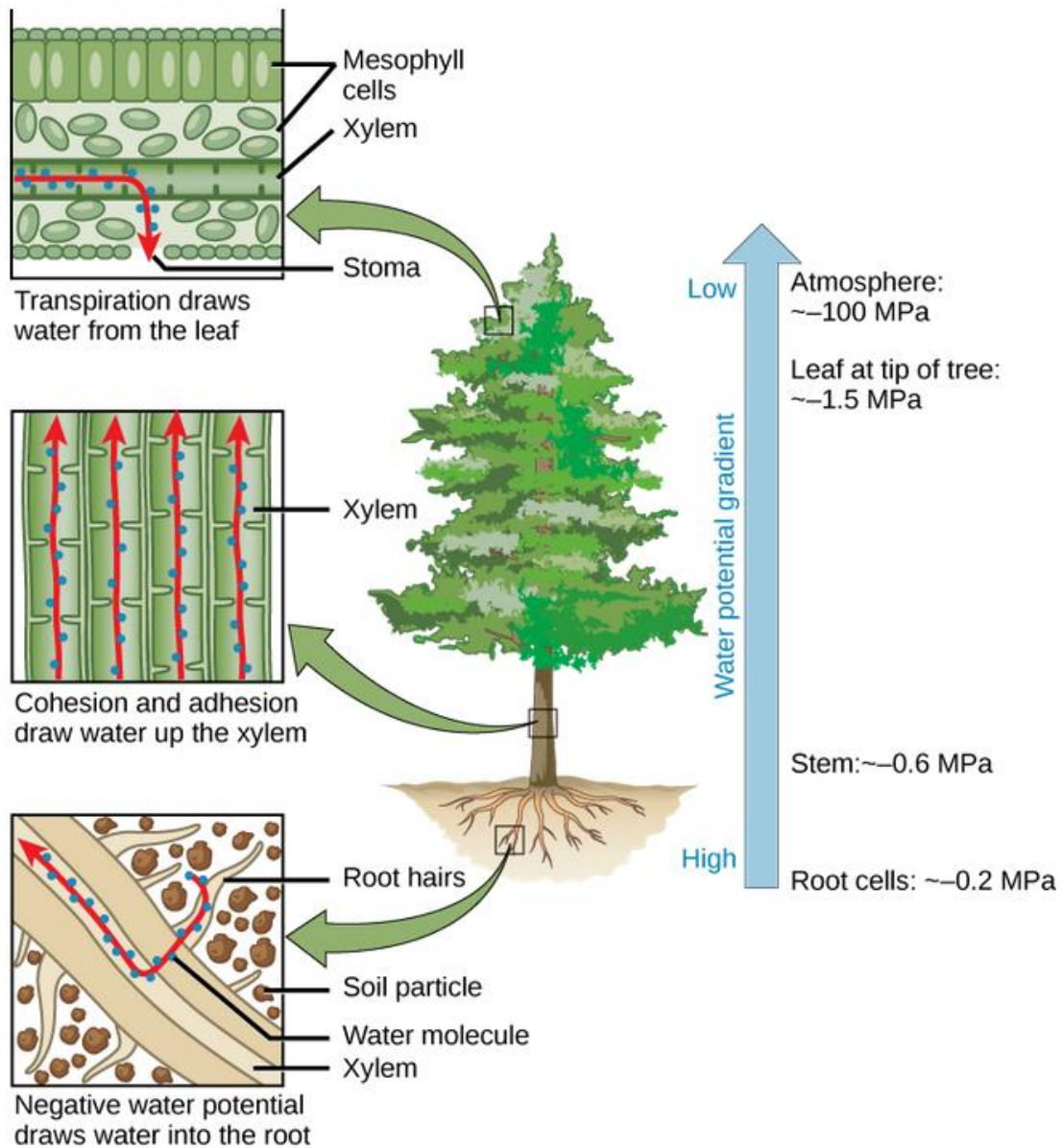


Figure 1.6 Schematic representation of the water movement in the soil-plant-atmosphere continuum (SPAC). Trees lose water through the stomata and because water molecules inside trees are bound to each other due to cohesive forces, water is pulled upward. This upward suction generates a water potential gradient, which is most negative in the atmosphere and less negative in the soil, resulting in upward water movement from roots to leaves through the xylem. Adapted from Lumen (2004).

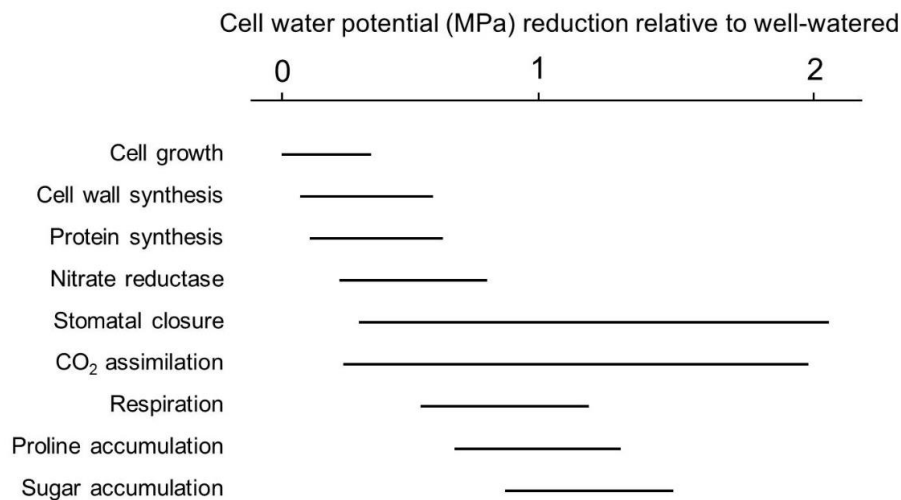


Figure 1.7 Typical values for reduction in cell water potential, compared to well-watered plants, which will affect cell processes. Some processes are more sensitive or responsive to water deprivation than others. Adapted from Porporato et al. (2001)

Physiological responses to elevated [CO₂] and temperature

Back to the effects of globally increasing [CO₂] levels. To take up CO₂, plants need to open their stomatal pores on the leaf surface. But opening stomata inevitably implies a loss of water. That is why stomata are so important for plants to regulate their water and carbon economy. In case of drought, signals are sent to stomata to close and minimise water loss (Porporato et al. 2001, Murata et al. 2015). Guard cells are designed in such a way that in case these cells lose turgor, typically caused by drought, they close the pore (Zeiger 1983, Leuning et al. 2004). Other factors also have an effect on stomatal aperture, such as temperature, relative humidity, light, and the photosynthetic pathway (C₃, C₄ or CAM). Furthermore, stomata are responsive to the internal [CO₂] to avoid that more CO₂ is taken up than needed by the metabolic processes at that time, and concomitantly water is lost (Zeiger 1983, Leuning et al. 2004, Shimazaki et al. 2007). Temperature influences all metabolic processes. A change in air temperature will therefore have multiple consequences on tree functioning (Boisvenue and Running 2006, Taiz and Zeiger 2010, Teskey et al. 2015). It affects photosynthesis via the activity of RuBisCO (Ribulose-1,5-bisphosphate carboxylase/oxygenase), respiration, and phosphate availability for chloroplasts. Temperature can be both high or too low, meaning that each species has its optimal temperature range to operate (Taiz and Zeiger 2010, Teskey et al. 2015).

Multiple photosynthetic pathways exist, but a large majority of species, including almost all tree species, function according to the C_3 pathway (Text box 1.1) (Yamori et al. 2014). The effect of elevated atmospheric $[CO_2]$ in C_3 plants is comparable with how C_4 and CAM (crassulacean acid metabolism) plants increase $[CO_2]$ over $[O_2]$ inside the leaf, and thus favour the carboxylase to oxygenase ratio of RuBisCO, making photosynthesis more efficient (Bowes 1993, Drake et al. 1997). Higher temperatures can give rise to a lower activation state of RuBisCO, while lower temperatures often leads to higher amounts of RuBisCO, but many plants are able to acclimate to prevailing temperatures, within a certain range (Yamori et al. 2014). In general, C_4 species show a higher optimal temperature range than C_3 species, while optimal temperatures in CAM plants are lower. Optimal temperatures in CAM are however related to nighttime temperatures and therefore CAM plants are less impacted by high daytime temperatures (Fig. 1.8) (Yamori et al. 2014).

Under changing climatic conditions, advantages and disadvantages of the different photosynthetic pathways could alter, as well as the success rate of one over another (Bowes 1993, Drake et al. 1997, Ainsworth and Rogers 2007, Bernacchi and VanLoocke 2015). For C_3 plants, which are most abundant, elevated $[CO_2]$ will generally result in a lower loss of water in exchange for taking up and assimilating CO_2 (i.e., increase in water-use efficiency, WUE), as a result of lowered stomatal conductance (Fig. 1.9) (Ainsworth and Rogers 2007, Allen et al. 2015). An increased WUE might mitigate the adverse effects of an increase in temperature and extreme events (such as drought), although C_4 plants are predicted to be better suited in higher temperatures (Ainsworth and Rogers 2007, Yamori et al. 2014, Allen et al. 2015). Besides an increase in WUE, maximum photosynthetic rates have been observed to be higher in C_3 species, despite acclimation and lower RuBisCO investment (Fig. 1.9) (Ainsworth and Rogers 2007, Leakey et al. 2009).

In summary, the response to an increase in $[CO_2]$ is expected to be positive, but species-dependent and varying between functional groups and photosynthetic pathways (Fig. 1.9) (Bowes 1993, Ainsworth and Rogers 2007). This species-dependent response on changes in CO_2 and other climatic factors will probably result in alterations in competitive force and thus species distribution. On top of this, many studies focus on one or several of the changing

factors, but much more rarely do they focus on the interaction of these factors, while it is clear that pure additivity is only seldom the case (Farrer et al. 2014).

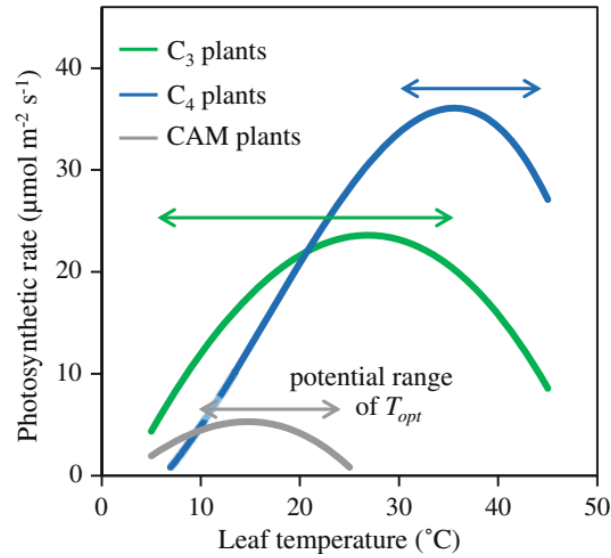


Figure 1.8 Typical optimal temperature ranges for different photosynthetic pathways (C_3 , C_4 and CAM). For C_3 and C_4 plants, temperatures are daytime temperatures and for CAM nighttime temperatures are shown. Adapted from Yamori et al. (2014).

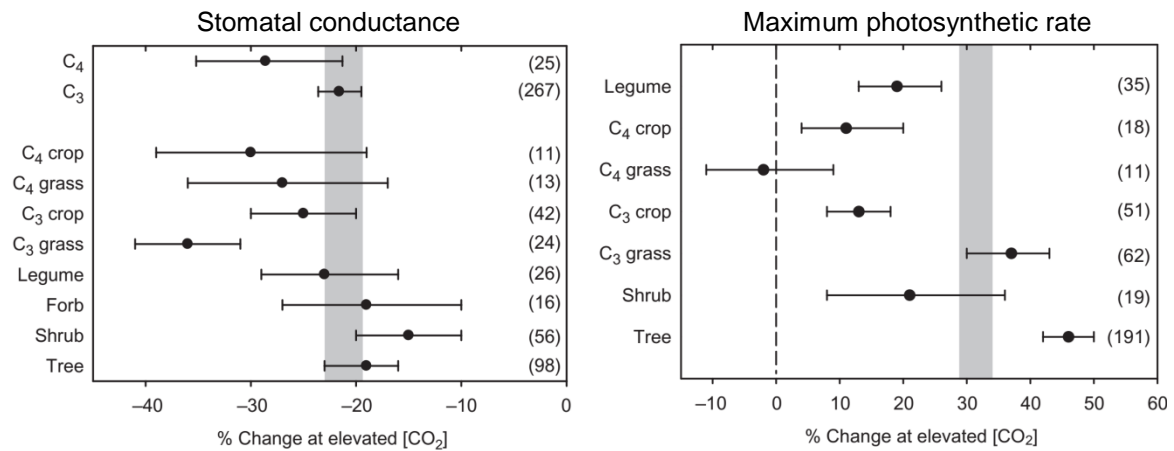


Figure 1.9 Observed relative effects of elevated CO_2 concentration ($[CO_2]$) on stomatal conductance and maximum photosynthetic rate in a meta-study of free-air CO_2 enrichment studies for several classes of functional groups. Number of studies used is indicated in parenthesis. Average $[CO_2]$ difference was 200 ppm. Adapted from Ainsworth and Rogers (2007).

Transport of photoassimilates in the phloem

The general principles of carbon transport were established almost a century ago by Münch (1930). The osmotically generated pressure gradient between sources and sinks drives the phloem flow (Fig. 1.11) (Münch 1930, Van Bel 2003, Turgeon and Wolf 2009, De Schepper et al. 2013b). Production of photoassimilates takes place in photosynthetic tissue of the plant, which is located mainly in the leaves. The surplus of carbon production inside the leaves will be exported through the phloem. Phloem consists of sieve elements through which transport occurs, and companion cells which are closely related to the sieve elements: Sieve elements and companion cells originate from the same mother cell and remain highly connected. A companion cell provides pivotal functions to the sieve element, which is stripped from important cell structures to facilitate bulk flow. Together they are called the sieve element-companion cell complex (SECCC) (De Schepper et al. 2013b).

Text box 1.1 Photosynthetic pathways: C₃, C₄, and CAM

Plants can be categorised in three groups, based on their photosynthetic pathway: C₃, C₄, and CAM (crassulacean acid metabolism) (Taiz and Zeiger 2010). Species with C₃ photosynthesis are by far the largest group with 85 % of all higher plant species, whereas 5 % of the species is C₄, and 10 % is CAM (Yamori et al. 2014). C₃ plants convert CO₂ entering the plant into 3-phosphoglycerate, a molecule consisting of three carbon atoms (and therefore called C₃ pathway) (Fig. 1.10). This reaction occurs in the Calvin cycle and is catalysed by RuBisCO (ribulose-1,5-bisphosphate carboxylase/oxygenase), the most important enzyme in photosynthesis.

This enzyme can catalyse reactions with both CO₂ and O₂. The reaction with CO₂, carboxylase, eventually results in the formation of sugars and starch. The reaction with O₂, oxygenase, is known as photorespiration and results in a loss of CO₂.

Plants with the C₄ or CAM photosynthetic pathway have a step in which CO₂ entering the leaf is first converted into an intermediary molecule (typically malate). In C₄ plants, this intermediary is transferred to bundle sheaths where CO₂ is released again, and the Calvin cycle processes the CO₂ (Fig. 1.10). In CAM plants, stomata are open and CO₂ is taken up during the night and stored as malate in the vacuoles (Fig. 1.10). During the day, stomata are closed and CO₂ is released internally when light reactions provide energy and the Calvin cycle can operate. Both C₄ and CAM plants separate the process of CO₂ uptake and the Calvin cycle (C₄ spatially, and CAM temporally). The main reason these pathways (C₄ and CAM) have been evolved is to lower the oxygenase activity of RuBisCO by increasing [CO₂] compared to [O₂].

Text box 1.1 Continued

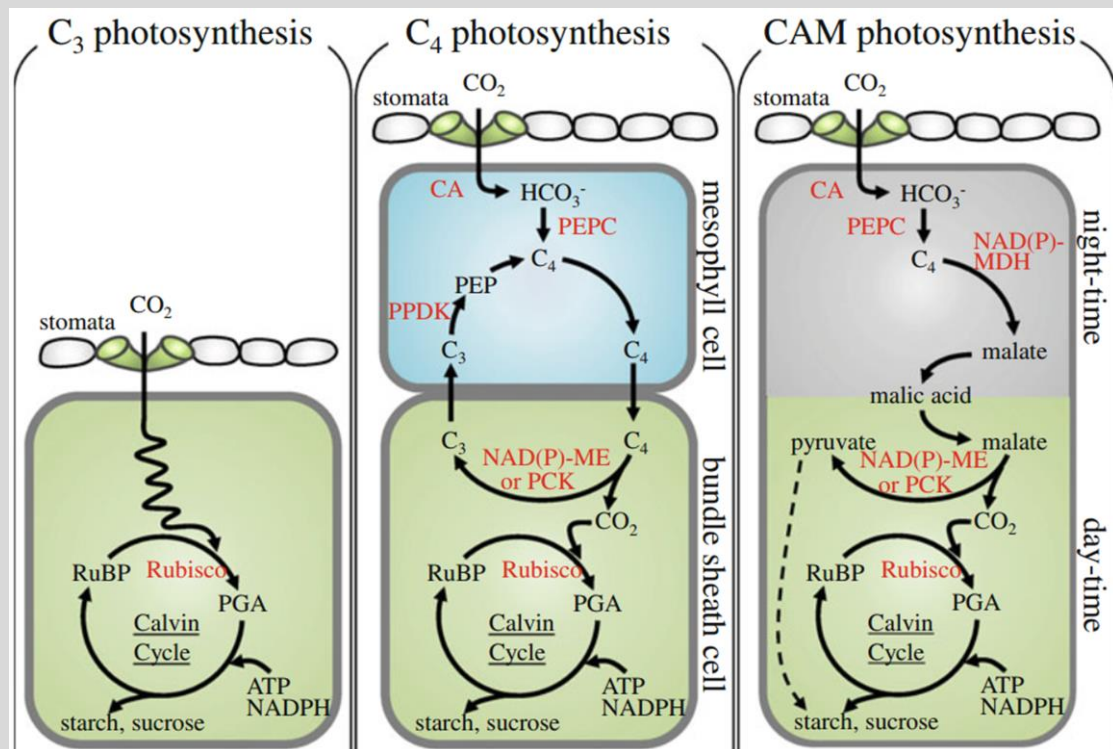


Figure 1.10 In C₃ plants, CO₂ is taken up and used in the Calvin cycle. In C₄ and CAM plants, CO₂ is first fixed in a C₄ molecule. In C₄ plants, the CO₂ is released in the bundle sheath cells and then used in the Calvin cycle. In CAM plants, CO₂ is taken up during the night, when stomata are open and CO₂ is released again during the day, when stomata are closed, but light is present to deliver energy for the Calvin cycle. The Calvin cycle consists of the reaction between ribulose-1,5-biphosphate (RuBP) and CO₂, catalysed by RuBisCO (ribulose-1,5-bisphosphate carboxylase/oxygenase), forming two molecules of 3-phosphoglycerate (PGA, consisting of three carbon molecules). This is used in further steps to produce sucrose and starch at the cost of energy (ATP and NADPH). The starting product of the Calvin cycle, RuBP is regenerated. Adapted from Yamori et al. (2014).

Photoassimilates meant for export out of the leaves (sources) are loaded into the SECCC, which increases the osmotic water potential and draws water into the sieve elements (Fig. 1.11). At sites where these photoassimilates are needed (sinks) the reverse process happens, and photoassimilates are unloaded with water concomitantly flowing out the sieve elements (Fig. 1.11). This will lead to an increase in turgor pressure at the source sites and a decrease at the sink sites. This generated pressure gradient results in the flow of water through the phloem, carrying high amounts of photoassimilates. Because of the need of water to drive this flow, an important coupling between phloem and xylem exists (Windt et al. 2006, De Schepper and Steppe 2010).

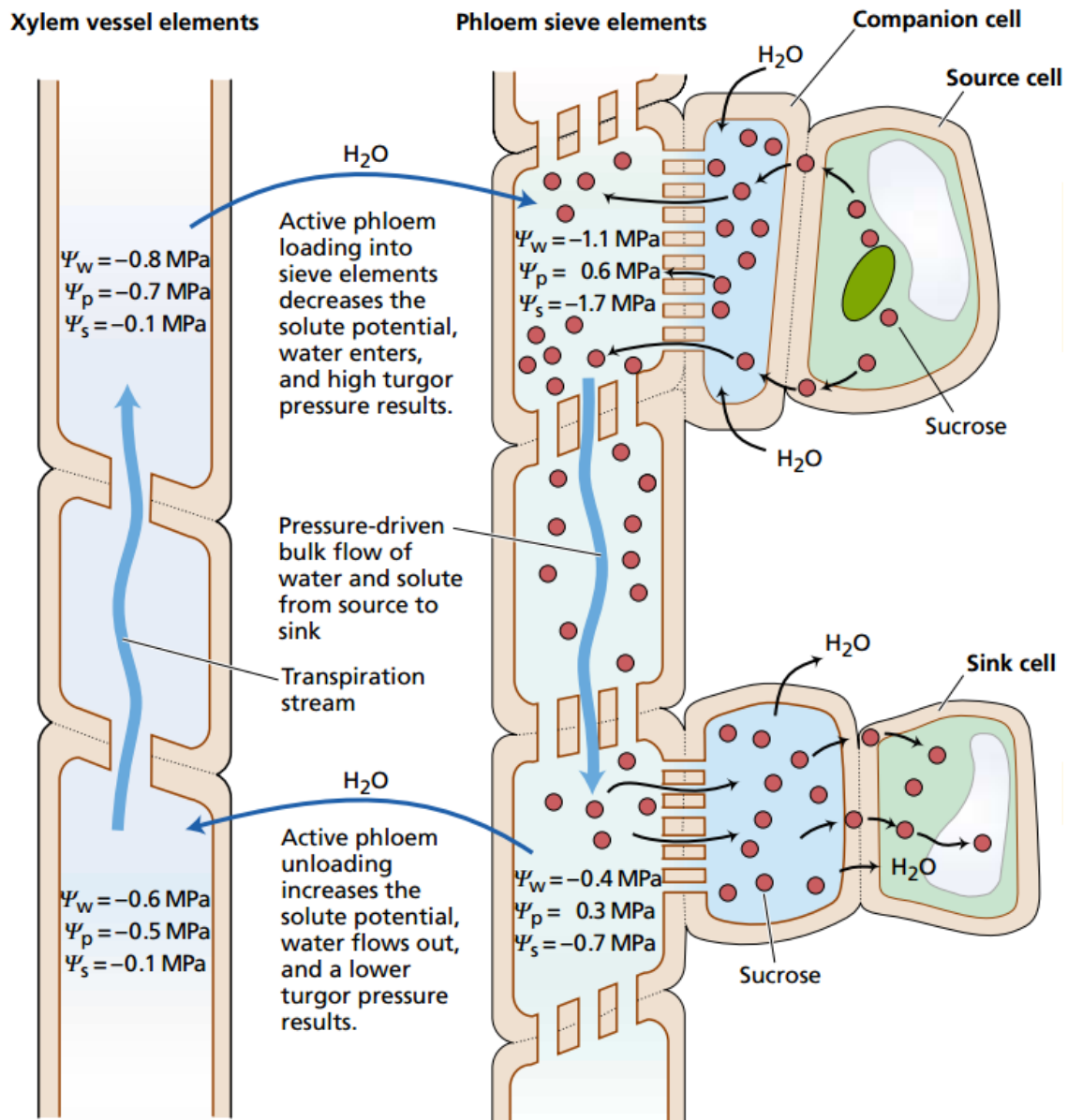


Figure 1.11 Schematic overview of the transport of sugars through phloem and its driving forces, with a clear interconnection between phloem and xylem. Photoassimilates, in this figure sucrose molecules, are loaded from the source into the phloem, which results in a pull on nearby water generating a flow in the phloem. At the sinks, photoassimilates are unloaded along with water, which results in a hydrostatic pressure driving source-to-sink flow in the phloem. Typically, water xylem flow is upwards and phloem flow is downwards. Ψ_w , Ψ_p and Ψ_s is total water potential, pressure potential, and osmotic potential, respectively. Adapted from Taiz and Zeiger (2010).

Phloem dynamics are regulated at many levels (De Schepper and Steppe 2010, Sevanto et al. 2011, Jensen et al. 2013, Sevanto 2014). Photosynthesis and loading rate influence the source strength (Ainsworth and Rogers 2007, Ainsworth and Bush 2011, De Schepper et al. 2013b), while the demand for

storage, growth or respirational energy influence sink strength (Sala et al. 2010, Sala et al. 2012, Wiley and Helliker 2012, De Schepper et al. 2013b). Also during transport, leakage-retrieval is finely equilibrated to ensure that enough sugars remain in the phloem, and enough sugars are allocated to lateral sinks (Minchin and Thorpe 1987, Thorpe et al. 2005, De Schepper et al. 2013b). This implies that environmental changes may alter phloem dynamics, and eventually also allocation and partitioning of available carbon will have their impact on phloem dynamics (Poorter and Nagel 2000, Minchin and Thorpe 2003, Sala et al. 2012, Ferrieri et al. 2013, Lemoine et al. 2013, Dietze et al. 2014, Savage et al. 2016). Although it is anticipated that climatic changes will influence phloem dynamics, complexities to measure phloem have resulted in only little available data on the influence of, for instance, drought, increased temperature or increased [CO₂] (Grimmer and Komor 1999, Komor 2000, Lemoine et al. 2013, Ryan and Asao 2014, Sevanto 2014), and much of the available knowledge comes from theoretical studies (Thompson and Holbrook 2003, Thompson 2006, Cabrita et al. 2013, Hall and Minchin 2013, Ryan and Asao 2014, Sevanto 2014, Woodruff 2014). Despite the incredible value of previous research, experimental data is needed to better predict how phloem will respond to a changing environment.

The reason why phloem is so complex to measure is because it consists of living cells, which are designed to be sensitive to intrusion and disturbances (Van Bel 2003, Turgeon and Wolf 2009). When a sieve element is damaged the plants would risk an enormous loss of valuable sap if there were no mechanism to seal this tube. Therefore, plants have developed defensive systems to clog and seal tubes with callose and P-proteins in case of a leakage (Van Bel 2003). These mechanisms make it not only harder for insects to feed on the phloem stream, but also for scientists to unravel all phloem secrets.

Better understanding of tree response to climate change through ecophysiology

Altogether, it remains very difficult to predict how a tree, forest, ecosystem or biome will respond to the combination of projected climatic changes. Yet, it is important to predict and understand future changes to a certain extent in order to assess which policy decisions are required, and what potential thresholds and tipping-points should be avoided.

In this PhD work, we will explore several ecophysiological responses that trees exhibit to climatic changes in air temperature, atmospheric [CO₂], and soil drought. Are the trees plastic enough to cope with elevated temperature and atmospheric [CO₂] combined with soil drought and how will this influence tree physiology? Will xylem and/or phloem be more resilient to the new challenges? If we can better understand the mechanisms behind the responses to these changes, we can come a step closer to fully comprehend how trees and forests will adjust. In this thesis, we use and integrate several innovative techniques to acquire a better picture of water and carbon relations and their coupling. We studied a temperate tree species, *Populus tremula* L., and determined how this species responded to climatic changes in terms of water and carbon transport, drought vulnerability of xylem and phloem, and growth. Using an ecophysiological research method we will not only investigate the outcome of climatic change of for instance stem growth but also come to a better understanding of what mechanisms lie behind the observed responses.

Thesis outline

A better ecophysiological understanding of how trees respond to forecasted climatic changes, such as elevated air temperature and atmospheric [CO₂], and altering precipitation patterns is important but complex (**Chapter 1**). Because climate change affects many factors at once, affecting trees both positively and negatively, learning what processes and mechanisms lie behind tree responses allow us to better understand and interpret observed plant functioning, but also increase our ability to foresee and project coming changes. Experiments were carried out on young *Populus tremula* L., a widespread Eurasian species, which grows in temperate and boreal forests (Fig. 1.12) (Myking et al. 2011, Caudullo et al. 2017). It is an angiosperm and a member of the Salicaceae family, commonly called aspen. *P. tremula* is a diffuse-porous tree species and known as a drought-sensitive and fast-growing species, with strong plasticity to soil moisture and climatic oscillations (Hall et al. 2007, Bjurhager et al. 2008, De Carvalho et al. 2010, Possen et al. 2011). Typically, this species does not grow larger than 30 m in height and 1 m in diameter. Its rapid growth and long branches make *P. tremula* well suited for the measurements performed in this PhD work. Although *P. tremula* has limited commercial importance, it is

ecologically important for many other species (Myking et al. 2011, Caudullo and de Rigo 2016). Furthermore, it is a pioneer species that establishes best on disturbed areas, mostly caused by forest fire (Myking et al. 2011). In the face of climate change, the occurrence of forest fires are expected to increase, which, in turn, might increase the importance of *P. tremula* (Allen et al. 2010, IPCC 2014c, Flannigan et al. 2016).



Figure 1.12 Distribution map of *Populus tremula* L., a widespread tree species, mostly occurring in temperate and boreal forests in Eurasia (Caudullo et al. 2017).

We have started our research with investigating how stem diameter growth is impacted in one-year-old *P. tremula* trees when grown under ambient conditions (ambient air temperature and atmospheric [CO₂] of 480 ppm) or climatic changes (elevated air temperature (+3°C) and atmospheric [CO₂] of 707 ppm), in combination with ample soil water or soil drought stress (Fig. 1.13) (**Chapter 2**). Tree stem growth is a good measure for tree vigour so treatments with highest stem growth indicate treatments with most favourable conditions. We investigated whether the effect of CO₂ fertilisation resulted in higher growth rates and whether the effects of soil drought would differ under different atmospheric [CO₂], by stomatal response. The latter effect was further investigated by measuring sap flow rates in all treatments and assessing water consumption per unit leaf area, from which the magnitude of stomatal response could be assessed. Stem diameter variation measurements were obtained on high temporal and spatial resolution in order to better interpret and understand underlying processes such as hydraulic capacitance and cell elasticity and extensibility.

After having assessed tree stem growth under constant soil conditions (well-watered or soil-drought), we characterised the resistance of the tree stems to drought-induced cavitation by determining hydraulic vulnerability curves (VC) and desorption curves (DC), from which hydraulic capacitances were determined in **Chapter 3** (Fig. 1.13). This way we investigated whether better growth rates (**Chapter 2**) come at the cost of higher hydraulic vulnerability or whether better growth rates indicated overall better “performances”, with also lower hydraulic vulnerability. Tree stems were dehydrated and the amount of cavitating vessels and stem water content was measured in function of a decreasing water potential. With these measurements, we were able to determine whether ambient vs. elevated, and well-watered vs. soil-drought induced plastic responses observable in drought vulnerabilities and hydraulic capacitances and whether interactions existed between these treatments. It was possible to assess whether trees under climatic changes are more vulnerable to effects of drought and elevated temperature, and whether elevated [CO₂] might mitigate drought vulnerability.

In **Chapters 4–6**, we focused on the transport of photoassimilates through the phloem. We explored the possibilities to work with ¹¹C, the short-lived carbon isotope, which emits a positron upon decay enabling its use in positron emission tomography (PET) (Fig. 1.13) (**Chapter 4**). This innovative technique has been used in plant science, but only scarcely. We have summarised the research that has been done with plant-PET and the possibilities that this technology provides to explore open questions persisting in plant research concerning phloem dynamics and the intimate xylem–phloem coupling.

In **Chapter 5**, the objective was to discover if ¹¹C could be used to determine phloem loading strategies in contrasting species (Fig. 1.13). ¹¹C-autoradiography is hardly ever used in the past because wet samples need to be used, which implies that positron range, the distance a positron can travel in aqueous media before interacting with matter to form gamma-rays, can influence autoradiographic measurements. We put contrasting species to the test, temperate and tropical tree species as well as herbaceous crop species, to investigate whether ¹¹C-autoradiography yields valid results and if this can be used as complementary tool with plant-PET scans to acquire a more comprehensive picture of phloem dynamics and how climate change might

influence different processes (such as loading in active or passive loading, or phloem transport dynamics, **Chapter 6**). Phloem transport dynamics were determined with a combination of plant-PET and compartmental modelling in **Chapter 6** (Fig. 1.13). We assessed how growth conditions of ambient (404 ppm) or elevated [CO₂] (659 ppm) impacted phloem velocity and exchange with surrounding tissue in native, well-watered state (leaf water potential -0.4 MPa) and after imposing a week of drought-stress (leaf water potential -1.8 MPa). We determined whether CO₂ fertilisation enhances the distribution of carbon, as well as whether elevated [CO₂] affects phloem vulnerability to drought, and if so, positively or negatively.

From **Chapter 1-6**, new insights were acquired, which enabled us to discuss how one-year-old *P. tremula* trees respond to climatic changes and how this impacts growth under unstressed conditions, and their vulnerability to drought in xylem and phloem (**Chapter 7**). Coupling between xylem and phloem complicate the response of trees to drought because drought-vulnerable xylem can cease phloem flow, but failing phloem transport can possibly also reduce the refilling capacity of xylem cavitated vessels. In the general discussion we propose how plant-PET can become more versatile in order to use it on a more routinely basis to further investigate phloem dynamics, phloem drought vulnerability and xylem–phloem coupling. Adaptational responses might not always prove to increase tree performance, but the Anthropocene will invoke unprecedented rates of changes, putting tree species which adapt and acclimate too slow at the brink of extinction. Ecophysiological tree and forest research will need to continue its efforts to further unravel how forests will change in the future.

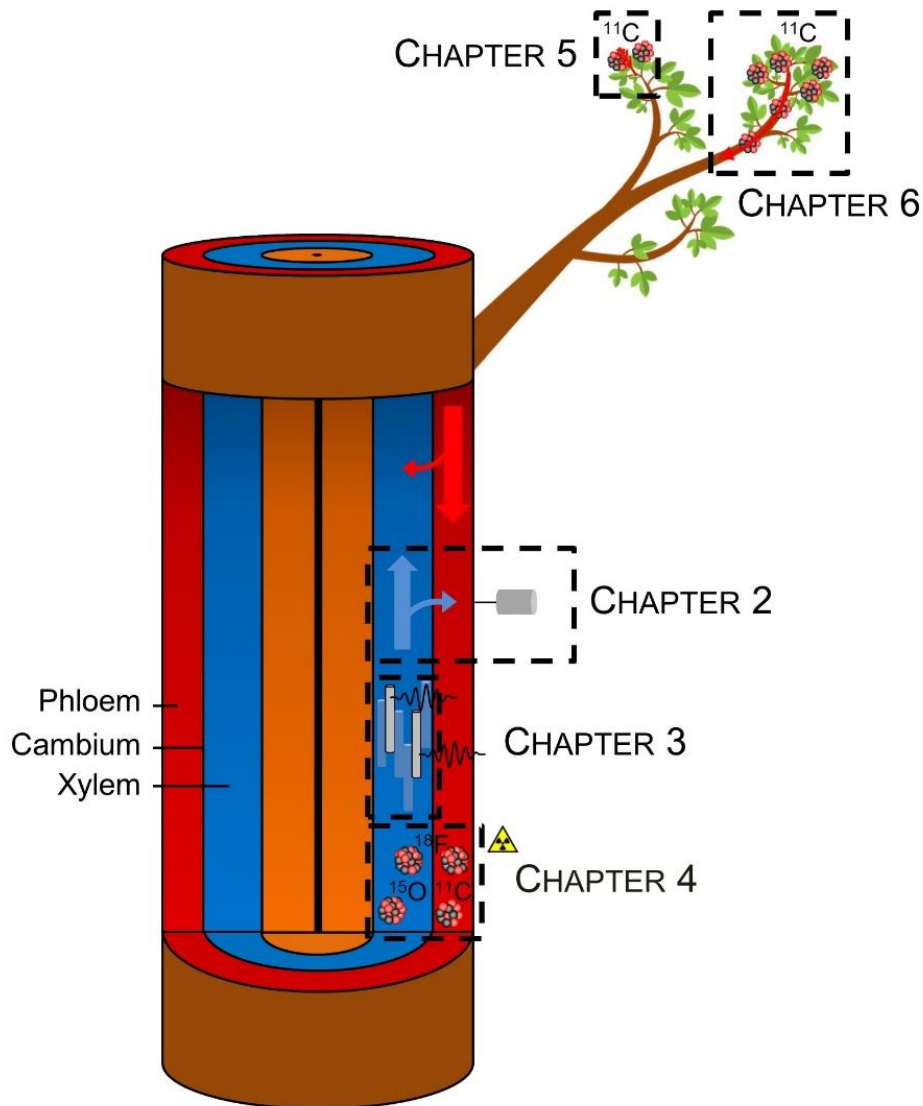


Figure 1.13 In this PhD, water and carbon relations in one-year-old *P. tremula* trees were investigated in the face of climatic changes. Chapter 2 focused on stem diameter variations and sap flow measurements to observe whether trees grown under ambient or climate change conditions grew best and which stem processes and mechanisms lay behind the growth responses. To know how well trees would cope with drought, xylem vulnerability to drought-induced cavitation and hydraulic capacitances during stem dehydration was studied. The emission of acoustic sound waves was used to determine the amount of cavitated vessels. Plant-PET (positron emission tomography) scanning was the focus of Chapter 4 and the use of short-lived positron emitting isotopes, ^{11}C , ^{15}O or ^{18}F in plant research was reviewed. In Chapter 5 and 6, the short-lived isotope of carbon, ^{11}C was used to measure phloem loading strategies in the leaf, and phloem transport velocity and exchange with surrounding tissue in the petioles, respectively.

2

CHAPTER 2

Growth responses of *Populus tremula*
trees to drought under changing climate
regimes: mitigation or amelioration?

Abstract

Despite the high interest in how the growth of trees will alter under climate change, little is known about how the internal mechanisms behind tree stem growth will be affected. We assessed the impact of a combination of elevated CO₂ concentration ([CO₂]) and air temperature on the responses of an important Eurasian tree species, *Populus tremula* L., and evaluated how drought additionally affected stem growth performance. To this end, one-year-old potted *P. tremula* trees were grown for four months in treatment chambers under ambient control (T_A, [CO₂] of 480 ppm and ambient air temperature) and predicted climate change (T_E, [CO₂] of 707 ppm and ambient +3°C) conditions. Half of the trees in both treatment chambers were well-watered (T_W, to a pF of 1.9 or a soil relative water content (RWC) of 42 %), and half were drought-stressed (T_D, to a pF of 3.1 or a soil RWC of 28 %). Stem diameter variations and sap flow rates were continuously measured with plant sensors. In general, T_E trees grew significantly better than T_A trees, but well-watered ones tended to grow significantly less than their drought-stressed counterparts, and showed smaller average daily shrinkages. We explained this observation by a difference in stem bulk elastic modulus between treatments. We reasoned that T_{EW} cells had a higher bulk elastic modulus, leading to less elastic cells, and reduced daily shrinkage, and that the associated decrease in cell extensibility resulted in smaller growth rates. Sap flow in T_A trees responded equally to changes in microclimate, whereas wet and dry trees in T_E showed opposite responses. Sap flow in T_{ED} trees increased less in response to drier atmospheric conditions compared to T_{AW} and T_{AD} trees. When atmospheric conditions were less demanding, sap flow per unit leaf area in T_{EW} trees was generally lower compared to the other treatments, but increased faster when atmospheric conditions became drier. These unanticipated results showed that whole-tree ecophysiological measurements in response to climate change are crucial if we aspire to predict how the forests of the future will grow and behave in a changing climate regime.

Introduction

Current research is intensively debating about how trees and forests will respond to the rapidly changing climate. Changes in climate are occurring at an unprecedented rate and it remains unknown whether trees and forests will be able to adapt sufficiently rapid to cope with the newly established environmental conditions (Franks et al. 2014, Valladares et al. 2014, Urban 2015). The most important expected climatic changes are substantial increases in atmospheric CO₂ concentration ([CO₂]), alterations in air temperature, changes in the frequency of extreme events (such as drought spells, fires or storms), and in precipitation patterns (IPCC 2014c, Allen et al. 2015). Predicting how these changes will influence individual trees and whole forests is a complicated and difficult task (Aitken et al. 2008, Leakey et al. 2009, Allen et al. 2015, Sperry and Love 2015, Domec et al. 2016). One daunting aspect is that there are many different factors exerting influence on tree responses, both positively and negatively, and in addition the factors influence one another. For instance, Silva and Anand (2013) compiled data on intrinsic water use efficiency and growth worldwide in response to increased [CO₂] over the past 50 years. They showed that despite a universally observed increase in water use efficiency, growth had been reduced in many areas, pointing to the presence of stressors.

Elevated atmospheric [CO₂] has been shown to have a positive effect on plant growth by reducing stomatal aperture for CO₂ uptake and lowering the associated transpirational water loss per amount of biomass, which is often called “CO₂ fertilisation” (Leakey et al. 2009, Allen et al. 2015). Elevated air temperature has a distinct effect depending on which climatic type is considered: in cold and wet regions, an increase in air temperature may prolong the growing season and reduce low-temperature associated damage (Allen et al. 2015); in other regions, an increase in air temperature may augment transpirational water demand and cause higher respiration rates (Allen et al. 2015). Furthermore, not only mean air temperature is expected to increase, but also the frequency of heat waves, typically leading to a decrease in biomass production (IPCC 2012, Bauweraerts et al. 2013, Teskey et al. 2015).

Drought stress affects plants because of the need to protect themselves against detrimental effects that water shortage can have on their functioning.

Almost all plant processes are negatively influenced when there is a shortage of water (Hsiao 1973, Porporato et al. 2001, McDowell et al. 2008, Sevanto 2014). A reduced water content lowers cell turgor, impeding cell division and growth and lowers water potential throughout the plant, putting more tension on the xylem water column, which can rupture when tension is too high and can ultimately result in complete hydraulic failure (Porporato et al. 2001, Sperry and Love 2015). Water shortage also leads to stomatal closure, reduced photosynthetic rates and lower phloem transport velocities, all negatively affecting the carbon metabolism thus increasing the chances for carbon starvation (Porporato et al. 2001, McDowell and Sevanto 2010, Pinheiro and Chaves 2011, Sevanto et al. 2011, Sala et al. 2012). Processes leading to carbon starvation are generally processes that preserve water for the tree, illustrating that in some conditions trees face the important trade-off between hydraulic failure escape or carbon starvation (McDowell et al. 2008). Drought duration and severity have an impact if trees face the threat of hydraulic failure or carbon starvation, but both will eventually result in tree death (McDowell et al. 2008, Sevanto et al. 2014). The combination of higher air temperatures and drought will probably lead to even worse effects and this phenomenon has recently been termed “hotter droughts” (Allen et al. 2015). When plants are subjected to hotter droughts, there is not only shortage of water inside the plant, but also an increased atmospheric water deficit causing an even larger water demand, not only from the plant, but also from the soil, further decreasing water availability (Allen et al. 2015, Teskey et al. 2015). Associated heat stress is also more severe when soil water availability to cool the leaves is reduced or even absent (Teskey et al. 2015).

The combination of continuous measurements of stem diameter variations and sap flow can be used to obtain information on both water and carbon relations, and their interactions (King et al. 2013, De Swaef et al. 2015, Steppe et al. 2015). Stem diameter variations are the result of (i) internal water depletion and replenishment and (ii) cell division and cell growth (Steppe et al. 2006, Drew and Downes 2009, De Swaef et al. 2015). Water depletion and replenishment is mainly determined by transpirational demand and soil water availability. Most important for growth are cell turgor and building stone (photoassimilates) availability (Lockhart 1965, Downes et al. 1999, Steppe et al. 2006, Deslauriers et al. 2007, De Schepper and Steppe 2010, Zweifel et al. 2010, De Swaef et al.

2015, Steppe et al. 2015). Sap flow measurements give an accurate assessment of the amount of water used by the tree and can, in many cases, be directly linked to microclimatic conditions and tree water status (Smith and Allen 1996, Ortuño et al. 2006, Kume et al. 2007, Oguntunde and Oguntuase 2007, Vandegehuchte and Steppe 2013). When sufficient soil water is available a tree will lose water shortly after dawn due to stomatal opening and accompanied leaf transpiration. With a small time lag, sap will start flowing to provide water to the transpiration stream. Therefore, sap flow is driven by leaf transpiration which, in turn, depends on the atmospheric water demand. Leaf transpiration can be roughly estimated from vapour pressure deficit (VPD) and canopy conductance. Atmospheric water demand is often expressed as potential evapotranspiration (ET_0), which represents the evapotranspiration of a hypothetical reference grass surface (Allen et al. 1998). Transpiration will cause internal water reserves to be depleted to a certain extent, which can be observed as shrinkage in stem diameter. After dusk, transpirational demand drops and trees will, when unstressed, replenish their water reserves with soil water and grow during the dark hours (Deslauriers et al. 2007, Drew and Downes 2009, Steppe et al. 2015). When soil water is not sufficiently available, sap flow rates will decrease and water reserves will no longer be fully replenished resulting in a reduction of nightly stem diameter growth.

The objective of this study was to assess individual and interactive effects of forecasted changes in microclimatic conditions (elevated air temperature and atmospheric $[CO_2]$) and soil water availability on young *Populus tremula* trees. We measured diel sap flow and stem diameter variations with high temporal resolution during one and three months, to assess the effects of climate change on individual tree physiology. We hypothesised higher sap flow rates and higher stem growth rates in trees with higher soil water availability. Trees grown under elevated $[CO_2]$ and temperature were hypothesised to perform best due to CO_2 fertilisation. We investigated whether higher $[CO_2]$ would reduce the amount of transpired water, possibly offset by higher air temperature, or whether trees maintain equal sap flow rates with a commensurate higher carbon uptake and productivity. Finally, we hypothesised that elevated $[CO_2]$ will mitigate drought, although the associated increase in air temperature could cause adverse effects linked to the hotter drought phenomenon.

Materials and methods

Plant material and growth conditions

Forty-eight one-year-old *Populus tremula* L. trees, with an average tree height of 76.0 ± 0.9 cm, were acquired from a nursery, grown from wild seeds from an unspecified European provenance (Sylva, Waarschoot, Belgium). All trees were planted on DOY 83 (23 March 2016) in 30 L cylindrical containers, filled with a commercial potting mixture (Greenyard Horticulture, Gent, Belgium) with specific weight of 680 kg m^{-3} and 15 % organic matter and slow-releasing (8 – 9 months) nutrient grains (Osmocote Exact 15-9-11-2 N-P-K-Mg, ICL Specialty Fertilizers, Geldermalsen, The Netherlands). The trees were equally distributed over four treatments in two treatment chambers. Treatment chambers were constructed in an open grass field at the experimental site of Ghent University (Proefhoeve, Melle, Belgium) (Fig. 2.1). Treatment chambers were half-cylindrical as in Wertin et al. (2010), based on a square of 4 m x 4 m. Trees in each treatment chamber were distributed over four subplots, with equal placing of trees in each treatment chamber. Each subplot consisted of six trees, with each treatment having two of these plots (Fig. 2.2). Both treatment chambers were identical in construction and were placed on the north-south axis relative to each other to minimise differences in shading and incoming radiation.

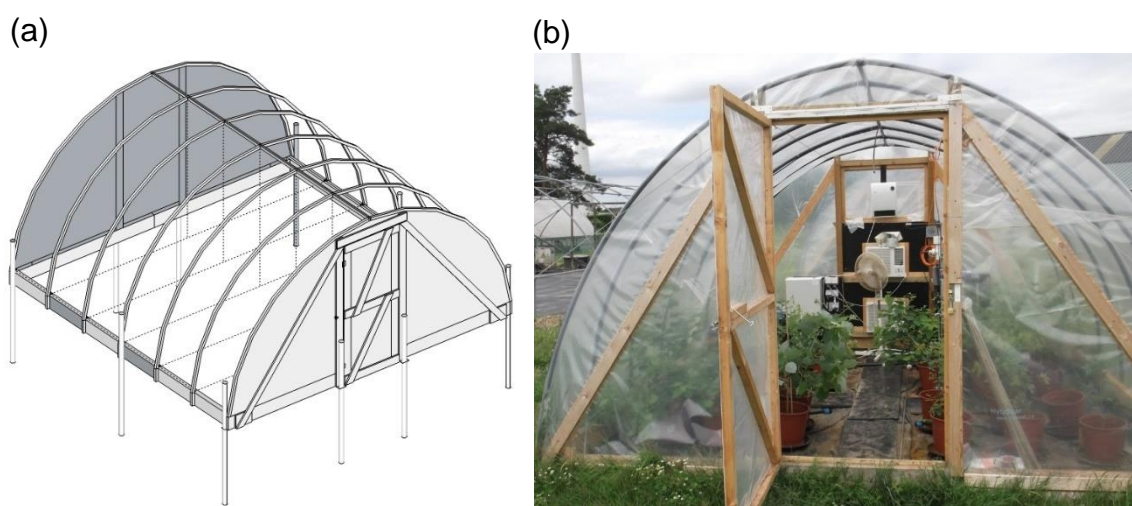


Figure 2.1 (a) Design and (b) picture of the treatment chambers. Two treatment chambers were built at the experimental site.

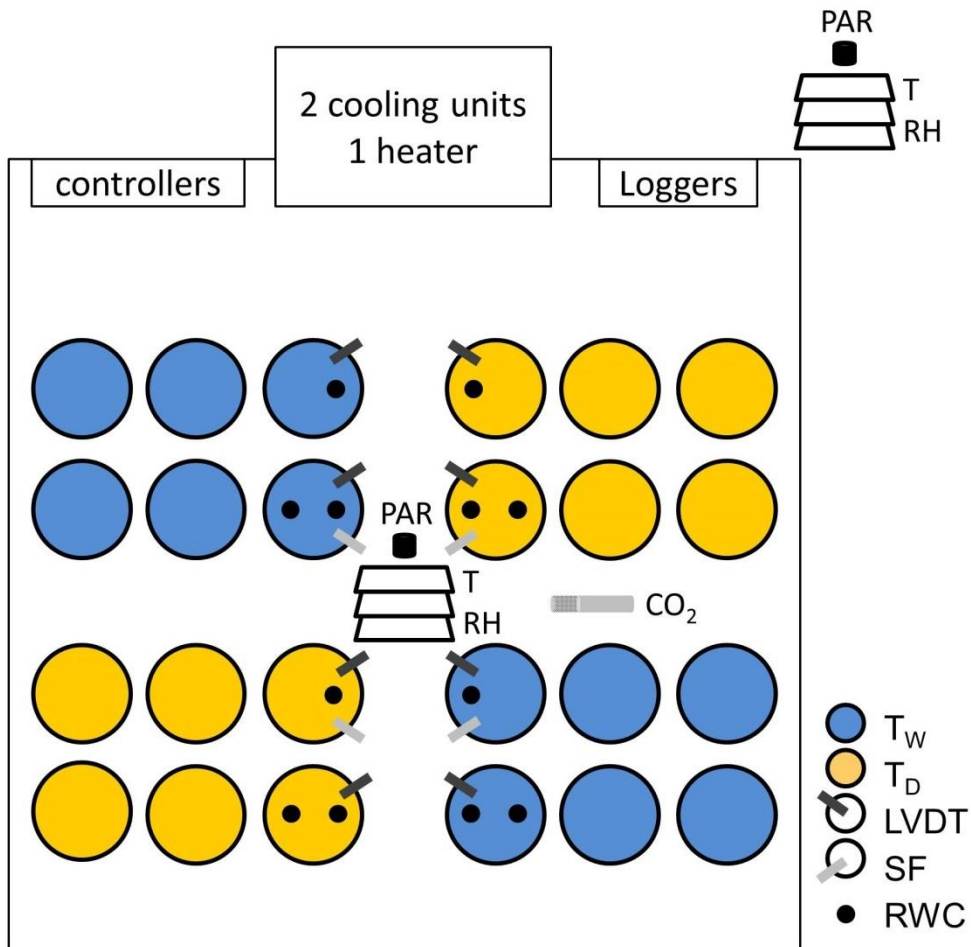


Figure 2.2 Lay-out of a treatment chamber. In each treatment chamber, trees were spaced per six in a subplot and each soil water treatment had two subplots. Per treatment, four trees were equipped with linear variable displacement transducers (LVDT) sensors and two with sap flow (SF) sensors. Soil relative water content (RWC) was measured in all the pots of the trees equipped with LVDTs with a total of six EC-5 soil sensors per treatment. Temperature, relative humidity (RH) and photosynthetic active radiation (PAR) was measured inside and outside the treatment chamber, whereas only inside atmospheric [CO₂] was measured. Output of sensors was sent to logger units for both data collection, microclimate control of atmospheric [CO₂] and air temperature with cooling units and a heater and irrigation control.

Data acquisition

Air temperature, relative humidity (RH), photosynthetic active radiation (PAR), atmospheric [CO₂], soil relative water content (RWC), stem diameter variation and sap flow (SF) rate were measured each minute and 5-minute averages were recorded with CR-1000 datalogger units (Campbell Scientific, Logan UT, USA) from DOY 119 (28 April 2016) to DOY 199 (17 July 2016). All measurements were automatically sent to the PhytoSense cloud service

(Phyto-IT, Mariakerke, Belgium), which has been developed for data collection and visualisation and enables a variety of calculations. Air Temperature was measured with 10k thermistors (Epcos, Munich, Germany), RH with hygrocip probes (Rotronic, Basserdorf, Switzerland), both inside a radiation shield, and PAR with JYP PAR sensors (SDEC, Rousset, France). Temperature, RH and PAR were measured inside each treatment chamber and also outside (Fig. 2.2). [CO₂] was measured in each treatment chamber with a GMT222 unit with sensor probe and controller (Vaisala, Helsinki, Finland).

Microclimatic treatments

Four treatments were produced by a combination of two atmospheric [CO₂] and air temperature treatments and two soil water treatments. Treatment chamber [CO₂] and temperature treatments were (i) ambient air temperature with an atmospheric [CO₂] of 400 ppm (T_A), and (ii) air temperature increase of +3°C compared to ambient and [CO₂] 700 ppm (T_E). In each treatment chamber, two commercial cooling units (Midea, Foshan City, Guangdong, China) and one heater unit (AEG, Nuernberg, Germany) were installed. These were connected to controlling loops programmed on CR-1000 datalogger units (Campbell Scientific, Logan UT, USA). Air temperature in T_A was set to ambient outside air temperature and temperature in T_E equalled air temperature in T_A +3°C. To optimise temperature control, measurements of PAR were used to fine-tune cooling protocol. In case of high PAR, anticipatory cooling ensured that temperature differences were not too high. Indoor [CO₂] was controlled by using the GMT222 sensor probe and a control algorithm in which the lower set point was used to activate an electronic relay and the higher set point to deactivate the relay. When the relay was activated, a solenoid valve (STNA1016 24 Vac, Air Liquide, Liege, Belgium) was opened, which supplied pure CO₂ at the top of the treatment chamber close to a small fan that ensured sufficient air mixing inside the treatment chamber.

Within each treatment chamber soil water treatments were (i) well-watered (T_W), and (ii) drought-stressed (T_D) (Fig. 2.2). Soil RWC was measured with six EC-5 sensors (Decagon, Pullman, WA) per treatment, installed in the potting mixture of trees equipped with linear variable displacement transducers (LVDT). Treatments in soil water were chosen so that T_W trees were well-watered (no

drought-stress) and tree survival was ensured in T_D , because *P. tremula* is known to be drought-sensitive (Johnson et al. 2002, Bogeat-Triboulot et al. 2007, Fichot et al. 2009). Based on previous research, well-watered plants (T_W) were irrigated to field capacity (i.e., soil RWC of 42 %), and drought-stressed plants (T_D) received 65 % of field capacity (i.e., soil RWC of 28 %) (Awad et al. 2010). This corresponded to a pF (i.e., the logarithm of soil water potential, expressed as a positive value) of 1.9 (= -8 kPa) and 3.1 (= -125 kPa), respectively. When soil RWC dropped below these set-points, an electronic valve was switched on and irrigation was provided to the trees by means of ring drip irrigation. To assess the impact of soil water potential on plant water potential, the soil-root resistance should be taken into account (Porporato et al. 2001).

Microclimatic calculations

Daily averages were used to depict prevailing microclimate inside the treatment chambers, whereas daytime averages were used to relate microclimatic variables to tree measurements, as daytime microclimate exerts the strongest impact on tree physiology and behaviour. Daytime averages were calculated for PAR higher than $5 \mu\text{mol m}^{-2} \text{s}^{-1}$. Diel patterns were calculated from hourly averages. As drivers, VPD, expressed in kPa, was calculated, because of its importance in quantifying the atmospheric water demand (Eq. 2.1 to 2.5 in Text box 2.1) (Buck 1981, Allen et al. 1998). Potential evapotranspiration (ET_0) was calculated, using the FAO-56 Penman-Monteith equations of Allen et al. (1998) (Eq. 2.6 to 2.8 in Text box 2.1). ET_0 , expressed in L d^{-1} , was related to the area each tree covered (0.55 m^2). Next to calculations on the individual tree level, ET_0 was calculated per unit leaf area (LA in m^2). This enabled upscaling to a per leaf area level, which made comparison between treatments possible. LA per tree was estimated to be 0.37 m^2 and 1.11 m^2 for T_A and T_E trees, respectively. These values were estimated in a follow-up experiment executed in 2017 in the same treatment chambers. Estimation was done by weighing all leaf material of three trees and defining the relationship between leaf area and leaf weight for nine leaves per treatment chamber. A crop coefficient (K_C) was calculated by dividing measured transpiration (= SF) with potential evapotranspiration (ET_0) ($K_C = \text{SF}/ET_0$) (Allen et al. 1998). Also for this parameter, a calculation was made on a per tree and per unit leaf area level. Finally, canopy conductance (g_s , in mmol

$\text{m}^{-2} \text{s}^{-1}$) was estimated from total transpiration per unit leaf area (i.e., SF, in $\text{mmol m}^{-2} \text{s}^{-1}$) and VPD_{mol} (expressed in mol mol^{-1} by dividing VPD by atmospheric pressure, 101.325 kPa) with the relation $g_s = \text{SF}/\text{VPD}_{\text{mol}}$ (Ewers and Oren 2000, Pearcy et al. 2000). This calculation assumes equal leaf and air temperature, and although we did not measure leaf temperature, this is a useful approximation to roughly assess differences in canopy conductance between treatments. Average g_s was calculated for VPD during daytime.

Tree measurements

Stem diameter variations were measured with LVDTs (Solartron, type DF-5.0, Leicester, UK) (Fig 2.3b). Per treatment, four trees were equipped with LVDTs, about 10 cm above root collar, on DOY 119. On two trees per treatment, sap flow (SF) was additionally measured. SF measurements began at DOY 163 (11 June 2016), when trees had sufficiently large stem diameters for sensor installation. Sap flow sensors were Dynagage stem heat balances (SHB, SGA10, Dynamax, Fresno, CA, USA) suited for stem diameters between 9 and 13 mm. SHBs were installed on a stem segment about 5 cm above the LVDTs, after application of Dow Corning 64 grease (Dow Corning, Midland, MI, USA) (Fig. 2.3a), which improves thermal contact and prevents fungal growth. Stem thermal conductivity was set to $0.42 \text{ W m}^{-1} \text{ K}^{-1}$, sensor-dependent heater resistance ranged from 139.8 to 149.4 Ω , thermocouple spacing was 4 mm and K_{sh} , the effective thermal conductance of the sheath of materials surrounding the heater, was automatically calculated in PhytoSense, as described in the manual between 2 and 3 h (Van Bavel and Van Bavel 2005). A low flow ΔT (temperature increase in sap) threshold and low flow P_{in} (heating power) percentage was applied to all sensors to filter out low flow conditions, which can give rise to noisy and faulty high measurements (Grime and Sinclair 1999, Van Bavel and Van Bavel 2005). Due to malfunctioning of one of the T_{AD} SHB sensors, measurements of one tree were used.

Text box 2.1 Microclimatic calculations.

1. Vapour pressure deficit

Dewpoint temperature (T_{dew}) is calculated using measured relative humidity (H_R , a number between 0 and 1), air temperature (T_a in °C), and a set of constants (Eq. 2.1-2.2) (Allen et al. 1998). With T_a and T_{dew} the saturated vapor pressure (e_s in kPa) (Eq. 2.3) and actual vapor pressure (e_a in kPa) (Eq. 2.4) can be calculated, respectively, which need to be subtracted to yield vapour pressure deficit (Δe in kPa) (Eq. 2.5) (Allen et al. 1998).

$$\alpha = \ln \left(H_R \exp \left[\left(18.678 - \frac{T_a}{234.5} \right) \left(\frac{T_a}{T_a + 257.14} \right) \right] \right) \quad (2.1)$$

$$T_{dew} = \frac{257.14\alpha}{18.678 - \alpha} \quad (2.2)$$

$$e_a = 0.6108 \exp \left(\frac{17.27T_{dew}}{T_{dew} + 237.3} \right) \quad (2.3)$$

$$e_s = 0.6108 \exp \left(\frac{17.27T_a}{T_a + 237.3} \right) \quad (2.4)$$

$$\Delta e = e_s - e_a \quad (2.5)$$

2. Potential evapotranspiration

Potential evapotranspiration (E_p , L m⁻² d⁻¹) is calculated from input incoming radiation, air temperature, relative humidity and wind speed. Because measurements were made inside a treatment chamber, not exposed to outside wind, wind speed was assumed to be low and constant, originating from the small fan, with a value of 0.5 m s⁻¹, which represents the breeze generated by the cooling units and small fan. Measured PAR values (R_{PAR} , μmol m⁻² s⁻¹) were converted to net radiation (R_n , W m⁻²) (Eq. 2.6) (Allen et al. 1998). With calculation of the slope of the vapour pressure curve (δ in kPa °C⁻¹) (Eq. 2.7), and some conversions to match units (see Allen et al. (1998)), E_p (L m⁻² d⁻¹) can be calculated (Eq. 2.8), with γ the psychrometric constant (kPa °C⁻¹) and u wind speed (0.5 m s⁻¹) (Allen et al. 1998).

$$R_n = 0.57 \cdot \frac{2 \cdot R_{PAR}}{4.62} \quad (2.6)$$

$$\delta = \frac{4098 \cdot e_s}{(T_a + 237.3)^2} \quad (2.7)$$

$$E_p = \frac{0.408\delta \cdot R_n + \gamma \frac{900}{T_a + 273} u \cdot \Delta e}{\delta + \gamma(1 + 0.34u)} \quad (2.8)$$

Stem diameter variations were used to calculate diel characteristic values of stem growth and maximum daily shrinkage. Diel stem growth was calculated as stem diameter increment between the maximum in the morning of a day and the maximum in the morning of the next day. Typically, maximum values were found around 6 h. Maximum daily shrinkage was calculated as the difference between maximum diameter in the morning of a day and minimum diameter during that day, typically observed around 15 h. Average diel patterns in stem diameter were calculated by averaging all hourly growth rates for each hour of the day. Cumulating these values resulted in a typical average diel pattern in stem diameter variation. For these cumulative values, no standard errors are given, because they depend on the error of previous values with which they are cumulated. This means that error propagation would be dependent on which hour the diel pattern is started, and so this does not represent a useful error estimation. For the average diel pattern in sap flow rates, hourly averages were calculated analogous to the diel hourly growth rates. As a measure for water use efficiency, the amount of wood volume that was formed in the period for which sap flow data was available (DOY 163-199), calculated as the volumetric increment of a coaxial cylinder (with measured stem diameter at DOY 163 and at DOY 199) of equal height, was divided by the total amount of water that was used during this period. Furthermore, aboveground leafless dry biomass was determined with a precision balance (PS4500/C/1, Radwag, Radorn, Poland), with an accuracy of 10 mg. Biomass was measured on eight individuals for T_{AW} , T_{AD} and T_{EW} and on six for T_{ED} .

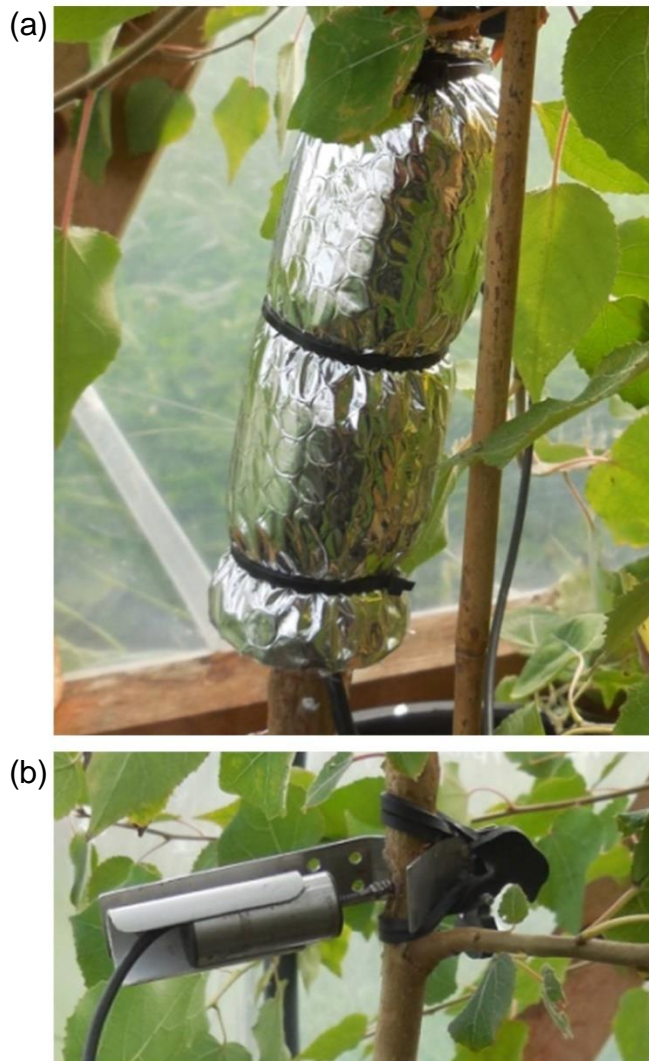


Figure 2.3 Pictures of installed (a) stem heat balance sap flow (SF) sensor packed in reflective foam for insulation, and (b) linear variable displacement transducer (LVDT).

Data analysis

Data were pooled per treatment (T_{AW} , T_{AD} , T_{EW} , T_{ED}) and shown as average values and standard errors. Unless specified otherwise, these values are based on 81 measurement days for the microclimate and stem diameter variation and 37 days for sap flow measurements. Differences are significant if P-values are smaller than 0.05 and tend to be significant if smaller than 0.1, which we included because the number of replicates per treatment is relatively low, and thus statistical power will be as well. All statistical calculations were performed in R (Rstudio v1.1.383, Boston, MA, USA) and graphs were produced with the ggplot2 package of R (Wickham 2016). Statistical effects of treatment were determined with linear mixed-effect models of the nlme package (Pinheiro et al. 2014), with treatment chamber and soil water treatment as two crossed factors

and tree number and day of measurement as random factors. Normality was checked with qqnorm plots, and no strong violation of normality was observed and linear mixed models are fairly robust towards normality assumptions. After checking plots of residuals to check for equality of variances, a constant variance function was applied in case of unequal variances. Post-hoc multiple comparison between all four treatments was performed with a Tukey test in the multcomp package (Hothorn et al. 2008). Coefficient of determination was calculated as R^2 values for mixed models with the piecewiseSEM package (Lefcheck 2016). Effects of microclimatic variables on diel stem growth, maximum daily shrinkage and daily sap flow rates were calculated per treatment using the daytime averages of temperature, RH, VPD and PAR with linear mixed-effect models and tree number as random effect. Again, a constant variance function was used where necessary.

Results

Microclimatic conditions

Figure 2.4 shows daily averages (Fig. 2.4a-f) and average diel patterns (Fig. 2.4g-l). Daytime $[CO_2]$ was 480.4 ± 4.0 ppm in T_A and 707.0 ± 1.7 ppm in T_E (Fig. 2.4a). In T_A , $[CO_2]$ was higher than the set 400 ppm, due to the influence of the trees on $[CO_2]$. The treatment chambers were relatively airtight, causing $[CO_2]$ to rise during night, dawn and dusk because of respiration by both trees and soil (Fig. 2.4g). Nighttime averages were 615.8 ± 11.6 ppm and 753.3 ± 8.4 ppm for T_A and T_E , respectively. During daytime, $[CO_2]$ decreased as trees used carbon for photosynthesis. Measurements of $[CO_2]$ in this experiment were taken directly above the tree canopy and in enclosed treatment chambers, and are therefore affected by the carbon uptake and release from the trees. In natural ecosystems, Brooks et al. (1997) measured $[CO_2]$ differences of around 200 ppm measurements between ground level and 9 m high in the canopy during the night, and 70 ppm during the day and Feigenwinter et al. (2008) measured a difference of 50 ppm between ground level and 6 m high in the canopy during the evening. In our experiment, the larger fluctuations in the T_A treatment chamber were probably caused by the small gradient between indoor and outdoor $[CO_2]$, resulting in a low CO_2 leakage compared to the T_E treatment chamber. Moreover,

CO₂ was only added, never scrubbed in this experiment. Average air temperature in T_A was $17.4 \pm 0.3^\circ\text{C}$, and in T_E $20.3 \pm 0.3^\circ\text{C}$ (Fig. 2.4b, h). Average daytime air temperature was $19.4 \pm 0.4^\circ\text{C}$ and $22.2 \pm 0.3^\circ\text{C}$ in T_A and T_E, respectively, which is a temperature difference of $2.9 \pm 0.1^\circ\text{C}$ during the whole day and $2.8 \pm 0.1^\circ\text{C}$ during daytime. VPD was on average 0.65 ± 0.03 kPa and 0.76 ± 0.03 kPa during the whole day and 0.88 ± 0.04 kPa and 0.94 ± 0.04 kPa during daytime for T_A and T_E, respectively (Fig. 2.4d, j). Daytime averages for PAR were 531 ± 22 $\mu\text{mol m}^{-2} \text{s}^{-1}$ and 516 ± 21 $\mu\text{mol m}^{-2} \text{s}^{-1}$ for T_A and T_E (Fig. 2.4e, k), respectively. Soil RWC was 42.0 ± 0.2 % and 42.2 ± 0.1 % (N = 456 = 6 sensors for 76 days) for T_{WA} and T_{WE}, and 27.5 ± 0.2 % and 27.6 ± 0.2 % (N = 456) for T_{DA} and T_{DE}, respectively (Fig. 2.4f, l). Corresponding soil water potentials of -8.7 ± 0.3 kPa and -8.4 ± 0.1 kPa for T_{WA} and T_{WE}, and -138 ± 6 kPa and -134 ± 5 kPa for T_{DA} and T_{DE}, respectively, were calculated using a soil specific pF-curve. This corresponds to a pF of 1.9 for T_W and 3.1 for T_D. Soil-root resistance has an important effect on how soil water potential is related to tree water potential and water status (Porporato et al. 2001, Zweifel et al. 2005, Jones 2007). Zweifel et al. (2005) modelled tree water deficit in *Quercus pubescens*, *Pinus sylvestris* and *Picea abies* and from these data we could deduce that our T_D trees experienced some degree of water deficit.

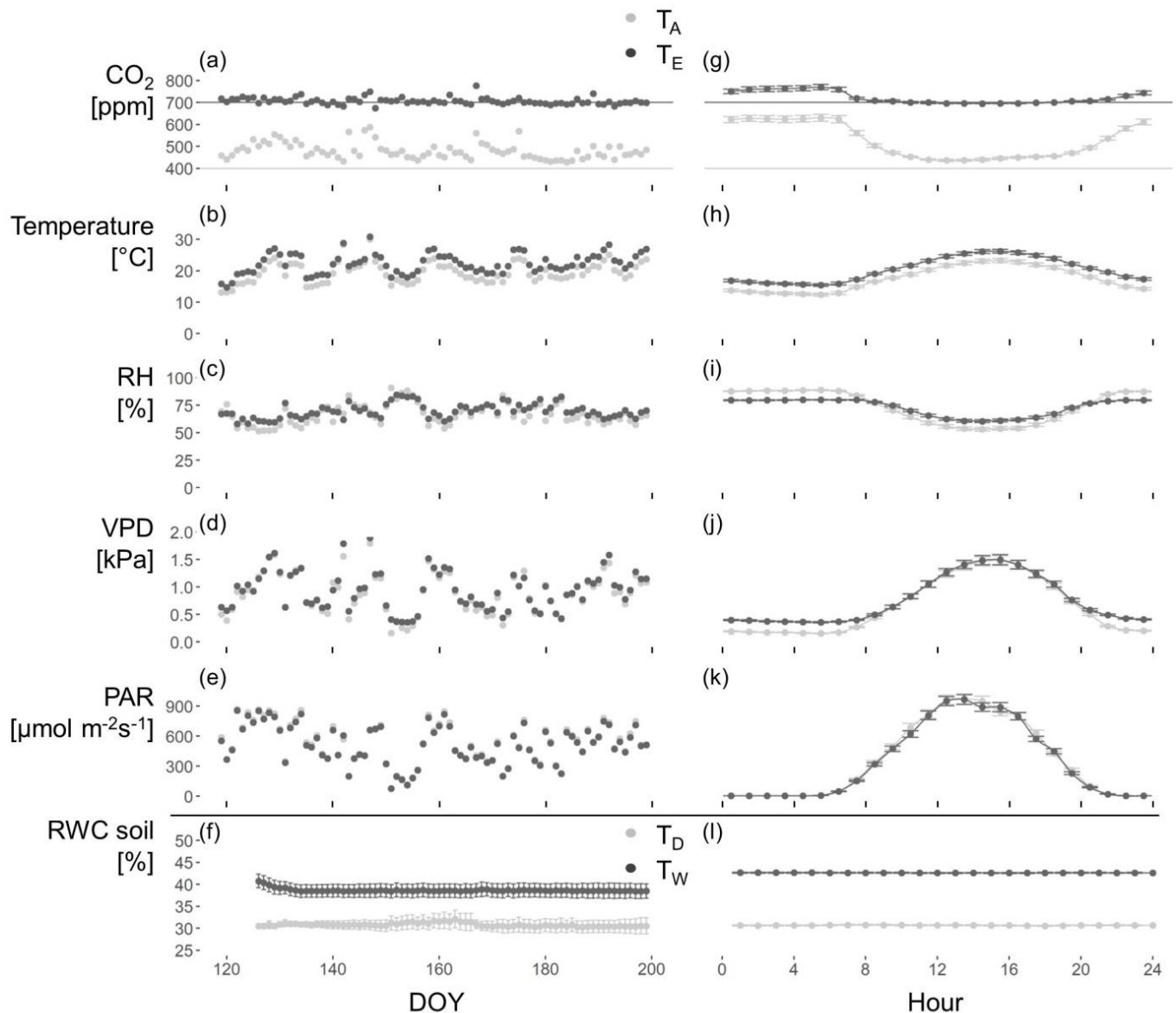


Figure 2.4 Overview of microclimatic variables in the treatment chambers with (a-f) daytime ($\text{PAR} > 5 \mu\text{mol m}^{-2} \text{s}^{-1}$) averages, and (g-l) average diel patterns: (a, g) atmospheric CO_2 concentration ($[\text{CO}_2]$), (b, h) air temperature, (c, i) relative humidity (RH), (d, j) vapour pressure deficit (VPD), (e, k) photosynthetic active radiation (PAR) with values in the ambient treatment (T_A , ambient air temperature and atmospheric $[\text{CO}_2]$ of 480 ppm) depicted in grey, and values in the elevated treatment (T_E , ambient air temperature $+3^\circ\text{C}$ and atmospheric concentration ($[\text{CO}_2]$) of 707 ppm) in black. (f, l). Relative water content (RWC) of the soil is measured per treatment regime with well-watered trees (T_W) in black, and soil-drought trees (T_D) in grey. Error bars in (f-l) are standard errors.

Tree measurements

Trees in T_{ED} showed a markedly stronger stem growth than in the other treatments (Fig. 2.5a-e). Initial stem diameters, measured at DOY 119, did not differ significantly, while final diameters, at DOY 199, in T_{ED} significantly differed from T_{AW} ($P < 0.01$) and T_{AD} ($P < 0.05$), and tended to be significantly different from T_{EW} ($P < 0.1$). Aboveground leafless dry biomass was significantly higher in T_{ED} than in the other treatments ($P < 0.01$) (Fig. 2.5f). At the start of the measurements (DOY 119-129) stem diameter growth was low and maximum daily shrinkage high in all treatments (Figs 2.5 and 2.6). In some periods, stem growth per day and maximum daily shrinkage showed marked differences between treatments (Fig. 2.6a, b), without microclimatic conditions being different from the surrounding periods (Fig 2.4a-f). Daytime averages of microclimatic variables exerted significant effects on both stem growth per day and maximum daily shrinkage, but in general low R^2 values were associated with these significant effects and no clear patterns were observed (Supplemental Table 2.1). Amongst treatments, stem growth per day tended to be significantly affected by soil water treatment ($P < 0.1$), and significantly by treatment chamber ($P < 0.01$) and by the interaction between both ($P < 0.001$). Stem growth per day in T_{ED} was significantly higher than in all the other treatments ($P < 0.001$) and higher growth was found in T_{EW} compared to T_{AW} ($P < 0.05$). Maximum daily shrinkage differed between all treatments ($T_{AW} - T_{EW}$ $P < 0.05$, $T_{AW} - T_{ED}$ $P < 0.01$ and all other combinations $P < 0.001$). Average maximum daily shrinkage decreased as follows, $T_{AD} > T_{AW} > T_{ED} > T_{EW}$. There was a strong significant negative correlation between stem growth per day and maximum daily shrinkage ($P < 0.001$), with the slope not significantly influenced by treatments. However, the relationship between stem growth per day and maximum daily shrinkage showed a large spread, as pointed out by a low R^2 of 0.42.

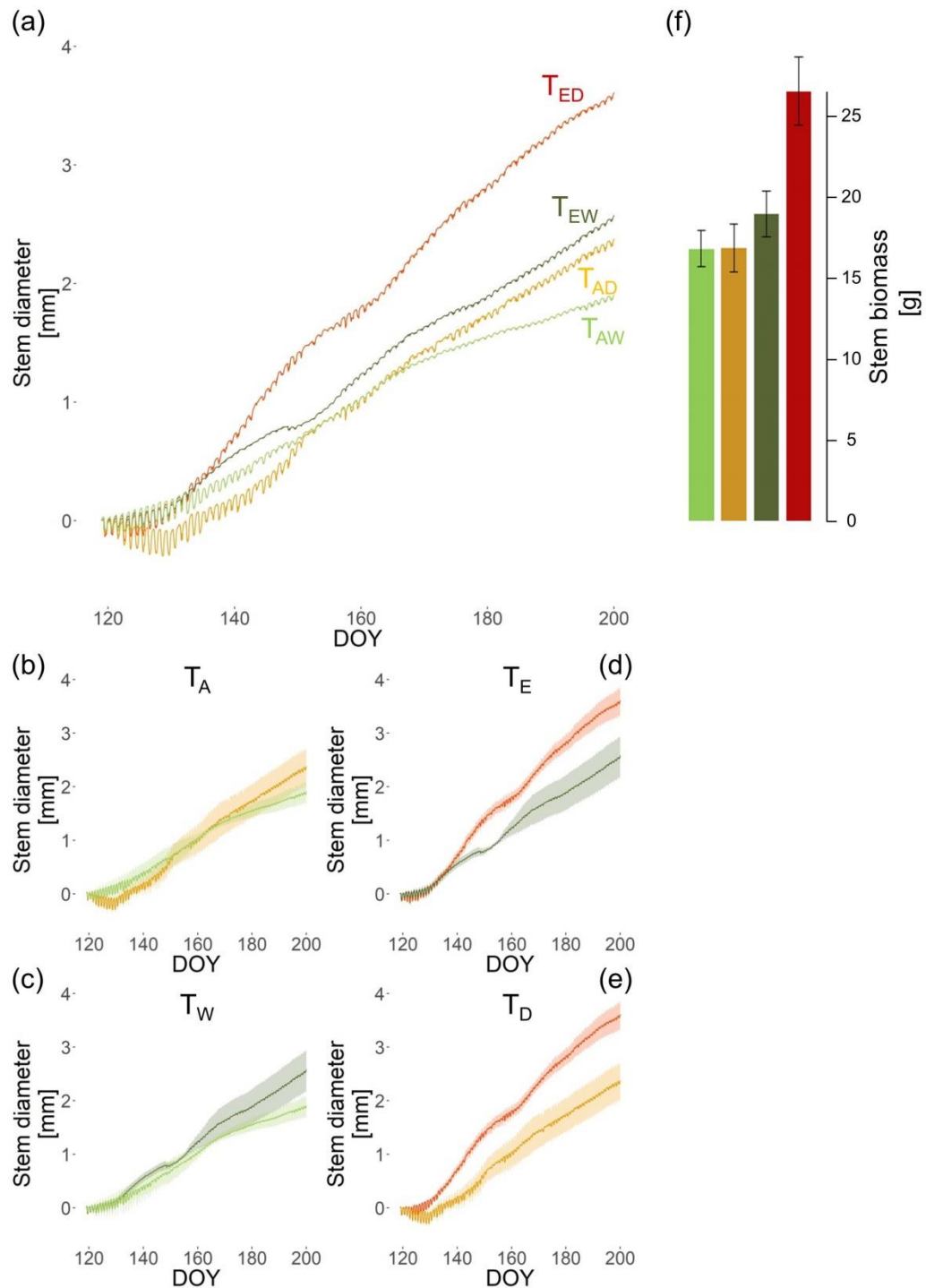


Figure 2.5 Average stem diameter variations for all treatments: (a) overview of stem diameter variations of all treatments, and (b-e) a comparison between different treatment combinations with error areas calculated as standard errors. (f) Average total aboveground leafless dry biomass per treatment at the end of the experiment, with error bars calculated as standard errors. Comparisons are between (b) $T_{AW} - T_{AD}$, (c) $T_{AW} - T_{EW}$, (d) $T_{EW} - T_{ED}$, (e) $T_{AD} - T_{ED}$. T_{AW} and T_{AD} are trees grown in a treatment chamber under ambient temperature and atmospheric $[CO_2]$ (480 ppm), well-watered and drought-stressed, respectively. T_{EW} and T_{ED} are trees grown in a treatment chamber under elevated temperature (+3°C) and atmospheric $[CO_2]$ (707 ppm), well-watered and drought-stressed, respectively.

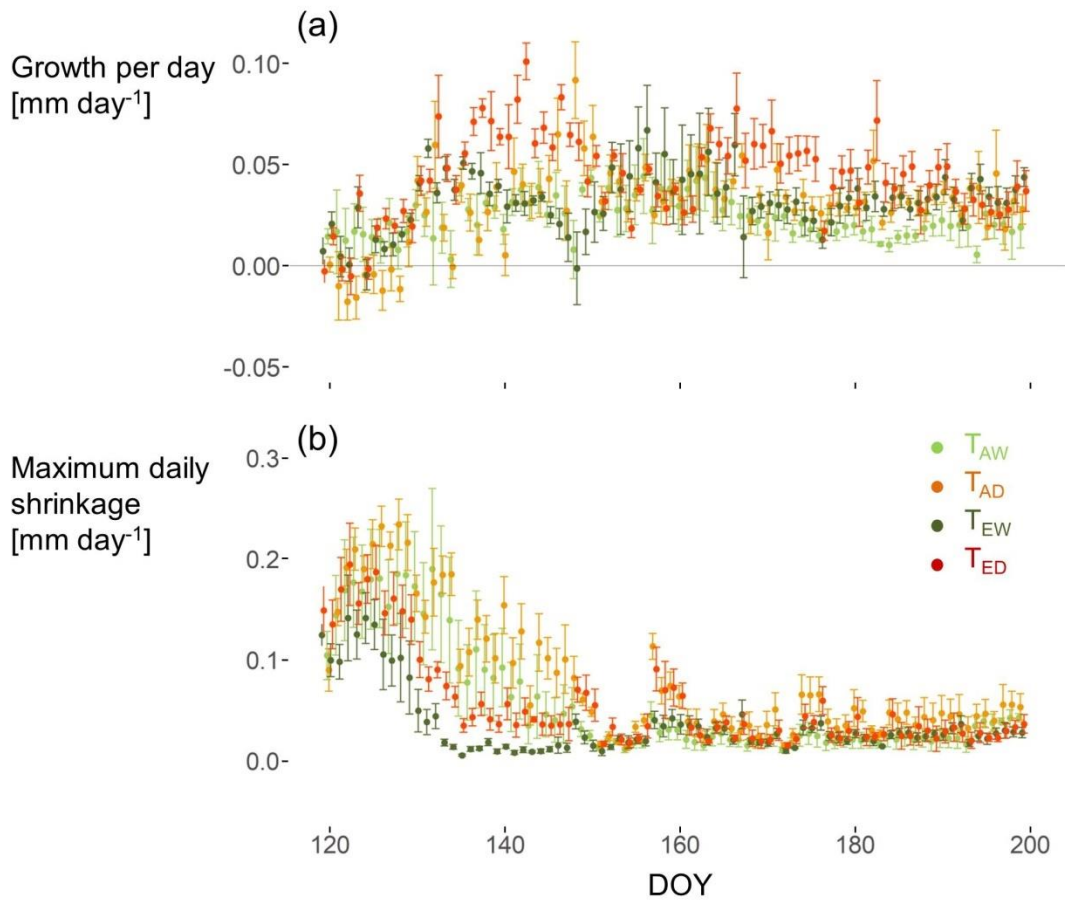


Figure 2.6. (a) Stem growth per day (GPD) and (b) maximum daily shrinkage (MDS). Error bars are standard errors. T_{AW} and T_{AD} are trees grown in a treatment chamber under ambient temperature and atmospheric [CO₂] (480 ppm), well-watered and drought-stressed, respectively. T_{EW} and T_{ED} are trees grown in a treatment chamber under elevated temperature (+3°C) and atmospheric [CO₂] (707 ppm), well-watered and drought-stressed, respectively.

Hourly stem growth rates were calculated to assess how growth processes in differently treated trees alter (Fig. 2.7). T_{EW} showed the least dynamics with smallest shrinkages during the daytime and smallest expansions in the evening and nighttime (Fig. 2.7). T_{AW} had comparable, but slightly higher, hourly stem growth rates when positive (i.e., net growth, Fig. 2.7b), but showed larger negative rates during daytime, eventually leading to a lower stem growth rate per day (and the lowest of all treatments) (Fig. 2.7a). The lower endpoint in T_{AW} trees (Fig. 2.7) corresponds with lower growth rates from DOY 170 onwards (Fig. 2.6a). T_{AD} showed the largest negative hourly growth rates during daytime (Fig. 2.7b), resulting in the largest depression in average diel stem diameter pattern (Fig. 2.7a). But, positive growth rates during evening and night in T_{AD}

were substantially higher than in T_{AW} and T_{EW} , offsetting the larger shrinking and resulting in growth rates comparable with T_{EW} . Finally, T_{ED} had hourly shrinkage rates most comparable with T_{AW} and hourly growth rates most comparable with T_{AD} (Fig. 2.7b), resulting in an average diel growth curve which during the day is in between the other treatments but with a markedly higher endpoint at the end of the growth phase (Fig. 2.7a).

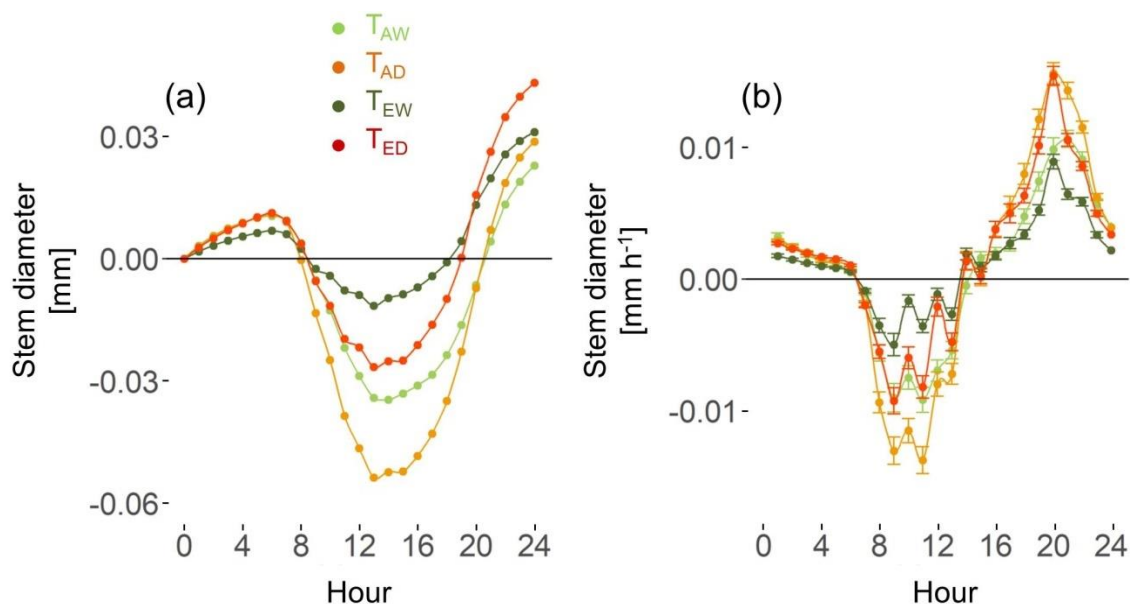


Figure 2.7 (a) Average diel pattern of stem diameter variations in each treatment and (b) hourly stem growth rates with error bars calculated as standard error for each hour. T_{AW} and T_{AD} are trees grown in a treatment chamber under ambient temperature and atmospheric $[CO_2]$ (480 ppm), well-watered and drought-stressed, respectively. T_{EW} and T_{ED} are trees grown in a treatment chamber under elevated temperature ($+3^\circ C$) and atmospheric $[CO_2]$ (707 ppm), well-watered and drought-stressed, respectively.

T_E showed significantly higher daily sap flow rates than T_A ($P < 0.001$) (Fig. 2.8b). On average, sap flow rates were 2.5 times higher in T_E compared to T_A ($364 \pm 16 \text{ g day}^{-1}$, $N = 148$ for T_E , and $144.9 \pm 6.1 \text{ g day}^{-1}$, $N = 111$ for T_A) (Fig. 2.8b). In general, daily sap flow was more correlated with maximum daily shrinkage (positive correlation) than with stem growth per day (negative correlation). Stem growth per day in T_{AD} was stronger related to sap flow than in T_{AW} , while no difference existed between T_{EW} and T_{ED} . Diel sap flow patterns also showed that treatment chamber was the main factor driving sap flow rates (Fig. 2.9). A large determinant of sap flow rates is the transpiring area of trees. Leaf area (LA) estimates were comparable between T_W and T_D treatments but

largely differed between T_A and T_E (LA in T_A was 2.96 times smaller than T_E). Figure 2.9b shows that, on average, sap flow per unit LA in T_E was lower compared to T_A . In general, T_{AD} had the highest midday sap flow per unit LA, followed by T_{AW} , T_{EW} , and T_{ED} . On average, sap flow per unit LA was reduced to 86 % in T_{EW} compared to T_{AW} and to 81 % in T_{ED} compared to T_{AD} .

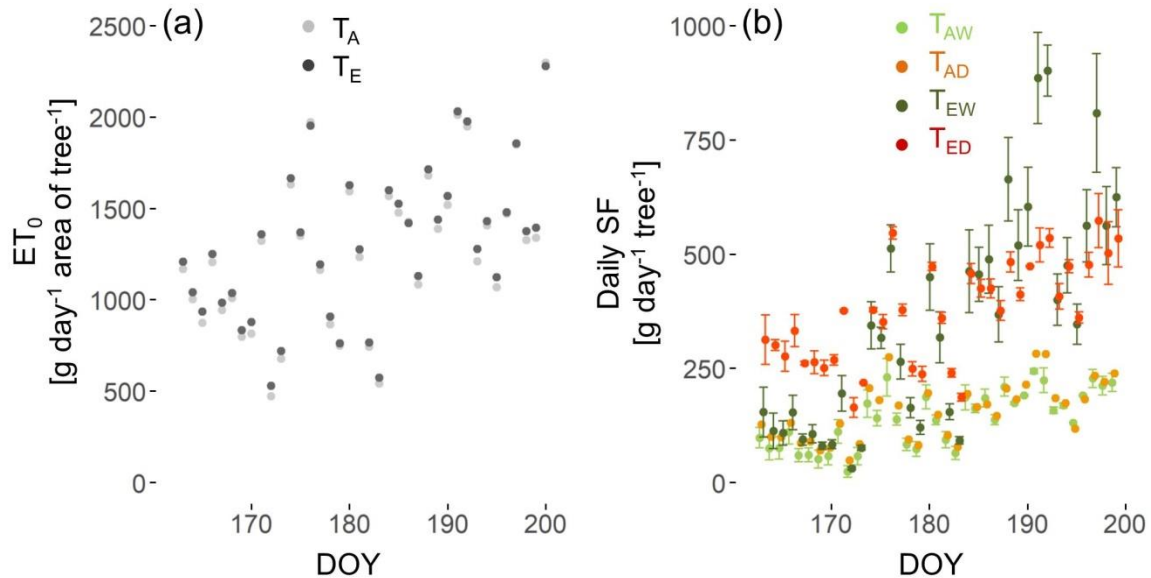


Figure 2.8 (a) Potential evapotranspiration (ET_0) expressed per area each tree covered (which was about $0.55\ m^2$). ET_0 in T_A is shown in grey and in T_E in black. (b) Averages of daily sap flow, with error bars calculated as standard error. For T_{AD} no error bars are shown because this is data from one SHB sensor. T_{AW} and T_{AD} are trees grown in a treatment chamber under ambient temperature and atmospheric $[CO_2]$ (480 ppm), well-watered and drought-stressed, respectively. T_{EW} and T_{ED} are trees grown in a treatment chamber under elevated temperature ($+3^\circ C$) and atmospheric $[CO_2]$ (707 ppm), well-watered and drought-stressed, respectively.

To assess whether differences in tree responses to prevailing microclimate existed between treatments, different approaches and approximations were applied. Potential evapotranspiration (ET_0) was calculated to assess how actual tree water use relates to potential water use (Fig. 2.8a). ET_0 in T_E was on average 3 % higher than in T_A . The temperature effect accounted for a 7 % increase, while higher RH and reduced PAR lowered the effective ET_0 . Sap flow clearly correlated with ET_0 , indicated by high R^2 values (Fig. 2.10). The relationship between sap flow and ET_0 was nearly equal for both T_A treatments, while there were large differences between T_{EW} and T_{ED} . They also showed differences compared to T_A . The intercept of T_{EW} was lower, which indicated that at low ET_0 , sap flow was low, while the higher slope indicated that sap flow rose

faster in response to increasing ET_0 (Table 2.1). T_{ED} had a different behaviour and responded less to rising ET_0 , as shown by the lower slope (Table 2.1). K_c was calculated, expressing the average relation between SF and ET_0 (Table 2.1). In general, K_c on a unit LA basis was larger in T_A than in T_E and within treatment chambers higher in T_D than in T_W . Daily sap flow rates were also closely related to VPD (Fig. 2.11). Differences between treatments are similar to the SF responses to ET_0 . Average canopy conductance was approximated by expressing the relationship between SF and VPD, and assuming equal leaf and air temperature, and was lower in T_E compared to T_A , with a reduction of 24 % in T_{EW} relative to T_{AW} , and 21 % in T_{ED} relative to T_{AD} . The amount of wood formation efficiency in terms of water use was nearly equal for T_{AW} and T_{ED} , but substantially higher for T_{AD} and lower for T_{EW} .

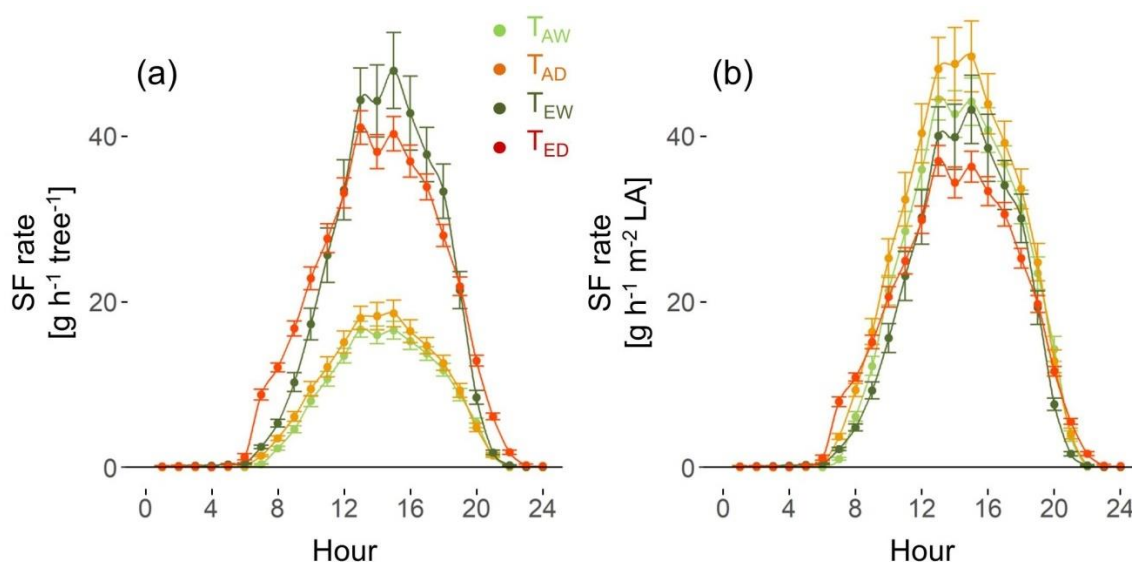


Figure 2.9 (a) Average diel pattern of whole-tree sap flow and (b) normalised per unit leaf area. Error bars are standard error. T_{AW} and T_{AD} are trees grown in a treatment chamber under ambient temperature and atmospheric $[CO_2]$ (480 ppm), well-watered and drought-stressed, respectively. T_{EW} and T_{ED} are trees grown in a treatment chamber under elevated temperature (+3°C) and atmospheric $[CO_2]$ (707 ppm), well-watered and drought-stressed, respectively.

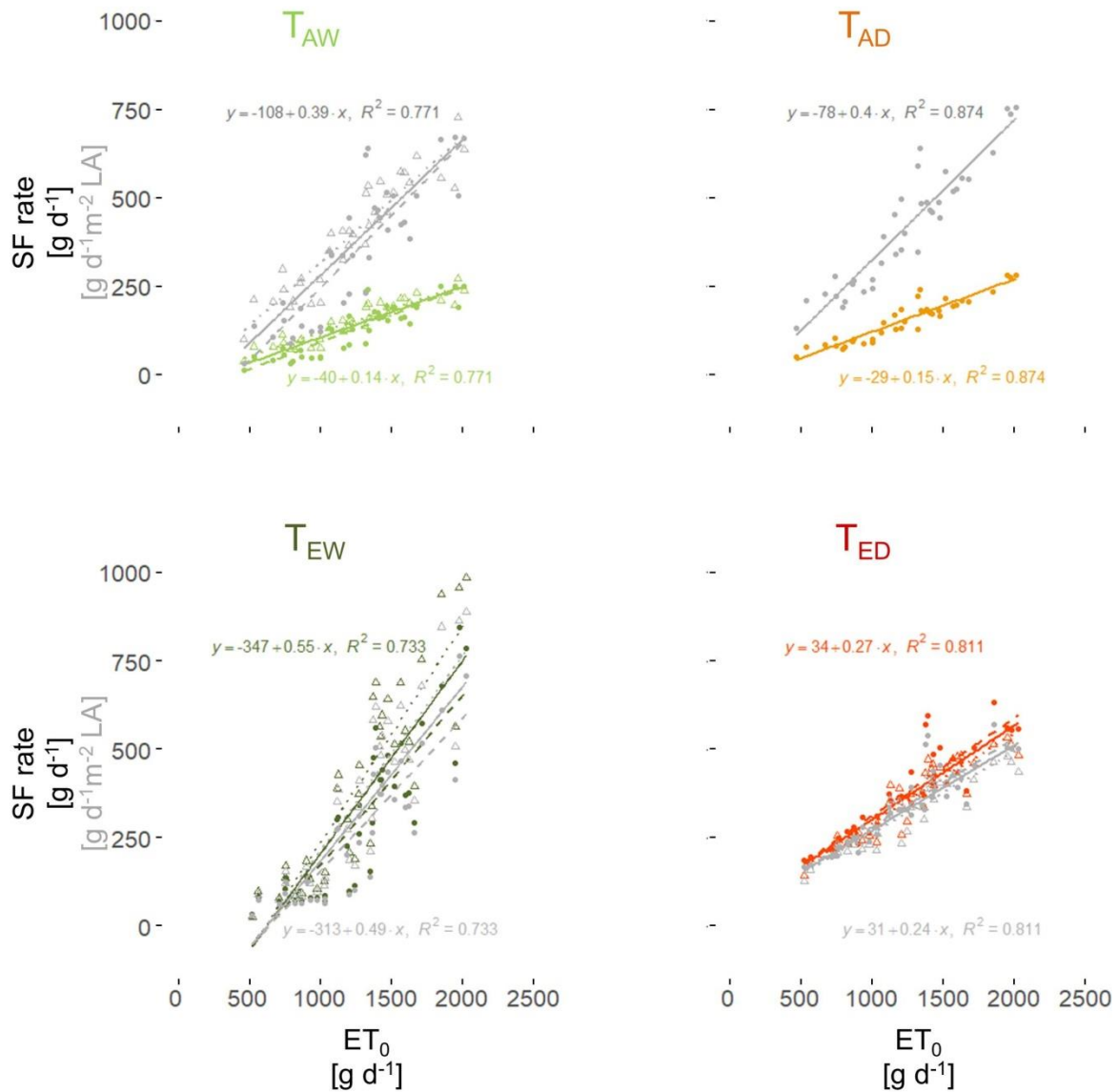


Figure 2.10 Relationship between sap flow (SF) rate and potential evapotranspiration (ET_0) for each treatment. ET_0 is expressed per unit surface area that each tree covered ($0.55\ m^2$) and SF rate is the sap flow rate expressed per tree in colour and per unit leaf area (LA) in grey. All regressions were significant ($P < 0.001$) and determination of coefficient (R^2) was high. T_{AW} and T_{AD} are trees grown in a treatment chamber under ambient temperature and atmospheric $[CO_2]$ (480 ppm), well-watered and drought-stressed, respectively. T_{EW} and T_{ED} are trees grown in a treatment chamber under elevated temperature ($+3^\circ C$) and atmospheric $[CO_2]$ (707 ppm), well-watered and drought-stressed, respectively.

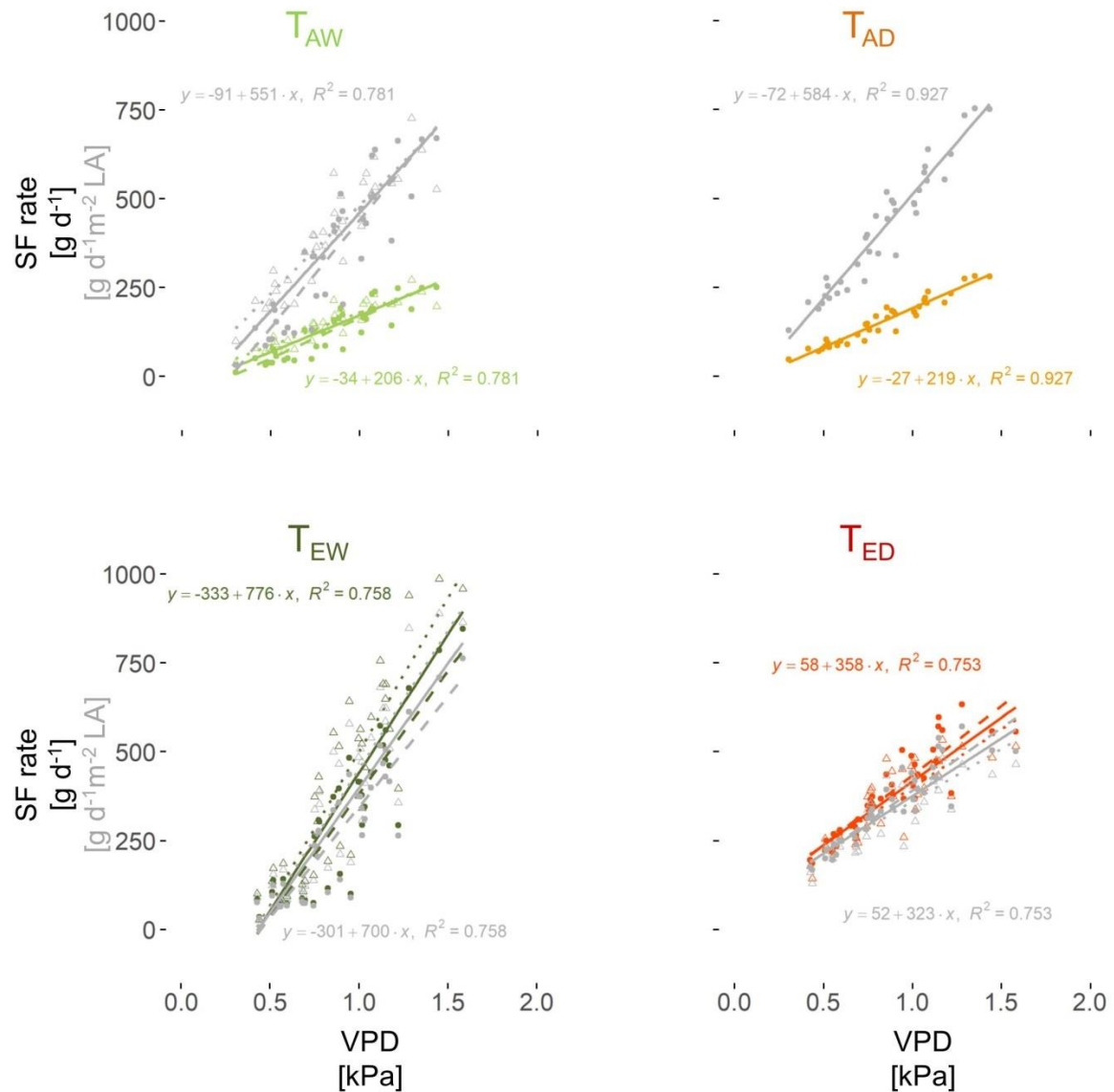


Figure 2.11 Relationship between sap flow (SF) rate and vapour pressure deficit (VPD) for each treatment. SF rate is the sap flow rate expressed per tree in colour and per unit leaf area (LA) in grey. All regressions were significant ($P < 0.001$) and determination of coefficient (R^2) was high. T_{AW} and T_{AD} are trees grown in a treatment chamber under ambient temperature and atmospheric $[CO_2]$ (480 ppm), well-watered and drought-stressed, respectively. T_{EW} and T_{ED} are trees grown in a treatment chamber under elevated temperature (+3°C) and atmospheric $[CO_2]$ (707 ppm), well-watered and drought-stressed, respectively.

Table 2.1 Crop coefficients (K_c) are calculated as SF/ET_0 , with SF whole-tree sap flow and ET_0 potential evapotranspiration per unit surface area covered by the tree (0.55 m^2). K_c is also shown per unit leaf area, where whole-tree SF is divided by LA ($K_{c,LA}$). Slopes of the relationships between SF and ET_0 (Fig. 2.10) are listed, for whole-tree SF and per unit LA. Calculated canopy conductances (g_s) are given, expressed per unit LA. K_c and g_s values are calculated with daily averages and standard errors are given with $N = 37 \times 2$, except for T_{AD} for which $N = 37 \times 1$. T_{AW} and T_{AD} are trees grown in a treatment chamber under ambient temperature and atmospheric $[CO_2]$ (480 ppm), well-watered and drought-stressed, respectively. T_{EW} and T_{ED} are trees grown in a treatment chamber under elevated temperature ($+3^\circ\text{C}$) and atmospheric $[CO_2]$ (707 ppm), well-watered and drought-stressed, respectively.

Treatment	T_{AW}	T_{AD}	T_{EW}	T_{ED}
K_c [-]	0.108 ± 0.003	0.124 ± 0.003	0.250 ± 0.015	0.296 ± 0.004
$K_{c,LA}$ [m^{-2}]	0.288 ± 0.010	0.330 ± 0.009	0.225 ± 0.013	0.267 ± 0.004
Slope SF~ ET_0 (whole-tree)	0.144	0.150	0.548	0.267
Slope SF~ ET_0 (per unit LA)	0.385	0.401	0.494	0.241
g_s [$\text{mmol m}^{-2} \text{ s}^{-1}$]	47.6 ± 1.5	54.5 ± 1.2	36.3 ± 2.1	43.1 ± 0.7

Table 2.2. Wood formation efficiency in terms of water use for the period of which sap flow was measured (DOY 163-199). Relative water use is the wood formation efficiency normalised for T_{AW} . T_{AW} and T_{AD} are trees grown in a treatment chamber under ambient temperature and atmospheric $[CO_2]$ (480 ppm), well-watered and drought-stressed, respectively. T_{EW} and T_{ED} are trees grown in a treatment chamber under elevated temperature ($+3^\circ\text{C}$) and atmospheric $[CO_2]$ (707 ppm), well-watered and drought-stressed, respectively.

Treatment	T_{AW}	T_{AD}	T_{EW}	T_{ED}
Stem wood formed/sap flow [mm^3 wood/g water]	4.15 ± 1.12	5.78 ± 0.63	2.73 ± 0.49	4.22 ± 0.62
Relative water use	1	1.39	0.66	1.02

Discussion

Interactions between microclimate and sap flow

We investigated combined effects of atmospheric $[CO_2]$ and air temperature, and soil water availability on young one-year-old *Populus tremula* trees, as we expected strongest responses and plasticity in young trees (Sultan 2000, Awad et al. 2010). Furthermore, young trees' behaviour eventually defines structure and composition of future forests (Classen et al. 2010). Tree sap flow

rates were higher in T_E than in T_A (Figs 2.8b and 2.9), which was caused by the large increase in LA in T_E by a factor of almost three. Sap flow rates per unit LA were lower in T_E than in T_A (Fig. 2.9b), which can be attributed to the effect of increased CO_2 on leaf stomatal conductance (Norby et al. 1999, Long et al. 2004, Ainsworth and Rogers 2007, Leuzinger and Körner 2007, Leuzinger and Bader 2012, Silva and Anand 2013). In their meta-analysis, Ainsworth and Rogers (2007) observed a reduction of 19 % on average in canopy conductance in trees when $[CO_2]$ rose by 200 ppm. Canopy conductance in our experiment agreed well to this meta-analysis with calculated reductions of 24 % for T_W and 21 % for T_D . This was also confirmed in $K_{c,LA}$, which was on average 26 % higher in T_A than in T_E (Table 2.1).

A strong relationship existed between sap flow rates and microclimatic variables (Figs 2.10 and 2.11), as has also been observed in previous studies (Ortuño et al. 2006, Kume et al. 2007, Oguntunde and Oguntuase 2007, Du et al. 2011, Leuzinger and Bader 2012). Response slopes showed that SF in T_{AW} and T_{AD} responded similarly to changes in ET_0 , while differences were observed between T_{EW} and T_{ED} . Pereira et al. (2006) reported comparable slopes in ambient conditions when SF was expressed per unit LA in mature orchard trees (apple, olive, walnut; values of 0.35-0.36). Given the calculated reduction in canopy conductance (Fig. 2.9b, Table 2.1), we also expected a reduced response of T_E sap flow to changes in microclimatic variables. This was confirmed in T_{ED} , but in contrast, T_{EW} showed a higher slope, indicating that whole-tree SF increased more pronounced in response to increasing ET_0 (Fig. 2.10, Table 2.1). Under less demanding atmospheric conditions (i.e., low ET_0 or VPD caused by a wetter atmosphere, lower temperatures or PAR-values), T_{EW} had the lowest SF rates per unit LA, while under more demanding atmospheric conditions (i.e., higher ET_0 or VPD) T_{EW} had highest amounts of SF (Figs 2.10 and 2.11). The expenditure of water in T_{EW} was high relative to the amount of stem growth (Table 2.2), indicating that its strategy was less efficient. Because our experiment was in confined treatment chambers, atmospheric conditions were never very dry, but based on the SF response to ET_0 and VPD it can be expected that under drier atmospheric conditions T_{EW} would have the highest SF rates of all treatments. This finding led us to speculate that T_{EW} trees showed a more risky behaviour towards microclimatic conditions, with less stomatal

regulation, a strategy with higher potential risks, but also higher potential benefits (Zweifel et al. 2006, Sade et al. 2012). Given the expected increase of hotter droughts, the potential risks might become more important when exposed to both drier atmospheric conditions and lower soil water availability (Allen et al. 2015). But, previous research on *Populus* spp. did not univocally show that more risky stomatal behaviour led to a reduced potential to recover from drought (Silim et al. 2009, Arango-Velez et al. 2011, Attia et al. 2015). For instance, Attia et al. (2015) reported that *Populus simonii* carr. (SI) had higher absolute water usage and lower agricultural WUE (tree weight gain per water use) than *P. balsamifera* L. (BS), but had the highest total growth and was not worse in recovering from drought. Other research on *Populus* spp. showed that the more drought-resistant species had a stronger stomatal regulation (Silim et al. 2009). T_{ED} trees were more efficient in wood formation with the water they used and showed a lower response to drier atmospheres, which indicates that this species would be less vulnerable to hotter droughts.

A strong feedback existed between trees and microclimate. By increasing the daytime air temperature by $2.8 \pm 0.1^\circ\text{C}$ in T_E , a higher VPD was expected, but T_E trees transpired three times more water, increasing RH during daytime, which cancelled the expected increase in daytime VPD and ET_0 . For instance, with only the temperature effect (and assuming RH and PAR in T_E equal to T_A), the increase in ET_0 would have been 7 % on average, compared to the current 3 %. Also, $[\text{CO}_2]$ in the T_E treatment chamber showed a step-wise decline during the first part of the day (Fig. 1j), which resulted from the trees taking up CO_2 , and in T_A , $[\text{CO}_2]$ was higher than the set level, because $[\text{CO}_2]$ inside the canopy is known to be influenced by tree carbon uptake and release (Brooks et al. 1997, Feigenwinter et al. 2008). This shows that not only microclimate influences tree physiology, but also tree physiology influences the microclimate. In treatment chambers, microclimatic conditions may vary faster than they would in forests, but even there, these interactions should not be disregarded. If in future conditions, unstressed trees have a low efficiency in terms of water use for wood formation (Table 2.2), hotter droughts might be mitigated by more water that is brought into the atmosphere. This added water to the atmosphere comes at the expense of a soil that would be more rapidly depleted, which would aggravate the effects of hotter droughts. Furthermore, in our experiment, VPD was nearly equal

during daytime in T_E and T_A , but higher in T_E during the night, which can increase nighttime transpiration (Dawson et al. 2007), and will increase the rate of drying out in soils.

Impact of climate change conditions on tree growth

We hypothesised that (i) trees grown in T_E will have higher growth rates than in T_A because of CO_2 fertilisation, and (ii) drought will lower growth rates, but that this effect will be less in T_E . Whereas trees grown in T_E indeed had higher stem growth and a 3-fold larger leaf area, stem growth was strongest in T_{ED} instead of T_{EW} (Fig. 2.5). Stem growth of T_{EW} was similar to those in T_A trees. During the initial measuring period, stem growth was low and shrinkage high for all treatments, which can be attributed to not yet fully expanded leaves and required allocation of stored carbon from the stem to the canopy (Urban et al. 2014). A comparison of stem diameter variations between T_E and T_A ($T_{AW} - T_{EW}$ and $T_{AD} - T_{ED}$) showed less daily shrinkage in T_E trees; especially in T_{EW} , despite a similar diel sap flow pattern between T_{EW} and T_{ED} (Figs 2.7 and 2.9). Also, Dawes et al. (2014) found smaller stem diameter shrinkages and expansions in 36-year-old *Larix decidua* L. trees exposed for nine years to elevated $[CO_2]$ (575 ppm) during daytime only, and found that stem shrinkage was delayed compared to the onset of sap flow. Dawes et al. (2014) showed that this combination of reduced shrinkage and increment, and increased time lag was caused by an increase in radial flow resistance between bark and xylem. Because we did not observe differences in the time of stem diameter shrinkage between treatments, we could not fully explain the reduction in stem shrinkage and increment by a reduced radial flow resistance. A lower xylem resistance might explain less pronounced shrinkages without a change in time lag, but this does not explain why radial stem growth in T_{ED} was larger. Factors that besides radial and xylem flow resistance influence diel stem diameter dynamics and wood formation are cell characteristics, and hydraulic capacitance of storage tissue (Zweifel and Häsler 2001, Steppe et al. 2006, De Swaef et al. 2015, Steppe et al. 2015).

Bulk elastic modulus as a measure of cell elasticity has been repeatedly investigated in regard to growth and turgor, and drought-induced tree responses (Steudle et al. 1977, Blake et al. 1991, Patakas and Noitsakis 1997, Steppe et al. 2006, Lechaudel et al. 2007, Martínez et al. 2007, De Swaef et al. 2015). Several

studies have measured a decrease in bulk elastic modulus in response to drought or as an acclimation to repeated drought and watering cycles (Blake et al. 1991, Patakas and Noitsakis 1997, Martínez et al. 2007). A decrease in bulk elastic modulus implies more elastic cells, which is related to an increased ability to maintain turgor, with increased turgor pressures and higher growth rates (Blake et al. 1991, Patakas and Noitsakis 1997, Steppe et al. 2006, Martínez et al. 2007) (see also Text box 2.2). Also for *Populus* spp., it has been reported that cell wall elasticity increased under drought stress (Giovannelli et al. 2007). In our study, we did not impose severe drought stress, but lowered soil RWC by 35 % in T_D during the development of the trees, which might have caused a plastic response in T_{ED} trees by lowering their elastic modulus. Trees in T_{EW} were assumed to be non-stressed, because access to both soil water and atmospheric $[CO_2]$ was high, which led us to speculate that bulk elastic modulus in T_{EW} was highest, and that drought in both T_E and T_A reduced bulk elastic modulus.

The putative higher bulk elastic modulus or reduced elasticity of stem cells in T_{EW} trees caused less shrinkage and swelling in stem diameter (Fig. 2.7) (Steppe et al. 2006, De Swaef et al. 2015). Lower elasticity and thus more rigid cells, will also result in lower cell wall extensibility, which might hamper cell growth, explaining the less pronounced stem growth observed in T_{EW} trees compared to T_{ED} trees (Lockhart 1965, Steppe et al. 2006, Cosgrove 2016). Another factor that is often related to elasticity is osmotic adjustments in response to stress, but for *Populus* spp. this has generally been reported to be small (Tschaplinski et al. 1998, Giovannelli et al. 2007).

Text box 2.2 Hydraulic capacitance and elasticity

A change in bulk elastic modulus can change tree hydraulic capacitance and, in turn, influence tree water relations and stem growth dynamics. Hydraulic capacitance (C) can be described as (Eq. 2.9) (Steppe et al. 2006):

$$C = \frac{dW}{d\psi} \quad (2.9)$$

with W the water content of the storage compartment (in g) in the stem and ψ the water potential in the storage compartment (in MPa).

The change in turgor pressure (ψ_p , MPa) is related to the change in volume (V , m³) with the bulk elastic modulus (ε , MPa) as proportionality constant (Eq. 2.10):

$$\frac{d\psi_p}{dt} = \frac{\varepsilon}{V} \frac{dV}{dt} \quad (2.10)$$

Furthermore, the change in water content is related to the change in volume by the density of water (ρ_w , g m⁻³):

$$\frac{dV}{dt} = \frac{1}{\rho_w} \frac{dW}{dt} \quad (2.11)$$

From these equations, it can be deduced that for a same change in turgor pressure, the volume change will be smaller if the bulk elastic modulus is higher (Eq. 2.10), and thus also the change in water content will be smaller (Eq. 2.11). In a tree with a higher bulk elastic modulus, a smaller hydraulic capacitance is expected because of the smaller change in water content per unit water potential.

With this deduction, changes in stem diameter with changing elastic modulus can be assessed. Bulk elastic modulus is proportional (ε_0 , m⁻¹) with the product of stem diameter (D , mm) and turgor pressure (Eq. 2.12):

$$\varepsilon = \varepsilon_0 D \psi_p \quad (2.12)$$

Elastic growth of the stem diameter is expressed in Eq. 2.13:

$$\left(\frac{dD}{dt}\right)_{el} = \frac{2d}{\varepsilon_0 D \psi_p} \frac{d\psi_p}{dt} \quad (2.13)$$

with d the thickness of the storage compartment (mm). Elastic stem growth reduces if the bulk elastic modulus is higher.

For an equal increase in storage water content, the effect on turgor will be dependent on the elastic bulk modulus (Eq. 2.10-2.11), which in turn affects many plant processes, including inelastic stem growth (i.e., irreversible growth), which is dependent on cell wall extensibility (ϕ , MPa s⁻¹) and the turgor threshold for growth (Γ , MPa) (Eq. 2.14):

$$\left(\frac{dd}{dt}\right)_{gr} = d\phi(\psi_p - \Gamma) \quad (2.14)$$

Although, in general, stem diameter growth is considered as a measure for tree vigour (Waring et al. 1980, Duchesne et al. 2003) it is not the only measure for success. The lower stem diameter in T_{EW} does not necessarily imply that these trees would have lower success rates than their T_{ED} counterparts. It is known that tree species can actively regulate their storage, and use these storages differently in response to environmental changes (Körner 2003, Sala et al. 2012, Sevanto et al. 2014, Adams et al. 2017). Carbon allocation might have been different between treatments, and thus T_{EW} might have been allocating more non-structural carbohydrates (NSC) to the stems, despite the smaller stem volume and aboveground biomass. Higher amounts of NSC reserves have been reported to be beneficial in case of a strong and prolonged drought episode (Sala et al. 2012, Wiley and Helliker 2012, Mitchell et al. 2014, Sevanto et al. 2014). Woodruff and Meinzer (2011) reported an increase in stored NSC in stems when water potentials dropped and trees suffered from drought stress. We however have no measurements of NSC and cannot conclude whether the T_{ED} and T_{EW} trees had different stem NSC.

Higher CO_2 uptake does not necessarily reflect increased stem growth. Despite an increased CO_2 absorption of 37 %, Klein et al. (2016) observed no effect on stem radial growth of 110-year-old *Picea abies* (L.) Karst. In their experiment, no stomatal response to elevated $[CO_2]$ and consequently no differences in whole-tree sap flow were measured, but possible changes in leaf area were not measured. This could also point to the importance of turgor. If additional carbon uptake is not accompanied by processes that increase cell turgor, no increase in growth is to be expected (see Text box 2.2).

Whole-tree ecophysiology to better understand the mechanisms underlying tree response to climate change

Whereas predictions on tree functioning in changing climate often focus on leaf level measurements, these measurements are difficult to translate to whole-tree functioning (Ainsworth and Rogers 2007, Leakey et al. 2009, Leuzinger and Bader 2012, Ryan 2013, Fatichi et al. 2014, Allen et al. 2015). We used whole-tree measurements to unravel the response of *Populus tremula* to elevated $[CO_2]$ and temperature, drought and their interactive effects. Diel

patterns in sap flow and stem diameter variation provided new insights of their growth and water use in different treatments.

It remains a challenge to scale up processes measured at the individual leaf level to the canopy, individual tree, forest and certainly ecosystem level (Leuzinger and Bader 2012). Our study aimed at contributing to this scaling exercise by taking measurements at the individual tree level in treatment chambers on seedlings, as treatment chambers have shown their added value in the past to better understand tree responses to elevated $[\text{CO}_2]$, and temperature (Norby et al. 1999, Bauweraerts et al. 2013, Teskey et al. 2015). To assess tree growth and biomass at stand level and interactions with other trees and soil, FACE (free-air CO_2 enrichment) experiments have been performed (Wullschlegel and Norby 2001, Long et al. 2004, Norby et al. 2005, Leakey et al. 2009, Norby and Zak 2011, Ryan 2013, Klein et al. 2016, Manderscheid et al. 2016), showing that increased photosynthesis under elevated $[\text{CO}_2]$ does not always translate in an equal increase in biomass (Leakey et al. 2009, Norby and Zak 2011, Ryan 2013).

We explained the reduced dynamic behaviour in stem diameters in T_{EW} trees by increased bulk elastic modulus and associated lower hydraulic capacitance (Text box 2.2). In trees with a small hydraulic capacitance, most of the water supplied to the transpiration stream comes from the soil rather than from internal stem water reserves. We further concluded that xylem flow resistance in T_{EW} trees was most likely relatively low, because otherwise a stronger stem shrinkage should be measured during active transpiration. Guet et al. (2015) showed in *Populus nigra* L. that genotypes with lower xylem resistance are less resistant to drought-induced cavitation

Despite their putative lower xylem resistance (efficient xylem), T_{EW} trees did not show a more efficient use of water, as they spent more water than T_A trees, while not growing more (Table 2.2). It may be clear that not only whole-tree water-use and stomatal regulation, but also internal cell water dynamics play a crucial role in how trees will respond when put in a new environment.

Conclusion

In this chapter, we showed that one-year-old *Populus tremula* trees did not always respond as expected to climate change regimes. The most striking result

was that the well-watered trees under elevated atmospheric [CO₂] and air temperature grew less than their drought-stressed counterparts. We used known mechanisms underlying stem diameter variation and proposed an increased bulk elastic modulus to explain the particular stem growth behaviour of the T_{EW} trees. This chapter aimed at contributing to a better understanding of tree functioning at the whole-tree level to further enhance our knowledge of the impacts of microclimatic changes on trees and forests, and of trees and forests on microclimate.

Supplemental material

Supplemental Table 2.1 Effects of microclimatic variables on GPD (growth per day) and MDS (maximum daily shrinkage) for each treatment for the entire period (DOY 119-199) or only second period (DOY 153-199), which is the period after which the effect of leaf emergence on MDS and GPD is thought to have disappeared, determined by statistical linear mixed-effect models. R^2 are levels of determination of the statistical models. Significance levels are denoted with * if $P < 0.05$, ** if $P < 0.01$, and *** if $P < 0.001$. T_{AW} and T_{AD} are trees grown in a treatment chamber under ambient temperature and atmospheric $[CO_2]$ (480 ppm), well-watered and drought-stressed, respectively. T_{EW} and T_{ED} are trees grown in a treatment chamber under elevated temperature (+3°C) and atmospheric $[CO_2]$ (707 ppm), well-watered and drought-stressed, respectively.

Full period (DOY 119-199)

Treatment		Temperature	PAR	RH	VPD	R^2
T_{AW}	MDS	-0.0062***	-	0.00086*	0.0747***	0.10
	GPD	-	-0.00007***	-0.00092*	0.0194***	0.04
T_{AD}	MDS	-0.0048***	0.00020***	0.0024***	-	0.10
	GPD	-	-0.00009***	-0.00183***	-	0.21
T_{EW}	MDS	-0.0174***	0.00020***	0.0038*	0.1689***	0.44
	GPD	0.0079***	-0.000084***	-0.0022**	-0.0592**	0.48
T_{ED}	MDS	-0.0156***	0.00015***	0.0028*	0.1270***	0.58
	GPD	0.0030***	-0.000051***	-	-	0.31

* $P < 0.05$, ** $P < 0.01$, *** $P < 0.001$

Only second period (DOY 153-199)

Treatment		Temperature	PAR	RH	VPD	R^2
T_{AW}	MDS	-	-	-	-	0.63
	GPD	-0.0033*	-0.000063**	-	0.0570**	0.22
T_{AD}	MDS	-	-	-0.00058***	-	0.36
	GPD	-	-0.000073***	-0.00151***	-	0.37
T_{EW}	MDS	-	0.00012***	0.00196***	-	0.80
	GPD	-	-	-	-	-
T_{ED}	MDS	-	0.00006***	0.00219***	0.0191*	0.81
	GPD	-	-	-	-	-

* $P < 0.05$, ** $P < 0.01$, *** $P < 0.001$

3

CHAPTER 3

Will *Populus tremula* trees be more vulnerable to drought-induced cavitation under climate change regimes?

Abstract

Within a climate that is rapidly changing, it is crucial to better understand how trees will respond to these changes. An important aspect to account for in climate change research is the predicted occurrence of hotter droughts. During drought spells, trees face the challenge to protect the integrity of their hydraulic system by avoiding cavitation. Previous research has shown that most trees operate within a small safety margin and that a small decrease in water potential might lead to considerably more cavitation. So far, the impact of the combination of elevated CO₂ concentration ([CO₂]) and air temperature under different soil water treatments on tree drought vulnerability remains poorly understood. Therefore, we assessed vulnerability to drought-induced cavitation in one-year-old *Populus tremula* L. trees grown under ambient and climate change projected conditions (i.e., atmospheric [CO₂] of 700 ppm, ambient air temperature +3°C) for two months. Trees were split between a well-watered and a drought-stressed treatment. First, potential differences in native state of cavitation between treatments were compared using micro-CT scans. Then, drought vulnerability was assessed using a combination of acoustic vulnerability curves and desorption curves. Trees subjected to drier growing conditions were significantly less vulnerable to drought-induced cavitation, whereas trees under elevated [CO₂] and temperature tended toward a higher vulnerability. Well-watered trees showed a smaller water potential range between safe and perilous levels of cavitation compared to their drought-stressed counterparts, making them more vulnerable to small decreases in water potential under drought. Well-watered trees under elevated [CO₂] and temperature conditions also showed lower hydraulic capacitance, explaining why they were most vulnerability to drought-induced cavitation. Our findings suggest that elevated [CO₂] might increase vulnerability to drought-induced, which might put future trees and forests in danger when confronted with hotter droughts.

Introduction

Climate change is expected to increase air temperature and the frequency of drought and heat periods. These so-called hotter droughts are projected to induce additional stress on trees, resulting in higher tree mortality rates (McDowell et al. 2008, Allen et al. 2010, McDowell et al. 2011, Bauweraerts et al. 2013, Bauweraerts et al. 2014, Teskey et al. 2014, Allen et al. 2015, Sperry and Love 2015). But predicting the actual effects of hotter droughts remains challenging because some climate change factors aggravate and others mitigate the consequences (Aitken et al. 2008, Allen et al. 2015). Higher temperatures and drier atmospheres increase the transpirational demand of trees, which, in combination with a dry soil, may lead to hydraulic failure due to cavitation (Xu et al. 2010, Meinzer and McCulloh 2013, Sperry and Love 2015). To prevent or limit hydraulic failure, most trees respond adequately to drought by closing their stomata, which reduces transpirational demand, but which also reduces carbon uptake, and hence photosynthetic potential (Porporato et al. 2001, Leuning et al. 2004, Xu et al. 2010). If carbon uptake is impeded for too long, a tree starts suffering from carbon starvation, a condition in which not enough energy is available for the tree to self-sustain (McDowell and Sevanto 2010, Sala et al. 2012). Elevated atmospheric CO₂ concentration ([CO₂]), as one of the main factors causing hotter droughts also influences tree carbon assimilation in a direct way. Increases in atmospheric [CO₂] have been shown to lower stomatal conductance (Beerling and Kelly 1997, Xu et al. 2016) and it is expected that this effect will increase further in the future (Ainsworth and Rogers 2007, Leakey et al. 2009, IPCC 2014a, Xu et al. 2016). Trees will require less gas exchange for the same amount of CO₂ when atmospheric [CO₂] increases, which results in a lower water use relative to carbon uptake. Consequently, it is expected that trees and forests may become less sensitive to drought, although this has not been confirmed by globally higher growth rates over the past decades (Silva and Anand 2013, Allen et al. 2015). In their review, Allen et al. (2015) contrasts existing studies reporting a “greater vulnerability” to hotter droughts under elevated [CO₂] with those predicting a “lesser vulnerability”. Because interactions between changing air temperatures, soil water availability and atmospheric [CO₂] are so complex, research is still struggling to confidently predict how tree species

and forests will respond and adapt to climate change (Wullschleger et al. 2002, Fischlin et al. 2007, Leakey et al. 2009, IPCC 2014a, Allen et al. 2015).

When trees are faced with drought, they are no longer able to withdraw sufficient water from the soil. This increases tension in the water-transporting xylem vessels, which also increases the amount of water withdrawn from the water storage compartments. The more negative xylem water potential (ψ_x) becomes, the more water-filled xylem vessels will succumb to the tension and cavitate (Sperry and Tyree 1988, Tyree and Sperry 1989, Sperry and Love 2015). Because cavitated or air-filled xylem vessels are no longer functional, the total conductive surface area decreases, which increases the resistance to water transport, further lowering ψ_x , and increasing cavitation risk for the remaining vessels. Under severe drought conditions, this may result into runaway cavitation, ultimately leading to total hydraulic failure and tree die-back (Tyree and Sperry 1989, Meinzer and McCulloh 2013).

A vulnerability curve (VC) is a very valuable and often used tool to assess a tree's capability to withstand drought and expresses the relationship between ψ_x and the loss of hydraulic conductivity caused by cavitation (Choat et al. 2012, Cochard et al. 2013). It has long been thought that species are faced with a trade-off between a more efficient or a more safe xylem transport system, but recent findings shows there is no strong evidence to support this (Gleason et al. 2016, De Baerdemaeker et al. in press). Hydraulic vulnerability to drought-induced cavitation has been found to be the best predictor for tree mortality (Anderegg et al. 2016), with tree species living in more drought-prone biomes (such as dessert or Mediterranean areas) generally more cavitation-resistant and able to withstand more negative ψ_x better (Maherali et al. 2004). From VCs typical values (i.e., ψ_{12} , ψ_{50} , ψ_{88} and ψ_{100} or ψ_x at which 12 %, 50 %, 88 % and 100 % of the conductivity is lost) are derived (Cochard et al. 2013), of which ψ_{50} is a widely used plant trait to compare drought resistance between species (Maherali et al. 2004, Delzon et al. 2010, Choat et al. 2012, Cochard et al. 2013, Lens et al. 2016). Trees from the same species growing in contrasting water regimes often show plastic responses and less drought vulnerability when grown under restricted water availability (Ladjal et al. 2005, Stiller 2009, Awad et al. 2010, Vilagrosa et al. 2012).

Hydraulic capacitance is tightly connected to vulnerability to drought, because it defines how much water can be supplied to the xylem water flow from water storage compartments in relation to a drop in ψ_x (Meinzer and McCulloh 2013, Vergelynst et al. 2015a). This buffers changes in transpirational demand and serves as a valuable water source during drought, and consequently reduces drops in ψ_x , relieving some tension from the water column (Steppe et al. 2006, Steppe et al. 2012, Meinzer and McCulloh 2013, Zhang et al. 2013, De Swaef et al. 2015, Steppe et al. 2015). Even when cavitation occurs, and a water column breaks, the water that is released during this process contributes to a capacitive water buffering (Tyree and Yang 1990, Lo Gullo and Salleo 1992, Hölttä et al. 2009, Vergelynst et al. 2015a).

To know whether trees and forests will be able to face the future, it is important to investigate how changing environmental factors affect trees' potential to cope with drought. As Allen et al. (2015) pointed out in their review, there exists contradicting evidence about climate change effects on vulnerability of forests. Some observe positive effects because of elevated $[\text{CO}_2]$ and associated decrease in water consumption, while others report adverse effects due to more frequent drought episodes accompanied with warmer temperatures. Comparing drought vulnerability data on a global scale, Choat et al. (2012) concluded that trees across biomes operate within a small hydraulic safety margin (HSM, defined as the difference between operating ψ in unstressed conditions and ψ_{50}). They reported that about 70 % of the investigated species had a narrow HSM (< 1 MPa). In general, angiosperms showed even lower, often negative, HSM, which indicates that many species would have at least half of their conductivity lost if ψ_x further decreases (Meinzer et al. 2001, Choat et al. 2012). If trees do not adapt, hotter droughts might become detrimental for their hydraulic system. To be able to better assess whether trees and by extension forests are in danger of massive drought-induced die-off, we need to know whether and how hydraulic vulnerability to drought changes when grown in future conditions.

To push some scientific frontiers in this research field, we studied the response of juvenile trees in a changing environment. We focussed on the integrated effect of elevated atmospheric $[\text{CO}_2]$ (700 ppm) and air temperature

(ambient +3°C) in combination with soil water availability on the vulnerability to drought-induced cavitation of one-year old *Populus tremula* L. trees. We assessed whether trees subjected to drought and elevated [CO₂] plus temperature adjusted their vulnerability to drought-induced cavitation and hydraulic capacitance. Our specific working hypothesis were: (i) Trees grown under lower soil water availability will be less vulnerable to cavitation due to acclimatisation, which has previously been reported by Awad et al. (2010) using VCs in hybrid poplars (*P. tremula* x *P. alba*). (ii) Trees grown under elevated atmospheric [CO₂] plus air temperature will lower stomatal conductance and will be acclimated to lower tensions in their hydraulic system. These trees will therefore be less acclimated to more negative ψ_x resulting from imposed drought, and will show more rapid progression of cavitation during dehydration. (iii) Trees grown under elevated atmospheric [CO₂] plus temperature will invest less in drought resilience, even when grown under drier conditions, because of their reduced stomatal conductance and associated water consumption, and will show a less plastic response to drought than trees grown under ambient and drought-stressed soil conditions.

Materials and methods

Sampling procedure and measurements

Twelve one-year-old *Populus tremula* L. trees were chosen from the treatment chambers described in Chapter 2: T_{AW} and T_{AD} trees were grown under ambient temperature and atmospheric [CO₂] (480 ppm), well-watered (soil relative water content (RWC) of 42 %), and drought-stressed (soil RWC of 28 %), respectively. T_{EW} and T_{ED} were grown in a treatment chamber under elevated temperature (+3°C) and atmospheric [CO₂] (707 ppm), well-watered (soil RWC of 42 %) and drought-stressed (soil RWC of 28 %), respectively. Three potted trees per treatment were transported from the treatment chambers at the experimental site of Ghent University (Proefhoeve, Melle, Belgium) to the Laboratory of Plant Ecology, Ghent University, Belgium before sunrise and one day before measurements. Trees were sequentially analysed from DOY 138 to 148 (17 May 2016 – 27 May 2016) (T_{EW} on DOY 138-139; T_{AW} on DOY 140-141; T_{ED} on DOY 144-145; T_{AD} on DOY 146-148). Trees were selected using as criteria

uniformity in length (75 ± 2 cm, SE, N = 12) and stem diameter (measured 5 cm above potting soil surface: 5.37 ± 0.03 mm, SE, N = 12).

Upon arrival in the lab, three trees per treatment were placed in a darkened treatment room with an operating green light to limit photosynthesis and transpiration (De Baerdemaeker et al. 2017, Epila et al. 2017a). Each tree stem was divided in two parts (Fig. 3.1). The upper part (with leaves) was used to measure acoustic vulnerability curves and the lower part (where leaves were removed) to measure desorption curves and associated hydraulic capacitances. A small stem section of ~ 3 cm was marked in the middle of the stem, separating upper from lower part, and was sampled upon cutting to determine wood characteristics (Fig. 3.1). All leaves of the upper stem part were wrapped in aluminium foil while the tree was still intact, to prevent transpiration and to allow equilibration between leaf and stem water potential. Next, all leaves from the lower part were removed and wounds were covered with petroleum jelly to avoid evaporation (Vergeynst et al. 2015a). Samples were first cut above the root zone, while submerged under water, to avoid air-entry artefacts (Cochard et al. 2013). Then, samples were shortly (5 s) relaxed to avoid artificial cavitation (Trifilò et al. 2014, De Baerdemaeker et al. 2017). Next, the marked middle stem section was cut, also while being submerged under water. Cut ends of both halves were covered with wet paper cloths, while still submerged in water to avoid premature dehydration after being taken out of the water for sensor installation.

The upper stem part was mounted in a custom-built holder (Fig. 3.1). On two fixed positions the bark (1.5×0.5 cm) was removed with a scalpel to expose the xylem to a broadband point-contact acoustic emission (AE) sensor (KRNBB-PC, KRN Services, Richland, WA, USA) and a point dendrometer (DD-S, Ecomatik, Dachau, Germany) (Vergeynst et al. 2016). The holder ensured a uniform positioning of the sensors between different samples (Epila et al. 2017a). The AE sensor was pressed to the exposed xylem via a compression spring (D22050, Tevema, Amsterdam, The Netherlands) in a small PVC tube. To allow for good acoustic contact, a droplet of vacuum grease (High-Vacuum Grease, Dow Corning, Seneffe, Belgium) was added between sensor tip and xylem, after which installation was validated via the pencil lead break test (Tyree and Sperry 1989, Hamstad et al. 1994, Sause 2011, Vergeynst et al. 2015b). In case of the dendrometer, petroleum jelly was also smeared between sensor tip and xylem to

prevent evaporation from the exposed wound (Epila et al. 2017a). The lower stem part was placed on continuous weight balances (DK 6200 with 0.01 g accuracy, Henk Maas, Veen, The Netherlands) (Fig. 3.1). Once both stem parts were installed, wet cloths were removed and room light turned on, to start bench-top dehydration.

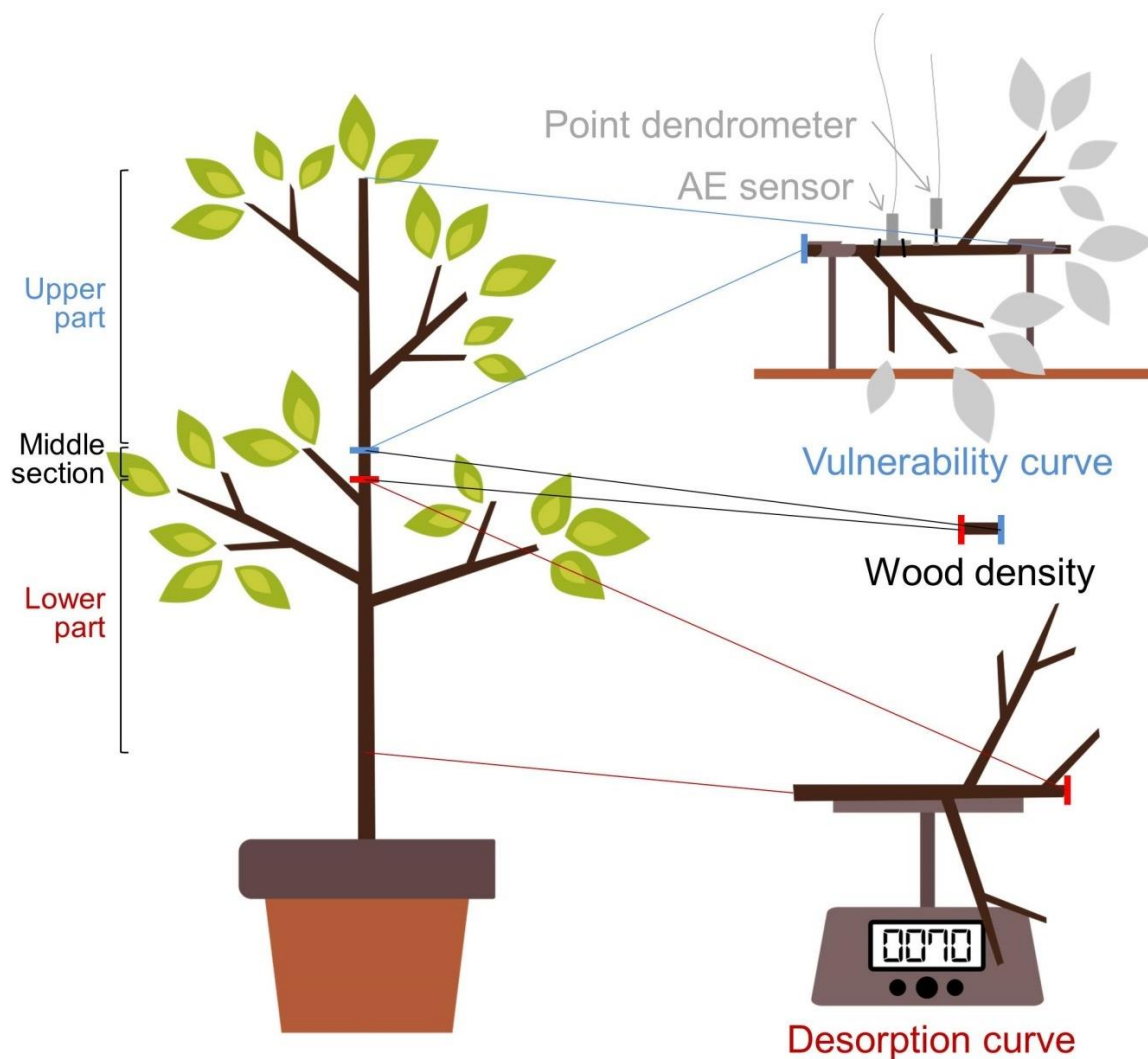


Figure 3.1 Schematic of the tree stem parts that are used for the determination of the vulnerability curve, desorption curve and wood density. Leaves are removed from the lower part and wounds are covered with petroleum jelly to prevent evaporation and the stem part was continuously logged on a weight balance. The small middle section was used to determine wood density from the dried weight. Vulnerability curves were determined on the upper stem part. All leaves were wrapped in aluminium foil to allow equilibration of leaf and stem water potential. These leaves were used to determine stem water potential several times during dehydration. Point dendrometers measured stem shrinkage during dehydration to convert stem water potential from discrete measurements to a continuous curve. An acoustic emissions (AE) sensor was used to measure sound originating from the dehydrating stem. The amount of AE can be linked to the amount of cavitated vessels. All cuts were made submerged under water.

Point dendrometer and balance read-outs were registered every minute via custom-built acquisition boards. AE signals were amplified by 35.6 dB (AMP-1BB-J, KRN Services, Richland, WA, USA) after which waveforms of 7168 samples length were acquired at 10 MHz sample rate. Signals were collected via 2-channel PCI boards and sent to the software program AEwin (PCI-2, AEwin E4.70, Mistras Group BV, Schiedam, The Netherlands). A 20-1000 kHz electronic band pass filter was applied, and only waveforms above the noise level of 28 dB were retained (Vergeynst *et al.* 2016).

Xylem water potential (ψ_x , MPa) was measured on wrapped leaves with a pressure chamber (PMS Instrument Company, Corvallis, OR, USA). Read-out frequency was between 30-60 minutes, based on visual inspection of the acoustic signal. More frequent ψ_x measurements were performed when AE increased. On average 20 ψ_x readings were done per tree during the course of the experiment. Experiments lasted about 24 h, starting in the morning with most ψ_x measurements taken during the first 9 h and a measurement the next morning which typically corresponded with 100 % cavitation, illustrated by too negative ψ_x for *Populus* spp. ($\psi_x < -5$ MPa). AE detection was paused during the cutting of the leaves to avoid disturbances in the acoustic detections (Epila *et al.* 2017a).

Acoustic vulnerability to drought-induced cavitation

The obtained AE signals were used to construct an acoustic VC (Mayr *et al.* 2011, Vergeynst *et al.* 2015a, Epila *et al.* 2017a). AE signals were cumulated over the measurement period. The first derivative was calculated from cumulated AE to construct an AE activity curve. The endpoint of the vulnerability curve (AE₁₀₀) was determined as the point at which the decrease in AE activity, following the AE activity peak, decreased most strongly (Vergeynst *et al.* 2016). This point corresponds to the local maximum of the third derivative (Vergeynst *et al.* 2016, Epila *et al.* 2017a). The AE activity was numerically calculated over a time interval of 15 minutes, while the third derivative was calculated over a time interval of 3 hours. Absolute cumulative AE was then rescaled between zero and the defined endpoint to obtain a relative percentage of cumulative AE. The x-axis of the VC ,i.e., ψ_x , was obtained using segmented linear regression (with one breakpoint) between the point measurements of ψ_x and xylem shrinkage

monitored by the point dendrometers to produce continuous water potential data (Vergeynst et al. 2015a, Epila et al. 2017a).

Volumetric water content and hydraulic capacitance

Precise diameter and length of the 3-cm middle section were measured with an electronic caliper (with 0.01 mm accuracy), and weighted with a precision balance (Sartorius precision balance with 0.001 g accuracy, Sartorius Weighing Technology GmbH, Goettingen, Germany). After bench-top dehydration, additional samples of equal length (3 cm) were taken from the ends of both the upper and the lower stem part, and diameter, length, and weight were measured to verify equal dehydration in both stem part (Vergeynst et al. 2015a). Because equal dehydration was found, water potentials measured on the upper part were assumed the same for the lower part. Each sample was then oven-dried (70°C) till constant weight. Length, diameter and weight were re-measured after drying and assuming a cylindrical form, basic wood density (ρ_b) (oven dry mass/green volume) was obtained (Vergeynst et al. 2015a). The wood samples were used to normalise weight loss data of the lower stem part to volumetric water content (VWC). This was obtained by multiplying mass fraction with ρ_b , while the change in VWC was determined by re-scaling the weight loss data to the range of water contents between initial and final water content of the wood samples (Vergeynst et al. 2015a, Epila et al. 2017a).

In addition to acoustic VCs, desorption curves (DC) were developed by plotting VWC against ψ_x . Three zones or regions of interest were determined, using the DC's breakpoints, calculated via the Segmented package in R (Muggeo 2008). The zone between the start point and first breakpoint is known as the initial phase or capillary water phase. The zone between first and second breakpoint is the elastic shrinkage phase, and the zone after the second breakpoint till ψ_{100} (derived from the acoustic VC) is the cavitation or inelastic shrinkage phase (Vergeynst et al. 2015a, Epila et al. 2017a). Hydraulic capacitance (in $\text{kg m}^{-3} \text{MPa}^{-1}$) of the distinct phases was calculated as the slope of the linear regression between VWC and ψ_x (Vergeynst et al. 2015a).

X-ray micro-computed tomography

To assess potential differences in native state of cavitation between treatments, one 30-cm long stem section cut from one additional tree per treatment was scanned with X-ray micro-computed tomography (micro-CT). The objective was assessing whether T_D would have a higher native state of cavitation compared to T_W . Often samples are artificially hydrated before determining VCs, but this comes with the risk to rehydrate non-functional vessels (Cochard et al. 2013, Sperry 2013, Trifilò et al. 2014). Instead, by starting our analysis from the native state, we ensured discarding all non-functional vessels from the VCs (De Baerdemaeker et al. 2017), but then information on differences in native state is required. For each treatment, one additional tree was transported to the Laboratory of Plant Ecology before sunrise (along with three trees used for the other measurements) and placed in the same darkened treatment room where trees for VC and DC were prepared. A 30-cm long section was cut from the middle of the tree, following the cutting procedure described for VCs, and all leaves were removed. Immediately after cutting, samples were entirely covered with a layer of paraffin, to prevent dehydration during the scanning process. The samples were fixed in a cylindrical carton holder, that was filled with foam to keep the samples in place. Scanning was executed at the NanoWood CT facility (Laboratory of Wood Technology, Faculty of Bioscience Engineering, Ghent University, Belgium) (Dierick et al. 2014). Samples were scanned for 28 minutes with an exposure time of 700 ms, where a total of 2000 projections were taken during a 360° rotation. In order to determine the amount of native embolism relative to the total amount of vessels, samples were re-scanned after complete dehydration at the same position, and under the same settings with the NanoWood CT scanner. 3-D volumes were reconstructed with the Octopus reconstruction software package (Dierick et al. 2004, Vlassenbroeck et al. 2007), and resulted in an approximate voxel pitch of 6 μm resolution.

Aside from assessing the native state of cavitation, we wanted to make sure that no artificial cavitated vessels originated from the cutting procedure, as many VC techniques are prone to such artefacts (Cochard et al. 2013). To this end, we scanned one additional intact tree selected from T_{AW} and T_{EW} with the HECTOR scanner at UGCT (Centre for X-ray scanning of Ghent University, Belgium) (Masschaele et al. 2013). In contrast to NanoWood, this custom-built

micro-CT scanner is capable of scanning small intact potted trees *in vivo*, because of the presence of a large rotation stage, which can carry and rotate small potted trees. On DOY 181 (29 June 2016), trees were transported from the treatment chambers in Melle to UGCT and scanned before sunrise. Scanned trees were aligned with the scanner via a custom-built Perspex holder (Vergeynst et al. 2015a), and scanned while being rotated for 21 minutes with an exposure time of 500 ms. This resulted in a total of 2400 projections taken during the 360° rotation. The Octopus reconstruction software rendered the 3-D volumes at an approximate voxel pitch of 6.5 μm .

Micro-CT images from both NanoWood and HECTOR were further processed with the image analysis software program Fiji (Schindelin et al. 2012). Images were first median filtered in the z-direction to enhance image quality and reduce background noise. Cavitated vessels were determined on NanoWood CT-images with the trainable weka segmentation plugin, in which a manual selection of filled and empty vessels was performed on a small section of the CT-sections before using the automated weka segmentation plugin (Arganda-Carreras et al. 2017). In this way, the native amount of cavitated vessels could be determined and compared between treatments.

Data analysis

To determine if treatments resulted in significant differences, a two-way ANOVA analysis was performed on key characteristics: (i) ψ_{12} , ψ_{50} , ψ_{88} and ψ_{100} for the VCs, (ii) transition from initial phase to phase I, and phase I to phase II, (iii) hydraulic capacitances of the initial phase, phase I, and phase II, (iv) initial stem volumetric water content, and (v) wood density. Before analysis, normality and homogeneity of variances were checked with a Shapiro-test and Levene's test, respectively, and ANOVA assumptions were considered fulfilled when p-values > 0.05. Treatment chamber and soil water treatment were two crossed factors. In case of significant differences, a post-hoc Tukey's honestly significant difference (Tukey's HSD) test was performed to see which treatments differed from each other. Outcomes of p-values tended to be significant in case of $p < 0.1$, and was significant in case of $p < 0.05$.

Results

Native state of cavitation

Because T_D trees could have more native cavitated vessels than T_W trees due to the drought treatment, native state of cavitation was compared between all treatments. With micro-CT scans, the reference technology to quantify cavitation (Cochard et al. 2015), native state and state after full dehydration were determined (Fig. 3.2). All scanned trees showed a considerable fraction of empty vessels in the native state, with empty vessels mainly located around the stem centre (Fig. 3.3). The percentage of native empty vessels was comparable among treatments, with no clear effect of treatment chamber ($T_A - T_E$) nor soil water treatment ($T_W - T_D$) (Table 3.1). Differences in soil water treatment did thus not affect the native state of cavitation. Because no effects of treatments were observed, we could assume that the empty vessels in native state were non-functional and did not contribute to water transport during the current growing season. To validate that the observed empty vessels were indeed non-functional and were not caused by a cutting artefact (Cochard et al. 2013), micro-CT scans were also made on an intact potted T_{AW} and T_{EW} (Fig. 3.4). Only the native state was measured here, so that quantification relative to the total amount of vessels was not possible. Comparison between NanoWood and HECTOR scans of regions with empty vessels in the native state resulted in no differences (Figs. 3.2, 3.4). Note that all NanoWood scans of the native state showed an empty ring with the width of one vessel between regions of filled vessels of the first and second growing year (Fig. 3.2). Because this empty ring was also visible in the HECTOR scans, we concluded no cutting artefacts were in play (Fig. 3.4). Therefore, all VCs could be constructed with confidence from the same starting point, being at 0 % AE-related cavitation.

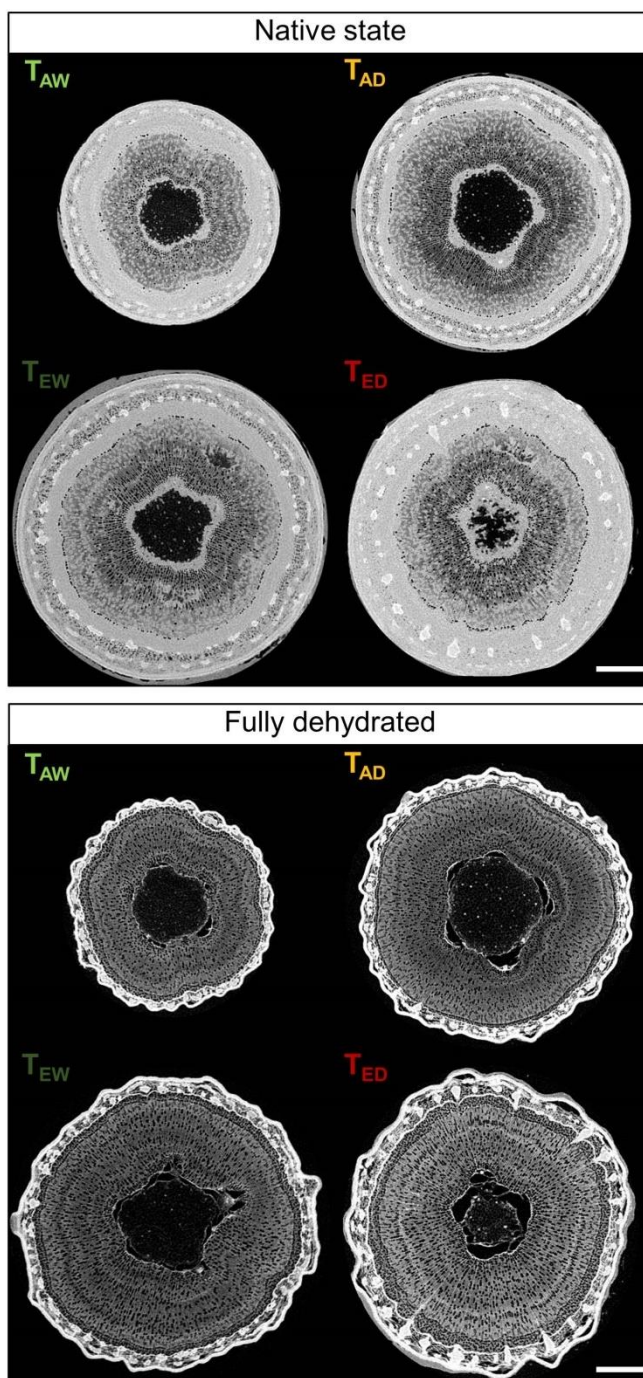


Figure 3.2 Comparison of micro-CT images from the NanoWood scanner between native states, prior to dehydration, and after full dehydration of each treatment. Images were used to identify possible differences in initial state of functional vessels (i.e., filled or empty) between treatments. White and grey areas point to the presence of water and black vessels are empty or air-filled regions. Fully dehydrated scans show the situation at full cavitation, and on these scans it was possible to count the total amount of vessels (as shown in Fig. 3.3). Bright white structures, positioned close to the cambium are probably bundles of phloem fibres with thickened secondary cell walls. T_{AW} and T_{AD} are trees grown in a treatment chamber under ambient temperature and atmospheric $[CO_2]$ (480 ppm), well-watered and drought-stressed, respectively. T_{EW} and T_{ED} are trees grown in a treatment chamber under elevated temperature (+3°C) and atmospheric $[CO_2]$ (707 ppm), well-watered and drought-stressed, respectively. Scale bars are 1 mm.

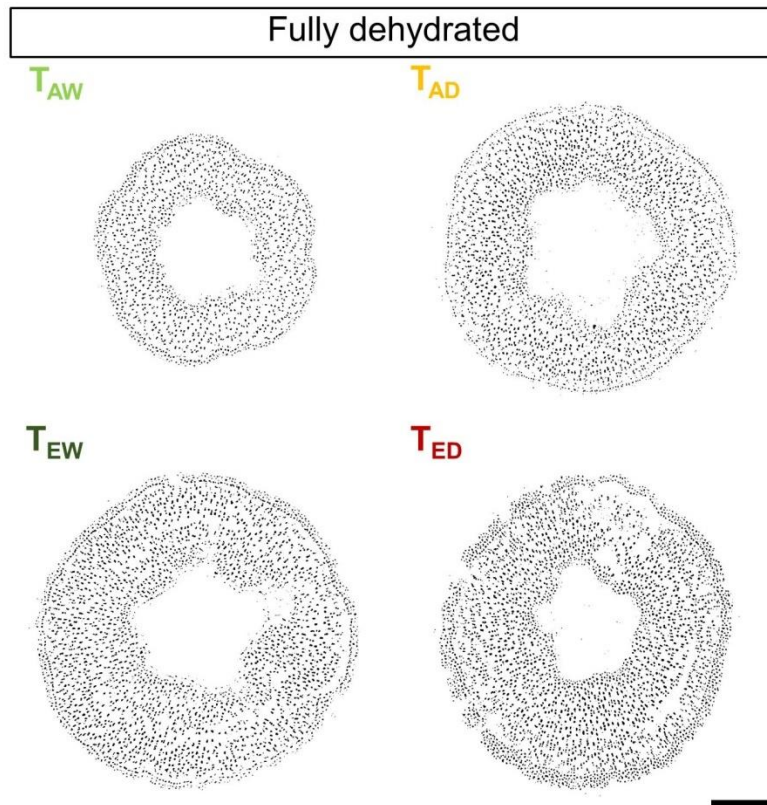


Figure 3.3 Binary map of micro-CT scans of the NanoWood scanner from fully dehydrated samples (as in Fig. 3.2). Black areas are empty vessels and were used to count the total number of xylem vessels (the same procedure was followed on native images). T_{AW} and T_{AD} are trees grown in a treatment chamber under ambient temperature and atmospheric $[CO_2]$ (480 ppm), well-watered and drought-stressed, respectively. T_{EW} and T_{ED} are trees grown in a treatment chamber under elevated temperature (+3°C) and atmospheric $[CO_2]$ (707 ppm), well-watered and drought-stressed, respectively. Scale bar is 1 mm.

Table 3.1 Number of empty vessels counted on the scans from the NanoWood scanner (Fig. 3.2.) Native state of empty vessels was compared with full dehydration to determine the percentage of non-functional vessels and compare treatments. T_{AW} and T_{AD} are trees grown in a treatment chamber under ambient temperature and atmospheric $[CO_2]$ (480 ppm), well-watered and drought-stressed, respectively. T_{EW} and T_{ED} are trees grown in a treatment chamber under elevated temperature (+3°C) and atmospheric $[CO_2]$ (707 ppm), well-watered and drought-stressed, respectively.

Treatment	Native state	Dehydrated	Native/dehydrated
T_{AW}	531	1742	30.5 %
T_{AD}	1248	3301	37.8 %
T_{EW}	1292	3725	34.7 %
T_{ED}	1204	3796	31.7 %
T_W			32.6 %
T_D			34.8 %

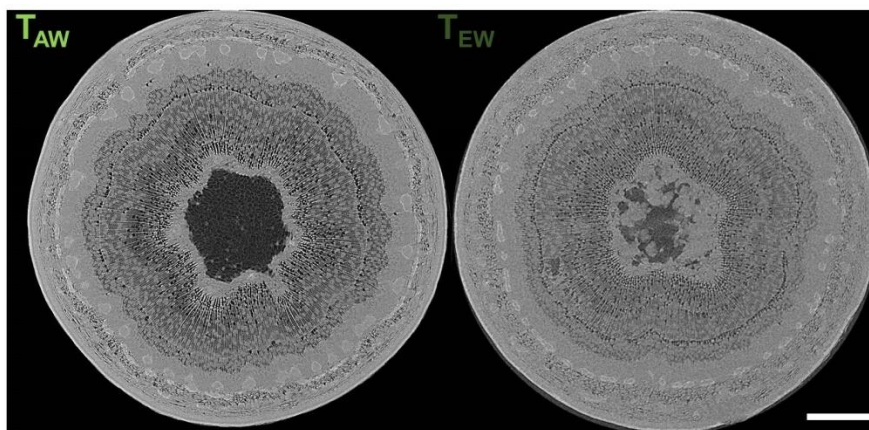


Figure 3.4 Micro-CT scans on an intact potted tree taken with the HECTOR scanner to assess the native state of cavitation *in vivo*. Grey areas show the presence of water and black areas point to empty, air-filled areas. T_{AW} is grown in a treatment chamber under ambient temperature and atmospheric $[CO_2]$ (480 ppm). T_{EW} is grown in a treatment chamber under elevated temperature ($+3^\circ C$) and atmospheric $[CO_2]$ (707 ppm). Both trees were well-watered. Scale bar is 1 mm.

Vulnerability to drought-induced cavitation

Figure 3.5 summarises the different acoustic VCs. In general, ψ_{12} , initial drought-induced cavitation, tended to be more negative for T_W than T_D (Table 3.2). This pattern changed for more negative ψ_x , which showed less negative values for T_D trees (ψ_{88} $p < 0.05$, ψ_{100} $p < 0.05$) (Table 3.2). T_{AD} and T_{EW} differed significantly, with T_{EW} more vulnerable to final drought-induced cavitation (ψ_{88} and ψ_{100} , $p < 0.05$) (Table 3.2). Within T_D and T_W , T_E showed on average a tendency of less negative values for ψ_{50} , ψ_{88} and ψ_{100} than T_A , but this difference was not significant (Table 3.2). Differences between ψ_{88} and ψ_{12} were calculated as a measure to determine how much ψ_x should drop for the trees to go from a relatively safe amount of drought-induced cavitation (ψ_{12}) to a dangerously high amount of drought-induced cavitation (ψ_{88}) (Table 3.2). $\psi_{88} - \psi_{12}$ was significantly larger ($p < 0.05$) in T_D compared to T_W . This factor was on average smallest for T_{EW} , which is visible as the steep VC slope under more negative ψ_x (Fig. 3.5).

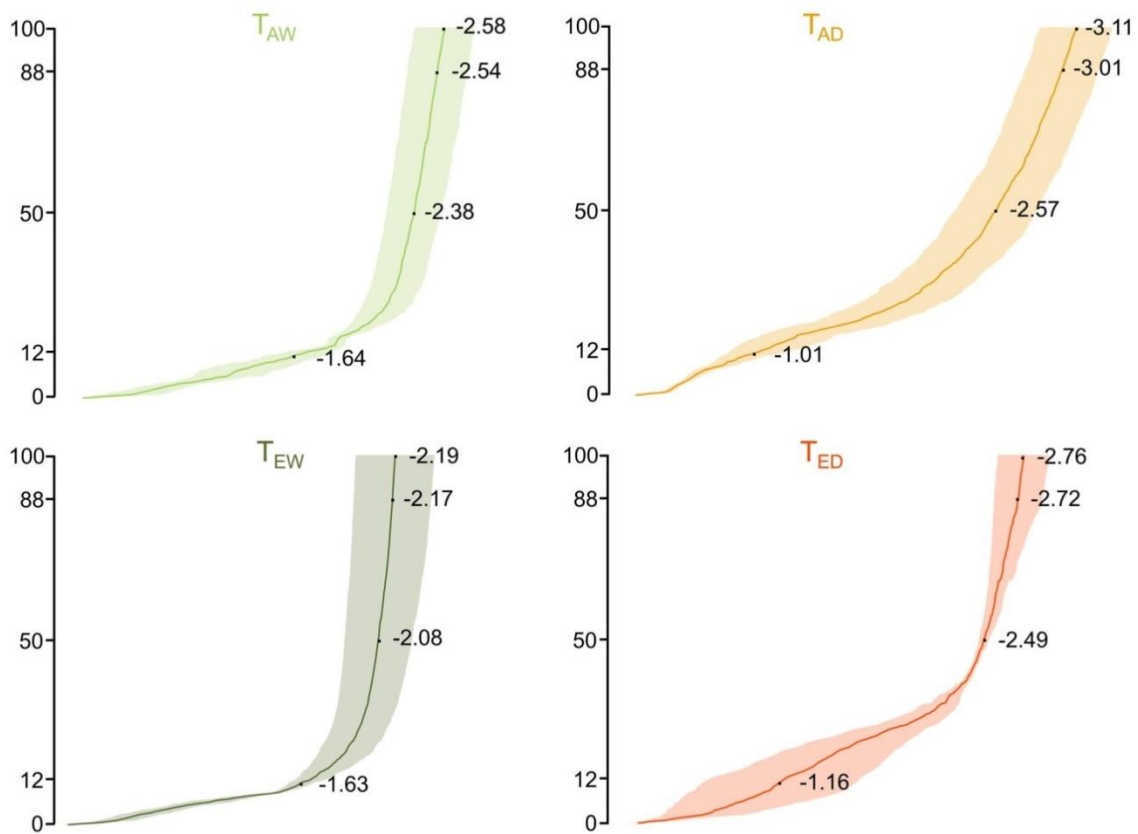
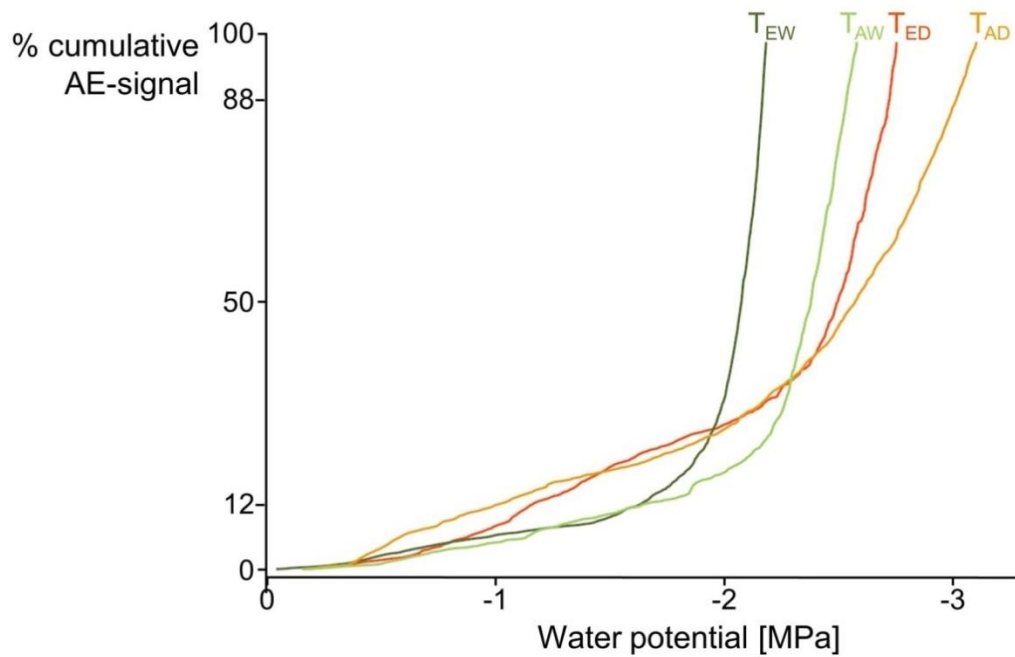


Figure 3.5 Summary of the acoustic vulnerability curves with a detailed panel for each treatment, showing the standard error band (N = 3). Values in the detailed panels show water potentials at 12 %, 50 %, 88 % and 100 % (ψ_{12} , ψ_{50} , ψ_{88} and ψ_{100} , respectively) of cumulated cavitation-related AE signals. T_{AW} and T_{AD} are trees grown in a treatment chamber under ambient temperature and atmospheric $[CO_2]$ (480 ppm), well-watered and drought-stressed, respectively. T_{EW} and T_{ED} are trees grown in a treatment chamber under elevated temperature (+3°C) and atmospheric $[CO_2]$ (707 ppm), well-watered and drought-stressed, respectively.

Table 3.2 Characteristic values derived from the acoustic vulnerability curves (Fig. 3.5): ψ_{12} , ψ_{50} , ψ_{88} and ψ_{100} are xylem water potentials (ψ_x) at 12 %, 50 %, 88 % and 100 % of cumulated cavitation-related AE signals, respectively. Values are averages \pm standard error (N = 3). Letters in superscript identify differences that are significant or tend to be (P < 0.1). Effects of soil water treatment ($T_W - T_D$) is denoted with $^{\circ}$ if the effect tends to be significant (P < 0.1), and with * if the effect is significant (P < 0.05). The effect of the treatment chamber ($T_A - T_E$) is not shown as no significant effects were observed. T_{AW} and T_{AD} are trees grown in a treatment chamber under ambient temperature and atmospheric [CO₂] (480 ppm), well-watered and drought-stressed, respectively. T_{EW} and T_{ED} are trees grown in a treatment chamber under elevated temperature (+3°C) and atmospheric [CO₂] (707 ppm), well-watered and drought-stressed, respectively.

ψ_x [MPa]	T_{AW}	T_{AD}	T_{EW}	T_{ED}	Effect T_W-T_D
ψ_{12}	-1.64 \pm 0.16	-1.01 \pm 0.20	-1.63 \pm 0.01	-1.16 \pm 0.50	$^{\circ}$
ψ_{50}	-2.38 \pm 0.18	-2.57 \pm 0.27	-2.08 \pm 0.13	-2.49 \pm 0.04	
ψ_{88}	-2.54 \pm 0.20 ^{ab}	-3.01 \pm 0.24 ^a	-2.17 \pm 0.15 ^b	-2.72 \pm 0.16 ^{ab}	*
ψ_{100}	-2.58 \pm 0.20 ^{ab}	-3.11 \pm 0.24 ^a	-2.19 \pm 0.15 ^b	-2.76 \pm 0.17 ^{ab}	*
$\psi_{88} - \psi_{12}$	-0.89 \pm 0.33 ^{ab}	-2.00 \pm 0.23 ^a	-0.54 \pm 0.11 ^b	-1.56 \pm 0.60 ^{ab}	*

The DCs of different dehydrating *P. tremula* stems are summarised in Figure 3.6, with the strongest difference observed between T_{AD} and T_{EW} for which hydraulic capacitance tended to differ in the elastic phase (P < 0.1) and differed significantly in the inelastic phase (P < 0.001) (Table 3.3). The transition from initial to elastic phase (breakpoint 1) tended to occur at lower values for T_E trees compared to T_A , and T_{EW} had on average the lowest first breakpoint and initial hydraulic capacitance (Table 3.3). Despite its significantly higher hydraulic capacitance in the elastic and inelastic phase compared to T_{AD} , the ψ_x range in which this stored water was used was relatively narrow (between -1.53 and -2.06 MPa) (Fig. 3.6, Table 3.3). On average, T_{EW} showed the lowest difference between initial stem water content and final stem water content (after full dehydration), which could mean that T_{EW} stems had the lowest amount of water available during dehydration, but these differences were not significant.

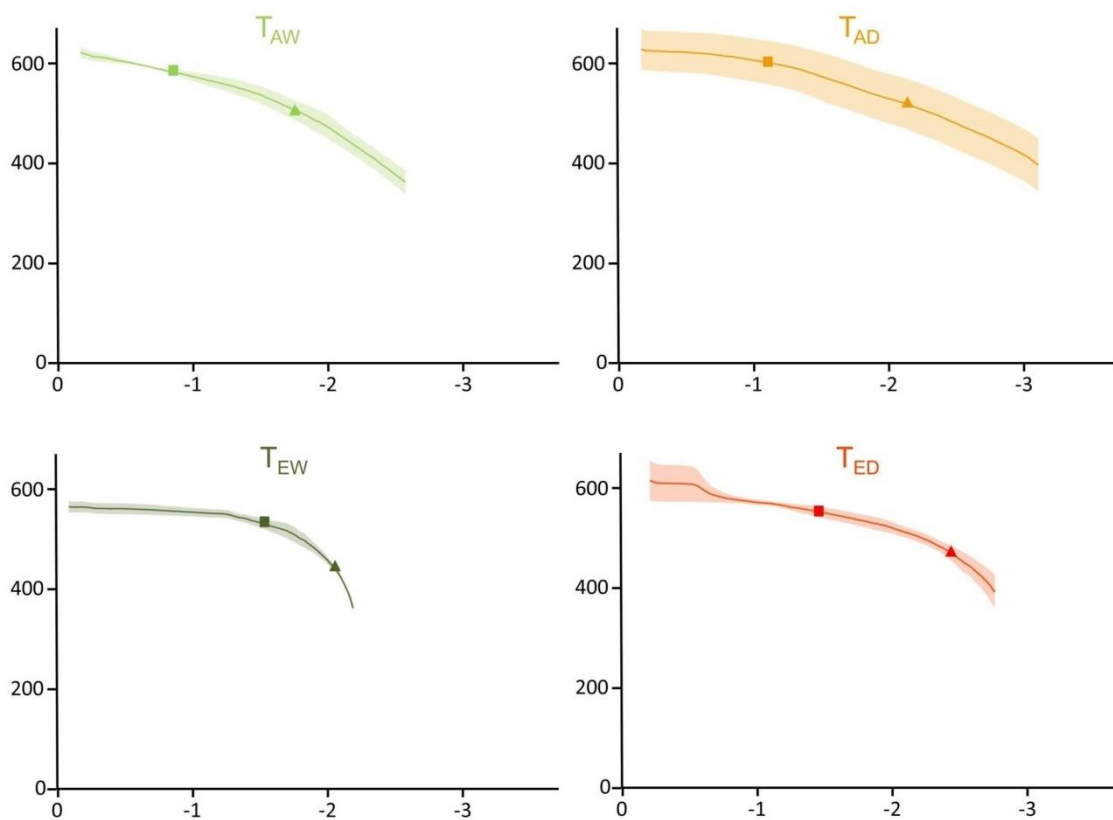
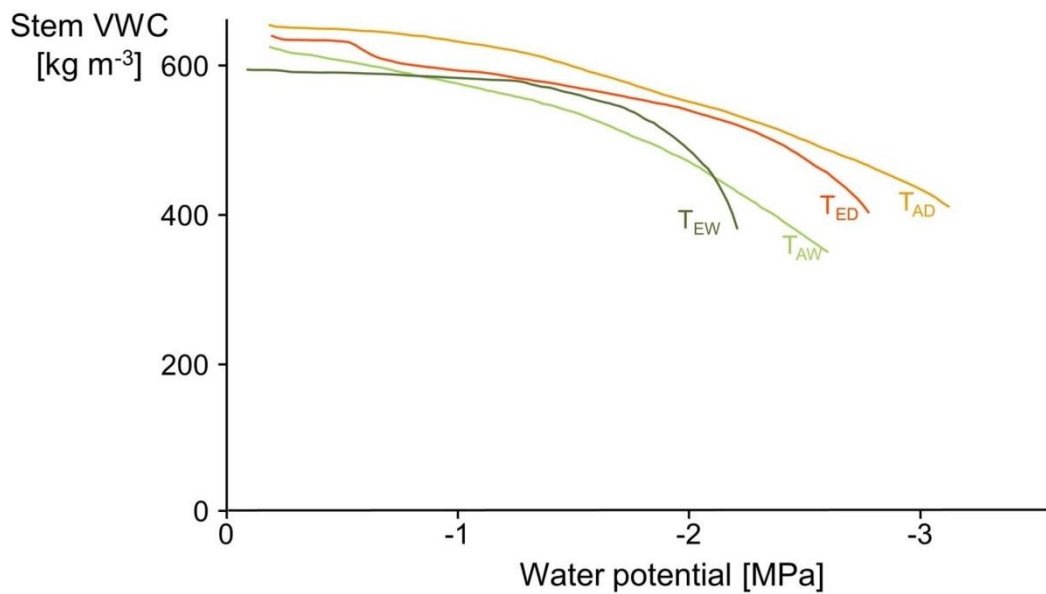


Figure 3.6 Summary of the desorption curves of all treatments with a detailed panel for each treatment, showing the standard error band, ($N = 3$). Squares show the first breakpoint, indicating the transition from capillary to elastic water loss and triangles show the second breakpoint, which is the transition from elastic to inelastic water loss. Breakpoints are identified as points where the curve shows a strong change in slope (i.e., hydraulic capacitance). T_{AW} and T_{AD} are trees grown in a treatment chamber under ambient temperature and atmospheric [CO_2] (480 ppm), well-watered and drought-stressed, respectively. T_{EW} and T_{ED} are trees grown in a treatment chamber under elevated temperature ($+3^\circ\text{C}$) and atmospheric [CO_2] (707 ppm), well-watered and drought-stressed, respectively.

Table 3.3 Stem water content at the start of bench-top dehydration, basic wood densities, water potential at the transition from initial to elastic phase (breakpoint 1) and from elastic to inelastic phase (breakpoint 2), and hydraulic capacitances derived from the slopes of the desorption curves (Fig. 3.6). Values are averages \pm standard error ($N = 3$). Effects of soil water treatment ($T_W - T_D$) and treatment chamber ($T_A - T_E$) are given with $^\circ$ if differences tend to be significant ($P < 0.1$), with $*$ if significant with $P < 0.05$, with $**$ if significant with $P < 0.01$ and with $***$ if significant with $P < 0.001$. T_{AW} and T_{AD} are trees grown in a treatment chamber under ambient temperature and atmospheric $[CO_2]$ (480 ppm), well-watered and drought-stressed, respectively. T_{EW} and T_{ED} are trees grown in a treatment chamber under elevated temperature ($+3^\circ C$) and atmospheric $[CO_2]$ (707 ppm), well-watered and drought-stressed, respectively.

	T_{AW}	T_{AD}	T_{EW}	T_{ED}	Effect T_W-T_D	Effect T_A-T_E
Initial stem water content [$kg\ m^{-3}$]	624 ± 11	652 ± 43	594 ± 11	634 ± 42		
Wood density [$kg\ m^{-3}$]	389 ± 23	349 ± 17	411 ± 9	367 ± 24	$^\circ$	
Breakpoints [MPa]						
Breakpoint 1	-0.88 ± 0.15	-1.12 ± 0.14	-1.53 ± 0.20	-1.46 ± 0.34		$^\circ$
Breakpoint 2	-1.78 ± 0.10	-2.15 ± 0.46	-2.06 ± 0.26	-2.43 ± 0.21	*	
Endpoint	-2.58 ± 0.20^{ab}	-3.11 ± 0.24^a	-2.19 ± 0.15^b	-2.76 ± 0.17^{ab}	*	
Capacitance [$kg\ m^{-3}\ MPa^{-1}$]						
Initial phase	54 ± 20	27 ± 9	18 ± 1	68 ± 50		
Elastic phase	103 ± 14^{ab}	83 ± 13^a	226 ± 72^b	92 ± 8^{ab}	$^\circ$	
Inelastic phase	201 ± 47^a	146 ± 26^a	619 ± 64^b	254 ± 55^a	**	***

Discussion

Native state of cavitation in P. tremula stems

In general, measurements of VC can be prone to cut artefacts upon sampling, which have led to erroneous VC derived traits in the past (Cochard et al. 2010, Cochard et al. 2013, Sperry 2013). A comparison between scans of potted intact trees and cut stems indicated that cut artefacts were not an issue in our experiment (Figs. 3.2, 3.4). We however observed a relatively large number of non-functional vessels in all scanned stems, ranging from 30.5 – 37.8 % (Table 3.1). If we had flushed our samples and had refilled by doing so, our

measurements would have been less reliable because also the non-functional vessels would have contributed to the acoustic VCs. This would make interpretation of the results more complex, as it remains difficult to know whether cavitation is caused by a treatment effect or by events from the past seasons (Sperry et al. 2012, Cochard et al. 2013, Trifilò et al. 2014). Although T_W trees received ample soil water, which limited the risk of cavitation, micro-CT scans in the native state showed empty vessels around the tree centre, which originated from the previous growing season. Similarities between regions and amounts of cavitation between T_W and T_D , showed that the drought treatment did not considerably impacted the number of functional vessels.

Trees are most vulnerable to drought-induced cavitation when well-watered and grown in elevated temperature and [CO₂]

Acoustic VCs showed that soil water had the strongest impact on vulnerability to drought-induced cavitation (Fig. 3.5, Table 3.2). When trees were well-watered (T_W), stems proved to be more vulnerable to cavitation in the more negative ψ_x range (ψ_{88} , ψ_{100}). In general, there is a high degree of plasticity in resistance towards drought-induced cavitation with species growing in more arid biomes showing more negative average ψ_{50} values, albeit a great interspecific variation exists within ecosystems (Maherali et al. 2004). Also intraspecific variation is not uncommon in response to different degrees of soil water availability (Ladjal et al. 2005, Stiller 2009, Awad et al. 2010, Vilagrosa et al. 2012). Our findings support the observation that most poplar hybrids are less vulnerable to drought-induced cavitation when grown under soil drought (VCs determined with centrifugation method; Awad et al. (2010), Fichot et al. (2010)). The difference between what is considered the onset of cavitation (ψ_{12}) and the lethal point, or point of no return (ψ_{88}), is a good indicator to express the shape of vulnerability curves (Domec and Gartner 2001, Fichot et al. 2015) and significantly differed between T_W and T_D , with T_W showing smallest ranges and thus steepest VCs (Table 3.2, Figure 3.5). These differences probably originated from anatomical acclimation to the soil water availability with likely smaller but more vessels in response to drier conditions as has been shown in poplar hybrids by Fichot et al. (2009).

Despite the early call of Tyree and Alexander, back in 1993, to perform research on the effect of elevated $[\text{CO}_2]$ on drought-induced cavitation, only four studies so far actually developing VCs to assess CO_2 effects have been performed to date (Tognetti et al. 1999, Tognetti et al. 2001, Domec et al. 2010, Warren et al. 2011), none of them investigating interaction effects with soil drought (Table 3.4). In Mediterranean species, a small reduction in vulnerability to drought-induced cavitation was found for trees grown near a natural CO_2 -spring (Table 3.4) (Tognetti et al. 1999, Tognetti et al. 2001). In North-American deciduous forests, FACE-experiments showed no effect or an increase in vulnerability to drought-induced cavitation under elevated $[\text{CO}_2]$ (Table 3.4) (Domec et al. 2010, Warren et al. 2011). These studies differed with ours in the method to construct VCs, in sample material (branches versus stems), and in flushing protocol (flushed versus native). When flushed, non-functional vessels will be refilled, potentially resulting in less negative ψ_x values for a percentage loss of conductivity (Sperry et al. 2012, Cochard et al. 2013, Trifilò et al. 2014). Upon flushing, we would have artificially increased the number of functional vessels by 50 % (Fig 3.2, Table 3.1).

Our results did not show a significant effect of elevated $[\text{CO}_2]$, but average values showed a tendency to more vulnerable stems in both T_W and T_D and the same response to drought (Fig. 3.5, Table 3.2). With a similar response to drought in ambient and elevated $[\text{CO}_2]$, predictions of stem vulnerability to drought-induced cavitation under elevated $[\text{CO}_2]$ might be done with the current knowledge on plastic drought responses, but accounting for a probable increase in vulnerability due to elevated $[\text{CO}_2]$. Differences in average values tended to be present and if so important, but variation within treatments was relatively high and the number of samples limited. Future experiments should be carried out with a higher number of replications to assess whether the revealed tendencies are treatment effects or caused by biological variation.

Table 3.4 Overview of studies investigating effect of elevated [CO₂] on VC measurements. Hydraulic method is explained in Sperry et al. (1988), and centrifuge method in Alder et al. (1997). h = height, D = diameter and l = length.

Species	Tree life stage	location	Elevated [CO ₂]	VC method	Native state	Main finding	Study
<i>Quercus ilex</i> L. <i>Quercus pubescens</i> Willd. <i>Fraxinus ornus</i> L. <i>Populus tremula</i> L. <i>Arbutus unedo</i> L.	Mature trees h = 3-9 m, D = 60-150 mm	Mediterranean forest Italy	Natural CO ₂ spring 700 ppm	Branches, 3-5 years old, cut in the field l = 150-200 cm Hydraulic method	Relaxated in water and flushed	Effects of elevated [CO ₂] were small and followed no particular trend.	Tognetti et al. (1999)
<i>Erica arborea</i> L. <i>Myrtus communis</i> L. <i>Juniperus communis</i> L.	Mature shrubs h = 1.5-3 m	Mediterranean forest Italy	Natural CO ₂ spring 700 ppm	Branches, 3-5 years old, cut in the field l = 60-110 cm Hydraulic method	Relaxated in water and flushed	Effects of elevated [CO ₂] were small, but a trend to lower vulnerability was observed	Tognetti et al. (2001)
<i>Liquidambar styraciflua</i> L. <i>Cornus florida</i> L. <i>Pinus taeda</i> L. <i>Ulmus alata</i> Michx.	Mature trees h = 4.6-6.4 m, D = 40-56 mm h = 4.1-5.8 m, D = 34-55 mm h = 13.7-15.8 m, D = 147-189 mm h = 5.1-7.8 m, D = 43-88 mm	Deciduous forest North Carolina USA	FACE since 1993 +200 ppm	Branches, cut in the field D = 2.8-7.6 mm l = 14.2 cm Centrifuge method	Flushed	Elevated [CO ₂] increased xylem vulnerability in <i>L. styraciflua</i> and <i>C. florida</i>	Domec et al. (2010)
<i>Liquidambar styraciflua</i> L.	Mature 19 years old h = 7.8-23.6 m, D = 25-125 mm	Deciduous forest Tennessee USA	FACE since 1998 525-555 ppm	Branches, 1 year old, cut in the field l = 20-35 cm, D = 5-10 mm Hydraulic method	Refilling under vacuum by submersion in solution	Elevated [CO ₂] increased xylem vulnerability in <i>L. styraciflua</i>	Warren et al. (2011)

Based on acoustic VCs, T_{EW} was on average most vulnerable to drought-induced cavitation (Figure 3.5, Table 3.2), and when considering associated DCs, T_{EW} displayed the most different behaviour (Fig. 3.6, Table 3.3). T_{EW} seemed to use capillary water across a larger ψ_x range compared to the other treatments (breakpoint 1 at -1.53 MPa) but associated hydraulic capacitance was low (Table 3.3). This implies that capillary stored water could only marginally buffer changes in xylem water potential during the initial phase of dehydration. The higher elastic and inelastic hydraulic capacitances observed in T_{EW} covered limited ranges at relatively low ψ_x , which might have hampered xylem protection from cavitation events. Water released during cavitation within the $\psi_{88} - \psi_{12}$ range considerably contributed to the high inelastic capacitance of T_{EW} (Tyree and Yang 1990, Lo Gullo and Salleo 1992, Hölttä et al. 2009, Vergeynst et al. 2015a). It also seemed that T_{EW} showed the lowest reduction in overall stem water content during dehydration, which supported the limited xylem buffering capacity (Fig. 3.6). The low hydraulic capacitance resulting from stored capillary water indicates that T_{EW} relied more on xylem structural features than on hydraulic capacitance to limit cavitation (Meinzer et al. 2009). But such structural features might make the trees more vulnerable when a threshold in ψ_x is exceeded, which might explain the steep increase in cavitation-related AE observed in T_{EW} . Domec et al. (2016) suggested that the higher availability of assimilates under elevated $[CO_2]$ might stimulate cell wall formation and increase vessel pore size, which enhances cavitation propagation (Choat et al. 2005, Wheeler et al. 2005). This would lead to an increase in wood density, and indeed, wood density was on average highest in T_{EW} , which supports the lower hydraulic capacitance under less negative ψ_x (Table 3.3). As explained in Chapter 2 (Text box 2.2), low capacitance is related to low cell wall elasticity and extensibility, caused by thicker cell walls (Lockhart 1965, Cosgrove 2016).

Will other physiological changes, related to elevated $[CO_2]$, guard trees against a higher cavitation vulnerability?

P. tremula trees showed a tendency to be more vulnerable to drought-induced cavitation when grown under elevated temperature and $[CO_2]$, with soil drought likely having caused a similar plastic response under ambient and elevated conditions. Although its VC-derived characteristics are considered as

good indicators to assess drought-vulnerability (Maherali et al. 2004, Meinzer et al. 2009, Choat et al. 2012, Cochard et al. 2013, Lens et al. 2016), trees have been shown to use different mechanisms to control water potential (Meinzer and McCulloh 2013). If trees are able to maintain less negative average ψ_x values, and limit large drops in ψ_x during drought, VC-based comparison between T_A and T_E of vulnerability to drought-induced cavitation becomes less straightforward. Elevated $[CO_2]$ indeed affects leaf gas exchange, causing a decrease in stomatal conductance and in leaf transpiration, which, in turn, increases ψ_x . A review by Domec et al. (2016) reports a small positive effect (less negative leaf water potential (ψ_l) under elevated $[CO_2]$) in ring-porous angiosperms, and a small (both positive and negative) or no effect in diffuse-porous species. In one-year-old peach (*Prunus persica* L.) and two-year-old cherry (*Prunus avicum* L.) trees, ψ_l was not affected by elevated $[CO_2]$ (700 ppm), both under well-watered and dry conditions (Centritto et al. 1999b, Centritto et al. 2002). Also in both young and mature trees of *Eucalyptus saligna* Sm., *E. sideroxylon* A.Cunn. ex Woolls, *E. radiata* Sieber ex DC., and *E. tereticornis* Sm. no consistent change in ψ_l was reported in response to elevated $[CO_2]$, both in greenhouse and free-air (Phillips et al. 2011, Duan et al. 2014, Gimeno et al. 2016). These studies suggest that ψ_l is not mitigated by elevated $[CO_2]$ and thus that more drought-vulnerable results from VCs under elevated $[CO_2]$ will also result in more drought-vulnerable trees, in spite of other physiological responses to elevated $[CO_2]$.

Despite the projected mitigation effect of elevated $[CO_2]$ via reduction in transpirational water loss, the limited number of available studies illustrate that often adjustments and acclimation to elevated $[CO_2]$ not necessarily make trees less vulnerable to drought (Heath and Kerstiens 1997, Centritto et al. 1999b, Warren et al. 2011, Duan et al. 2014, Allen et al. 2015, Domec et al. 2016). Elevated $[CO_2]$ often increases biomass production and leaf development (Centritto et al. 1999a, De Luis et al. 1999, Ferris et al. 2001, Wullschleger et al. 2002, Calfapietra et al. 2003, Gielen et al. 2005, Allen et al. 2015), which results in a higher water-use (see also Chapter 2) and thus a more rapid soil water depletion (Heath and Kerstiens 1997, Wullschleger et al. 2002). Since elevated $[CO_2]$ does not seem to (i) improve water status (with ψ_l as important proxy) or (ii) decrease vulnerability to drought-induced cavitation (Fig. 3.5, Table 3.2), the

small HSM in which trees currently operate globally might prove insufficiently safe in future conditions (Choat et al. 2012). With only a narrow HSM, increased growth rates, and lack of drought-proof adaptations, trees and forests may face great challenges in case of hotter droughts, which are predicted to become only more frequent and harsh in the future (Allen et al. 2015).

Conclusion

A two-months growing period under elevated air temperature and atmospheric [CO₂] in different soil water regimes caused substantial changes in vulnerability to drought-induced cavitation in one-year old *P. tremula* trees: vulnerability decreased when grown under lower soil water availability and showed a tendency to increase under elevated temperature and [CO₂]. Well-watered trees grown in elevated [CO₂] were most vulnerable to drought as demonstrated by their vulnerability and desorption curves. The low hydraulic capacitance, which only increased under considerably negative water potential, might have contributed to this pronounced response to drought, in addition to the narrow margin in water potential between safe and perilous levels of cavitation in T_{EW} trees. Such response might turn out to be adverse in the outlook of more and harsher hotter droughts.

4

CHAPTER 4

Plant-PET scans: *in vivo* mapping of xylem and phloem functioning

Redrafted from: Hubeau, M. and K. Steppe. 2015. Plant-PET scans: *in vivo* mapping of xylem and phloem functioning. Trends in Plant Science **20**:676-685.

Abstract

Knowledge on plant-carbon relations is much more limited compared to plant-water relations, because of the difficulties to measure carbon transport. Positron emission tomography (PET) is advancing as a powerful functional imaging technique to decipher *in vivo* the function of xylem water flow (with ^{15}O or ^{18}F), phloem sugar flow (with ^{11}C or ^{18}F), and the importance of their strong coupling. Both under present and future climate regimes, much remains to be learned about how water flow and sugar distribution are coordinated in intact plants. Here, we review and explore the use of plant-PET to visualise and generate the necessary yet missing data about integrated xylem and phloem transport, which is imperative for us to understand how a given environment will affect plant physiological processes and growth.

PET scanners are ready to bridge the gap between medical and plant sciences

PET (positron emission tomography) scanners have been developed to give the medical world a tool to measure the activity of organs, cell aggregates, or brain zones. With the positron-emitting radioactive molecule fluorodeoxyglucose (^{18}F FDG), a proxy for sugar, cancerous lesions can now be readily located because of their higher metabolic activity, and brain functioning can be mapped by imaging active and passive brain zones (Raichle 2009, Wehrl et al. 2013). Whereas ^{18}F FDG is currently the most widely used radiopharmaceutical in PET, many other positron-emitting radionuclides are available for clinical use (Vallabhajosula et al. 2011). Despite the wide use of PET in the medical field, only a few plant-PET experiments have been undertaken. There is, however, no reason why PET could not be widely used in plant science, because humans and plants are similar at cellular and biochemical level (Alberts et al. 2013), which makes the use of PET scanners transferable to plant research. In addition to mapping spots with higher or lower metabolic activity, the dynamic information that can be derived from plant-PET is of particular interest. Where does water and sugar flow to and at what speed, how are axial and lateral movements coordinated, and what is the importance of xylem–phloem interactions? In the same way as medical PET scans led to major breakthroughs in explaining organ function and detecting health issues in humans, PET has the potential to rapidly advance our understanding of xylem and phloem function, the dynamic interactions that exist between xylem and phloem, and the extent to which these two long-distance transport pathways aid or hamper each other's function in a given environment (Thompson 2006, Zwieniecki and Holbrook 2009, Knoblauch and Peters 2010, Secchi and Zwieniecki 2011, Anderegg et al. 2012, Ryan and Asao 2014, Sevanto 2014, Steppe et al. 2015).

Water and sugar as the alpha and omega of plants

For centuries, scientists have been fascinated by water and sugar flow in plants, because of their vital importance for plant growth and life. If we aspire to explain plant growth or to increase forest conservation and management, but also

agriculture productivity, it is crucial that we understand the dynamics and the controls of water and sugar flow, as well as their interactions. This is essential to unravel how plants function, how they cope with stress, and which features determine whether a plant thrives or dies. Water transport through the xylem is essential for plants and any malfunction may result in some degree of drought stress (Porporato et al. 2001, Anderegg et al. 2012). The phloem, responsible for the distribution of sugars throughout the plant, ensures that all cells are supplied with fuel for maintenance and growth (Sala et al. 2012, De Schepper et al. 2013b, Steppe et al. 2015). If the supply of sugar is reduced, a plant will have fewer resources to grow and maintain its living cells (Epron et al. 2012, De Schepper et al. 2013b, Steppe et al. 2015). These two long-distance transport pathways are also highly interlinked. For instance, phloem transport will only operate under the requisite of both sufficient water and sugars, and stomatal regulation controls carbon uptake and water loss and is responsive to leaf water status, but also carbon assimilation and phloem loading (Nikinmaa et al. 2013).

The importance of highly interconnected xylem and phloem also emerges in drought-related plant studies. It is well known that drought hampers photosynthesis (Pinheiro and Chaves 2011, Bauweraerts et al. 2013, Teskey et al. 2014). Nevertheless, this drought-related reduction in photosynthesis also results in a smaller water flow from xylem to phloem at the sources owing to a decrease in phloem loading (Steppe et al. 2015). Furthermore, it has been speculated that drought may lead to lower cell wall permeability, which may result in reduced water supply to the phloem, as well as increased viscosity because of the decreased dilution of sugars (Sevanto 2014). A too-syrupy fluid and a weak pressure gradient in the sieve elements will hamper the proper function of phloem transport and sugar distribution (Sevanto 2014), and may greatly weaken the plant (Anderegg et al. 2012). These examples illustrate that, without a proper functioning of the xylem also phloem functioning will be constrained, but these interactions are currently understudied, because methodological approaches have not advanced sufficiently to routinely study these interactions. Many open questions remain about xylem–phloem interactions in a changing environment. Will the reduction in sugar or rather the reduction in water have the largest impact (Sevanto et al. 2014)? Will reduced turgor pressure cause problems for phloem transport or will it be instead the increased viscosity of the sugar sap (Sevanto

2014)? Will sources and sinks behave and compete differently under a changing climate regime (Minchin and Thorpe 2003)? To what extent will plants be able to adapt or avoid these above-mentioned problems? Plant-PET scans and, by extension, all functional medical imaging techniques, may help answering these vital questions to further our knowledge of drought tolerance and resilience, growth, reproduction, and yield.

Measurements of water and sugar flow with PET

PET scanners make use of high-energy decay of short-lived radioactive isotopes to visualise their distribution (Text Box 4.1, Fig. 4.1a for the physical principles behind PET). PET can be used to visualise water flow in intact plants with H_2^{15}O or ^{18}F (Fig. 4.2) (Mori et al. 2000, Kiyomiya et al. 2001, Nakanishi et al. 2002, Kiser et al. 2008, Ohya et al. 2008, Kang et al. 2009, Converse et al. 2015). The fluorine atom is used as an apoplastic proxy for water because the size of fluorine and hydrogen are comparable and thus both behave and bond similarly (Vallabhajosula et al. 2011). Because of its higher half-life (respectively, 109.8 min versus 2.03 min; Table 4.1), ^{18}F is preferred over ^{15}O in experiments where water transport needs to be studied over a longer period (Kiser et al. 2008, Kang et al. 2009, Converse et al. 2015). With H_2^{15}O , Ohya et al. (2008) demonstrated the occurrence of lateral water exchange during water transport towards the leaves. This lateral water supply is not only important for sugar transport when it is directed from xylem to phloem (De Schepper et al. 2013b, Sevanto 2014), but it also plays a crucial role as hydraulic capacitance when water is released from internal phloem water reserves to help buffering abrupt changes in xylem water potential (Steppe et al. 2006, Steppe et al. 2012). In addition, aquaporins are expected to play an important role in this lateral water movement (Ohya et al. 2008, Steppe et al. 2012, Li et al. 2014).

Text box 4.1 A brief introduction to PET

Positron emission tomography (PET) is a non-invasive and *in vivo* functional imaging technique that, when applied with plants, produces a 3-D image of transport and distribution in the vascular tissues (Kiser et al. 2008, Jahnke et al. 2009, Kim et al. 2013). PET is based on coincident detection of antiparallel γ -rays (180°) with an energy of 511 keV, produced by the annihilation of an electron (e^-) and a positron (β^+), the latter being emitted by a short-lived radionuclide tracer upon decay (Fig. 4.1a) (Minchin and Thorpe 2003, Verel et al. 2005). The most important short-lived radionuclides used in biological studies are ^{11}C , ^{13}N , ^{15}O , and ^{18}F (Table 4.1) (Minchin and Thorpe 2003, Kiser et al. 2008, Kim et al. 2013). These isotopes have a short half-life time ($t_{1/2}$), which makes them ideal for studying short-term processes (minutes to hours) because of their high signal output during the short time period they exist. The downside is that positrons have to travel a small distance before they annihilate (Table 4.1, Fig. 4.1a), which fundamentally limits the maximum attainable resolution of PET (Bailey et al. 2005, Kiser et al. 2008, Jahnke et al. 2009, Bühler et al. 2011, Moses 2011).

Scintillators detect γ -rays, formed during annihilation, and the signal is enhanced by photomultipliers (Fig. 4.1a). Typically, a trade-off between resolution (~ 1 mm) and sensitivity (~ 1 %) is set by specifying the acceptance angle for opposite scintillators and defining the time interval in which coincident events may occur, typically < 20 ns (Uchida et al. 2004, Jahnke et al. 2009, Kim et al. 2013). A smaller acceptance angle or shorter time interval increases resolution but decreases sensitivity. In large PET systems (such as full-body PET), positron acolinearity needs to be accounted for (Park et al. 2007).

In leaves, many decay events occur close to the surface, which results in a large fraction (up to 60 %) that escapes into the atmosphere before annihilating (Alexoff et al. 2011, Partelová et al. 2016). This undetected fraction can be strongly reduced by placing positron shields made of plastic or aluminium foil, but interferences with plant physiology (e.g., transpiration or light interception) should be accounted for (Alexoff et al. 2011). Unless thick wood samples are measured, attenuation and scatter should not cause significant effects (Kim et al. 2013).

To generate an accurate image, data handling is required – including corrections for scatter and random events, attenuation, detector efficiency, geometry, and system dead-time (Beer et al. 2010, Kim et al. 2013). Furthermore, the exponentially decreasing tracer activity needs to be decay-corrected, which increases noise with time, and limits scanning time to about 7 – 9 half-lives (Table 4.1) (Ewers and Oren 2000, Kiser et al. 2008, Minchin 2012). A PET scanner only detects a line of response (connecting opposing scintillators) where the annihilation took place, and during data handling the signal is spread with a software-based probability distribution over several pixels. New developments are underway that will further improve the resolution (to sub-mm resolution) and quantitative accuracy (Alessio et al. 2010, Moses 2011).

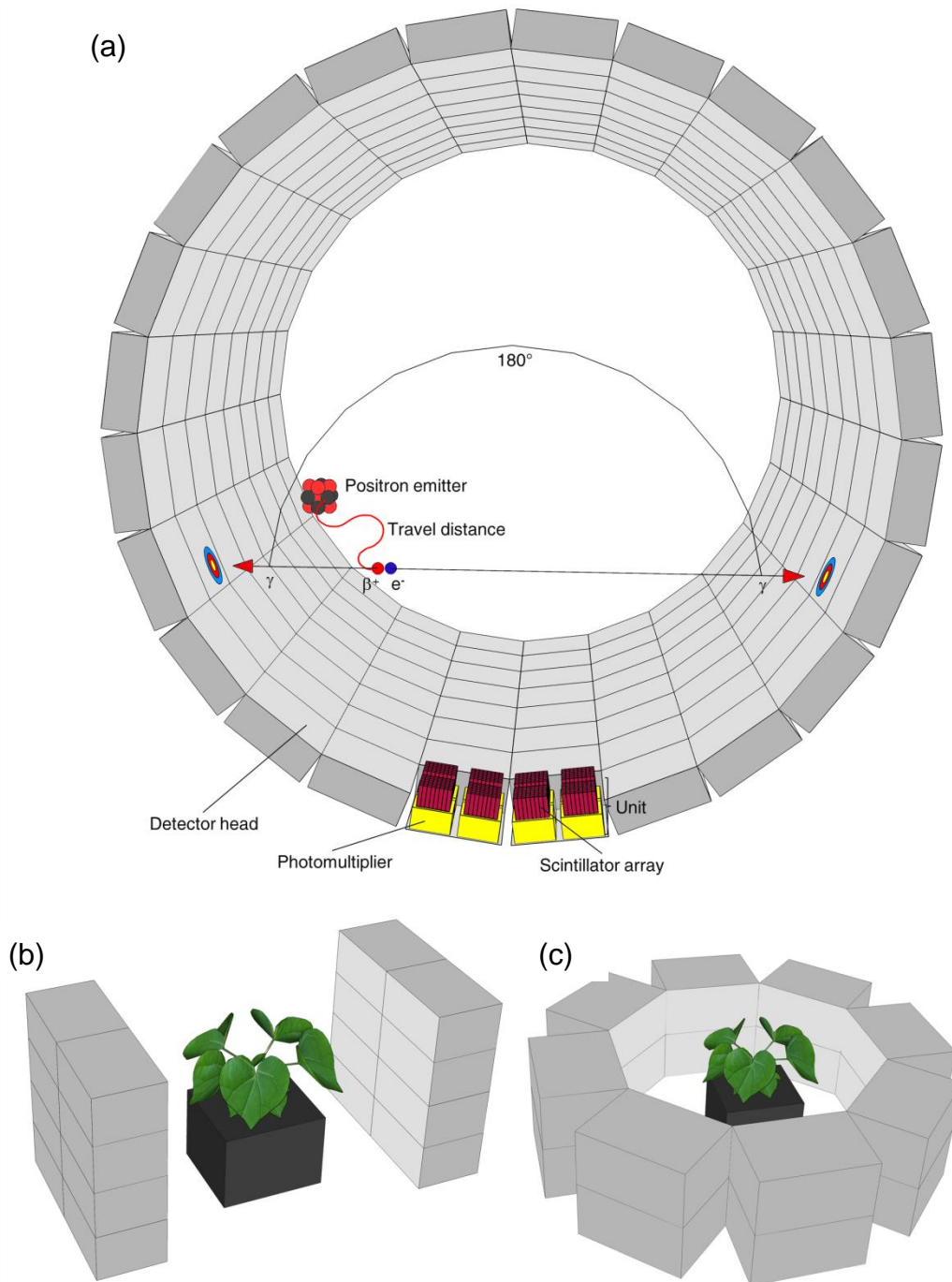


Figure 4.1 Positron emission tomography (PET) detection systems. (a) The most commonly used clinical PET scanner configuration is a ring detection system. A detection ring consists of many detectors with several units. Each unit has an array of scintillators connected to a photomultiplier. The reaction inside the cylinder depicts annihilation: a decaying radionuclide emits a positron (β^+), which meets an electron (e^-) within a short travel distance, leading to annihilation that resulting in the back-to-back (180°) emission of two γ -rays with an energy of 511 keV. Both γ -rays can be detected by scintillators within a specified time interval, and are registered as a coincident signal. Non-coincident signals are rejected, making the use of collimators redundant. Other arrangements of PET modules are possible, and exist, and (b) the planar and (c) the circular configuration, representing the most promising developments in plant-PET applications (Weisenberger et al. 2013).

Table 4.1. Overview of the most commonly used short-lived positron-emitting radionuclides in biological research (Bailey et al. 2005, Jødal et al. 2012). $t_{1/2}$ is Half-life time of the radionuclides and mean travel distance in water is the distance which the emitted positron travels on average before annihilating with an electron. This is an important factor in determining the resolution of PET.

Radionuclide	$t_{1/2}$ [min]	Mean travel distance in water [mm]
^{11}C	20.4	1.1
^{13}N	9.96	1.5
^{15}O	2.03	2.5
^{18}F	109.8	0.6

Whereas many alternatives exist to quantify water flow *in vivo*, ranging from the use of heat as a tracer (Chapter 2) (Vandegheuchte and Steppe 2013), to magnetic resonance imaging (Windt et al. 2006, Sardans et al. 2010, Borisjuk et al. 2012) and neutron imaging (Defraeye et al. 2014), the options are much more limited for *in vivo*, non-invasive carbon quantification. This is where the isotope ^{11}C may contribute significantly (Keutgen et al. 2005, Matsushashi et al. 2005, Kikuchi et al. 2008, Kiser et al. 2008, Jahnke et al. 2009, Kawachi et al. 2011, Garbout et al. 2012, De Schepper et al. 2013a, Weisenberger et al. 2013) (Fig. 4.2). This short-lived isotope can be widely used because of the presence of carbon in many plant molecules. The most straightforward way to make use of ^{11}C is to feed gaseous $^{11}\text{CO}_2$ to a leaf. Uptake of this primary substrate for photosynthesis will be incorporated into photoassimilates, and the distribution of the ^{11}C -labelled sugars can be imaged with PET for several hours (Text box 4.1). PET scanning has been used to examine the dynamics of carbon distribution in roots and fruits. Roots, that are otherwise difficult to investigate, can be imaged with PET (Garbout et al. 2012), which enabled a clear analysis of the active root tips (Wang et al. 2014). In storage organs, including roots and fruits, sectoriality has been observed, with specific leaves supplying assimilates to specific parts of the organ (Kikuchi et al. 2008, Jahnke et al. 2009). Consecutive PET measurements on these storage organs can map the active zones as well as the distribution of assimilates, which is imperative for us to better understand growth and development of such important structures (Kikuchi et al. 2008, Jahnke et al. 2009, Kawachi et al. 2011). Carbon transport and its sectoriality can also be studied in stems with PET (De Schepper et al. 2013a). Blockage and subsequent

changes in the phloem transport pathway throughout the entire tree following girdling were visualised with PET, demonstrating that, already after one day, new paths were used to bypass the interrupted phloem vessels (De Schepper et al. 2013a).

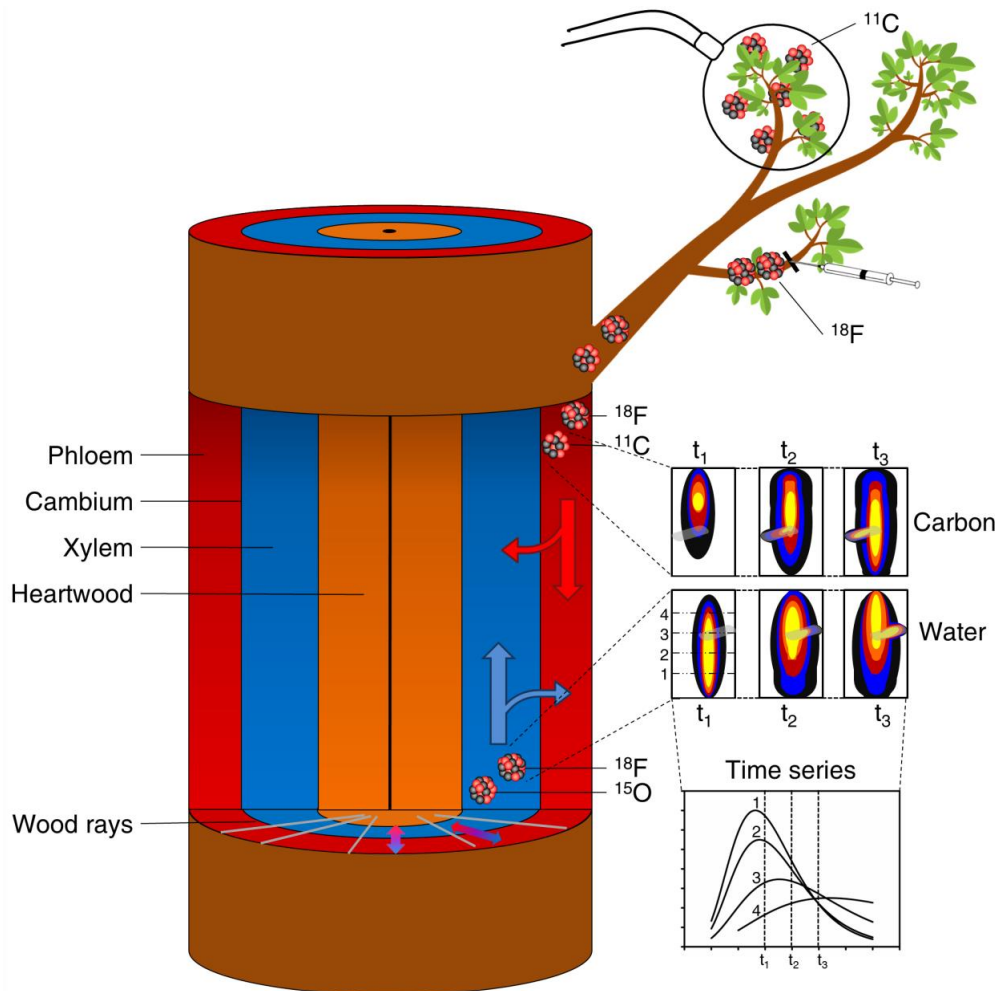


Figure 4.2. Schematic of transport processes in xylem and phloem which can be mapped with positron emission tomography (PET). In general, carbon is transported downward in the phloem and water is transported upward in the xylem. Lateral exchanges of both water and carbon takes place between phloem and xylem. Transport of water can be imaged by supplying a solution of water containing ^{15}O (H_2^{15}O) or ^{18}F . Carbon transport can be visualised by exposing leaves to airborne ^{11}C ($^{11}\text{CO}_2$) or by administering a solution with ^{18}F -fluorodeoxyglucose (^{18}FDG) through an incision. Subsequent transport can be monitored with PET, generating dynamic tracer profiles from which time-series can be derived, and transport characteristics determined. Grey zones in the tracer profiles represent wood rays.

As an alternative to $^{11}\text{CO}_2$, sugar transport can also be traced with ^{18}FDG (Fig. 4.2). Similarly to its use in the medical world, where ^{18}FDG serves as a surrogate for glucose to identify cancer cells, it might help in visualising plant

sugar metabolism using PET. Autoradiographic imaging has shown that plants can uptake ^{18}F FDG. For administration of this tracer, it is necessary to damage the plant surface (Fig. 4.2), after which it is transported, and incorporated into secondary metabolites. Because intact ^{18}F FDG is transported, questions arise whether it really mimics actual sugar transport (Ferrieri et al. 2012), and this might explain why ^{18}F FDG has not yet found a wide application in plant research (Hattori et al. 2008).

^{11}C has already proven its importance in plant sciences

Phloem vessels are known to be notoriously difficult to investigate because they operate under high pressures (Turgeon and Wolf 2009). They are highly sensitive to any perturbation, resulting in immediate blockage when they are damaged (Turgeon and Wolf 2009, Knoblauch and Peters 2010). An important merit of ^{11}C studies is the ability to visualise sugar flow *in vivo* without damaging the phloem or altering its characteristics, which is essential to unravel phloem transport in living plants. In the past, Minchin and co-workers have extensively contributed to the current understanding of phloem transport by their ^{11}C experiments (Minchin and Thorpe 2003, Kiser et al. 2008). Using collimated detectors, their most pioneering discovery was the leakage and retrieval of carbohydrates along the phloem pathway (Minchin and Thorpe 1987, Minchin and Thorpe 2003, Kiser et al. 2008). This leakage-retrieval mechanism is now considered to be of great importance for plants in supplying intermediate cells between sources and sinks with sugars, and for maintaining the pressure gradient driving phloem transport (De Schepper et al. 2013b).

Although many interesting phloem features have been discovered with collimated detectors, PET might further our knowledge, as a more complete picture of phloem transport and its characteristics is acquired. Since the introduction of PET technology, which makes use of coincidence detection (Text box 4.1), collimators became redundant and 3-D imaging was enabled. Whereas a collimated detector dynamically registers single radiation intensities from an entire field of view (FOV), PET generates a complete 3-D image with voxel-based intensities across the FOV, which can be a leaf, a fruit, a root, or a stem segment. Furthermore, the flexibility offered by PET to define regions of interest or to place virtual detectors (similar to collimated detectors, but software-based) in retrospect

makes it possible to analyse the data with respect to how the tracer has been transported throughout the plant, which, in turn feeds into model calculations of phloem transport velocities, exchange, and unloading rates (Keutgen et al. 2005, Matsushashi et al. 2005, Kikuchi et al. 2008, Jahnke et al. 2009, Bühler et al. 2011, De Schepper et al. 2013a).

Quantitative data from PET measurements can be obtained by applying one of several mathematical frameworks (Bühler et al. 2011, Minchin 2012, Bühler et al. 2014). Initially, ^{11}C tracer profiles obtained with several collimated detectors were analysed with the input-output framework developed by Minchin and co-workers (Minchin and Thorpe 1987, Minchin and Thorpe 2003, Minchin 2007, Kiser et al. 2008, Minchin 2012). Although this framework has been widely and successfully used, including for PET data (Keutgen et al. 2005), it is not entirely uncontested and has been criticised because the analysis is considered to be data-driven, not restricting model outcomes with physical boundaries or posing realistic ranges of solute transport characteristics (Bühler et al. 2011, Bühler et al. 2014). To tackle some of these issues, mechanistic compartmental models have been developed to analyse PET tracer profiles (Bühler et al. 2011, Bühler et al. 2014). These models simulate long-distant transport and exchange of solutes within a chosen number of compartments, which may include phloem conduits, tissue where solute from the conduit is exchanged, and tissue where solute is immobilised and stored (Bühler et al. 2011, Bühler et al. 2014). By optimising the parameters, these models output translocation velocities and tracer exchange between compartments, and their modular design makes it possible to readily merge with other existing mechanistic plant models (Steppe et al. 2006, De Schepper and Steppe 2010). When merged, data on sugar transport velocity and lateral exchange rates can be linked to other data, such as measured stem diameter changes and sap flux densities, to develop integrative water and carbon relationships (Hölttä et al. 2006, De Schepper and Steppe 2010, Sevanto et al. 2011, Steppe et al. 2012, Steppe et al. 2015), which will advance our understanding of xylem–phloem interactions.

An important advantage of working with short-lived isotopes is the ability to pulse repeatedly the same individual, for which the plant then serves as its own control. Because of the short half-life time (Table 4.1), tracer levels are reduced swiftly, enabling multiple measurements per day. Because short-lived isotopes do

not need destructive harvesting of the plant, and there is no build-up of tracer from previous pulses (Minchin and Thorpe 2003), including no radioactive waste, a sequence of independent pulses can be used to investigate *in vivo* the effects of a given treatment in the same individual, significantly reducing the number of replicates needed and improving experimental consistency. With this feature, variability in phloem transport within a single individual, between individuals, and between species can be thoroughly examined with plant-PET both on a spatial and a temporal scale.

Combining imaging techniques to see the whole picture

MRI (magnetic resonance imaging) scans provide a high-resolution (up to $30 \mu\text{m}^3$ per voxel) anatomical and structural background, and allow quantification of water flow in both xylem and phloem. However, the low phloem water flow is difficult to detect and, in contrast to PET, it does not represent the amount of sugar that is transported with the water (Windt et al. 2006, Jahnke et al. 2009, Borisjuk et al. 2012, Van de Wal et al. 2017). With the combination of ^{11}C -PET and MRI, carbon flow can be displayed on a highly detailed structural background, while imaging the water flows (Jahnke et al. 2009, De Schepper et al. 2013a), which will assist us in unravelling the contribution of water and carbon to both xylem and phloem flow, as well as their interaction (Windt et al. 2006). The hypothesis of carbon-assisted embolism repair could, for instance, be tested in a set-up where cavitation in xylem vessels is scanned with MRI (Holbrook et al. 2001, Borisjuk et al. 2012, Zwieniecki et al. 2013), carbon transport from inner bark to sapwood is shown by PET, and the subsequent water refilling of embolised vessels is again displayed by MRI.

SPECT (single photon emission computed tomography) might be another interesting option to visualise xylem and phloem functioning in intact plants. While its technical applicability has been proven in a few plant studies with $^{99\text{m}}\text{Tc}$ as a proxy for water transport (Krijger et al. 1999, Walker et al. 2015), no plant physiological insights have yet been derived from SPECT, because most biological molecules of interest are covered by PET (Text box 4.1), whereas SPECT employs non-biological tracers (Krijger et al. 1999, Rahmim and Zaidi 2008, Walker et al. 2015). Nevertheless, SPECT has potential in plant research because, by using heavier γ -ray emitting atoms, there is no loss of resolution

resulting from positron travel distance as there is in PET (Text box 4.1) (Rahmim and Zaidi 2008). However, the overall sensitivity of SPECT is lower than for PET (two to three orders of magnitude), because shielded collimators are used instead of coincidence detection (Rahmim and Zaidi 2008). Today, higher resolutions can be achieved with the development of new collimators such as multi-pinhole SPECT (Deleye et al. 2013) or clustered-pinhole SPECT (Goorden and Beekman 2010), which have higher resolution than PET. The energy levels in SPECT are lower than for PET (140 keV for ^{99m}Tc compared to 511 keV for positron emitters), but both are sufficiently high to penetrate thick wood samples (Wei et al. 2011). Recent developments also make it possible to use positron emitters (for instance ^{11}C) with SPECT detectors, resulting in an improved resolution for a limited FOV (Goorden and Beekman 2010). While it is technically possible to image ^{99m}Tc -water and ^{11}C -carbon flow in plants with SPECT, the technique is still in its infancy, but further developments in this area are to be expected in the future.

Opportunities in plant research remain to be seized

Phloem function and transport have been, and still are (Ryan and Asao 2014, Savage et al. 2016), an important subject of debate, and while on-going research provides new insights on phloem traits and its operating principles, it lacks visualisation of the fate of carbon inside plants (e.g., Minchin and Thorpe (2003), De Schepper and Steppe (2010), Knoblauch and Peters (2010), Slewinski and Braun (2010), Turgeon (2010), Sevanto et al. (2011), Cabrita et al. (2013), De Schepper et al. (2013b), Hall and Minchin (2013), Sevanto (2014)). To improve our knowledge about the ecological implications of xylem and phloem function, as well as their interactions, several missing links need to be deciphered. Plant-PET may play an important role in this quest, in particular when quantitative analysis of PET data is pursued. To date, PET scanners are not readily available for plant scientists, but plant researchers can profit from the advances that have been made in medical imaging, and can use, as temporary solution, clinical PET scanners (Buck et al. 2010, Garbout et al. 2012). Access to custom-built, plant-dedicated PET scanners, with a configuration that is better suited for plants than the horizontal orientated medical scanners, is expected to rapidly develop (Fig. 4.1b, c).

To quantify the overall carbon budget of plants, a better understanding of both the short- and the long-term plant-carbon relations is needed. Longer-term dispersal of carbon within plants can be determined with the long-lived radioactive isotope of carbon, ^{14}C ($t_{1/2} = 5730$ years), or with the stable isotope, ^{13}C (Epron et al. 2012). Both methods give information on carbon sinks, fractionation, or remobilization of carbon reserves, but they do require destructive harvesting of the plant (where ^{11}C -PET does not), and build-up of the tracer prevents independent repeated measurements on the same subject (Minchin and Thorpe 2003). The short-lived radioactive isotope ^{11}C does not have these issues, making this tracer preferable over its longer-lived counterparts to unravel short-term carbon relationships. For instance, a recent study on the fate of xylem-transported CO_2 at leaf level showed a more detailed spatial distribution of CO_2 within a single tissue, which facilitated a more accurate quantification of differences between different leaf tissues when using ^{11}C - compared with ^{13}C -labelled CO_2 (Bloemen et al. 2015). In addition, compartmental analysis of PET data enables quantification of the allocation of carbon to different storage compartments (Fig. 4.2). Carbon allocation to storage is currently the focus of an intense debate because open questions remain about whether it is a passive overflow system or is actively regulated, and how it relates to tree mortality (Sala et al. 2012, Wiley and Helliker 2012, Dietze et al. 2014). It is hypothesised that stored carbohydrates are not solely used as reserves, but that they also play a role in maintaining plant hydraulic functioning during drought, which may create an incentive to actively regulate it in a given environment (Sala et al. 2012). Another challenge in understanding carbon allocation is to quantify the contribution of woody tissue photosynthesis to stem growth (Bloemen et al. 2014, Steppe et al. 2015). Lateral phloem solute leakage, which can be quantified from PET data, might differ between stems with and without woody tissue photosynthesis. Stems with a reduced or absent local production of sugars might have an increased carbon supply from the leaves through the phloem. In addition, the function of wood rays and their role in xylem–phloem coupling (Pfautsch et al. 2015) could be assessed using plant-PET, because radial transport through these rays occurs over distances which can be directly visualised by PET (Fig. 4.2).

Driven by medical impetus, on-going technical advances continue to improve the versatility, compactness and resolution of PET scanners (Schulz et al. 2011, Yamamoto et al. 2011, Yao et al. 2012, España et al. 2014, Wang et al. 2014), of which plant-PET could fruitfully make use in future applications. Plant-PET scanners with modules allowing different configurations (Fig. 4.1b, c) are a first step in making the scanners more mobile and applicable to measure plants, even when they have larger dimensions (e.g., De Schepper et al. (2013a), Weisenberger et al. (2013)). Medical mobile PET systems, that have been configured to fit around the head of a small laboratory animal, could easily be mounted on a branch or small stem segment (Schulz et al. 2011) and portable MRI systems, dedicated to plant research, have recently been developed (Windt et al. 2011, Windt and Blümler 2015). These are all advances that can bring us a step closer to measuring plants in their natural environment.

Concluding remarks and future perspectives

PET technology and other medical imaging techniques present promising avenues to decipher a broad range of unknown or poorly understood vital plant mechanisms and functions. Despite its huge potential, there have been only a few plant-PET studies to date. Nevertheless, studies using clinical PET scanners or custom-made devices have clearly demonstrated their applicability and usefulness, but have mainly been restricted to short-term qualitative analyses. Quantitative analysis of plant-PET scans may reinforce integrated studies that link water and carbon dynamics, and their interplay with growth. Simultaneous observation, visualisation and analysis of the dynamic behaviour of water and sugar movement in intact plants is one of the greatest challenges in modern plant science, and represent an untapped resource that will deepen our current and future fundamental understanding of the coordination of water and sugar flow in plants, and its impact on plant development, environmental suitability, and yield.

5

CHAPTER 5

¹¹C-autoradiographs to image phloem loading

Abstract

Most tree species passively load photoassimilates into the phloem, according to a concentration gradient, while most herbaceous species use active loading, against a concentration gradient with the expenditure of energy. Phloem loading strategies have implications for phloem sugar concentration and growth potential. In past research, ¹⁴C-autoradiography has been mainly used to explore and identify phloem loading strategies in plants. Here, we suggest the application of ¹¹C-autoradiography, because of its compatibility with plant-PET scans. Because so far plant ¹¹C-autoradiography is hardly used, we assessed its suitability to characterise phloem loading in contrasting plant species: five tree species consisting of one temperate species, *Populus tremula* L. (common aspen), and four tropical species, *Erythrophleum suaveolens* (Guill. & Perr.) Brenan, *E. ivorense* A. Chev. (both tali), *E. africanum* (Benth.) Harms (African blackwood), and *Maesopsis eminii* Engl. (umbrella tree), and two herbaceous crop species *Solanum lycopersicum* L. (tomato) and *S. tuberosum* L. (potato). For the study species with known loading strategies, we were able to confirm that *P. tremula* used passive loading and showed equal or lower tracer amounts in major veins, and that *Solanum* spp. were active loaders with higher tracer amounts in major veins. Also *Erythrophleum* spp. and young leaves of *M. eminii* showed the expected passive loading strategy, but mature leaves of *M. eminii* showed an uncommon pattern. Images corrected for leaf tissue thickness supported that mature leaves of *M. eminii* used active phloem loading of assimilates. Active loading has been related to continuous investment in growth and new leaves, and likely, *M. eminii* continuously invests in new leaf material, also supporting the typically lower storage levels observed in tropical tree species. With this study, we demonstrated that ¹¹C-autoradiography is a powerful tool to acquire detailed tracer distribution in leaves to typify phloem loading strategies in plant species.

Introduction

Leaves are designed like little factories in which mass production of photoassimilates takes place by the photosynthesis process. After production, the logistics need to be taken care of, and this is where phloem comes into play. Plants have developed several ways to load photoassimilates into the phloem, with or without expenditure of energy (Fig. 5.1) (Rennie and Turgeon 2009, Turgeon 2010, Fu et al. 2011, De Schepper et al. 2013b). Most plant species produce sucrose as photoassimilates, but alternatively polymers such as raffinose or stachyose, or sugar alcohols, such as mannitol or sorbitol can also be assimilated (Reidel et al. 2009, Rennie and Turgeon 2009). Plants use one or multiple ways of phloem loading (Slewiniski et al. 2013), which are classified in three strategies: (i) passive symplastic (Fig. 5.1a, d), (ii) polymer trapping (Fig. 5.1b, e), and (iii) active apoplastic (Fig. 5.1c, f). Studies have shown that trees generally exhibit passive loading of sugars into the phloem (strategy i), that both herbaceous and trees apply polymer trapping (strategy ii) and that most herbaceous species have active apoplastic loading (strategy iii) (Rennie and Turgeon 2009, Turgeon 2010, Davidson et al. 2011, Fu et al. 2011). Passive loading means that leaf mesophyll and phloem are symplastically connected via plasmodesmata and that sugars flow into the phloem according to a governing gradient inside the leaf (Fig. 5.1a) (Turgeon 1996, Rennie and Turgeon 2009, Turgeon 2010, Fu et al. 2011, De Schepper et al. 2013b). During active loading, energy is spent to increase sugar concentration inside the phloem (Fig. 5.1e, f). In case of polymer trappers, photoassimilates flow passively from mesophyll to companion cells, where they are converted into oligosaccharides (such as raffinose and stachyose) (Fig. 5.1b) (Rennie and Turgeon 2009, De Schepper et al. 2013b). These larger molecules can still pass through plasmodesmata between companion cells and sieve elements but they cannot flow back through plasmodesmata connecting companion cells to mesophyll cells. Inside the companion cells, the concentration of primary photoassimilates remains low and passive influx continues. This way, polymer trapping makes use of a size-exclusion strategy to increase the concentration of oligosaccharides inside the phloem at the expense of energy to convert the sugars. In case of apoplastic loading, active pumping is required to load sucrose into the phloem (Fig. 5.1c).

Apoplastic loaders have very few plasmodesmata between mesophyll cells and sieve element companion cell complexes (SECCC), and are practically symplastically isolated from each other (Turgeon 1996, Rennie and Turgeon 2009, De Schepper et al. 2013b). The only way for sugars to enter the SECCC is to enter the apoplast and then being actively pumped into the symplast of the SECCC by sucrose/ H^+ co-transporters. To create the required proton motive force, protons are pumped by proton-ATPase against their concentration gradient at the expense of the energy carrier ATP (Lemoine 2000, Williams et al. 2000, De Schepper et al. 2013b).

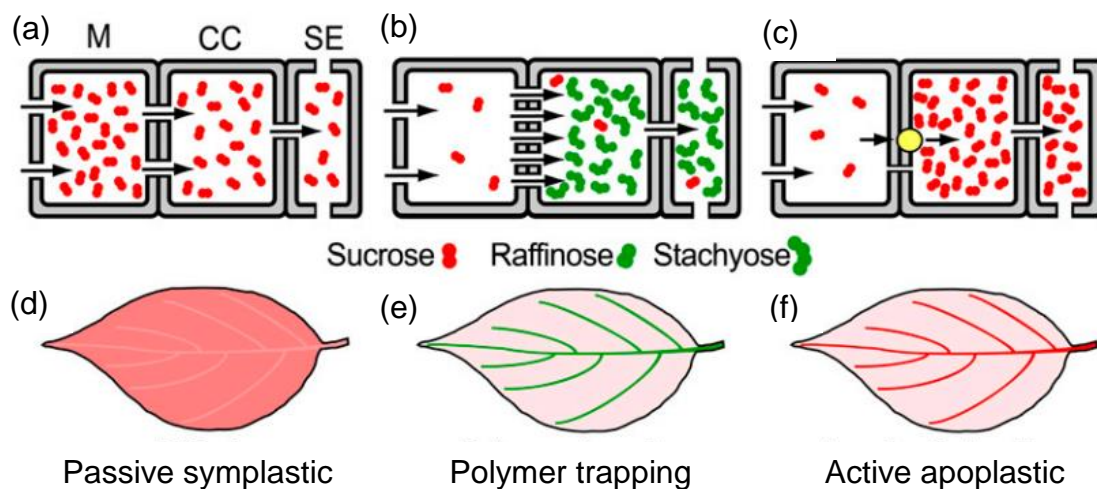


Figure 5.1 Plants use passive or active strategies to load sugars into the phloem. (a) In passive loading sucrose diffuses through many present plasmodesmata according to a gradient in concentration, which is higher in the mesophyll (M), and smaller in the companion cells (CC) and sieve elements (SE). (b) Polymer trapping is an active loading strategy in which sucrose from the mesophyll enters the companion cells through plasmodesmata and is converted into a polymer such as raffinose and stachyose at the expense of energy. These molecules are too large to pass through plasmodesmata back into the mesophyll but fit the plasmodesmata connecting the companion cell to the sieve element, and are loaded into the sieve element according to a concentration gradient. (c) In active apoplastic loading, almost no plasmodesmata connect mesophyll to companion cells, which requires an apoplastic route to load the companion cells. Loading occurs with a sucrose/ H^+ co-transporter (yellow bullet), which consumes ATP and thus costs energy. (d) Passive loading follows a concentration gradient from higher sugar concentration in the mesophyll to lower concentration in the major veins (indicated by lighter colour). (e, f) Active loading occurs against a concentration gradient, which is visualised by higher concentrations in major veins (indicated by brighter colours) compared to mesophyll. Adapted from Turgeon (2010).

Evolution has led to different loading strategies because using an active or a passive loading strategy is the result of an interesting trade-off. Active loaders

do not need a high sugar concentration in the mesophyll to load sugar into the phloem (Fig. 5.1e, f). No or very little negative feedback signals will be sent to the photosynthetic apparatus, which reduces its activity when mesophyll sugar concentrations are high (Körner et al. 1995, Turgeon 2010, De Schepper et al. 2013b). Phloem concentration is also higher in active loaders, which increases the gradient in hydrostatic pressure between production (source) and consumption (sink) site, maximising sugar transport efficiency (Jensen et al. 2013, Savage et al. 2016). In general, active loaders maintain low leaf carbon inventories and continuously grow new leaves, leading to fast growth. Because their growth potential is higher, active loading is suited for herbaceous species, who invest in year-round growth (Turgeon 2010). Also, many herbs have a short life duration and need to invest in growth as much and as quick as possible. The drawback of high investment in growth is that less carbon is allocated to storage. In trees, this drawback is critical and the main reason why trees in general are passive loaders. As trees have a longer lifespan than herbaceous species, they need to be able to survive less favourable circumstances, and thus need higher amounts of storage to rely on (Turgeon 2010, Sala et al. 2012). Also, they typically do not continuously invest in leaf growth but rather in flushes, during which a high portion of storage is mobilised (Turgeon 2010). This is only possible when there has been a sufficient investment in storage.

In their recent review, Savage et al. (2016) call for more research to acquire a comprehensive picture of sugar distribution in plants. Moreover, the coupling between xylem and phloem is important but still far from fully understood (Chapter 4) (Hölttä et al. 2006, Windt et al. 2006, Mencuccini and Hölttä 2010, Sevanto et al. 2011, Ryan and Asao 2014, Steppe et al. 2015, Savage et al. 2016). Not only growth strategies are dependent on how phloem is loaded, but also the response to environmental challenges such as climate change may be different (Savage et al. 2016). How plants cope with, for instance, drought will become increasingly important (Wullschleger et al. 2002, IPCC 2014c, Sevanto 2014, Allen et al. 2015, Teskey et al. 2015). Active loaders have a higher solute concentrations inside their phloem (Fig. 5.1e, f), which results in a higher osmotic potential and thus a stronger pull on available water (Sevanto et al. 2011). Also, to accommodate the need of water in the phloem, the xylem water potential should not be too negative, because then water will flow from phloem to xylem,

ceasing phloem transport (Sevanto et al. 2011, Sevanto 2014, Sevanto et al. 2014). Alternatively, high solute concentration inside the phloem will draw water into the phloem, increasing tension on the water column and resulting in more cavitation. In case of limited water availability, phloem solute concentration will up-concentrate, potentially resulting in a too syrupy stream with a viscosity that high that transport will come to a stop (Sevanto 2014).

In this study, we propose ^{11}C -autoradiography as powerful tool to assess *in vivo* carbon distributions and phloem loading strategies after exposing attached leaves to gaseous $^{11}\text{CO}_2$. Seven contrasting plant species, ranging from temperate and tropical tree species to herbaceous crops, were investigated and study species with known loading strategies were used as validation to then explain patterns in species with unknown loading strategies. Because ^{11}C is a positron emitter, it can also be used to obtain plant-PET scans. A combination of plant-PET scans and autoradiography might then be able to image the entire pathway from phloem loading to phloem transport.

Introduction to autoradiography

Autoradiography is a visualisation method that is used in combination with radiation emitting isotopes. These isotopes are unstable and emit radiation that can be measured with autoradiographic phosphor plates. In this way, distribution and amount of an administered radioactive tracer can be imaged. In plants, carbon isotopes are often used, as they can mimic photoassimilates. Whereas ^{14}C , the long-lived unstable carbon isotope (half-life time 5730 years), has often been used in autoradiographic plant studies, ^{11}C , the short-lived unstable isotope (half-life time 20.4 min), is new to the field of autoradiography (Thorpe et al. 2007, Epron et al. 2012, Bloemen et al. 2015). ^{11}C emits a high-energy positron (mean energy 390 keV, and maximum energy 970 keV) upon decay (Phelps et al. 1975, Jødal et al. 2012). When exposing an object or a source that contains positron emitters to a phosphor autoradiographic plate, crystals in the plate will be ionised by the positrons and can be imaged in 2-D.

Annihilation is the interaction between a positron and an electron, which results in the emission of 2 γ -rays (Text box 4.1, Fig. 4.1). This process is important to consider when imaging thin material such as plant leaves in autoradiography (Alexoff et al. 2011, Partelová et al. 2016). When a positron is

traveling through matter, it will lose energy due to collisions and scattering until it reaches a low enough energy to annihilate (Bailey et al. 2005). Because of the many interactions before annihilation, the path of the positron will be deflected, which makes it difficult to predict the distance it travelled from the source (i.e., the decaying ^{11}C atom) through matter, the so-called positron range. The positron range is hence not a fixed number, but rather consists of a probability distribution (Phelps et al. 1975, Levin and Hoffman 1999, Jødal et al. 2012). In water or tissue, the mean positron range of ^{11}C is about 1.13 mm, with a maximum of 4.46 mm, while in air, the positron range becomes very large, in the range of several meters (Phelps et al. 1975, Levin and Hoffman 1999, Alexoff et al. 2011, Jødal et al. 2012). This will influence measured intensities on the autoradiographic phosphor plates, because γ -rays have a much lower chance than particles (positrons) of interacting with the phosphor plate, and being registered as activity. Typically, major veins (midvein, first- and second-order veins) are specialised in transport of carbon and water, and are thickened parts of the leaf compared to the leaf lamina (Sack and Scoffoni 2013). Depending on where in the vein the vascular bundle is positioned, the range a positron will travel through matter and the density of this matter will vary, as well as the chance to annihilate and be left undetected. Also, resolution of autoradiography is not easy to determine, because the emitted high energy of ^{11}C positrons will excite a larger range of crystals in the plate.

Autoradiography has been used in the past to discover phloem loading strategies in plant species. Back in the 1970s, autoradiography in combination with [^{14}C]sucrose has been used to study transport and loading of sugars in phloem (Geiger 1975, Giaquinta 1976). Turgeon and Wimmers (1988) delivered the first proof of different loading pathways using [^{14}C]sucrose-autoradiography. Surprisingly and despite being the simplest loading strategy, it was not until the ^{14}C -autoradiography studies of Eschrich and Fromm (1994) and Turgeon and Medville (1998) that passive loading was detected. Later, Rennie and Turgeon (2009) and Fu et al. (2011) performed large multi-species (45 species) studies in which they assessed the uptake and distribution of [^{14}C]sucrose, [^{14}C]mannitol and [^{14}C]sorbitol to investigate whether study species increased sugar concentration in the veins and if they used sugar alcohols or sucrose. Most

¹⁴C-autoradiographic research has been performed by floating small cut leaf discs in a solution containing [¹⁴C]sugars to bring the labelled sugar in contact with the loading sites of the phloem, which are typically located in the minor veins (De Schepper et al. 2013b). Higher tracer intensities were found in veins of active loaders, while no clear difference in tracer intensity was found in passive loaders (Reidel et al. 2009, Rennie and Turgeon 2009, Fu et al. 2011).

Materials and methods

Plant material

We assessed ¹¹C-autoradiography as method to characterise carbon distribution and phloem loading in seven contrasting plant species: five tree species consisting of one widely distributed temperate species, *Populus tremula* L. (common aspen), and four tropical species, *Erythrophleum suaveolens* (Guill. & Perr.) Brenan, *Erythrophleum ivorense* A. Chev. (both tali), *Erythrophleum africanum* (Benth.) Harms (African blackwood), and *Maesopsis eminii* Engl. (umbrella tree) (Table 5.1). *Erythrophleum* spp. occur along an ecosystem gradient from savannah to rainforest system. In case differences in carbon distribution and loading exist, this might be related to their habitat. *Maesopsis eminii* is a pioneer species of African tropical rainforest and has been the subject of other studies in which it showed interesting leaf behaviour (Epila et al. 2017a, Epila et al. 2017b, Epila et al. 2018, Van Camp et al. 2018). Two herbaceous crop species, *Solanum lycopersicum* L. (tomato) and *Solanum tuberosum* L. (potato), were measured with *S. lycopersicum* being interested for its fruits and *S. tuberosum* for its tubers. Mature leaves were sampled for all species and additionally young leaves of *M. eminii* were sampled. Trees were expected to show a passive loading strategy and herbaceous species an active loading strategy.

Table 5.1 Summary of the study species and experimental details. Growth habit is tree (Tr) or herbaceous (Herb). Measurement date, starting activity and cuvette volume refer to the autoradiographs shown in Fig. 5.4. Cuvette design is the small plexiglas cuvette (SP), the large plexiglas cuvette (LP) or the branch bag (BB). N is the total number of scans for the species. Soil substrate is potting soil (PS) or rockwool (RW). Substrate volume represents potting soil or rockwool volume. All plants were well-watered and grown inside a controlled greenhouse. Underlined text indicates the option chosen to image the leaves shown in Fig. 5.4. Note that *Erythrophleum* spp. were labelled together in the same branch bag.

Plant species	Common name	Growth habit	Typical height [m]	Measurement date Fig. 5.4	Starting activity [MBq]	Volume cuvette [L]	Cuvette	N	Soil substrate	Substrate volume [L]
<i>Populus tremula</i>	common aspen	Tr	1.5 – 2	August 2015	550	2.9	LP + <u>BB</u>	6	PS	15 + <u>30</u>
<i>Erythrophleum suaveolens</i>	tali	Tr	0.20 – 0.25	March 2017	1110	24.2	<u>BB</u>	1	PS	<u>3</u>
<i>E. ivorense</i>	tali	Tr	0.15 – 0.20	March 2017	1110	24.2	<u>BB</u>	1	PS	<u>3</u>
<i>E. africanum</i>	African blackwood	Tr	0.10 – 0.15	March 2017	1110	24.2	<u>BB</u>	1	PS	<u>3</u>
<i>Maesopsis eminii</i>	umbrella tree	Tr	1.5 – 2	October 2015	550	3.6	SP + <u>LP</u>	8	PS	<u>35</u>
<i>Solanum lycopersicum</i>	tomato	Herb	2 – 3	December 2016	610	2.9	<u>BB</u>	2	RW	<u>15</u>
<i>S. tuberosum</i>	potato	Herb	0.3 – 0.4	May 2015	40	2.9	<u>BB</u>	1	PS	<u>15</u>

Exposure to gaseous $^{11}\text{CO}_2$

Across 2015–2017, attached leaves of contrasting plant species were exposed to gaseous $^{11}\text{CO}_2$ to assess carbon distribution patterns and phloem loading strategies. Because of its compatibility with PET scanning (see next Chapter), exposures to ^{11}C were performed in a PET scanner with a bore diameter of 15 cm (LabPET8, TriFoil Imaging, Chatsworth, CA, USA).

Three designs of fully airtight cuvettes that fitted the PET bore were employed (Fig. 5.2). A first design was a small solid plexiglas cuvette (diameter 13.5 cm, depth 7 cm), in which one or two leaves could be fixed between two positron shields (plexiglas plates, Text box 4.1), but the installation protocol was prone to leaf damage, and therefore this design had been abandoned after a testing period. A second design consisted of a larger solid plexiglas cuvette (diameter 13.5 cm, depth 25 cm), without positron shields. A third cuvette design comprised a flexible fully airtight branch bag (see details in Chapter 6). In these cuvettes, attached leaves or distal parts of attached branches (in case of *Solanum* spp. this was one leaf consisting of several leaflets) were exposed to ^{11}C . For safety reasons at any time, any contamination of the air with airborne radioactive molecules was prevented by constructing an airtight seal with putty (Opstosil Putty, Kulzer, Hanau, Germany), adhesive (Teroson Terostat-IX, Henkel, Düsseldorf, Germany) and grease (Vacuum Grease, Dow Corning, Auburn, MI, USA). A controlled flow of air was sent in and out of the cuvettes to maintain stable atmospheric conditions in the cuvette. Flow rate was adjusted to cuvette volume in order to refresh one cuvette volume every 5 min.



Figure 5.2 Different cuvette designs to administer gaseous $^{11}\text{CO}_2$ to leaves attached to intact branches. (a) Small plexiglas cuvette in which one or two leaves could be fixed between two plexiglas plates, serving as positron shields (Text box 4.1). (b) Larger plexiglas cuvette without positron shields that could fit an entire distal part of a branch with multiple leaves. (c) Versatile and airtight branch bag (details in Chapter 6).

$^{11}\text{CO}_2$ was administered to the cuvette via a pulse, through a thin tube. Outflowing air was scrubbed from CO_2 to capture the remaining activity before releasing it back into the air. To ensure photosynthetic activity during the experiments, a light source (red and blue LED-light (GreenPower LED string, Philips, Amsterdam, The Netherlands), except for *S. tuberosum* which was exposed to a combination of white LED-light (PH1LP Teaching Photosynthesis, Qubit Systems, Kingston, Canada) and fibre-optic light (Model FL-4000, Walz Mess und Regeltechnik, Effeltrich, Germany)) was positioned above the labelled leaves, yielding between 200 and 250 $\mu\text{mol PAR m}^{-2} \text{s}^{-1}$ at leaf surface. Leaves were left in the cuvette for one hour after pulse-labelling and the branch was then cut at a distance of 10 cm from the labelled region, and removed from the cuvette. After cutting, phloem transport and movement of tracer are expected to slow down to eventually stop (Van Bel 2003, Turgeon and Wolf 2009). The cut branch was then exposed to the phosphor autoradiographic plates. Exposed parts were hence allowed to take up, metabolise and transport tracer for one hour, which has been considered a good exposure time to investigate phloem loading (Rennie and Turgeon 2009, Fu et al. 2011). In general, species were labelled separately, with the exception of the *Erythrophleum* spp., which were labelled together in one large branch bag.

Autoradiography

Used phosphor plates consisted of BaFBr:Eu_2^+ crystals and were 25.2 cm x 12.5 cm in size (MultiSensitive, PerkinElmer, Waltham, MA, USA) (Fig. 5.3). The cut branch with attached leaves was placed on a thin layer of cellophane and then covered with another layer to prevent contamination of the plates, and leaves were separated by tape to limit overlap. The phosphor plates were put on top of the adaxial sides of the leaves inside an autoradiographic cassette, which pressed the plates onto the leaves, ensuring a tight contact. Contact time was optimised to have sufficient activity captured by the phosphor plate and typically lasted for 10 min (being about 30 % emitted activity from the leaf given the exponential decay with a half-life of 20.4 min). After these 10 min of exposure, the crystals of the phosphor plates that were excited by the radiation energy were scanned by a laser and digitised in a Cyclone Plus Phosphor imager in OptiQuant

software (Perkin Elmer, Waltham, MA, USA). These images were further processed with Fiji, an image processing software (Schindelin et al. 2012).

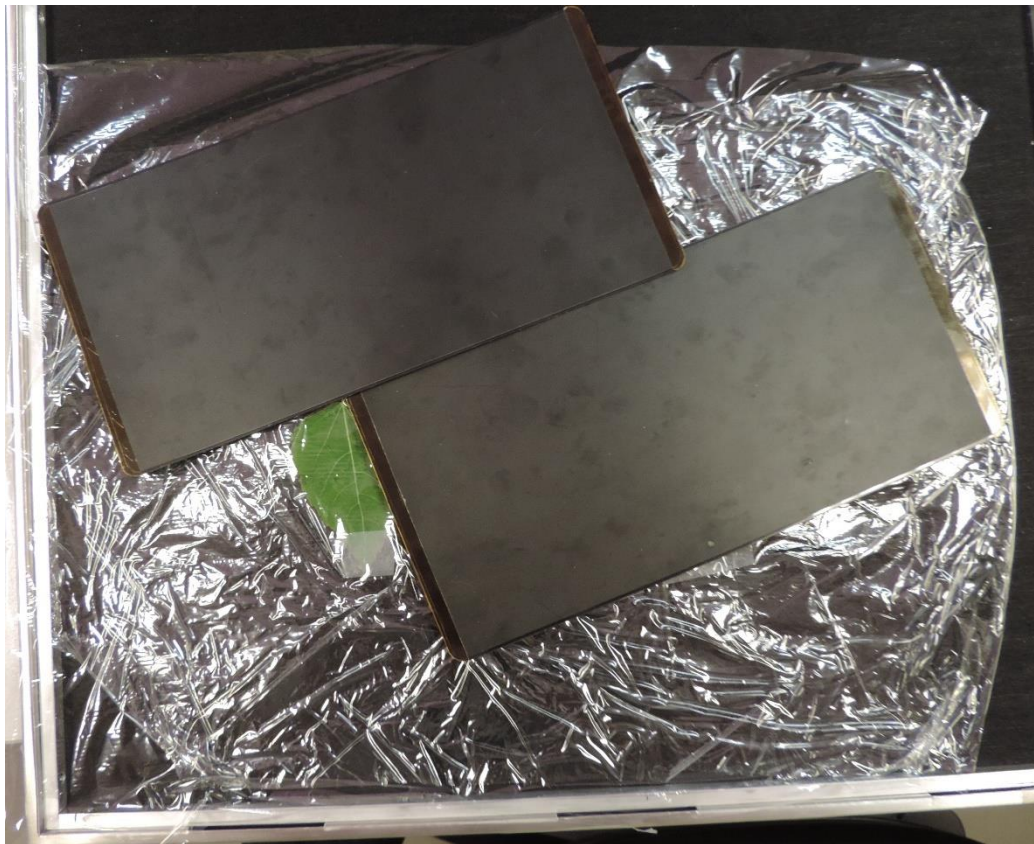


Figure 5.3 Open top-view of an autoradiographic cassette. Leaves are placed between one layer of cellophane to prevent contamination of the phosphor plates. The back side of the black phosphor plates is visible, while the front side covers the adaxial side (upper surface) of the leaves. The cassette is closed to firmly press the plates against the leaves and to ensure close contact. Exposure during 10 min, and final digitalisation, is performed in dark conditions.

Vein anatomy

Anatomical cross-sections were prepared when required for specific pattern recognition in *Maesopsis eminii*. To this end, stored leaf segments were rehydrated overnight in 1 % (v/v) Aerosol OT (Cytec) and 25 % (v/v) methanol. They were excised in such a way that sections perpendicular to the veins of the first, second and third order could be made. After rinsing in demineralised water, samples were embedded in 7 % (w/v) agarose (Sigma Aldrich). Blocks of agarose containing leaf segments were glued onto the vibratome stage using superglue (Roticoll, Carl Roth). 40 μ m thick sections, prepared with a vibrating microtome (HM 650V, ThermoScientific, Germany), were stained with 0.5 % w/v astra blue, 0.5 % w/v chrysoidine and 0.5 % w/v acridine red and mounted in

Euparal after dehydration in isopropyl alcohol. Slides were observed with a Nikon Ni-U microscope and images were recorded using a Nikon DS-Fi1c camera. Length measurements on the cross-section were performed with Fiji (Schindelin et al. 2012), and expressed as average values with standard error.

Results

A compilation of ^{11}C -autoradiographs illustrates different tracer distributions in leaves of contrasting trees and crops (Fig. 5.4). Across leaves or leaflets of the same plant species, similar patterns were found. Overall, images showed a close agreement with leaf venation, and mainly major veins showed a different intensity of detected signal. Uneven lighting during ^{11}C exposure caused the observed leaf patchiness in the images. Leaf surfaces in the relatively small PET-bore did not receive equal light intensities, and likely shaded each other.

In *P. tremula* and the *Erythrophleum* spp., midvein and secondary veins were the regions with lower ^{11}C activity. Lower activity was more pronounced in midvein than secondary veins in *E. africanum*, probably because of its small leaf size (1.6 cm in length) and associated resolution limits. Also young leaves of *M. eminii* showed a lower activity in midvein and secondary veins compared to mesophyll. In the older leaves, however, a different pattern was observed, with tracer signal accumulating around primary and secondary veins, while inside the veins registered activities were lower.

In *S. lycopersicum*, a clear distribution was imaged with higher ^{11}C activity in midvein and secondary veins of the leaflets compared to mesophyll. Also in *S. tuberosum*, the midvein and some secondary veins showed higher activities, while in other parts of the leaflet a less clear distribution and lower intensity of the carbon tracer was detected, probably because of leaf shading and the relatively low starting activity (Table 5.1) resulting in a lower resolution.

Also thickness of overlying tissue can affect the signal strength in autoradiography. In *S. lycopersicum* and *S. tuberosum*, major veins in leaflets are typically structured in a thickened part extending in abaxial direction (Hayward 1951, McCauley and Evert 1988b, a). Tissue thickness between the vascular bundles and the adaxial leaflet surface is thus larger than lamina thickness, implying that measured tracer activity in the major veins is an underestimation of the actual activity.

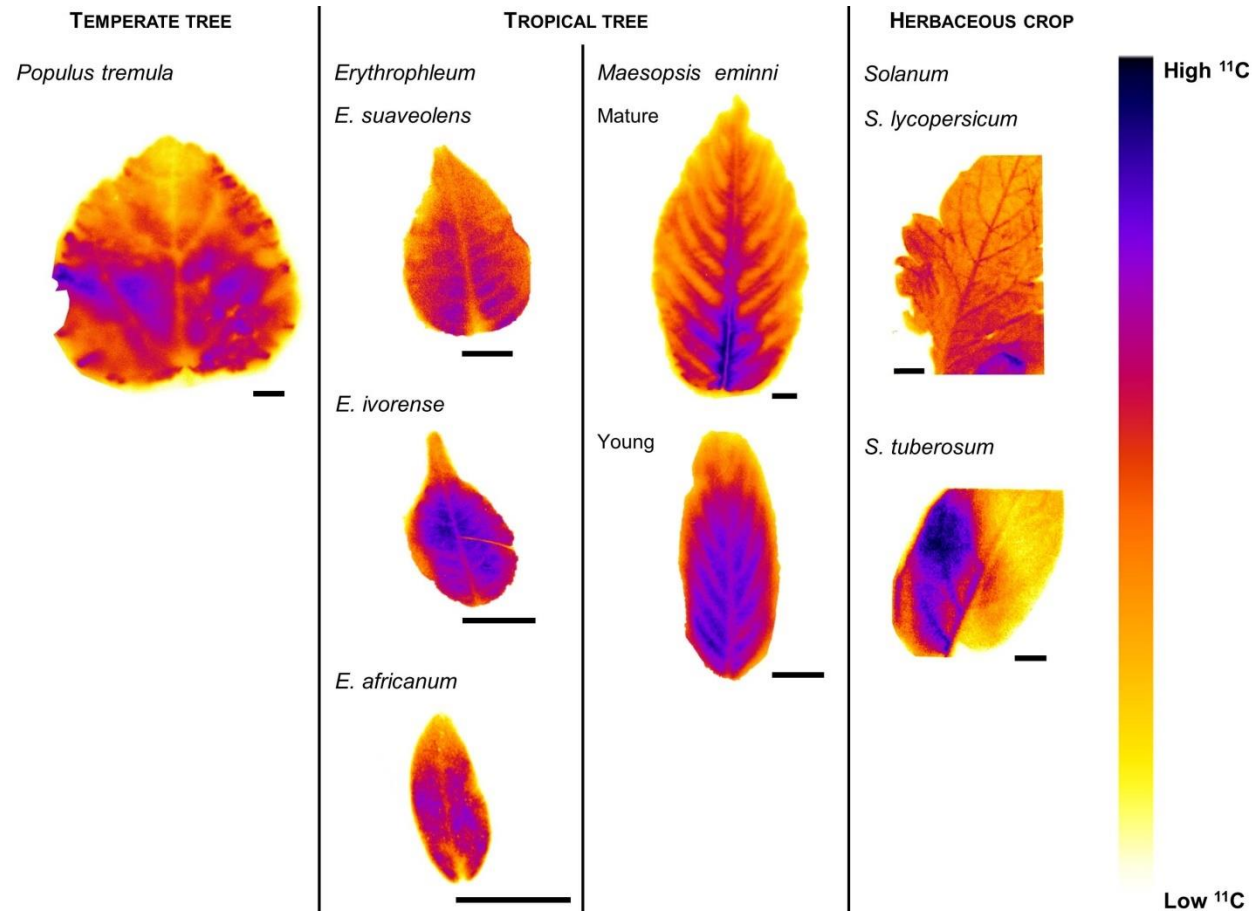


Figure 5.4 Compilation of typical autoradiographs displaying ^{11}C tracer intensities in leaves of contrasting plant species. *Populus tremula* is a known passive loader, illustrating lower tracer intensities in major veins compared to mesophyll. *Erythrophleum* spp. are tropical tree species, all showing the projected passive loading strategy with lower activities measured in the major veins. Also young *Maesopsis eminii* leaves showed lower intensities in major veins compared to mesophyll indicating passive loading, but their mature counterparts showed highest tracer intensities around the major veins. *Solanum* spp. are known to be active loaders and showed higher intensities in major veins than in mesophyll. Scale bars are 1 cm.

Because only the mature leaves of *M. eminii* showed an uncommon tracer distribution pattern, their anatomy was further investigated (Fig. 5.5). Vascular bundles in the midvein and secondary veins were located just above halfway the leaf cross-section, whereas tertiary veins were found just below halfway the section. Leaf thickness was measured to assess the effect of increased probability of annihilation when moving from smaller to larger veins. Distances were measured between points in the vascular bundle and the adaxial side of the leaf (i.e. the side that was exposed to the phosphor plates) to derive average distances that positrons had to travel before reaching the phosphor plates. These distances were $206 \pm 23 \mu\text{m}$, $88.0 \pm 5.4 \mu\text{m}$, and $67.41 \pm 0.92 \mu\text{m}$ ($N = 8$ each) for the midvein, secondary and tertiary veins, respectively. Thickness of the leaf lamina was on average $123 \pm 14 \mu\text{m}$ ($N = 12$). In mesophyll, it is difficult to assess where ^{11}C is mainly present. Probably, most of the tracer will be present in the photosynthetically most active palisade cells close to the adaxial side. Average distance between palisade cells and the adaxial side of the leaf was $28.0 \pm 2.4 \mu\text{m}$ ($N = 8$). If we assume ^{11}C tracer to be located in the palisade tissue when in the mesophyll and in the vascular bundle when in the veins, we can quantify the reduction in positron escape according to Jødal et al. (2012), and thus associated reduction in detected signal on the phosphor plates. A reduction of 3 %, 4 % and 12 % due to overlying tissue in tertiary, secondary and midveins, respectively, was calculated.

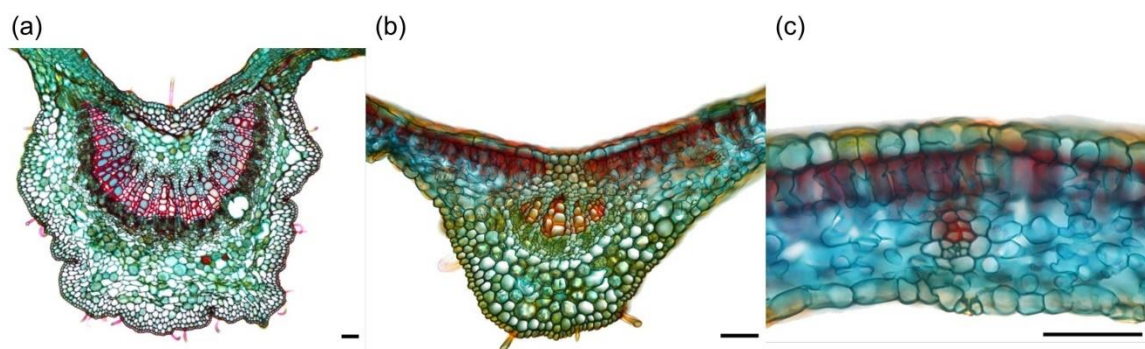


Figure 5.5 Anatomical cross-section of (a) the major vein, (b) a secondary vein and (c) a tertiary vein of a mature leaf vein of *Maesopsis eminii*. Images were used to determine the distance between the phloem in the vascular bundle and the adaxial side of the leaf (top of the image), which was exposed to the phosphor plates for autoradiography. This allowed calculating a correction factor for the positron range. Scale bar is $50 \mu\text{m}$.

Also in *P. tremula*, positron range associated correction factors were calculated from vein thickness measurements along the midvein. Correction factors ranged from 25 % in the thickest part to 11 % in the thinner endings of the midvein. These correction factors were applied across the centre of the midvein, and half of the correction was applied at the edges of the midvein as an estimate to account for the cylindrical vein shape. When correcting midveins values for these percentages, tracer activity in the midvein in *P. tremula* increased and almost equalled measured intensities in the mesophyll, whereas in *M. eminni* accumulation of tracer occurred towards the midvein (Fig. 5.6). Furthermore, the apparent drop in tracer activity in the midvein of *M. eminni* was almost entirely eliminated after correction. Tracer activity in the midvein was about as high as in the surrounding mesophyll. These corrections should only be used indicatively on the acquired autoradiographs, but demonstrated that in mature leaves of *M. eminni* active loading occurred.

Discussion

Carbon export requirement when imaging ^{11}C distribution during phloem loading

To identify a plant's phloem loading strategy with ^{11}C -autoradiography, relatively constant export rates of carbon out of the leaf between the time of pulse-labeling and imaging are required. If this steady-state requirement is met, relative differences in tracer accumulation characterise how carbon is distributed in the leaf after uptake. We measured tracer distribution after one hour of ^{11}C exposure, which is comparable with ^{14}C -autoradiography studies (Turgeon and Medville 1998, Rennie and Turgeon 2009, Zavaliev et al. 2010, Fu et al. 2011). In their study with scintillation detectors, Jahnke et al. (1998) showed a continuous and relatively constant export rate of carbon tracer out of the leaves for at least two hours on young *Fraxinus excelsior* L. and *Sorbus aucuparia* L. trees using $^{11}\text{CO}_2$ pulse-labelling. Also, export rates of carbon in leaves of *Triticum aestivum* cv. Consort remained high and relatively constant for about two hours, based on $^{14}\text{CO}_2$ pulse-labelling measurements (Dilkes et al. 2004). We therefore assumed a steady-state of phloem loading one hour after labelling.

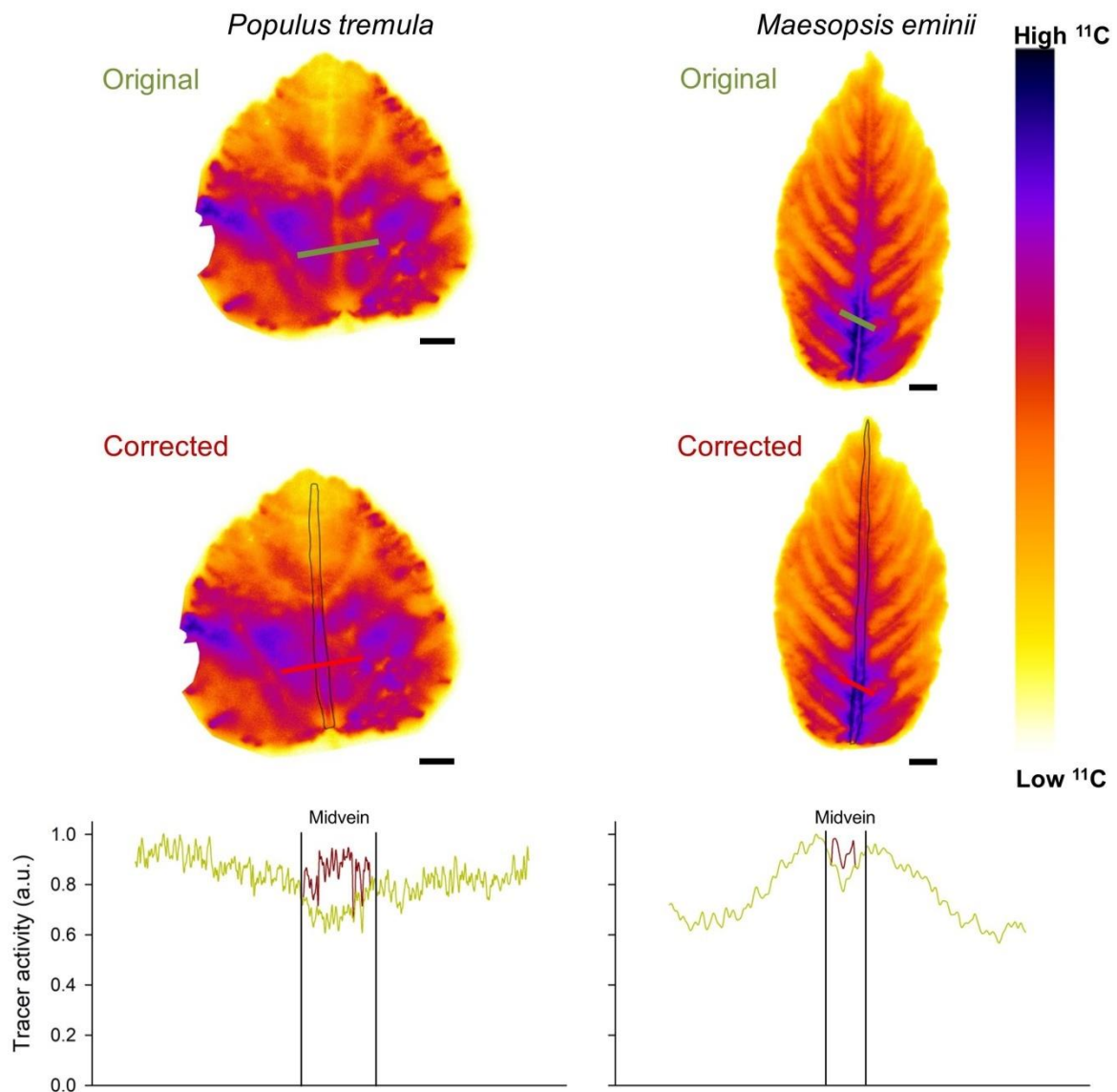


Figure 5.6 Leaf ^{11}C -autoradiographs of *Populus tremula* and *Maesopsis eminii*. Correction is illustrated for the midvein, with the region indicated with a black line is corrected using the approach of Jødal et al. (2012). The profile plots show how the measured tracer intensity varies in and around the midvein, when corrected (red line) and uncorrected (green line). Tracer activity is expressed in arbitrary units (a.u.) with 1 the maximum intensity measured in the profile. Scale bars are 1 cm.

^{11}C -autoradiography as valuable tool to define loading strategies in leaves

The ^{11}C -autoradiographs of *P. tremula* leaves pointed to a passive phloem loading strategy (Figs 5.1d, 5.4 and 5.6). Passive loading was expected, as *P. tremula* is a tree species and also previous measurements (anatomical, genetical and ^{14}C -autoradiography) in other *Populus* spp. showed the passive phloem loading strategy, which can be defined as a family trait (Gamalei 1989, Turgeon 2010, Fu et al. 2011, Jensen et al. 2013, Zhang et al. 2014). The

^{11}C -autoradiography method to define loading strategies was further validated for the *Solanum* spp., which are described in literature as active apoplastic loaders (Fu et al. 2011) and were identified as active loaders on the ^{11}C -autoradiographs (Figs 5.1f, 5.4). In leaves of the tropical species (Gorel et al. 2015, Epila et al. 2017c), we projected to find the passive loading strategy, because study species were trees (Gamalei 1991, Davidson et al. 2011), but no previous studies exist to verify our ^{11}C image analysis.

All ^{11}C -autoradiographs (Fig. 5.4) showed differences in ^{11}C intensity between the major veins, where transport phloem is located, and the mesophyll. This is similar to ^{14}C -autoradiographs where differences between minor veins and mesophyll are measured to distinguish between passive and active loaders (Reidel et al. 2009, Rennie and Turgeon 2009, Fu et al. 2011). In the passive loaders, ^{11}C intensities in the midvein and secondary veins were lower than in the surrounding mesophyll (Fig. 5.4). Based on leaf and vein thickness measurements and the positron range probability relations of Jørdal et al. (2012), corrected tracer intensities in major veins and the leaf lamina in *P. tremula* leaves returned nearly equal (Fig. 5.6). This corresponds with the findings of Rennie and Turgeon (2009) and Fu et al. (2011), who reported lower or equal intensities of ^{14}C tracer inside the veins of passive loaders. In the active loaders an increase in ^{11}C activity was found in midvein and secondary veins (Fig. 5.4). Taking into account that overlying tissue in major veins was thicker than the leaf lamina, meaning that high activities measured in midvein and secondary veins underestimated actual ones, the images led us conclude that after one hour of exposure to $^{11}\text{CO}_2$, much tracer had been loaded into the phloem to be transported out of the leaf. This higher tracer intensities in major veins also corresponds to the earlier ^{14}C findings of Rennie and Turgeon (2009) and Fu et al. (2011) in active loaders. Despite the challenges regarding overlying tissue effects, tracer distribution differences in ^{11}C -autoradiographs were sufficiently large to ensure a reliable assessment of passive and active phloem loading strategies in leaves of contrasting species.

Phloem loading in tropical tree species

Whereas all *Erythrophleum* spp. leaves showed the anticipated passive phloem loading strategy, only young leaves of *M. eminii* could be identified as

passive loaders (Fig. 5.4). Mature leaves showed a tracer pattern that suggested active loading, but with this difference that accumulation of tracer was observed near the midvein and secondary veins instead of inside the veins. When images were corrected for signal reduction induced by differences in overlying tissue thickness (Fig. 5.5), similar tracer intensities inside and next to the veins were found (Fig. 5.6). This accumulation pattern from mesophyll towards major veins indicates active loading. Alternatively, this tracer distribution pattern could also be explained by a rapid export of tracer out of the mesophyll, with most of the tracer already within the major veins after pulse-labelling, which would also indicate active loading (Lalonde et al. 2003). The remainder of tracer in the mesophyll in this case could be carbon that remains as storage (for instance, in the form of starch). ¹⁴CO₂-autoradiographs of *Nicotiana tabacum* cv. Samsun (NN), an active loader with high export rates, also showed elevated tracer amounts in the major veins, with a lower evenly distributed amount of tracer in the mesophyll, measured 1 hour after labelling (Zavaliev et al. 2010). Although active phloem loading is uncommon in a woody tree species, it is certainly not impossible (Fu et al. 2011, Thoms et al. 2017). Interestingly, *M. eminii*, like many tropical species, is only deciduous in response to drought (Epila et al. 2017c) and thus resembles herbaceous species for this trait. Meta-studies on phloem loading strategies reveal that hardly any data is available for tropical species (Rennie and Turgeon 2009, Fu et al. 2011, Jensen et al. 2013). Anatomical studies by Gamalei (1989, 1991) demonstrated that tropical tree species typically have open cell types (with many plasmodesmata), which is associated with passive loading, while a follow-up study by Davidson et al. (2011) found no clear link between climate zone and loading type. But the Gamalei studies classified phloem loading cells of the family Rhamnaceae (of which *M. eminii* is a member) as an intermediate type, between open (passive loading) and closed (with few plasmodesmata, active loading) (Gamalei 1989). This type of cells can be found in tree and herbaceous species, and has been related to both active and passive loading (Gamalei 1989, Reidel et al. 2009, Davidson et al. 2011, Fu et al. 2011). As non-deciduousness is a typical trait in the tropics, it would be interesting to expand the existing anatomical studies with studies directly visualising phloem loading in tropical species. Körner (2003) showed that leaves of tropical tree species contain lower levels of non-structural carbohydrates (NSC) than

temperate species. Lower levels of NSC in leaves would be the norm in active loaders, as they keep a lower carbon inventory (Turgeon 2010). Also branch wood NSC levels were observed to be lower in tropical trees, pointing to a lower investment in storage, again in line with the behaviour of herbaceous active loaders. But, large variation exists in foliar NSC so jumping to conclusions would be too simplistic (Martínez-Vilalta et al. 2016). It does however highlight that tropical species, certainly in Africa, deserve more attention as they are underrepresented despite their large significance in worldwide carbon stocks and cycling (Cao et al. 2001, Bonan 2008, Fisher et al. 2013, Epila et al. 2018).

¹¹C- versus ¹⁴C-autoradiography

We have successfully used ¹¹C-autoradiography to assess carbon tracer distribution and phloem loading strategies in leaves of contrasting plant species. Compared to ¹⁴C, working with ¹¹C as a tracer results in autoradiographs with lower resolution, because the higher energy of the emitted positrons ionises more crystals in the phosphor plate. In ¹⁴C-autoradiography, leaves are typically freeze-dried, to prevent that emitted radiation travels through aqueous tissue and undergoes interactions. For ¹¹C-autoradiography, this would prevent the issue of positron range because in dry matter, the probability of annihilation would be negligible, but the process of freeze-drying can take a period ranging from half a day to multiple days (personal communication R. Turgeon). With ¹⁴C, activity will hardly reduce over the course of drying because of its half-life time of 5730 years. In ¹¹C-autoradiography however, much less time is available to process samples (such as freeze-drying), because of ¹¹C's short half-life time (20.4 min). Taking the ¹¹C-autoradiograph after, for instance, half a day drying will have reduced ¹¹C activity inside the samples below the detection limit. Because freeze-drying is not an option in ¹¹C-autoradiography, we resolved the overlying tissue issue on reduced tracer detection by correcting for tissue thickness using anatomical information. These corrections can be further improved by using detailed 2-D or even 3-D scans, which could be acquired with 3-D laser or CT scanning, if technological challenges are overcome (Dhondt et al. 2010, Dupuis et al. 2017). Also, ¹¹C positrons possess higher energy (mean energy 390 keV) than ¹⁴C betas (mean energy 49 keV), which will result in a lower resolution of ¹¹C-autoradiography, because resolution is a function of energy (personal

communication R. Edler) (Phelps et al. 1975, Levin and Hoffman 1999, Chiu et al. 2007, Jødal et al. 2012).

An advantage of using ^{11}C , over ^{14}C , as a tracer is that ^{11}C is a positron emitter, and can thus be used in PET scanners (Chapter 4). A combination of carbon transport dynamics in 3-D with PET complemented with a 2-D higher-resolution ^{11}C -autoradiograph of resulting carbon distribution contributes to the call for and suit of new methodologies to establish a more comprehensive picture of sugar distribution in plants (Savage et al. 2016).

Conclusion

We demonstrated that ^{11}C -autoradiography is a powerful tool to identify phloem loading strategies in leaves of contrasting species. Although ^{11}C has a too short half-life to freeze-dry samples, corrections for leaf and tissue thickness were adequate to classify species as active or passive loaders. Because ^{11}C is also compatible with plant-PET scanners carbon distribution, loading and transport dynamics can be imaged and analysed together, which contributes to the need of new methods to acquire a more comprehensive picture of phloem dynamics and carbon regulation.

6

CHAPTER 6

Plant-PET reveals phloem vulnerability to drought in *Populus tremula* under changing climate regimes

Abstract

Phloem transport is of great importance in trees to distribute assimilated carbon across the entire tree. Nevertheless, knowledge of phloem is incomplete, because of the complexity to measure phloem transport and its characteristics. Only few studies address how phloem transport might change with climate with most data originating from theoretical studies. We measured phloem characteristics in leaves of young *Populus tremula* L. trees grown during 5 months under ambient (T_A) and elevated (T_E) atmospheric CO_2 concentration ($[CO_2]$) using a combination of positron emission tomography (PET) and compartmental modelling. Short-term phloem dynamics were measured *in vivo* and non-invasively using the short-lived isotope of carbon, ^{11}C (half-life 20.4 min). Trees were scanned in well-watered and dry conditions to assess changes in phloem characteristics induced by drought. Reliability of the PET-generated data was verified with reported observations in literature. Phloem velocity was highest in well-watered T_E trees, but completely ceased under drought, while phloem velocity reduced only 60 % in T_A at the same level of drought. These findings suggest that phloem transport in T_E trees might be more vulnerable to drought. We discuss how a higher phloem vulnerability to drought in a changing climate could hinder the putative role of sugars in cavitation repair or as surfactants for nanobubble stabilisation. In summary, trees grown for 5 months under elevated $[CO_2]$ appeared to be less well-acclimated to face the projected hotter droughts in a changing climate.

Introduction

Phloem transport of sugars and other building stones is of pivotal importance for growth and maintenance of non-photosynthesising plant parts (Sala et al. 2012, De Schepper et al. 2013b, Steppe et al. 2015). However, it remains a great challenge to investigate phloem, and to fully understand how it works, what it controls, and how climate change might impact it (Van Bel 2003, Thompson 2006, McDowell et al. 2008, Turgeon and Wolf 2009, Knoblauch and Peters 2010, Sala et al. 2010, Sala et al. 2012, Hall and Minchin 2013, Sevanto 2014, Sevanto et al. 2014, Savage et al. 2016, Savage et al. 2017). Current understanding of phloem flow is based on source-sink dynamics, proposed back in 1930 by Münch. Since then, remarkably little has changed to this theory, which basically states that solutes are loaded into the phloem close to the site where they are produced (sources: typically leaves), and are unloaded at sites where they are needed (sinks: roots, shoots or storage tissue) (Van Bel 2003, De Schepper et al. 2013b). Phloem flow between sources and sinks is driven by water drawn into the sieve elements because of the negative osmotic potential, generated by the concentration of solutes, which need to be transported (Van Bel 2003, De Schepper et al. 2013b). One important addendum that has been made to Münch's theory since its introduction is the leakage-retrieval mechanism of solutes during transport (De Schepper et al. 2013b). Leakage and retrieval is important to feed lateral sinks (such as stem tissues), and has been proposed to play an important function in maintaining phloem flow over long distances (Van Bel 2003, Thorpe et al. 2005, Van Bel and Hafke 2005, De Schepper et al. 2013b).

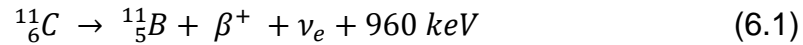
As a consequence of climatic changes, trees are expected to face hotter droughts, which might impede phloem transport due to water shortage and put cells and organs to danger that rely on transported assimilates (McDowell et al. 2008, Sala et al. 2010, Sevanto 2014, Sevanto et al. 2014, Allen et al. 2015, Steppe et al. 2015). Assessing impacts of climate change is especially difficult, because both water and carbon relations are profoundly affected, in positive and negative ways, while also being strongly interrelated (Chapter 4) (Steppe et al. 2015, Savage et al. 2016). Functioning of phloem strongly depends on both water and carbon, making the consequences of climate change uncertain (Ainsworth

and Lemonnier 2018). Furthermore, phloem is a complex chain of living cells with high sensitivity. When phloem is damaged, the sudden release of hydrostatic pressure can destroy multiple phloem cells, change molecular shapes of proteins, and result in the release of clogging substances to shut off and protect the phloem from losing valuable phloem sap, making phloem even harder to investigate (Turgeon and Wolf 2009, Knoblauch and Peters 2010).

To overcome some of these experimental difficulties we propose PET (positron emission tomography), as PET scanners enable to capture radioactive tracers dynamically, *in vivo* and non-invasively (Chapter 4). We used plant-PET scans to visualise phloem transport in intact leaves of one-year-old potted *Populus tremula* L. trees by simultaneously exposing and measuring branches with multiple leaves to gaseous ^{11}C -labelled CO_2 ($^{11}\text{CO}_2$). Prior to the PET measurements, trees were grown in ambient (T_A ; 404 ppm) and elevated (T_E ; 659 ppm) atmospheric CO_2 conditions during 5 months. Trees were scanned when well-watered and after some days of drought to assess changes in specific phloem characteristics. Compartmental modelling was applied to compute phloem velocity and several exchange parameters. Two main questions were addressed: (i) Do climate change conditions affect native dynamics of phloem transport and (ii) have trees grown under climate change conditions a phloem system with altered vulnerability to drought? Our specific working hypotheses were that carbon fertilisation will cause (i) higher phloem velocities, because of increased source strength and (ii) higher resilience to drought because of higher carbon storage and lower impact of drought due to stomatal down-regulation.

Tracing the flow of photoassimilates in plants with ^{11}C

The short-lived carbon isotope ^{11}C can be successfully used to trace phloem sugar flow (Chapter 4). If a plant is exposed to $^{11}\text{CO}_2$, leaves will take up and photosynthesise it, just like naturally occurring CO_2 , eventually incorporating the ^{11}C -atoms in all sorts of building blocks, typically sucrose, if it is meant for transport (Minchin and Thorpe 2003). These photoassimilates can be allocated to leaf tissue or can be loaded into the phloem and transported out of the leaf. The half-life of ^{11}C is 20.4 minutes, implying that within a relatively short time span (a few hours) nearly all of the administered ^{11}C will have decayed to a stable boron atom (B) as in Eq. 6.1:



β^+ is a positron (which is the antimatter conjugate of an electron), ν_e is an electron neutrino, and 960 keV is the released amount of energy (Bailey et al. 2005). The resulting boron atom will not exert any considerable influence because the total absolute amount of used tracer is very small and boron naturally occurs in plants (Blevins and Lukaszewski 1998). Given the typical starting activities used in our experiments (555 ± 27 MBq), and assuming that all administered ${}^{11}\text{CO}_2$ would be incorporated, a total of only 1.6 pmol boron would be added to the plant.

Like in ${}^{11}\text{C}$ -autoradiography (Chapter 5), positron range poses challenges to PET when measuring thin objects. Whereas in autoradiography annihilation reduces the chance for detection, in PET it is a necessity to measure activity. Leaves are amongst the most important plant organs, but are thus an obstacle when performing PET. Because of their thin dimensions, positrons have a relatively high chance of exiting the leaves before annihilating (Alexoff et al. 2011, Partelová et al. 2016). As soon as positrons reach the empty air, the probability of annihilating drops tremendously and thus most tracer will be left undetected. One possible solution is to surround leaves by positron shields, i.e. material in which the chance of annihilation is very high, such as aluminium foil or plastic (Kiser et al. 2008, Alexoff et al. 2011, Partelová et al. 2016). But this solution has an important trade-off about how close to position these shields to the leaves. Placing them too close will influence leaf gas exchange and thus plant physiology, but placing them too far will considerably reduce resolution because the positrons fly out of the leaf under any angle. Another possible approach is to determine the expected fraction of positron escape by the use of phantoms, mimicking a leaf, as performed by Partelová et al. (2016). A high-detailed correction map would require high-resolution data on leaf thickness, which could, in theory, be generated with 3-D laser or CT-scanning (Dhondt et al. 2010, Dupuis et al. 2017).

These quantification issues can be avoided by using relative dynamic evolution in activity instead of absolute amounts. When doing so, it is important to only consider dynamics in plant parts with the same structure and dimension. Analysis of dynamic tracer activity along organs that remain uniform in structure

and dimension is then valid without the need to account for positron escape. As soon as dimensions change, such as transport from leaf blade to veins, veins to petiole or petiole to branch, the different fractions of positron escape should be taken into account (Alexoff et al. 2011, Partelová et al. 2016).

Compartmental modelling to compute phloem characteristics

Compartmental modelling is one of the approaches to derive specific phloem characteristics, such as phloem velocity and exchange of tracer, from dynamic PET scans. A compartmental model based on Bühler et al. (2011) was implemented in the plant modelling software PhytoSim (Phyto-IT, Mariakerke, Belgium) and fed with data derived from ROIs (regions of interest) along the petioles of measured leaves (Fig. 6.1). The model of Bühler et al. (2011) was modified to account for respiration and loss of tracer out of the ROI (parameter c). Dynamic evolutions of tracer amounts in each ROI, called time-series (Fig. 4.2), were used to calibrate the model that consisted of three compartments per ROI (Fig. 6.1). The resolution of PET (about 1 mm) integrates processes in several tissues and therefore compartmental modelling is used to disentangle these processes from measured time-series (Bühler et al. 2011). Compartment 1 represents the phloem and is characterised by the phloem velocity v (cm h^{-1}) and the exchange parameter a (min^{-1}), which is the flow of tracer from compartment 1 to 2. In compartment 2, tracer can enter from the phloem (via a) and exit to a third compartment (via b (min^{-1})) or to the atmosphere, outside the ROI (via c , (min^{-1})). Loss of tracer to the atmosphere is linked to respiration, which produces gaseous CO_2 that can escape to the atmosphere. In compartment 3, the tracer is immobilised and movement or exchange with other compartments is no longer possible, representing a storage compartment. All parameters are assumed to be constant during measurements (i.e. 1 hour). While this model suited our measurements best, other model formulations with a different number of compartments or parameters can be developed in a similar way (Bühler et al. 2014).

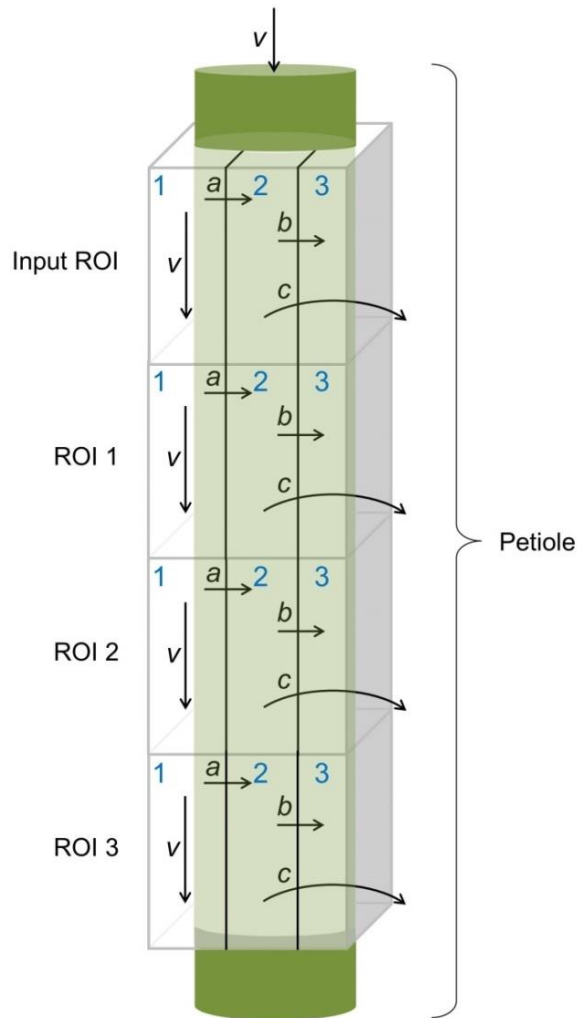


Figure 6.1 Schematic of the compartmental model used to simulate evolution of tracer amounts in the defined regions of interest (ROI) along the petiole of leaves. Tracer that enters an ROI is defined by bulk phloem velocity v (cm h^{-1}) and exchange parameters a , b and c (min^{-1}). Parameter v describes the phloem velocity (compartment 1). Tracer will move from the phloem to compartment 2 through a , and can enter compartment 3, via b where it is immobilised and stored, or can exit to the atmosphere (outside the ROI) through c . Parameters are assumed equal in each ROI, and data for the input ROI data is directly derived from measured activity.

For each ROI, evolution of tracer amounts in the three compartments was simulated and exchange between ROIs was determined by phloem velocity and the amount of tracer in the phloem compartment of the ROIs upstream. Equations 6.2 – 6.4 describe the change in tracer amount in each compartment for ROI i :

$$\frac{dT_{C_i}^1}{dt} = \frac{v}{l} \cdot T_{C_{i-1}}^1 - \frac{v}{l} \cdot T_{C_i}^1 - a \cdot T_{C_i}^1 \quad (6.2)$$

$$\frac{dT_{C_i}^2}{dt} = a \cdot T_{C_i}^1 - b \cdot T_{C_i}^2 - c \cdot T_{C_i}^2 \quad (6.3)$$

$$\frac{dT_{C_i}^3}{dt} = b \cdot T_{C_i}^2 \quad (6.4)$$

T_C (number of detections) is the amount of ^{11}C -tracer with in superscript the compartment number and in subscript the ROI number (numbered in downstream order). Constant l (mm) is the length of the ROI. Parameter a is the net result of leakage and retrieval, comparable with the fixed ratio implemented by Bühler et al. (2011), because separate leakage and retrieval parameters were not identifiable.

For the first time-frame, we assumed that all measured tracer was present in compartment 1. We tested this assumption and found the parameter outcome to be insensitive to whether initial activity was allocated to compartment 1 only or distributed over all 3 compartments.

In the model, the input ROI (with all other ROIs being located downstream from this) does not receive any tracer from upstream ROIs. In reality, however, tracer will enter this ROI (from the leaf), so values for this input ROI were directly derived from the total amount of tracer ($T_{C_{total}}$) measured in the input ROI (for each time step) according to equations 6.5 – 6.7:

$$T_{C_{input}}^1 = T_{C_{total}} - T_{C_{input}}^2 - T_{C_{input}}^3 \quad (6.5)$$

$$\frac{dT_{C_{input}}^2}{dt} = a \cdot T_{C_{input}}^1 - b \cdot T_{C_{input}}^2 - c \cdot T_{C_{input}}^2 \quad (6.6)$$

$$\frac{dT_{C_{input}}^3}{dt} = b \cdot T_{C_{input}}^2 \quad (6.7)$$

Model sensitivity and identifiability were assessed according to De Pauw et al. (2008), and the four model parameters were identifiable, with each parameter having a high sensitivity in the model output. Model simulations were performed by using an adaptive step size fourth order Runge-Kutta solver (accuracy 10^{-6} , minimum step size 0.01 min) (Runge 1895, Kutta 1901, De Pauw et al. 2008). The model was then calibrated using Phytosim with time-series that were extracted from the PET scans by first performing a global random search twice

with 1500 evaluations to narrow down the initial parameter calibration ranges, followed by simulated annealing calibrations (Cardoso et al. 1996) with an iteration multiplier of 10, a cooling rate of 1, and 1500 evaluations. Calibration was terminated when the difference between simulated and measured time-series of total amount of tracer per ROI was minimised. Correspondence between model simulation and measurements was expressed using the coefficient of determination (R^2) calculated for each ROI.

Materials and methods

Plant material and experimental design

PET-scans were made of young *Populus tremula* L. trees in their second growing season. Trees were planted 31 March 2017 and grown in treatment chambers (introduced in Chapters 2 and 3) under ambient (T_A : 404 ± 5 ppm during daytime, SE, N = 119) or elevated (T_E : 659 ± 3 ppm during daytime, SE, N = 119) atmospheric conditions for five months, prior to the PET scans. Air temperature in both treatment chambers was controlled to equal outdoor air temperature. Trees were well-watered, and grew in cylindrical 30 L containers, filled with a commercial potting soil mixture with a density of 680 kg m^{-3} and 15 % organic matter complemented by slow-releasing (8 – 9 months) nutrient grains (Osmocote Exact 15-9-11-2 N-P-K-Mg, ICL Specialty Fertilizers, Geldermalsen, The Netherlands).

Trees, ranging in height between 1.75 and 2 m, were transported from the treatment chambers to the INFINITY lab of Ghent University at UZ Gent at least 24 h before measurement to ensure that phloem transport was undisturbed upon scanning, because it is known that moving trees can influence phloem functioning for several hours (Pickard et al. 1993, Minchin and Thorpe 2003). At INFINITY, four 2 m-long arrays of red and blue LED-lights provided about $250 \mu\text{mol m}^{-2} \text{ s}^{-1}$ photosynthetic active radiation (PAR) at the top of the trees.

Trees from both treatments (T_A and T_E) were kept well-watered for the first scan (T_{AC} and T_{EC} , with C control), with leaf water potentials (ψ_l) measured with a pressure chamber (Model 1000, PMS instruments, Albany, OR, USA), averaging -0.40 ± 0.05 MPa (SE, N = 4 leaf measurements on T_{AC} tree 1, assumed the same for T_{AC} tree 2 and T_{EC} for which no measurements were

made). Trees of treatments T_A and T_E were measured a second time after one week of drought (T_{AD} and T_{ED} , with D drought), with average ψ_l of -1.80 ± 0.05 MPa (SE, $N = 9$ leaf measurements on the T_{AD} and T_{ED} tree). A T_A tree was also measured halfway dehydration (T_{ASD} , with SD semi-dry) when average ψ_l reached -1.28 ± 0.04 MPa (SE, $N = 4$ leaf measurements). In total, four T_A PET scans (two in well-watered control (T_{AC}), one in semi-dry (T_{ASD}) and one in dry (T_{AD}) conditions), and two T_E PET scans (one in well-watered control (T_{EC}) and one in dry (T_{ED}) conditions) were performed.

Leaf cuvette fitting the PET scanner

When performing experiments with gaseous $^{11}\text{CO}_2$ it has to be fed to the leaves in a fully airtight environment, because air contamination with radioactivity should be avoided at all times. In our study trees, the region that was labelled was scanned, whereas most studies label some leaves and scan roots, stem, fruits or other leaves (Chapter 4). The branch bag cuvette (Fig. 6.2 and design c in Fig 5.2) was used to expose between five and ten leaves at the distal part of intact branches, selected at breast-height, to gaseous $^{11}\text{CO}_2$. A wedge seal in the plastic was made with a kitchen vacuum packing machine (Vacupack Plus F380, Krups, Fleurus, Belgium) to minimise the opening between branch bag and branch. To ensure a fully airtight seal, a small 3-cm-long piece of plastic tubing was cut longitudinally, and covered on the inside with vacuum grease (Dow Corning, Auburn, MI, USA) and was installed around the branch (Fig. 6.3). The branch bag was then closed with cable ties around the tubed piece of branch. By using plastic tubing with vacuum grease, pressure on the branch was kept to a minimum in order to prevent damage to the outer cells of the branch, which is important because also this zone contains transport phloem. The branch bag cuvette was then introduced into the PET scanner bore with detector rings (Fig. 6.2). Four 20-cm-long arrays, alternating containing six red or six blue LED-lights, were positioned above the leaves, providing them with about $250 \mu\text{mol PAR m}^{-2} \text{s}^{-1}$.

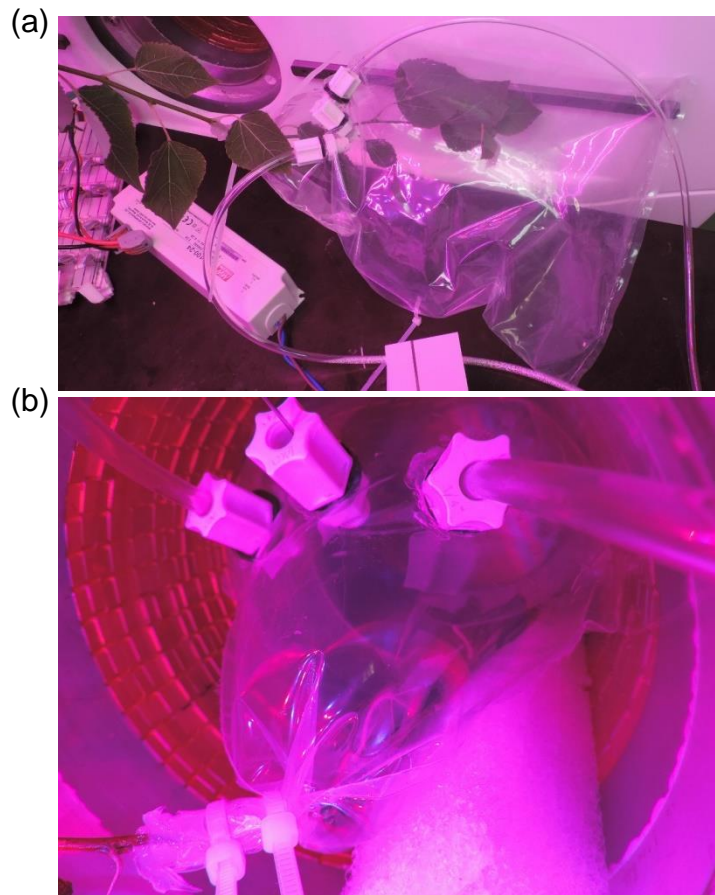


Figure 6.2 (a) Branch bag cuvette used to expose leaves of an intact branch to gaseous $^{11}\text{CO}_2$, and (b) air-stream inflated branch bag cuvette inserted into the PET scanner. The gold squared PET detectors are arranged in a cylinder of 15 cm diameter and 8 cm depth. The white foam, used to position the branch inside the scanner, will not interact with the positrons because of its low density.



Figure 6.3 Detail of the plastic tubing, covered with vacuum grease on the inside and encapsulating the intact branch to ensure an airtight seal without damaging the branch surface.

Flowchart

Leaves enclosed in the cuvette were continuously supplied with fresh air to prevent a drop in $[\text{CO}_2]$ or an increase in relative humidity (RH) caused by leaf gas exchange. A continuous airflow passed through two tubes (inner diameter

4.0 mm and outer diameter 5.6 mm) connected to the cuvette (Fig. 6.4). The inflow was controlled by means of a LI-6400 (LI-COR, Biosciences, Lincoln, NE, USA). Air was supplied to the cuvette at a rate of 0.58 L min^{-1} with an RH of 41 % at a temperature of 22°C . Atmospheric $[\text{CO}_2]$ was set at 400 ppm for T_A and 700 ppm for T_E trees. In- and outflow were sent through flow meters (AWM5101, Honeywell, Morris Plains, NJ, USA) to monitor equal flows. Outflowing air was directed through a 50-cm-long CO_2 scrubbing column, consisting of soda lime pellets (calcium hydroxide on sodium carbonate carrier, Merck, Overijse, Belgium) to purify the emitted air and strip it from CO_2 , also capturing all radioactive $^{11}\text{CO}_2$. A third tube was connected to the branch bag through which the gaseous $^{11}\text{CO}_2$ was administered to the leaves (Fig. 6.4). This tube was smaller (inner diameter 0.9 mm and outer diameter 1.5 mm) and was connected to the cuvette by a needle (inner diameter 0.5 mm) inserted through a septum. $^{11}\text{CO}_2$ arrived in solution with a base (NaOH), and was released by adding a small excess of equimolar acidic solution (H_2SO_4). Air from the room was blown through a second needle (inner diameter 0.5 mm), which was submerged in the solution, to direct released $^{11}\text{CO}_2$ through a third wider needle (inner diameter 1 mm) positioned in the headspace of the vial and which was connected to the small tube supplying the $^{11}\text{CO}_2$ to the cuvette. During $^{11}\text{CO}_2$ administering, bulk airflow was kept constant causing dilution of the gaseous $^{11}\text{CO}_2$ concentration during the first few minutes while being taken up by the leaves. Cuvettes had a volume of 2.9 L with a refresh rate of 5 minutes.

Production of $^{11}\text{CO}_2$

$^{11}\text{CO}_2$ was produced in a cyclotron (18 MeV protons, IBA, Belgium), at UZ Gent, about 100 m from the PET scanner. Proximity of the cyclotron to the scanner is important to minimise activity loss during transport. Inside the cyclotron, ions are accelerated towards a N_2/H_2 (5 %) target, resulting in the production of $^{11}\text{CH}_4$. This product was cryogenically concentrated and released by heating, passing over a small flow of He through a heated reactor with cobalt oxide to eventually be converted into $^{11}\text{CO}_2$. This $^{11}\text{CO}_2$ was captured in basic NaOH by bubbling it through a 1 M solution of NaOH. Starting activities were $555 \pm 27 \text{ MBq}$ (SE, N = 6).

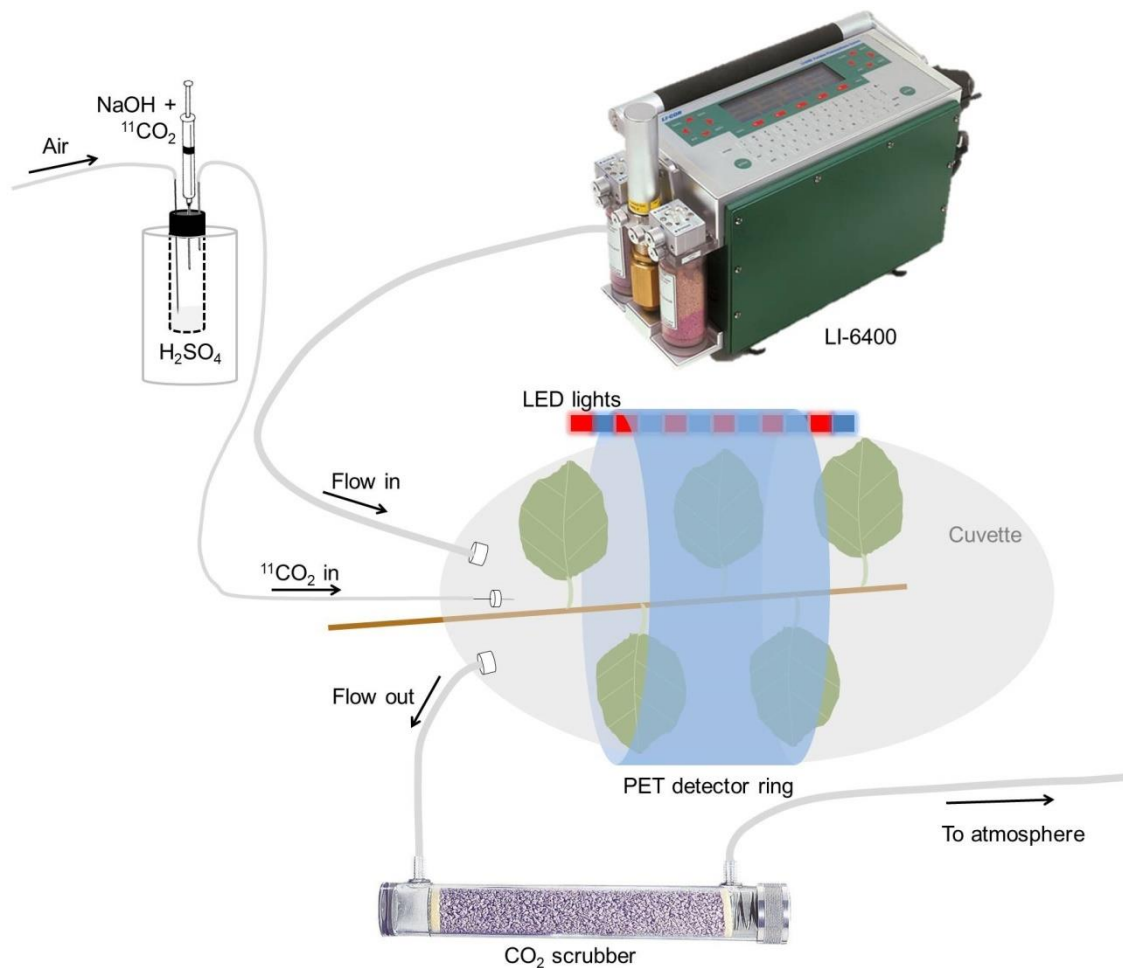


Figure 6.4 Overview of the set-up and flowchart to take PET scans. The distal part of a selected intact branch was inserted into an airtight cuvette and positioned inside the PET scanner, which had LED lights at the top. Bulk air flow that was controlled (flow rate, CO_2 concentration, temperature, and relative humidity of the air) by a LI-6400 system was sent through the cuvette. Outflowing air was directed through a CO_2 scrubber before being released into the atmosphere. Dissolved ${}^{11}\text{CO}_2$ in NaOH arrived in a syringe that was emptied in a vial filled with a small excess of equimolar H_2SO_4 , which released the ${}^{11}\text{CO}_2$. Air was blown through the solution to direct the gaseous ${}^{11}\text{CO}_2$ into the cuvette.

PET scanner

In this study, we used the LabPET8 scanner (TriFoil Imaging, Chatsworth, CA, USA), located at INFINITY. This scanner has been designed to image small animals (mice and rats) for preclinical research. Detectors consist of LGSO ($\text{Lu}_{0.4}\text{Gd}_{1.6}\text{SiO}_5:\text{Ce}$) and LYSO ($\text{Lu}_{1.9}\text{Y}_{0.1}\text{SiO}_5:\text{Ce}$) scintillation crystals and avalanche photodiodes are used for read-out. The detection ring has a diameter of 15 cm and a depth of 8 cm, which results in a relatively small field of view (FOV) for plant imaging. Twice a year, the detectors are normalised and the scanner is calibrated.

The PET-scanner registered activity for 1 hour after exposing the intact branch with leaves to gaseous $^{11}\text{CO}_2$. After scanning, dynamic reconstruction of the acquired signals was done by the LabPET reconstruction software (Version 1.12.1, TriFoil Imaging, Chatsworth, CA, USA), using the 2-D maximum-likelihood expectation-maximization algorithm, with a setting of 50 iterations and 5-min time frames. The result is a decay-corrected 4-D image (x,y,z,t) consisting of 12 time-frames with 63 slices of 200 x 200 pixels. Each pixel had a bit depth of 16 bits. These images were imported in Amide (amide.sourceforge.net) and a 3-D median filter with a kernel size of 3 was applied to reduce noise and highlight plant structures. On these images petioles were identified and box-shaped ROIs were drawn around the petioles. Petioles were selected to measure phloem velocity, because, (i) dimensions remain similar along the length of the petiole (average diameter of 0.975 ± 0.057 mm (SE, N = 30 leaves from studied trees)), which avoids positron escape problems during analysis, and (ii) only transport phloem is present. Four consecutive ROIs (input ROI + ROI 1–3) were drawn along the direction of phloem flow (Fig. 6.1) with each ROI being 5 mm in length. The cumulative activity in each ROI was calculated per time-frame, and these time-series were exported to be used as input for the compartmental model.

Results

In general, at least one leaf was entirely visible within the FOV, on which the petiole could be identified and ROIs drawn (Fig. 6.5). Leaf material was checked to ensure that petiole dimensions did not change with ROI. In T_{ED} , tracer was detected inside the petiole, but the amount did not change during the experiment, indicating that there was tracer uptake but no bulk flow inside the phloem. Therefore, no phloem velocity or exchange parameters could be computed. Simulated and measured time-series closely corresponded (Fig. 6.6), as pointed out by the high R^2 values (≈ 0.9 for most simulations).

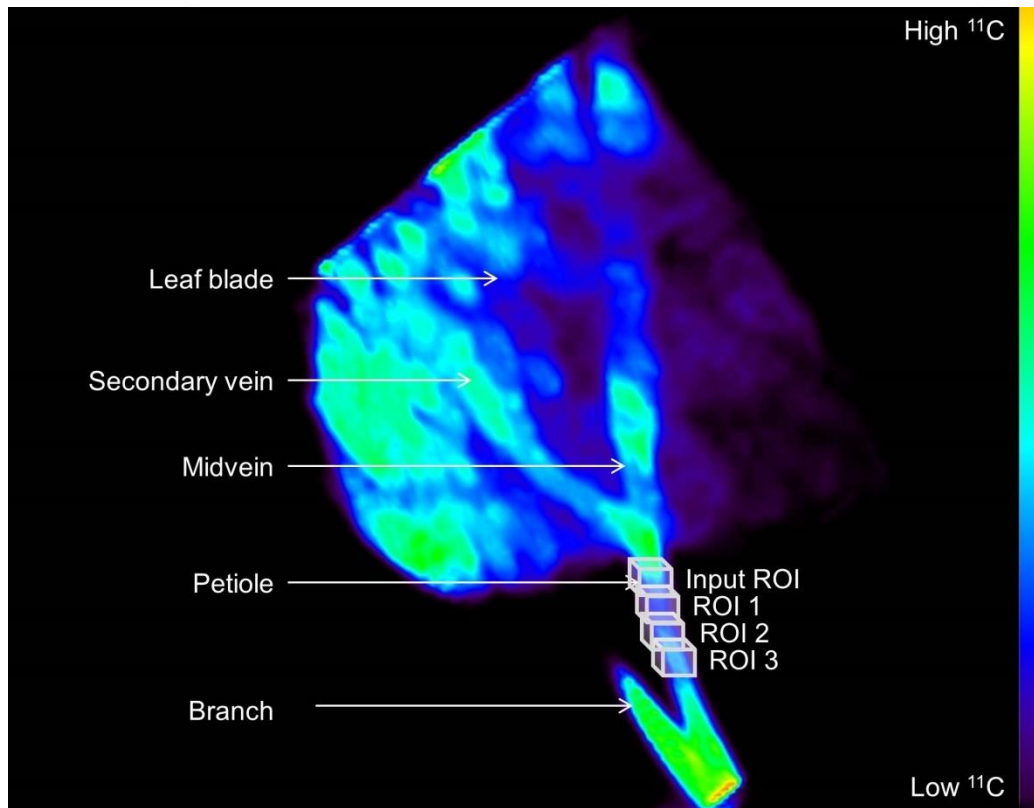


Figure 6.5 Example of cumulated detected activity for a 1-hour PET scan of a *Populus tremula* L. leaf developed under well-watered conditions in an elevated CO₂ atmosphere (659 ppm) (T_{EC}). The leaf contour is clearly visible. The midvein and several secondary veins show higher detected ¹¹C activity. The sharp contour at the upper left edge of the leaf is where the field of view (FOV) ends. Connection of the leaf to a branch is visible at the lower edge of the image. Box-shaped regions of interest (ROIs) are drawn around the petiole which is attached to the intact branch.

In the study leaves, phloem velocity in T_E was 50 % larger than in T_A when well-watered. When subjected to drought v in the study leaves strongly reduced (Fig. 6.7a). Drought caused a reduction in v of about 60 % (i.e., reduction by a factor 2.7) in T_A leaves compared to well-watered control ones, while the same level of drought stress reduced v by 100 % (i.e., phloem transport ceases) in T_E leaves. The exchange parameter a defines how much tracer leaked out of the phloem, with a higher value indicating less tracer being left for transport further down the phloem. In general, net leakage was higher in T_A than in T_E leaves with the highest values found in T_{AC} followed by T_{AD} and T_{ASD} (Fig. 6.7b). The amount of tracer that flowed into the storage compartment 3 (parameter b) was in general very low, except in T_{AD} leaves (Fig. 6.7b). The amount of tracer that left the petiole (parameter c), was low in T_{ASD} and T_{EC}, intermediate in T_{AC}, and high in T_{AD} leaves (Fig. 6.7b).

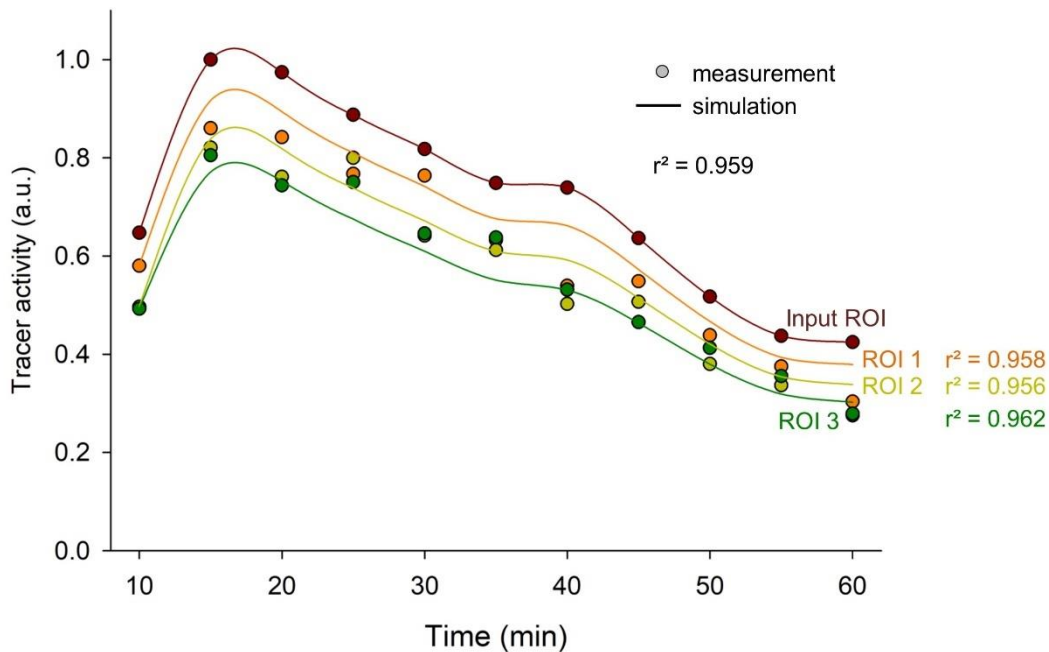


Figure 6.6 Example of measured (circles) and simulated (lines) time-series for four regions of interest (input ROI + ROI 1–3) (as in Fig. 6.1 and 6.5) on a petiole of a *Populus tremula* L. leaf developed under well-watered conditions in an elevated CO₂ atmosphere (659 ppm) (T_{EC}). Input ROI measurements are used as input for the compartmental model. Time is expressed as minutes after pulse-labelling ¹¹C₂ and the simulation is performed starting ten minutes after the pulse to ensure that air inside the cuvette is refreshed and void of ¹¹C₂ tracer originating from the pulse. The coefficients of determination (R²) are calculated per simulation result and a general average is also shown. Arbitrary units were used with the maximal value set to 1.

Discussion

Elevated CO₂ changes phloem velocity and its response to drought

Phloem transport characteristics, such as phloem velocity and net leakage from phloem to surrounding tissues of *P. tremula* leaves were successfully assessed using a combination of PET scans and compartmental modelling. The compartmental model was able to simulate the phloem behaviour in petioles well, resulting in a close agreement between measured and simulated time-series of ¹¹C activity (Fig. 6.6). A range of methods have been applied since the 1950s to measure phloem velocities in stems or branches ranging from the use of stable (¹³C) and radioactive (¹¹C, ¹⁴C) carbon-tracers, to magnetic resonance imaging, stylet exudation and calculations from sieve element conductivity (see reviews by Epron et al. (2012), Jensen et al. (2012), Liesche et al. (2015)). Because

substantial differences exist in stem phloem velocity between angiosperms and gymnosperms, *P. tremula*'s velocities were compared with those of angiosperms, which range between 19 and 450 cm h⁻¹ under ambient conditions (well-watered, ambient atmospheric [CO₂]) (Fig. 6.8) (Jensen et al. 2012, Liesche et al. 2015). *P. tremula*'s average T_{AC} phloem velocity of 49.5 cm h⁻¹ fell into the reported range (Fig. 6.8), and is close to the value of 43 cm h⁻¹ reported by Babst et al. (2005), who measured with ¹¹C phloem velocity in *Populus nigra*. This convergence between phloem velocity data from literature and our data points indicated that the compartmental modelling provided realistic values.

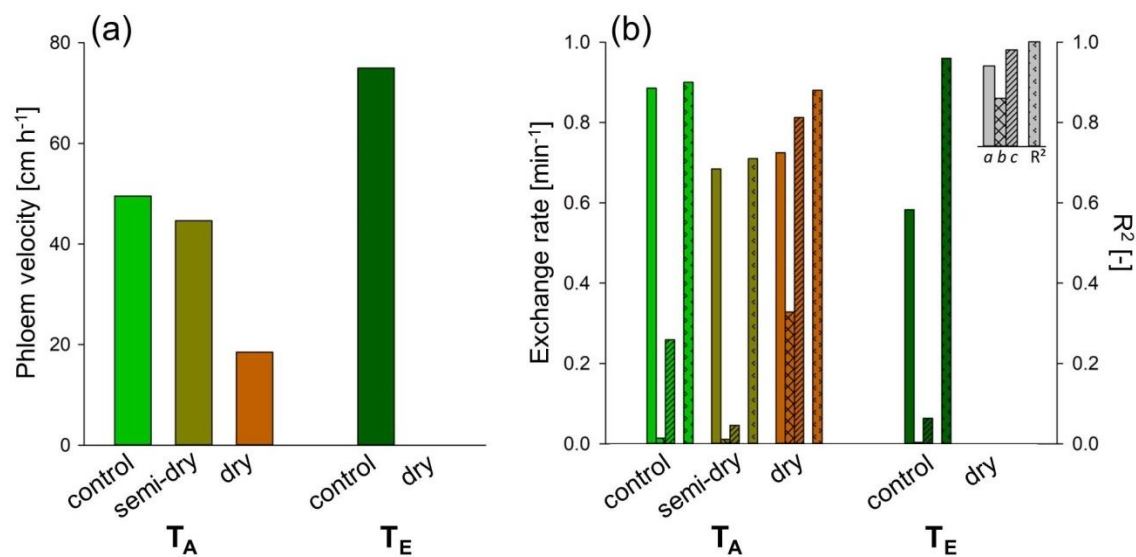


Figure 6.7 Calibrated parameter values for the compartmental model as defined in Fig. 6.1, with (a) v as phloem velocity and (b) a , b and c as exchange parameters, and coefficient of determination (R^2), calculated per ROI and averaged. T_A and T_E are trees grown under ambient (404 ppm) or elevated (659 ppm) atmospheric CO₂ conditions, respectively. T_A trees were scanned when well-watered control (average value of two measured trees), and then subjected to drought and measured in semi-dry and dry state. T_E trees were scanned when well-watered control and dry, but no values are shown for dry measurements because no bulk flow was observed. Average leaf water potentials were -0.40 ± 0.05 MPa, -1.28 ± 0.04 MPa, -1.80 ± 0.05 MPa for control, semi-dry and dry state, respectively.

According to our single observation, phloem velocity increased with 51 % when trees were grown under elevated atmospheric [CO₂] supporting our first working hypothesis. The observed increase in phloem velocity can be caused by an increase in source strength because of photosynthetic stimulation under elevated atmospheric [CO₂] (Davey et al. 2006, Ainsworth and Rogers 2007,

Ainsworth and Bush 2011, Ainsworth and Lemonnier 2018). Davey et al. (2006) reported that this photosynthetic stimulation was sustained over four growing seasons in three *Populus* spp. and that carbon use (difference between photosynthetic assimilation and non-structural carbohydrates (NSC)) and distribution over the tree increased with 50 to more than 100 % in response to the increase in [CO₂] of 180 ppm.

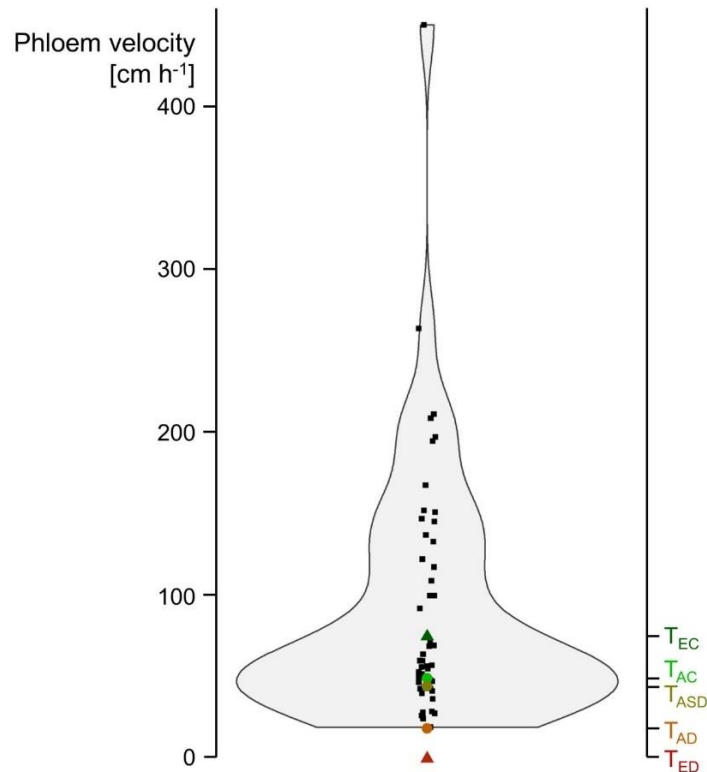


Figure 6.8 Range of phloem velocities reported in angiosperms (N = 52). Phloem velocities (black squares) were measured under ambient growing conditions (i.e., well-watered, ambient atmospheric [CO₂]) with different methods. Wider areas in the graph indicate more reported values in that range (based on data from Jensen et al. (2012) and Liesche et al. (2015)). Phloem velocities measured in *Populus tremula* leaves are added in colour: T_A and T_E represent leaves from trees developed under ambient (404 ppm) and elevated (659 ppm) [CO₂], respectively. T_{AC} refers to ambient, well-watered control, T_{ASD} to ambient, semi-dry, T_{AD} to ambient, dry, T_{EC} to elevated [CO₂], well-watered control, and T_{ED} to elevated [CO₂], dry.

Drought tended to cause a decrease in phloem velocity in *P. tremula* leaves (Fig. 6.7a). While drought strongly reduced phloem velocity in T_{AD}, tracer and hence phloem flow completely stopped in T_{ED}, which might suggest that phloem velocity is more prone to drought when trees grow under elevated atmospheric [CO₂]. To date, directly measured data on phloem drought research

is scarce. The data that is available mostly originates from measurements using the delay in transport between canopy and soil measured with ^{13}C pulses. Although useful for purposes of comparison, they do not yield the same information on short-distance transport as our method, because photoassimilates can still interact in many ways during transfer in the phloem, by fixation and/or remobilisation (De Schepper et al. 2013b). Certainly under drought, also the lack of internal water, changes in conduit wall permeability or alterations in temporal storage and remobilization can strongly influence the retention time in the phloem system (Gessler et al. 2014, Sevanto 2014, Blessing et al. 2015). Using the ^{13}C -based delay in phloem transport between the canopy of young beech (*Fagus sylvatica* L.) trees and the soil, Barthel et al. (2011) found a drought-induced reduction factor in velocity of 2.5, which closely agrees with our measured reduction factor of 2.7 in T_{AD} . Ruehr et al. (2009) found a reduction in phloem transport velocities up to 1 cm h^{-1} also in young beech trees after imposing drought. Blessing et al. (2015) did not observe any effect of drought on the delay in transport in young beech trees, but they found an effect of temperature which they related to increased storage along the transport pathway.

Leakage-retrieval, carbon storage and respirational carbon loss

In general, a substantial amount of tracer leaked out of the phloem transport system in *P. tremula* leaves (leakage-retrieval parameter *a*) of which only a small fraction was stored (parameter *b*) (Fig. 6.7b). Carbon storage however tended to increase under drought (T_{AD} : Fig. 6.7b). Storing more carbon when confronted with drought has been attributed to a reduced metabolic demand for growth in sink tissue (Körner 2003, Hummel et al. 2010, Lemoine et al. 2013). Turgor-induced sink limitation resulting from water deficit demonstrates that drought does not lead to lower supply from sources, but rather induces reduction in sink demand (Wiley and Helliker 2012). Growth is indeed faster suppressed than photosynthesis when plants are exposed to drought, resulting in a positive C-balance and thus an increase in allocation to storage (Körner 2003, Sala et al. 2010, McDowell 2011). Also the respirational carbon loss from the petiole (parameter *c*) increased under drought (T_{AD} : Fig. 6.7b). Although there have been few studies, there is evidence of increased vascular bundle respiration in petioles of sugar beet petioles in early response to drought (Shugaeva et al.

2007). While effects of elevated $[\text{CO}_2]$ on respiration are still under intense debate, respirational carbon loss in *P. tremula* petioles showed a decrease in response to an increase in atmospheric $[\text{CO}_2]$ when trees were well-watered ($T_{AC} > T_{EC}$) (Gonzalez-Meler et al. 1996, Drake et al. 1999, Way et al. 2015). Lower c in T_{EC} might result from the lower a value, with less tracer leaking out of the phloem resulting in a lower rate of tracer respiration. Results should however not be generalized because respiration in petioles might be differently impacted than in the leaf blade.

Effect of drought on phloem functioning under elevated $[\text{CO}_2]$

Although only a single observation was available (and two for T_{AC}), the obtained values that could be compared to data from other studies corresponded well. If these data points are hence true, we might speculate that despite a higher phloem velocity in *P. tremula* petioles of leaves developed under elevated $[\text{CO}_2]$ when trees were well-watered, drought might affect phloem velocity much stronger (Fig 6.7a). A drought level ($\psi_1 = -1.8$ MPa) that caused a 60 % decrease in phloem velocity under ambient conditions caused a stop in phloem transport under elevated conditions. This might suggest a greater vulnerability of phloem to drought when *P. tremula* trees are grown under elevated $[\text{CO}_2]$. If phloem transport ceases, sinks that are dependent on energy and building stones delivered by the phloem will be affected. Much then depends on the pre-drought amount of storage of NSC and the capability of mobilising it. According to Dietze et al. (2014), trees prefer to use recently assimilated carbon, which may become limited more rapidly under drought in T_E compared to T_A because of the putative stronger response to drought. If readily available storage is low or absent in T_E (because of the lack of storage or the inability to remobilise it), trees will face carbon starvation (Sevanto et al. 2014). Given the higher phloem velocity observed under well-watered conditions in T_{EC} , the drought-induced decrease most likely occurred more sudden than in T_A . Such a decrease would then lower the amount of recently assimilated sugars that are still in “transit” or lower the ability to mobilise present NSC, because of the sudden lack in phloem flow, both reducing the amount of immediately available carbon (Carpenter et al. 2008, Sala et al. 2010, Sala et al. 2012). If phloem flow stops faster, the period of carbon starvation experienced by the tree will be longer, with the mechanism of carbon

starvation to explain tree mortality becoming more important than anticipated, certainly in the face of hotter droughts (Sala et al. 2012, Sevanto 2014, Sevanto et al. 2014, Allen et al. 2015).

But phloem is also intimately linked to xylem and both exert influences on each other. For instance, it has been suggested that sugars play an important role in the refilling of cavitated vessels (Zwieniecki and Holbrook 2009, Secchi and Zwieniecki 2011, Sevanto et al. 2011). If phloem would fail under less negative water potentials when grown under elevated $[\text{CO}_2]$, this might make a tree more vulnerable to drought-induced cavitation, because of the lower immediate sugar availability needed for refilling (Sevanto et al. 2011, Sevanto 2014, Sevanto et al. 2014). More recently, studies have indicated that the presence of sugars in xylem sap may stabilise nanobubbles, preventing these bubbles to expand and cause cavitation below a critical pressure threshold (Schenk et al. 2015, De Baerdemaeker et al. 2017, Schenk et al. 2017). If these results were true for phloem functioning throughout the entire plant, it might help explaining the less negative average values at which ψ_{88} and ψ_{100} were measured in trees grown under elevated $[\text{CO}_2]$ and temperature (Chapter 3). Alternatively, the indicated higher vulnerability to drought-induced cavitation of trees grown under elevated $[\text{CO}_2]$ and temperature (Chapter 3) could be the reason why phloem flow fails more rapidly, because delivery of water to the phloem is interrupted (Sevanto et al. 2011, Sevanto et al. 2014). Stopping phloem flow might also be an active process to preserve water inside the xylem, kicking in faster in trees that are likely more vulnerable to drought-induced cavitation (T_{EW} trees in Chapter 3). Such a mechanism could be in place if carbon storages are already sufficiently filled and sink strength is actively downregulated (Sala et al. 2010, Sala et al. 2012). It however remains unclear whether the finding in this chapter, with only an increase in atmospheric $[\text{CO}_2]$ are comparable with drought vulnerability measured on trees exposed to both elevated $[\text{CO}_2]$ and temperature.

Opportunities to improve our understanding of phloem functioning

No prior studies provided direct measurements of the effect of drought and elevated atmospheric $[\text{CO}_2]$ on phloem flow characteristics. Indirect measurements, resulting from changes in residence time or the arrival of a pulse-

label have significantly increased our knowledge on the response of phloem to drought, but do not provide information on what happens during phloem transport (Ruehr et al. 2009, Barthel et al. 2011, Epron et al. 2012, Blessing et al. 2015). Our current understanding of phloem functioning is mainly hampered because of the complexity to measure phloem. Plant-PET provides the possibility to study short-term dynamics of phloem flow in high-detail, but is a complex method which is not readily available. We have used a small-animal scanner, with which we have generated valuable data for some individuals, but it also showed the need for larger and more versatile plant-dedicated PET-scanners (e.g., Jahnke et al. (2009), Wang et al. (2014)). With the small-animal scanner, we could only analyse the distal part of intact branches with attached leaves, and it should be verified in larger, more versatile PET scanners whether the selected and analysed ROIs are most representative for an entire tree.

Nevertheless, we observed clear and logical trends, certainly in phloem velocities, which were in line with previously reported values. Our approach further enabled us to assess the effect of elevated $[\text{CO}_2]$ on phloem functioning, which remains largely unknown and is nearly unexplored, while being crucial if we aspire to understand tree functioning in the face of climate change (Ainsworth and Lemonnier 2018). Not only CO_2 concentrations, but also other climatological factors such as temperature and precipitation will alter. Therefore, we see an important role for plant-PET scans and compartmental modelling to further confirm or reject hypotheses and unravel mechanism that have been proposed concerning phloem functioning. How will the reduction in xylem water potential lower the availability of water for phloem flow (Mencuccini and Hölttä 2010, Hölttä et al. 2014, Savage et al. 2016)? Will higher temperature or less water increase viscosity resulting in a more syrupy and slower phloem flow (Jensen et al. 2013, Sevanto 2014, Savage et al. 2016)? What is the role of turgor under water deficit on the driving force of phloem (De Schepper et al. 2013b, Sevanto 2014)? How will altered carbon assimilation under elevated atmospheric $[\text{CO}_2]$ affect source strength, and the source-sink gradient (Pinheiro and Chaves 2011, Steppe et al. 2015)?

Conclusion

In our study, we observed indications that under well-watered conditions, trees grown under elevated [CO₂] tended to have an advantage, as a higher phloem velocity was measured. However, these trees appeared to stop phloem flow more rapidly when subjected to sudden drought, which would most likely make them more vulnerable to the adverse effects of drought and carbon starvation. If valid, this would contradict the often described mitigation of drought effects caused by a higher [CO₂] and the resulting decrease in stomatal conductance (Ainsworth and Rogers 2007, Xu et al. 2013, AbdElgawad et al. 2015, Allen et al. 2015). Plant-PET scanning in combination with compartmental modelling has proven to be a tool that can be used to gather the much-needed data on phloem transport and how this is impacted by atmospheric [CO₂] and drought. Further use of this technology can help in confirming whether the findings presented in this chapter are single case observations or more general trends.



CHAPTER 7

General discussion and outlook

Research justification

Climate change is a much-discussed topic since many years now, but it remains a difficult task and challenge to accurately project if and how it will reshape forests. To predict the consequences of an increase in air temperature or a change in precipitation pattern it is often possible to look at forests of other biomes across the world (**Chapter 1**). The impact of elevated atmospheric CO₂ concentration ([CO₂]) is, however, harder to predict, because almost no natural points of comparison exist in the world, apart from a few natural CO₂ springs (Badiani et al. 1999, Paoletti et al. 2005). How elevated [CO₂] will impact tree ecophysiology, and which effect the interaction between [CO₂], temperature and drought will have remains largely unanswered (Way 2013).

Because of many open questions, we have investigated the effects of elevated temperature and [CO₂], in combination with drought (hereafter called climatic changes). Because elevated [CO₂] directly affects carbon assimilation, but also indirectly transpiration due to stomatal regulation, it was important to assemble data of both water and carbon transport. A variety of methods were used with the aim to relate tree ecophysiological responses to climatic changes. With this PhD we have been the first to: (i) assess the combination of stem diameter variations and sap flow changes in trees grown under climatic changes, with and without drought; (ii) determine interactive effects of short-term (two months) plastic responses to elevated [CO₂] and temperature, and drought on stem hydraulic vulnerability to drought-induced cavitation; and (iii) measure the effect of elevated [CO₂] on phloem transport *in vivo* with plant-PET (positron emission tomography) and on phloem vulnerability to drought.

We conducted our research on *Populus tremula* L. trees, which is a species with high importance for biodiversity and an important constituent of boreal and temperate ecosystems across Eurasia (Myking et al. 2011, Caudullo et al. 2017). On the one hand, populations of *P. tremula* could come under pressure because of hotter droughts in the near future as it is a drought sensitive species (Johnson et al. 2002, Bogeat-Triboulot et al. 2007, Fichot et al. 2009), but on the other hand, this species is a widespread species with plastic and adaptive traits, and a pioneer species that establishes well after disturbances

(Hall et al. 2007, Fichot et al. 2009, De Carvalho et al. 2010, Myking et al. 2011, Possen et al. 2011).

Indirect measurements of cell characteristic adjustments

We planted one-year-old *P. tremula* trees in treatment chambers to expose them to altered conditions from the beginning of the growing season so that trees could respond to the imposed conditions. In **Chapter 2**, we observed that growth dynamics were influenced by treatments. Trees exposed to elevated air temperature and atmospheric [CO₂] increased growth rates and invested more in leaf biomass. They showed a lower rate of sap flow per unit leaf area, which pointed to stomatal response to higher [CO₂]. Other than expected, well-watered trees, exposed to elevated atmospheric [CO₂] and air temperature (T_{EW}), showed reduced growth rates compared to trees confronted with soil drought (T_{ED}). These lower growth rates were however not accompanied by typical stress responses that are observable as stronger stem shrinkage. These trees showed reduced growth, but also reduced shrinkage, which we explained by stiffer cells with lower elasticity and extensibility. This means that absolute values of maximum daily shrinkage, currently used to assess plant water status and optimal growing conditions, might become a less useful indicator under climatic changes (Moreno et al. 2006, Steppe et al. 2008, Badal et al. 2010, Fernández and Cuevas 2010, Ortuño et al. 2010, De Swaef et al. 2015). In **Chapter 3**, we analysed the hydraulic capacitance of these well-watered stems exposed to climatic changes (T_{EW}) and measured hydraulic capacitances which were on average lowest of all treatments in case of less negative stem water potential. This was in line with the putative treatment effects on cell characteristics, resulting in stiffer cells with a smaller stem water storage content, which was also hypothesised by Domec et al. (2016) in response to elevated atmospheric [CO₂]. Trees that were exposed to elevated atmospheric [CO₂] and air temperature but also soil drought (T_{ED}) did not show this trait of stiff cell walls, and showed higher growth rates than all other treatments (**Chapter 2**).

Vulnerability to drought and cavitation

Growth conditions of the trees in **Chapter 2** were fairly unstressed, also for the trees exposed to soil drought, because the aim was to ensure tree survival at

all times during the experiment. By constructing vulnerability curves of stems in **Chapter 3**, we could evaluate how vulnerable trees from different treatments were, if they were exposed to progressive levels of drought (resulting in more negative stem water potentials). Trees exposed to elevated atmospheric [CO_2] and air temperature tended towards higher vulnerability to drought-induced cavitation, and drought acclimatisation reduced vulnerability with the same degree in both ambient and elevated treatment chambers (T_A and T_E , respectively). Growth under drought conditions evoked a stronger plastic response than growth under elevated atmospheric [CO_2] and air temperature.

Sucrose from the phloem or hydrolysed starch from the storage is thought to play an important role in cavitation repair (Salleo et al. 2004, Zwieniecki and Holbrook 2009, Secchi and Zwieniecki 2011). More recently, it has been proposed that the presence of locally produced sugars serve as surfactants to stabilise nanobubbles, and prevent them from expanding and cavitating the vessel they are in (Schenk et al. 2015, De Baerdemaeker et al. 2017). Because of the higher or easier availability to carbon if grown under elevated atmospheric [CO_2], a higher allocation of carbon to stem storage tissues, and increased levels of non-structural carbohydrates (NSC) could be expected. We did not measure NSC levels, but despite its potential to mitigate vulnerability to drought-induced cavitation, a tendency towards higher vulnerability was observed in **Chapter 3** in trees grown under elevated atmospheric [CO_2] and air temperature (compared to their counterparts grown under ambient conditions). In case sucrose leaking out of the phloem avoids cavitation or helps in cavitation repair, measurements of drought-induced cavitation on cut stem parts with all leaves wrapped in aluminium foil could give a distorted result if the phloem dynamics are impacted. But this seemed to be refuted by the plant-PET measurements from **Chapter 6**, where we observed ceased phloem transport in T_{EW} at water potential levels for which phloem transport still occurred at 40 % in T_{AW} . Comparison should however be carried out with care because in **Chapter 6** only elevated atmospheric [CO_2], but no elevated air temperature was imposed. Findings suggest that phloem would probably not be able to play an important role in the prevention of cavitation under severe soil drought stress in T_{EW} . Although it might be expected that trees grown under elevated [CO_2] would have less negative xylem water potentials because of stomatal regulation, no evidence is found for

this in recent studies (reviewed by Domec et al. (2016)). In conclusion, for *P. tremula* trees exposed to the same level of drought, the ones grown under elevated atmospheric [CO₂] and air temperature showed a tendency to higher vulnerability to drought-induced cavitation compared to the ones grown under ambient conditions. To confirm these results, it would be advisable to investigate the effect of a prolonged exposure to climatic change conditions and carry out experiments on more individuals to verify whether the observed differences and trends are caused by treatments effects or by within treatment variation. To reveal how vulnerable trees to drought are when grown under climatic changes, severe drought could be imposed *in vivo*. The natural change in water potential and the determination of a critical water potential for survival would be valuable.

Phloem loading and climate change

In this work, we assessed phloem loading and transport with ¹¹C. In **Chapter 4** we discussed how this isotope of carbon is useful in mapping phloem transport *in vivo* and non-invasively, which is important given the disturbance sensitivity of phloem, with a high temporal and relatively high spatial resolution. In **Chapter 5**, we demonstrate that ¹¹C-autoradiography can successfully be used to map carbon tracer distribution inside leaves and define phloem loading strategies. In this chapter, we also concluded that one of the tropical species displayed an active loading strategy, which is less common for tree species, certainly in the tropics. But because tropical species are typically understudied compared to temperate species, more research is warranted on this topic (Cao et al. 2001, Bonan 2008, Fisher et al. 2013).

Phloem loading has a distinct effect on phloem sap concentration and species with different loading strategies could be contrastingly influenced by climatic changes. Under current climatic conditions, no clear correlation is found between loading type and climate zone (Davidson et al. 2011), but this could alter when atmospheric [CO₂] changes. Higher solute concentration inside the phloem of active loaders, which elevated atmospheric [CO₂] might cause, is more likely to render the phloem sap too syrupy. A higher phloem concentration (active loaders) would be able to osmotically attract water longer under drought and keep the phloem sap flowing, while species with lower concentrations (passive loaders) would probably have more vulnerable phloem, but also a lower pull on

xylem water under drought, which could then lead to a lower vulnerability to drought-induced cavitation of the xylem. Higher assimilation rates inside the leaves, associated with elevated atmospheric $[CO_2]$ (Ainsworth and Rogers 2007), could have different effects on species with different loading strategies. Passive loaders would have a stronger concentration gradient between mesophyll and SECCC, and probably increased phloem loading, but a study by Körner et al. (1995) has shown that leaf starch inventory increases, rather than loading rates, possibly leading to levels of starch, inhibiting photosynthesis and even levels causing chloroplast malfunctioning. Active loaders would be less close to these inhibitory levels of starch or more general of NSC on photosynthesis and might therefore be better competitors, but they would need to upregulate the phloem loading capacity by regulating the amount of sucrose symporters. (Körner et al. 1995, Turgeon 2010, Ainsworth and Bush 2011, De Schepper et al. 2013b). The amount of sucrose symporters (by increased cell wall invaginations) has been observed as an adaptation to environmental factors, such as increased light levels, so they might also adapt to higher levels of $[CO_2]$ (Amiard et al. 2005, Adams et al. 2014, Ainsworth and Lemonnier 2018), while the production of more plasmodesmata to transport more sucrose in passive loaders has not been observed in response to higher light levels (Amiard et al. 2005).

It has been observed that species with heterogeneous strategies of phloem loading are not uncommon, and can switch between strategies or use multiple strategies at the same time (Slewiniski et al. 2013). In spite of the potential effects on the plant's ecophysiology and consequences on competitive power, only little research is available that has investigated possible differences in climate change response between active and passive loaders (Körner et al. 1995, Ainsworth and Lemonnier 2018).

Plant-PET scans: innovative method to measure phloem characteristics

From the above discussion about different possible outcomes of responsiveness to elevated $[CO_2]$, it is clear that not only phloem loading strategy has an impact, but that also photosynthetic rates, phloem transport characteristics and metabolic responses will play their role. In this respect, the

added value of using ^{11}C is large because not only phloem loading strategies can be assessed (**Chapter 5**), but also phloem transport characteristics (**Chapter 6**). Linking both phloem loading and transport can significantly improve knowledge and projections of how trees, but also crops, will respond to climate change and where bottlenecks appear (e.g., photosynthetic, loading or transport rates). Identifying these factors could lead to better forest management or agricultural practice as well as more directed searches to the most suitable species in future climates.

In **Chapter 6**, we have used plant-PET (positron emission tomography) scanning and ^{11}C to investigate the effect of elevated atmospheric $[\text{CO}_2]$ on phloem transport of *P. tremula* in well-watered conditions and in response to sudden drought. PET is a fairly new and not often used technology in plant sciences (**Chapter 4**). We examined the feasibility of using this technology and assessed the effects of different treatments on phloem transport. Higher phloem velocity was measured in well-watered trees grown under elevated atmospheric $[\text{CO}_2]$ (**Chapter 6**), which indicated that the additional carbon was exported and that symplastic loading did not prevent this tree to transport a surplus of carbon. We did not measure leaf starch levels, but because measured phloem transport velocity was higher when grown in elevated $[\text{CO}_2]$ (**Chapter 6**), we assume that for this passive loader the additional atmospheric carbon and probably uptake did not cause adverse effects inside the leaves. But in these trees the response of phloem to drought was more severe and caused the phloem sap to stop flowing. The apparent stronger response of phloem in T_E to drought might have resulted from an earlier ceasing of xylem transport in these trees (**Chapter 3**). It would be interesting to investigate if active loaders would be able to keep flowing phloem under more negative water potentials because their phloem sap has a higher concentration and would exert a stronger pull on xylem water. Such experiments could be accompanied by measurements of xylem and phloem diameter fluctuations to determine how this coupling influences phloem transport characteristics measured with plant-PET (Sevanto et al. 2011, Chan et al. 2016). In general, we have shown that plant-PET scans can be used to measure phloem characteristics, and how these characteristics alter in response to climatic changes. To learn more in detail how trees will respond to climatic changes, we

need data of multiple species to assess whether responses are going to be highly species-dependent or rather general.

To perform more systematic plant-PET research, there is a strong need for plant-dedicated scanners that are more versatile than the small-animal PET scanner used in **Chapter 6**. The scanner that we used supported only measurements on distal branch parts, long enough to fit the scanner, and had a relatively small field of view (FOV). Despite these limitations, we gathered useful data on the response of phloem to climatic changes in *P. tremula*. Few plant-dedicated PET scanners, typically oriented vertical instead of horizontal, exist worldwide (Uchida et al. 2004, Hattori et al. 2008, Kiser et al. 2008, Jahnke et al. 2009, Kawachi et al. 2011, Weisenberger et al. 2013, Wang et al. 2014) with the plant-PET scanner described in Wang et al. (2014) looking most promising. In their set-up, a custom-built plant-PET scanner is positioned inside a growth chamber with controlled temperature, photosynthetic active radiation, relative humidity and atmospheric [CO₂]. Furthermore, they can directly inject ¹¹CO₂ inside the chamber from the cyclotron directly beneath it. Also their modular PET system configuration can be changed whenever warranted. This means that a highly controlled environment can be created and measurements can be performed with a minimum handling of the plant. Because ¹¹C is short-lived, repeated measurements on the same individual can be taken (e.g., several times during the growing season or in response to any kind of treatment). Although the height of plants is limited to the magnitude of the growth chamber, experiments on young trees of multiple species could be carried out in such set-ups and would certainly help to accurately map the effects of climatic changes, such as temperature, atmospheric [CO₂] and drought, separately and integratively.

Another way to make plant-PET scanners more versatile is by miniaturising them, such as the ratCAP system that has been designed to fit around the head of a rat (**Chapter 4**) (Schulz et al. 2011). The great benefit of this design is that the scanner itself can be opened and closed, allowing it to be positioned around any part of the plant. This way, the scanner is more mobile and can be easier applied in measurements on multiple trees by moving the scanner instead of moving the trees. The FOV of the existing ratCAP design is small (diameter 38 mm, length 25 mm), but could be extended (Bauer et al. 2016).

Climate change research in treatment chambers

Despite the complexity involved in climate change research, we have been able to generate improved mechanistic understanding of the effects of climate change on the tree species *P. tremula*. In this work, we have provided a strong case to use innovative methods and technology to shed new light on the responses of trees to changing climate. The described experiments could now be further improved by using (i) more individuals, (ii) more stable microclimatic control, (iii) prolonged experimental duration, (iv) more experimental treatments, (v) multiple species, and (vi) field trials.

By using more replications, it will be easier to distinguish biological variation from treatment effects. We often found differences in averages per treatment, but also a high degree of within treatment variation. This resulted in fewer significant treatment effects, while the treatments might have caused actual differences.

Control of temperature and [CO₂] in the treatment chambers was established with on/off controls, resulting in typical over- and undershooting of the set microclimatic conditions. A more advanced control loop might smoothen such over- and undershooting effects.

The current experiments looked at mid-term responses over the course of several months. However, the stimulating effect of elevated atmospheric [CO₂] on photosynthetic rate is known to reduce over time (Ainsworth and Rogers 2007, Leakey et al. 2009) and might change when trees are exposed to multiple growing seasons under climatic changes. Therefore, a prolonged experimental duration might be of interest.

We have imposed an average increase in atmospheric [CO₂], temperature, and drought, while in reality problematic climate change events rather cause ecosystem disruptions than climate change trends (Jentsch et al. 2007), such as heat waves (Teskey et al. 2015) or hot and severe droughts (Allen et al. 2015).

We have assessed the effect of climatic changes on one tree species and despite some convergence exists between our measurements and literature data, it should be verified whether our observations are species-specific responses or generally present in a broad scale of tree species.

Finally, potted plants in non-natural settings are useful for improving mechanistic understanding, but if possible the resulting findings should be verified in natural ecosystems (De Boeck et al. 2015). Soil characteristics, competition, or disturbances can all have a profound impact on how climate change will impact forest dynamics (Leakey et al. 2009, Pereira et al. 2010, Ramsfield et al. 2016). Open-top chamber experiments are widely used to enrich [CO₂] under field conditions, but care should be taken that leaf temperatures do not become unrealistically high because of wind shielding (De Boeck et al. 2012). Free-air CO₂ enrichment systems (FACE) do not shield trees from wind, but require a much higher input of CO₂ and thus come at a greater cost. FACE experiments have the advantage that they allow naturally occurring species competition and other ecological interactions (Long et al. 2004, Ainsworth and Long 2005, Leakey et al. 2009). Whereas in this study temperature was controlled in a treatment chamber, manipulation of temperature in field conditions can be performed by infrared lamps or using heat-resistance cables, aboveground or belowground (Aronson and McNulty 2009, De Boeck and Nijs 2011).

The outlook of climate change on *Populus tremula* and other trees

From stem diameter variation measurements (**Chapter 2**), vulnerability and desorption curves (**Chapter 3**), and plant-PET scans (**Chapter 6**), it was observed that *P. tremula* showed different responses in different treatments, and thus acclimated to its growing conditions. While it was expected that well-watered and climate change acclimated trees (T_{EW}) would have the lowest degree of stress and would perform most optimal, they tended to have the highest vulnerabilities across chapters and grew less than trees grown under equal atmospheric conditions but subjected to soil-drought stress (T_{ED}). It almost seemed as if T_{EW} trees were too little stressed, because ample carbon and water was available, and that plastic responses in T_{EW} made these trees perform suboptimal, as they did not show the largest stem or biomass increment. What does this imply for the potential of *P. tremula* to adapt to climate change? Climate change will not only increase average air temperatures and atmospheric [CO₂], but it will also increase climate variability (IPCC 2012). In currently modelled climate change, both the frequency of drought spells and heavy or extreme rain

events is forecasted to increase. This indicates that the occurrence of tree recruitment in soils that are drier than average, but also wetter than average, will increase. *P. tremula* trees recruited and acclimated to such “well-watered” soil conditions, may turn out to be drought-sensitive generations, which will not be resilient when faced with drought. To be able to make better predictions of the species success rate, we should additionally investigate whether the plastic potential to the governing environmental conditions remains high from year-to-year, because if that is the case, trees could acclimate to wetter and drier years. But, years with wet springs and harsh summer droughts could turn out to be problematic for the species survival rate. To test this, we should look not only to drought vulnerability traits but also to mortality traits, such as what levels of drought cause lethal damage or which amount of successive droughts cause a point-of-no-return (Anderegg et al. 2012, Allen et al. 2015), which have not been investigated during this PhD work. Furthermore, it should be tested how measurements from potted trees grown in treatment chambers are translatable to field-grown trees in which interaction with other species occurs. It is also important to study whether the plastic traits (stiffer cells, more leaf area, changed drought vulnerability of xylem and phloem) measured in response to elevated [CO₂] are universal or species-dependent. Overall, the conclusions that apply on *P. tremula* reveal a dangerous trend. Trees from a species like *P. tremula* with strong plastic potential (Hall et al. 2007, Fichot et al. 2009, De Carvalho et al. 2010, Possen et al. 2011), could acclimate to become relatively vulnerable under climatic changes, while trees of species with less plastic potential could succumb because the current pace of change is unprecedentedly high (Hoffmann and Sgrò 2011, Corlett and Westcott 2013, Franks et al. 2014, Valladares et al. 2014, Duputié et al. 2015, Lenoir and Svenning 2015, Urban 2015, Harsch et al. 2017).

Climate change is often referred to as the greatest experiment on earth. No doubt, it is also one of the most dangerous experiments on earth. It seems very likely that many species will be affected by climate change, both positively and negatively. If we want to be able to mitigate the adverse effects, expanding our knowledge on tree species' responses to climate change will be of utmost importance. This way, forest management, assisted migration and other protective measures may reduce the impact of climate change on trees, forests, ecosystems and biodiversity.

R

REFERENCES

- AbdElgawad, H., E. R. Farfan-Vignolo, D. de Vos, and H. Asard. 2015. Elevated CO₂ mitigates drought and temperature-induced oxidative stress differently in grasses and legumes. *Plant Science* **231**:1-10.
- Adams, H. D., M. J. B. Zeppel, W. R. L. Anderegg, H. Hartmann, S. M. Landhäusser, D. T. Tissue, T. E. Huxman, P. J. Hudson, T. E. Franz, and C. D. Allen. 2017. A multi-species synthesis of physiological mechanisms in drought-induced tree mortality. *Nature Ecology & Evolution* **1**:1285.
- Adams, W., C. Cohu, V. Amiard, and B. Demmig-Adams. 2014. Associations between the acclimation of phloem-cell wall ingrowths in minor veins and maximal photosynthesis rate. *Frontiers in Plant Science* **5**:24.
- Ainsworth, E. A. and D. R. Bush. 2011. Carbohydrate export from the leaf: a highly regulated process and target to enhance photosynthesis and productivity. *Plant Physiology* **155**:64-69.
- Ainsworth, E. A. and P. Lemonnier. 2018. Phloem function: a key to understanding and manipulating plant responses to rising atmospheric [CO₂]? *Current Opinion in Plant Biology* **43**:50-56.
- Ainsworth, E. A. and S. P. Long. 2005. What have we learned from 15 years of free-air CO₂ enrichment (FACE)? A meta-analytic review of the responses of photosynthesis, canopy properties and plant production to rising CO₂. *New Phytologist* **165**:351-372.
- Ainsworth, E. A. and A. Rogers. 2007. The response of photosynthesis and stomatal conductance to rising [CO₂]: mechanisms and environmental interactions. *Plant, Cell & Environment* **30**:258-270.
- Aitken, S. N., S. Yeaman, J. A. Holliday, T. Wang, and S. Curtis-McLane. 2008. Adaptation, migration or extirpation: climate change outcomes for tree populations. *Evolutionary Applications* **1**:95-111.
- Alberts, B., D. Bray, K. Hopkin, A. Johnson, J. Lewis, M. Raff, K. Roberts, and P. Walter. 2013. *Essential cell biology*. Garland Science.
- Alder, N. N., W. T. Pockman, J. S. Sperry, and S. Nuismer. 1997. Use of centrifugal force in the study of xylem cavitation. *Journal of Experimental Botany* **48**:665-674.
- Alessio, A. M., C. W. Stearns, T. Shan, S. G. Ross, S. Kohlmyer, A. Ganin, and P. E. Kinahan. 2010. Application and evaluation of a measured spatially variant system model for PET image reconstruction. *IEEE Transactions on Medical Imaging* **29**:938-949.
- Alexoff, D. L., S. L. Dewey, P. Vaska, S. Krishnamoorthy, R. Ferrieri, M. Schueller, D. J. Schlyer, and J. S. Fowler. 2011. PET imaging of thin objects: measuring the effects of positron range and partial-volume averaging in the leaf of *Nicotiana tabacum*. *Nuclear Medicine and Biology* **38**:191-200.
- Allen, C. D., D. D. Breshears, and N. G. McDowell. 2015. On underestimation of global vulnerability to tree mortality and forest die-off from hotter drought in the Anthropocene. *Ecosphere* **6**:1-55.

- Allen, C. D., A. K. Macalady, H. Chenchouni, D. Bachelet, N. McDowell, M. Vennetier, T. Kitzberger, A. Rigling, D. D. Breshears, E. H. Hogg, P. Gonzalez, R. Fensham, Z. Zhang, J. Castro, N. Demidova, J.-H. Lim, G. Allard, S. W. Running, A. Semerci, and N. Cobb. 2010. A global overview of drought and heat-induced tree mortality reveals emerging climate change risks for forests. *Forest Ecology and Management* **259**:660-684.
- Allen, R. G., L. S. Pereira, D. Raes, and M. Smith. 1998. Crop evapotranspiration-Guidelines for computing crop water requirements-FAO Irrigation and drainage paper 56. FAO, Rome **300**:D05109.
- Amiard, V., K. E. Mueh, B. Demmig-Adams, V. Ebbert, R. Turgeon, and W. W. Adams. 2005. Anatomical and photosynthetic acclimation to the light environment in species with differing mechanisms of phloem loading. *Proceedings of the National Academy of Sciences of the United States of America* **102**:12968-12973.
- Anderegg, W. R. L., J. A. Berry, and C. B. Field. 2012. Linking definitions, mechanisms, and modeling of drought-induced tree death. *Trends in Plant Science* **17**:693-700.
- Anderegg, W. R. L., J. A. Hicke, R. A. Fisher, C. D. Allen, J. Aukema, B. Bentz, S. Hood, J. W. Lichstein, A. K. Macalady, N. McDowell, Y. Pan, K. Raffa, A. Sala, J. D. Shaw, N. L. Stephenson, C. Tague, and M. Zeppel. 2015. Tree mortality from drought, insects, and their interactions in a changing climate. *New Phytologist* **208**:674-683.
- Anderegg, W. R. L., T. Klein, M. Bartlett, L. Sack, A. F. A. Pellegrini, B. Choat, and S. Jansen. 2016. Meta-analysis reveals that hydraulic traits explain cross-species patterns of drought-induced tree mortality across the globe. *Proceedings of the National Academy of Sciences* **113**:5024-5029.
- Arango-Velez, A., J. J. Zwiazek, B. R. Thomas, and M. T. Tyree. 2011. Stomatal factors and vulnerability of stem xylem to cavitation in poplars. *Physiologia Plantarum* **143**:154-165.
- Arganda-Carreras, I., V. Kaynig, C. Rueden, K. W. Eliceiri, J. Schindelin, A. Cardona, and H. Sebastian Seung. 2017. Trainable Weka Segmentation: a machine learning tool for microscopy pixel classification. *Bioinformatics* **33**:2424-2426.
- Aronson, E. L. and S. G. McNulty. 2009. Appropriate experimental ecosystem warming methods by ecosystem, objective, and practicality. *Agricultural and Forest Meteorology* **149**:1791-1799.
- Attia, Z., J.-C. Domec, R. Oren, D. A. Way, and M. Moshelion. 2015. Growth and physiological responses of isohydric and anisohydric poplars to drought. *Journal of Experimental Botany* **66**:4373-4381.
- Awad, H., T. Barigah, E. Badel, H. Cochard, and S. Herbette. 2010. Poplar vulnerability to xylem cavitation acclimates to drier soil conditions. *Physiologia Plantarum* **139**:280-288.
- Babst, B. A., R. A. Ferrieri, D. W. Gray, M. Lerdau, D. J. Schlyer, M. Schueller, M. R. Thorpe, and C. M. Orians. 2005. Jasmonic acid induces rapid changes in carbon transport and partitioning in *Populus*. *New Phytologist* **167**:63-72.

- Badal, E., I. Buesa, D. Guerra, L. Bonet, P. Ferrer, and D. S. Intrigliolo. 2010. Maximum diurnal trunk shrinkage is a sensitive indicator of plant water, stress in *Diospyros kaki* (Persimmon) trees. *Agricultural Water Management* **98**:143-147.
- Badiani, M., A. Raschi, A. R. Paolacci, and F. Miglietta. 1999. Plants responses to elevated CO₂: a perspective from natural CO₂ springs. Pages 45-81 in S. B. Agrawal and M. Agrawal, editors. *Environmental Pollution and Plant Response* Lewis Publishers, Boca Raton.
- Bailey, D., J. Karp, and S. Surti. 2005. Physics and instrumentation in PET. Pages 13-39 in D. Bailey, D. Townsend, P. Valk, and M. Maisey, editors. *Positron Emission Tomography*. Springer.
- Barthel, M., A. Hammerle, P. Sturm, T. Baur, L. Gentsch, and A. Knohl. 2011. The diel imprint of leaf metabolism on the δ¹³C signal of soil respiration under control and drought conditions. *New Phytologist* **192**:925-938.
- Bauer, C. E., J. Breczynski-Lewis, G. Marano, M.-B. Mandich, A. Stolin, P. Martone, J. W. Lewis, G. Jaliparthi, R. R. Raylman, and S. Majewski. 2016. Concept of an upright wearable positron emission tomography imager in humans. *Brain and Behavior* **6**:e00530.
- Bauweraerts, I., M. Ameye, T. M. Wertin, M. A. McGuire, R. O. Teskey, and K. Steppe. 2014. Water availability is the decisive factor for the growth of two tree species in the occurrence of consecutive heat waves. *Agricultural and Forest Meteorology* **189–190**:19-29.
- Bauweraerts, I., T. M. Wertin, M. Ameye, M. A. McGuire, R. O. Teskey, and K. Steppe. 2013. The effect of heat waves, elevated [CO₂] and low soil water availability on northern red oak (*Quercus rubra* L.) seedlings. *Global Change Biology* **19**:517-528.
- Beer, S., M. Streun, T. Hombach, J. Buehler, S. Jahnke, M. Khodaverdi, H. Larue, S. Minwuyelet, C. Parl, G. Roeb, U. Schurr, and K. Ziemons. 2010. Design and initial performance of PlanTIS: a high-resolution positron emission tomograph for plants. *Physics in Medicine and Biology* **55**:635-646.
- Beerling, D. and C. Kelly. 1997. Stomatal density responses of temperate woodland plants over the past seven decades of CO₂ increase: a comparison of Salisbury (1927) with contemporary data. *American Journal of Botany* **84**:1572-1572.
- Bernacchi, C. J. and A. VanLoocke. 2015. Terrestrial Ecosystems in a Changing Environment: A Dominant Role for Water. *Annual Review of Plant Biology* **66**:599-622.
- Bjurhager, I., L. A. Berglund, S. L. Bardage, and B. Sundberg. 2008. Mechanical characterization of juvenile European aspen (*Populus tremula*) and hybrid aspen (*Populus tremula* × *Populus tremuloides*) using full-field strain measurements. *Journal of Wood Science* **54**:349-355.
- Blake, T. J., E. Bevilacqua, and J. J. Zwiazek. 1991. Effects of repeated stress on turgor pressure and cell elasticity changes in black spruce seedlings. *Canadian Journal of Forest Research* **21**:1329-1333.

- Blessing, C. H., R. A. Werner, R. Siegwolf, and N. Buchmann. 2015. Allocation dynamics of recently fixed carbon in beech saplings in response to increased temperatures and drought. *Tree Physiology* **35**:585-598.
- Blevins, D. G. and K. M. Lukaszewski. 1998. Boron in plant structure and function. *Annual Review of Plant Physiology and Plant Molecular Biology* **49**:481-500.
- Bloemen, J., M. M. Anne, D. P. Aubrey, R. O. Teskey, and K. Steppe. 2014. Internal recycling of respired CO₂ may be important for plant functioning under changing climate regimes. *Plant Signaling & Behavior* **8**:e27530.
- Bloemen, J., I. Bauweraerts, F. De Vos, C. Vanhove, S. Vandenberghe, P. Boeckx, and K. Steppe. 2015. Fate of xylem-transported ¹¹C- and ¹³C-labelled CO₂ in leaves of poplar. *Physiologia Plantarum* **153**:555-564.
- Blunden, J. and D. S. Arndt. 2017. State of the Climate in 2016. *Bulletin of the American Meteorological Society* **98**:Si-S280.
- Boden, T. A., G. Marland, and R. J. Andres. 2017. Global, Regional, and National Fossil-Fuel CO₂ Emissions. Carbon Dioxide Information Analysis Center, Oak Ridge National Laboratory, U.S. Department of Energy, Oak Ridge, TN, USA.
- Bogeat-Triboulot, M.-B., M. Brosché, J. Renaut, L. Jouve, D. Le Thiec, P. Fayyaz, B. Vinocur, E. Witters, K. Laukens, T. Teichmann, A. Altman, J.-F. Hausman, A. Polle, J. Kangasjärvi, and E. Dreyer. 2007. Gradual soil water depletion results in reversible changes of gene expression, protein profiles, ecophysiology, and growth performance in *Populus euphratica*, a poplar growing in arid regions. *Plant Physiology* **143**:876-892.
- Boisvenue, C. and S. W. Running. 2006. Impacts of climate change on natural forest productivity – evidence since the middle of the 20th century. *Global Change Biology* **12**:862-882.
- Bonan, G. B. 2008. Forests and Climate Change: Forcings, Feedbacks, and the Climate Benefits of Forests. *Science* **320**:1444.
- Borisjuk, L., H. Rolletschek, and T. Neuberger. 2012. Surveying the plant's world by magnetic resonance imaging. *The Plant Journal* **70**:129-146.
- Bowes, G. 1993. Facing the Inevitable: Plants and Increasing Atmospheric CO₂. *Annual Review of Plant Physiology and Plant Molecular Biology* **44**:309-332.
- Brooks, J. R., L. B. Flanagan, G. T. Varney, and J. R. Ehleringer. 1997. Vertical gradients in photosynthetic gas exchange characteristics and refixation of respired CO₂ within boreal forest canopies. *Tree Physiology* **17**:1-12.
- Buck, A. K., K. Herrmann, T. Stargardt, T. Dechow, B. J. Krause, and J. Schreyögg. 2010. Economic evaluation of PET and PET/CT in oncology: evidence and methodologic approaches. *Journal of Nuclear Medicine* **51**:401-412.
- Buck, A. L. 1981. New Equations for Computing Vapor Pressure and Enhancement Factor. *Journal of Applied Meteorology* **20**:1527-1532.
- Bühler, J., G. Huber, F. Schmid, and P. Blümler. 2011. Analytical model for long-distance tracer-transport in plants. *Journal of Theoretical Biology* **270**:70-79.

- Bühler, J., E. von Lieres, and G. Huber. 2014. A class of compartmental models for long-distance tracer transport in plants. *Journal of Theoretical Biology* **341**:131-142.
- Cabrita, P., M. Thorpe, and G. J. Huber. 2013. Hydrodynamics of steady state phloem transport with radial leakage of solute. *Frontiers in Plant Science* **4**:531.
- Calfapietra, C., B. Gielen, A. N. J. Galema, M. Lukac, P. De Angelis, M. C. Moscatelli, R. Ceulemans, and G. Scarascia-Mugnozza. 2003. Free-air CO₂ enrichment (FACE) enhances biomass production in a short-rotation poplar plantation. *Tree Physiology* **23**:805-814.
- Cao, M. K., Q. F. Zhang, and H. H. Shugart. 2001. Dynamic responses of African ecosystem carbon cycling to climate change. *Climate Research* **17**.
- Cardoso, M. F., R. L. Salcedo, and S. Foyo de Azevedo. 1996. The simplex-simulated annealing approach to continuous non-linear optimization. *Computers & Chemical Engineering* **20**:1065-1080.
- Carpenter, L. T., S. R. Pezeshki, and F. D. Shields. 2008. Responses of nonstructural carbohydrates to shoot removal and soil moisture treatments in *Salix nigra*. *Trees* **22**:737-748.
- Caudullo, G. and D. de Rigo. 2016. *Populus tremula* in Europe: distribution, habitat, usage and threats. Page e01f148+ in J. San-Miguel-Ayanz, D. De Rigo, G. Caudullo, T. Houston Durrant, and A. Mauri, editors. *European Atlas of Forest Tree Species*. Publ. Off. EU, Luxembourg.
- Caudullo, G., E. Welk, and J. San-Miguel-Ayanz. 2017. Chorological maps for the main European woody species. *Data in Brief* **12**:662-666.
- Centritto, M., H. S. J. Lee, and P. G. Jarvis. 1999a. Increased growth in elevated [CO₂]: an early, short-term response? *Global Change Biology* **5**:623-633.
- Centritto, M., M. E. Lucas, and P. G. Jarvis. 2002. Gas exchange, biomass, whole-plant water-use efficiency and water uptake of peach (*Prunus persica*) seedlings in response to elevated carbon dioxide concentration and water availability. *Tree Physiology* **22**:699-706.
- Centritto, M., F. Magnani, H. S. J. Lee, and P. G. Jarvis. 1999b. Interactive effects of elevated [CO₂] and drought on cherry (*Prunus avium*) seedlings II. Photosynthetic capacity and water relations. *New Phytologist* **141**:141-153.
- Čermák, J., J. Kučera, W. L. Bauerle, N. Phillips, and T. M. Hinckley. 2007. Tree water storage and its diurnal dynamics related to sap flow and changes in stem volume in old-growth Douglas-fir trees. *Tree Physiology* **27**:181-198.
- Chan, T., T. Hölttä, F. Berninger, H. Mäkinen, P. Nöjd, M. Mencuccini, and E. Nikinmaa. 2016. Separating water-potential induced swelling and shrinking from measured radial stem variations reveals a cambial growth and osmotic concentration signal. *Plant, Cell & Environment* **39**:233-244.
- Chen, I. C., J. K. Hill, R. Ohlemüller, D. B. Roy, and C. D. Thomas. 2011. Rapid range shifts of species associated with high levels of climate warming. *Science* **333**:1024.

- Chiu, T.-C., R. G. Fairbanks, L. Cao, and R. A. Mortlock. 2007. Analysis of the atmospheric ^{14}C record spanning the past 50,000 years derived from high-precision $^{230}\text{Th}/^{234}\text{U}/^{238}\text{U}$, $^{231}\text{Pa}/^{235}\text{U}$ and ^{14}C dates on fossil corals. *Quaternary Science Reviews* **26**:18-36.
- Choat, B., S. Jansen, T. J. Brodribb, H. Cochard, S. Delzon, R. Bhaskar, S. J. Bucci, T. S. Feild, S. M. Gleason, U. G. Hacke, A. L. Jacobsen, F. Lens, H. Maherali, J. Martinez-Vilalta, S. Mayr, M. Mencuccini, P. J. Mitchell, A. Nardini, J. Pittermann, R. B. Pratt, J. S. Sperry, M. Westoby, I. J. Wright, and A. E. Zanne. 2012. Global convergence in the vulnerability of forests to drought. *Nature* **491**:752-755.
- Choat, B., E. C. Lahr, P. J. Melcher, M. A. Zwieniecki, and N. M. Holbrook. 2005. The spatial pattern of air seeding thresholds in mature sugar maple trees. *Plant, Cell & Environment* **28**:1082-1089.
- Classen, A. T., R. J. Norby, C. E. Company, K. E. Sides, and J. F. Weltzin. 2010. Climate change alters seedling emergence and establishment in an old-field ecosystem. *PLOS ONE* **5**:e13476.
- Cochard, H., E. Badel, S. Herbette, S. Delzon, B. Choat, and S. Jansen. 2013. Methods for measuring plant vulnerability to cavitation: a critical review. *Journal of Experimental Botany* **64**:4779-4791.
- Cochard, H., S. Delzon, and E. Badel. 2015. X-ray microtomography (micro-CT): a reference technology for high-resolution quantification of xylem embolism in trees. *Plant, Cell & Environment* **38**:201-206.
- Cochard, H., S. Herbette, T. Barigah, E. Badel, M. Ennajeh, and A. Vilagrosa. 2010. Does sample length influence the shape of xylem embolism vulnerability curves? A test with the Cavitron spinning technique. *Plant, Cell & Environment* **33**:1543-1552.
- Converse, A., E. Ahlers, T. Bryan, J. Hetue, K. Lake, P. Ellison, J. Engle, T. Barnhart, R. Nickles, P. Williams, and O. DeJesus. 2015. Mathematical modeling of positron emission tomography (PET) data to assess radiofluoride transport in living plants following petiolar administration. *Plant Methods* **11**:1-7.
- Corlett, R. T. and D. A. Westcott. 2013. Will plant movements keep up with climate change? *Trends in Ecology & Evolution* **28**:482-488.
- Cosgrove, D. J. 2016. Plant cell wall extensibility: connecting plant cell growth with cell wall structure, mechanics, and the action of wall-modifying enzymes. *Journal of Experimental Botany* **67**:463-476.
- Davey, P. A., H. Olcer, O. Zakhleniuk, C. J. Bernacchi, C. Calfapietra, S. P. Long, and C. A. Raines. 2006. Can fast-growing plantation trees escape biochemical down-regulation of photosynthesis when grown throughout their complete production cycle in the open air under elevated carbon dioxide? *Plant, Cell & Environment* **29**:1235-1244.
- Davidson, A., F. Keller, and R. Turgeon. 2011. Phloem loading, plant growth form, and climate. *Protoplasma* **248**:153-163.

- Dawes, M. A., R. Zweifel, N. Dawes, C. Rixen, and F. Hagedorn. 2014. CO₂ enrichment alters diurnal stem radius fluctuations of 36-yr-old *Larix decidua* growing at the alpine tree line. *New Phytologist* **202**:1237-1248.
- Dawson, T. E., S. S. O. Burgess, K. P. Tu, R. S. Oliveira, L. S. Santiago, J. B. Fisher, K. A. Simonin, and A. R. Ambrose. 2007. Nighttime transpiration in woody plants from contrasting ecosystems. *Tree Physiology* **27**:561-575.
- De Baerdemaeker, N. J. F., N. Hias, J. Van Den Bulcke, W. Keulemans, and K. Steppe. in press. The effect of polyploidization on tree hydraulic functioning. *American Journal of Botany*.
- De Baerdemaeker, N. J. F., R. L. Salomón, L. De Roo, and K. Steppe. 2017. Sugars from woody tissue photosynthesis reduce xylem vulnerability to cavitation. *New Phytologist* **216**:720-727.
- De Boeck, H. J., T. De Groot, and I. Nijs. 2012. Leaf temperatures in glasshouses and open-top chambers. *New Phytologist* **194**:1155-1164.
- De Boeck, H. J. and I. Nijs. 2011. An alternative approach for infrared heater control in warming and extreme event experiments in terrestrial ecosystems. *Journal of Ecology* **99**:724-728.
- De Boeck, H. J., S. Vicca, J. Roy, I. Nijs, A. Milcu, J. Kreyling, A. Jentsch, A. Chabbi, M. Campioli, T. Callaghan, C. Beierkuhnlein, and C. Beier. 2015. Global change experiments: challenges and opportunities. *Bioscience* **65**:922-931.
- De Carvalho, D., P. K. Ingvarsson, J. Joseph, L. Suter, C. Sedivy, D. Macaya-Sanz, J. Cottrell, B. Heinze, I. Schanzer, and C. Lexer. 2010. Admixture facilitates adaptation from standing variation in the European aspen (*Populus tremula* L.), a widespread forest tree. *Molecular Ecology* **19**:1638-1650.
- De Frenne, P., D. A. Coomes, A. De Schrijver, J. Staelens, J. M. Alexander, M. Bernhardt-Römermann, J. Brunet, O. Chabrierie, A. Chiarucci, J. den Ouden, R. L. Eckstein, B. J. Graae, R. Gruwez, R. Hédli, M. Hermy, A. Kolb, A. Mårell, S. M. Mullender, S. L. Olsen, A. Orczewska, G. Peterken, P. Petřík, J. Plue, W. D. Simonson, C. V. Tomescu, P. Vangansbeke, G. Verstraeten, L. Vesterdal, M. Wulf, and K. Verheyen. 2014. Plant movements and climate warming: intraspecific variation in growth responses to nonlocal soils. *New Phytologist* **202**:431-441.
- De Frenne, P., B. J. Graae, F. Rodríguez-Sánchez, A. Kolb, O. Chabrierie, G. Decocq, H. De Kort, A. De Schrijver, M. Diekmann, O. Eriksson, R. Gruwez, M. Hermy, J. Lenoir, J. Plue, D. A. Coomes, and K. Verheyen. 2013a. Latitudinal gradients as natural laboratories to infer species' responses to temperature. *Journal of Ecology* **101**:784-795.
- De Frenne, P., F. Rodríguez-Sánchez, D. A. Coomes, L. Baeten, G. Verstraeten, M. Vellend, M. Bernhardt-Römermann, C. D. Brown, J. Brunet, J. Cornelis, G. M. Decocq, H. Dierschke, O. Eriksson, F. S. Gilliam, R. Hédli, T. Heinken, M. Hermy, P. Hommel, M. A. Jenkins, D. L. Kelly, K. J. Kirby, F. J. G. Mitchell, T. Naaf, M. Newman, G. Peterken, P. Petřík, J. Schultz, G. Sonnier, H. Van Calster, D. M. Waller, G.-R. Walther, P. S. White, K. D. Woods, M. Wulf, B. J. Graae, and K. Verheyen. 2013b. Microclimate moderates plant responses to macroclimate warming. *Proceedings of the National Academy of Sciences* **110**:18561.

- De Luis, I., J. J. Irigoyen, and M. Sánchez-Díaz. 1999. Elevated CO₂ enhances plant growth in droughted N₂-fixing alfalfa without improving water status. *Physiologia Plantarum* **107**:84-89.
- De Pauw, D. J. W., K. Steppe, and B. De Baets. 2008. Identifiability analysis and improvement of a tree water flow and storage model. *Mathematical Biosciences* **211**:314-332.
- De Schepper, V., J. Bühler, M. Thorpe, G. Roeb, G. Huber, D. van Dusschoten, S. Jahnke, and K. Steppe. 2013a. ¹¹C-PET imaging reveals transport dynamics and sectorial plasticity of oak phloem after girdling. *Frontiers in Plant Science* **4**:200.
- De Schepper, V., T. De Swaef, I. Bauweraerts, and K. Steppe. 2013b. Phloem transport: a review of mechanisms and controls. *Journal of Experimental Botany* **16**:4839–4850.
- De Schepper, V. and K. Steppe. 2010. Development and verification of a water and sugar transport model using measured stem diameter variations. *Journal of Experimental Botany* **61**:2083-2099.
- De Swaef, T., V. De Schepper, M. W. Vandegehuchte, and K. Steppe. 2015. Stem diameter variations as a versatile research tool in ecophysiology. *Tree Physiology* **35**:1047-1061.
- Defraeye, T., D. Derome, W. Aregawi, D. Cantré, S. Hartmann, E. Lehmann, J. Carmeliet, F. Voisard, P. Verboven, and B. Nicolai. 2014. Quantitative neutron imaging of water distribution, venation network and sap flow in leaves. *Planta* **240**:423-436.
- Deleye, S., R. Holen, J. Verhaeghe, S. Vandenberghe, S. Stroobants, and S. Staelens. 2013. Performance evaluation of small-animal multipinhole μ SPECT scanners for mouse imaging. *European Journal of Nuclear Medicine and Molecular Imaging* **40**:744-758.
- Delzon, S., C. Douthe, A. Sala, and H. Cochard. 2010. Mechanism of water-stress induced cavitation in conifers: bordered pit structure and function support the hypothesis of seal capillary-seeding. *Plant, Cell & Environment* **33**:2101-2111.
- Denning, A. S., I. Y. Fung, and D. Randall. 1995. Latitudinal gradient of atmospheric CO₂ due to seasonal exchange with land biota. *Nature* **376**:240.
- Deslauriers, A., S. Rossi, and T. Anfodillo. 2007. Dendrometer and intra-annual tree growth: What kind of information can be inferred? *Dendrochronologia* **25**:113-124.
- Dhondt, S., H. Vanhaeren, D. Van Loo, V. Cnudde, and D. Inzé. 2010. Plant structure visualization by high-resolution X-ray computed tomography. *Trends in Plant Science* **15**:419-422.
- Dierick, M., B. Masschaele, and L. V. Hoorebeke. 2004. Octopus, a fast and user-friendly tomographic reconstruction package developed in LabView®. *Measurement Science and Technology* **15**:1366.
- Dierick, M., D. Van Loo, B. Masschaele, J. Van den Bulcke, J. Van Acker, V. Cnudde, and L. Van Hoorebeke. 2014. Recent micro-CT scanner developments at UGCT.

- Nuclear Instruments and Methods in Physics Research Section B: Beam Interactions with Materials and Atoms **324**:35-40.
- Dietze, M. C., A. Sala, M. S. Carbone, C. I. Czimczik, J. A. Mantooth, A. D. Richardson, and R. Vargas. 2014. Nonstructural carbon in woody plants. *Annual Review of Plant Biology* **65**:667-687.
- Dilkes, N. B., D. L. Jones, and J. Farrar. 2004. Temporal dynamics of carbon partitioning and rhizodeposition in wheat. *Plant Physiology* **134**:706.
- Dlugokencky, E. and P. Tans. 2017. NOAA/ESRL. Trends in atmospheric carbon dioxide. Globally averaged marine surface annual and monthly mean data.
- Domec, J.-C. and B. L. Gartner. 2001. Cavitation and water storage capacity in bole xylem segments of mature and young Douglas-fir trees. *Trees* **15**:204-214.
- Domec, J.-C., K. Schäfer, R. Oren, H. S. Kim, and H. R. McCarthy. 2010. Variable conductivity and embolism in roots and branches of four contrasting tree species and their impacts on whole-plant hydraulic performance under future atmospheric CO₂ concentration. *Tree Physiology* **30**:1001-1015.
- Domec, J.-C., D. D. Smith, and K. A. McCulloh. 2016. A synthesis of the effects of atmospheric carbon dioxide enrichment on plant hydraulics: implications for whole-plant water use efficiency and resistance to drought. *Plant, Cell & Environment* **40**:921–937.
- Downes, G., C. Beadle, and D. Worledge. 1999. Daily stem growth patterns in irrigated *Eucalyptus globulus* and *E. nitens* in relation to climate. *Trees* **14**:102-111.
- Drake, B. G., J. Azcon-Bieto, J. Berry, J. Bunce, P. Dijkstra, J. Farrar, R. M. Gifford, M. A. Gonzalez-Meler, G. Koch, H. Lambers, J. Siedow, and S. Wullschleger. 1999. Does elevated atmospheric CO₂ concentration inhibit mitochondrial respiration in green plants? *Plant, Cell & Environment* **22**:649-657.
- Drake, B. G., M. A. González-Meler, and S. P. Long. 1997. More efficient plants: a consequence of rising atmospheric CO₂? *Annual Review of Plant Physiology and Plant Molecular Biology* **48**:609-639.
- Drew, D. M. and G. M. Downes. 2009. The use of precision dendrometers in research on daily stem size and wood property variation: A review. *Dendrochronologia* **27**:159-172.
- Du, S., Y.-L. Wang, T. Kume, J.-G. Zhang, K. Otsuki, N. Yamanaka, and G.-B. Liu. 2011. Sapflow characteristics and climatic responses in three forest species in the semiarid Loess Plateau region of China. *Agricultural and Forest Meteorology* **151**:1-10.
- Duan, H., R. A. Duursma, G. Huang, R. A. Smith, B. Choat, A. P. O'Grady, and D. T. Tissue. 2014. Elevated [CO₂] does not ameliorate the negative effects of elevated temperature on drought-induced mortality in *Eucalyptus radiata* seedlings. *Plant, Cell & Environment* **37**:1598-1613.
- Duchesne, L., R. Ouimet, and C. Morneau. 2003. Assessment of sugar maple health based on basal area growth pattern. *Canadian Journal of Forest Research* **33**:2074-2080.

- Dupuis, J., C. Holst, and H. Kuhlmann. 2017. Measuring leaf thickness with 3D close-up laser scanners: possible or not? *Journal of Imaging* **3**:22.
- Duputié, A., A. Rutschmann, O. Ronce, and I. Chuine. 2015. Phenological plasticity will not help all species adapt to climate change. *Global Change Biology* **21**:3062-3073.
- Epila, J., N. J. F. De Baerdemaeker, L. L. Vergeynst, W. H. Maes, H. Beeckman, and K. Steppe. 2017a. Capacitive water release and internal leaf water relocation delay drought-induced cavitation in African *Maesopsis eminii*. *Tree Physiology* **37**:481-490.
- Epila, J., M. Hubeau, and K. Steppe. 2018. Drought effects on photosynthesis and implications of photoassimilate distribution in ¹¹C-labeled leaves in the African tropical tree species *Maesopsis eminii* Engl. *Forests* **9**:109.
- Epila, J., W. H. Maes, H. Verbeeck, J. Van Camp, J. B. L. Okullo, and K. Steppe. 2017b. Plant measurements on African tropical *Maesopsis eminii* seedlings contradict pioneering water use behaviour. *Environmental and Experimental Botany* **135**:27-37.
- Epila, J., H. Verbeeck, T. Otim-Epila, P. Okullo, E. Kearsley, and K. Steppe. 2017c. The ecology of *Maesopsis eminii* Engl. in tropical Africa. *African Journal of Ecology*.
- Epron, D., M. Bahn, D. Derrien, F. A. Lattanzi, J. Pumpanen, A. Gessler, P. Högberg, P. Maillard, M. Dannoura, D. Gérard, and N. Buchmann. 2012. Pulse-labelling trees to study carbon allocation dynamics: a review of methods, current knowledge and future prospects. *Tree Physiology* **32**:776-798.
- Eschrich, W. and J. Fromm. 1994. Evidence for two pathways of phloem loading. *Physiologia Plantarum* **90**:699-707.
- España, S., R. Marcinkowski, V. Keereman, S. Vandenberghe, and R. Van Holen. 2014. DigiPET: sub-millimeter spatial resolution small-animal PET imaging using thin monolithic scintillators. *Physics in Medicine and Biology* **59**:3405-3420.
- Ewers, B. E. and R. Oren. 2000. Analyses of assumptions and errors in the calculation of stomatal conductance from sap flux measurements. *Tree Physiology* **20**:579-589.
- Farrer, E. C., I. W. Ashton, J. Knape, and K. N. Suding. 2014. Separating direct and indirect effects of global change: a population dynamic modeling approach using readily available field data. *Global Change Biology* **20**:1238-1250.
- Fatichi, S., S. Leuzinger, and C. Körner. 2014. Moving beyond photosynthesis: from carbon source to sink-driven vegetation modeling. *New Phytologist* **201**:1086-1095.
- Feigenwinter, C., C. Bernhofer, U. Eichelmann, B. Heinesch, M. Hertel, D. Janous, O. Kolle, F. Lagergren, A. Lindroth, S. Minerbi, U. Moderow, M. Mölder, L. Montagnani, R. Queck, C. Rebmann, P. Vestin, M. Yernaux, M. Zeri, W. Ziegler, and M. Aubinet. 2008. Comparison of horizontal and vertical advective CO₂ fluxes at three forest sites. *Agricultural and Forest Meteorology* **148**:12-24.
- Fernández, J. E. and M. V. Cuevas. 2010. Irrigation scheduling from stem diameter variations: A review. *Agricultural and Forest Meteorology* **150**:135-151.

- Ferrieri, A. P., B. Agtuca, H. M. Appel, R. A. Ferrieri, and J. C. Schultz. 2013. Temporal changes in allocation and partitioning of new carbon as ^{14}C elicited by simulated herbivory suggest that roots shape aboveground responses in arabidopsis. *Plant Physiology* **161**:692-704.
- Ferrieri, A. P., H. Appel, R. A. Ferrieri, and J. C. Schultz. 2012. Novel application of 2-[^{18}F]fluoro-2-deoxy-d-glucose to study plant defenses. *Nuclear Medicine and Biology* **39**:1152-1160.
- Ferris, R., M. Sabatti, F. Miglietta, R. F. Mills, and G. Taylor. 2001. Leaf area is stimulated in *Populus* by free air CO_2 enrichment (POPFACE), through increased cell expansion and production. *Plant, Cell & Environment* **24**:305-315.
- Fichot, R., T. S. Barigah, S. Chamaillard, D. Le Thiec, F. Laurans, H. Cochard, and F. Brignolas. 2010. Common trade-offs between xylem resistance to cavitation and other physiological traits do not hold among unrelated *Populus deltoides* × *Populus nigra* hybrids. *Plant, Cell & Environment* **33**:1553-1568.
- Fichot, R., F. Brignolas, H. Cochard, and R. Ceulemans. 2015. Vulnerability to drought-induced cavitation in poplars: synthesis and future opportunities. *Plant, Cell & Environment* **38**:1233-1251.
- Fichot, R., F. Laurans, R. Monclus, A. Moreau, G. Pilate, and F. Brignolas. 2009. Xylem anatomy correlates with gas exchange, water-use efficiency and growth performance under contrasting water regimes: evidence from *Populus deltoides* × *Populus nigra* hybrids. *Tree Physiology* **29**:1537-1549.
- Fischlin, A., G. F. Midgley, J. T. Price, R. Leemans, B. Gopal, C. Turley, M. D. A. Rounsevell, O. P. Dube, J. Tarazona, and A. A. Velichko. 2007. Ecosystems, their properties, goods, and services. Pages 211-272 in M. L. Parry, O. F. Canziani, J. P. Palutikof, P. J. van der Linden, and C. E. Hanson, editors. *Climate Change 2007: Impacts, Adaptation and Vulnerability. Contribution of Working Group II to the Fourth Assessment Report of the Intergovernmental Panel on Climate Change*. Cambridge University Press, Cambridge, UK.
- Fisher, J. B., M. Sikka, S. Sitch, P. Ciais, B. Poulter, D. Galbraith, J.-E. Lee, C. Huntingford, N. Viovy, N. Zeng, A. Ahlström, M. R. Lomas, P. E. Levy, C. Frankenberg, S. Saatchi, and Y. Malhi. 2013. African tropical rainforest net carbon dioxide fluxes in the twentieth century. *Philosophical Transactions of the Royal Society B: Biological Sciences* **368**:20120376.
- Flannigan, M. D., B. M. Wotton, G. A. Marshall, W. J. de Groot, J. Johnston, N. Jurko, and A. S. Cantin. 2016. Fuel moisture sensitivity to temperature and precipitation: climate change implications. *Climatic Change* **134**:59-71.
- Franks, S. J., J. J. Weber, and S. N. Aitken. 2014. Evolutionary and plastic responses to climate change in terrestrial plant populations. *Evolutionary Applications* **7**:123-139.
- Fu, Q., L. Cheng, Y. Guo, and R. Turgeon. 2011. Phloem Loading Strategies and Water Relations in Trees and Herbaceous Plants. *Plant Physiology* **157**:1518-1527.
- Gamalei, Y. 1989. Structure and function of leaf minor veins in trees and herbs. *Trees* **3**:96-110.

- Gamalei, Y. 1991. Phloem loading and its development related to plant evolution from trees to herbs. *Trees* **5**:50-64.
- Garbout, A., L. Munkholm, S. Hansen, B. Petersen, O. Munk, and R. Pajor. 2012. The use of PET/CT scanning technique for 3D visualization and quantification of real-time soil/plant interactions. *Plant and Soil* **352**:113-127.
- Geiger, D. B. 1975. Phloem loading and associated processes. Pages 251-295 in S. Aronoff, J. Dainty, P. R. Gorham, L. M. Srivastava, and C. A. Swanson, editors. *Phloem transport*. Springer, Boston, MA, USA.
- Gessler, A., J. P. Ferrio, R. Hommel, K. Treydte, R. A. Werner, and R. K. Monson. 2014. Stable isotopes in tree rings: towards a mechanistic understanding of isotope fractionation and mixing processes from the leaves to the wood. *Tree Physiology* **34**:796-818.
- Giaquinta, R. 1976. Evidence for phloem loading from the apoplast: chemical modification of membrane sulfhydryl groups. *Plant Physiology* **57**:872-875.
- Gielen, B., C. Calfapietra, M. Lukac, V. E. Wittig, P. De Angelis, I. A. Janssens, M. C. Moscatelli, S. Grego, M. F. Cotrufo, D. L. Godbold, M. R. Hoosbeek, S. P. Long, F. Miglietta, A. Polle, C. J. Bernacchi, P. A. Davey, R. Ceulemans, and G. E. Scarascia-Mugnozza. 2005. Net carbon storage in a poplar plantation (POPFACE) after three years of free-air CO₂ enrichment. *Tree Physiology* **25**:1399-1408.
- Gimeno, T. E., K. Y. Crous, J. Cooke, A. P. O'Grady, A. Ósvaldsson, B. E. Medlyn, and D. S. Ellsworth. 2016. Conserved stomatal behaviour under elevated CO₂ and varying water availability in a mature woodland. *Functional Ecology* **30**:700-709.
- Giovannelli, A., A. Deslauriers, G. Fragnelli, L. Scaletti, G. Castro, S. Rossi, and A. Crivellaro. 2007. Evaluation of drought response of two poplar clones (*Populusxcanadensis* Mönch 'I-214' and *P. deltoides* Marsh. 'Dvina') through high resolution analysis of stem growth. *Journal of Experimental Botany* **58**:2673-2683.
- Gleason, S. M., M. Westoby, S. Jansen, B. Choat, U. G. Hacke, R. B. Pratt, R. Bhaskar, T. J. Brodribb, S. J. Bucci, K.-F. Cao, H. Cochard, S. Delzon, J.-C. Domec, Z.-X. Fan, T. S. Feild, A. L. Jacobsen, D. M. Johnson, F. Lens, H. Maherali, J. Martínez-Vilalta, S. Mayr, K. A. McCulloh, M. Mencuccini, P. J. Mitchell, H. Morris, A. Nardini, J. Pittermann, L. Plavcová, S. G. Schreiber, J. S. Sperry, I. J. Wright, and A. E. Zanne. 2016. Weak tradeoff between xylem safety and xylem-specific hydraulic efficiency across the world's woody plant species. *New Phytologist* **209**:123-136.
- Gonzalez-Meler, M. A., M. Ribas-Carbo, J. N. Siedow, and B. G. Drake. 1996. Direct inhibition of plant mitochondrial respiration by elevated CO₂. *Plant Physiology* **112**:1349.
- Goorden, M., C. and F. Beekman, J. 2010. High-resolution tomography of positron emitters with clustered pinhole SPECT. *Physics in Medicine and Biology* **55**:1265-1277.

- Gorel, A. P., A. Fayolle, and J. L. Doucet. 2015. Ecology and management of the multipurpose *Erythrophleum* species (Fabaceae-Caesalpinioideae) in Africa. A review. *Biotechnologie, Agronomie, Société et Environnement* **19**:415-429.
- Grime, V. L. and F. L. Sinclair. 1999. Sources of error in stem heat balance sap flow measurements. *Agricultural and Forest Meteorology* **94**:103-121.
- Grimmer, C. and E. Komor. 1999. Assimilate export by leaves of *Ricinus communis* L. growing under normal and elevated carbon dioxide concentrations: the same rate during the day, a different rate at night. *Planta* **209**:275-281.
- Guet, J., R. Fichot, C. Lédée, F. Laurans, H. Cochard, S. Delzon, C. Bastien, and F. Brignolas. 2015. Stem xylem resistance to cavitation is related to xylem structure but not to growth and water-use efficiency at the within-population level in *Populus nigra* L. *Journal of Experimental Botany* **66**:4643-4652.
- Hall, A. J. and P. E. H. Minchin. 2013. A closed-form solution for steady-state coupled phloem/xylem flow using the Lambert-W function. *Plant, Cell & Environment* **36**:2150-2162.
- Hall, D., V. Luquez, V. M. Garcia, K. R. St Onge, S. Jansson, and P. K. Ingvarsson. 2007. Adaptive population differentiation in phenology across a latitudinal gradient in European aspen (*Populus tremula* L.): a comparison of neutral markers, candidate genes and phenotypic traits. *Evolution* **61**:2849-2860.
- Hamstad, M. A., S. L. Quarles, and R. L. Lemaster. 1994. Experimental far-field wideband acoustic waves in wood rods and plates. Pages 30-44 *in* Proceedings of the 9th International Symposium on Nondestructive Testing of Wood. Conferences and Institutes, Washington State University, Pullman, WA, USA.
- Harsch, M. A., A. Phillips, Y. Zhou, M.-R. Leung, D. S. Rinnan, and M. Kot. 2017. Moving forward: insights and applications of moving-habitat models for climate change ecology. *Journal of Ecology* **105**:1169-1181.
- Hattori, E., H. Uchida, N. Harada, M. Ohta, H. Tsukada, Y. Hara, and T. Suzuki. 2008. Incorporation and translocation of 2-deoxy-2-[¹⁸F]fluoro-d-glucose in *Sorghum bicolor* (L.) Moench monitored using a planar positron imaging system. *Planta* **227**:1181-1186.
- Hayward, H. E. 1951. The structure of economic plants. The Macmillan Company, New York, NY, USA.
- Heath, J. and G. Kerstiens. 1997. Effects of elevated CO₂ on leaf gas exchange in beech and oak at two levels of nutrient supply: consequences for sensitivity to drought in beech. *Plant, Cell & Environment* **20**:57-67.
- Hoffmann, A. A. and C. M. Sgrò. 2011. Climate change and evolutionary adaptation. *Nature* **470**:479.
- Holbrook, N. M., E. T. Ahrens, M. J. Burns, and M. A. Zwieniecki. 2001. *In vivo* observation of cavitation and embolism repair using magnetic resonance imaging. *Plant Physiology* **126**:27-31.

- Hölttä, T., H. Cochard, E. Nikinmaa, and M. Mencuccini. 2009. Capacitive effect of cavitation in xylem conduits: results from a dynamic model. *Plant, Cell & Environment* **32**:10-21.
- Hölttä, T., M. Mencuccini, and E. Nikinmaa. 2014. Ecophysiological Aspects of Phloem Transport in Trees. Pages 25-36 *in* M. Tausz and N. Grulke, editors. *Trees in a Changing Environment: Ecophysiology, Adaptation, and Future Survival*. Springer Dordrecht, The Netherlands.
- Hölttä, T., T. Vesala, S. Sevanto, M. Perämäki, and E. Nikinmaa. 2006. Modeling xylem and phloem water flows in trees according to cohesion theory and Münch hypothesis. *Trees* **20**:67-78.
- Hothorn, T., F. Bretz, and P. Westfall. 2008. Simultaneous Inference in General Parametric Models. *Biometrical Journal* **50**:346-363.
- Hsiao, T. C. 1973. Plant responses to water stress. *Annual Review of Plant Physiology* **24**:519-570.
- Hummel, I., F. Pantin, R. Sulpice, M. Piques, G. Rolland, M. Dauzat, A. Christophe, M. Pervent, M. Bouteillé, M. Stitt, Y. Gibon, and B. Muller. 2010. Arabidopsis plants acclimate to water deficit at low cost through changes of carbon usage: an integrated perspective using growth, metabolite, enzyme, and gene expression analysis. *Plant Physiology* **154**:357.
- IPCC. 2012. Managing the risks of extreme events and disasters to advance climate change adaptation: special report of the intergovernmental panel on climate change. Cambridge University Press, Cambridge, UK and New York, NY, USA.
- IPCC. 2014a. Climate change 2013: the physical science basis: Working Group I contribution to the Fifth assessment report of the Intergovernmental Panel on Climate Change. Cambridge University Press, United Kingdom and New York, NY, USA.
- IPCC. 2014b. Climate Change 2014: Impacts, adaptation, and vulnerability. Part A: global and sectoral aspects. contribution of working group II to the fifth assessment report of the intergovernmental panel on climate change. Cambridge University Press, Cambridge, UK and New York, USA.
- IPCC. 2014c. Climate change 2014: synthesis report. Contribution of Working Groups I, II and III to the fifth assessment report of the Intergovernmental Panel on Climate Change. Cambridge University Press, United Kingdom and New York, NY, USA.
- Jahnke, S., M. I. Menzel, D. Van Dusschoten, G. W. Roeb, J. Bühler, S. Minwuyelet, P. Blümler, V. M. Temperton, T. Hombach, M. Streun, S. Beer, M. Khodaverdi, K. Ziemons, H. H. Coenen, and U. Schurr. 2009. Combined MRI-PET dissects dynamic changes in plant structures and functions. *The Plant Journal* **59**:634-644.
- Jahnke, S., U. Schlesinger, G. B. Feige, and E. J. Knust. 1998. Transport of photoassimilates in young trees of *fraxinus* and *sorbus*: measurement of translocation *in vivo*. *Botanica Acta* **111**:307-315.
- Jensen, K. H., J. Liesche, T. Bohr, and A. Schulz. 2012. Universality of phloem transport in seed plants. *Plant, Cell & Environment* **35**:1065-1076.

- Jensen, K. H., J. A. Savage, and N. M. Holbrook. 2013. Optimal concentration for sugar transport in plants. *Journal of the Royal Society Interface* **10**:20130055.
- Jentsch, A., J. Kreyling, and C. Beierkuhnlein. 2007. A new generation of climate-change experiments: events, not trends. *Frontiers in Ecology and the Environment* **5**:365-374.
- Jødal, L., C. L. Loirec, and C. Champion. 2012. Positron range in PET imaging: an alternative approach for assessing and correcting the blurring. *Physics in Medicine and Biology* **57**:3931.
- Johnson, J. D., R. Tognetti, and P. Paris. 2002. Water relations and gas exchange in poplar and willow under water stress and elevated atmospheric CO₂. *Physiologia Plantarum* **115**:93-100.
- Jones, H. G. 2007. Monitoring plant and soil water status: established and novel methods revisited and their relevance to studies of drought tolerance. *Journal of Experimental Botany* **58**:119-130.
- Kang, D.-J., T. Nakanishi, T. Kume, and R. Ishii. 2009. Determination of the rate of ¹⁸F-labeled water movement to the leaf and its association with water relations in acid soil-tolerant rice varieties. *Journal of Crop Science and Biotechnology* **12**:261-265.
- Kawachi, N., K. Kikuchi, N. Suzui, S. Ishii, S. Fujimaki, N. S. Ishioka, and H. Watabe. 2011. Imaging of carbon translocation to fruit using carbon-11-labeled carbon dioxide and positron emission tomography. *IEEE Transactions on Nuclear Science* **58**:395-399.
- Keeling, C. D., R. B. Bacastow, A. E. Bainbridge, C. A. J. Ekdahl, P. R. Guenther, L. S. Waterman, and J. F. S. Chin. 1976. Atmospheric carbon dioxide variations at Mauna Loa Observatory, Hawaii. *Tellus* **28**:538-551.
- Keutgen, A. J., N. Keutgen, S. Matsushashi, C. Mizuniwa, T. Ito, T. Fujimura, N.-S. Ishioka, S. Watanabe, A. Osa, T. Sekine, H. Uchida, A. Tsuji, and S. Hashimoto. 2005. Input–output analysis of *in vivo* photoassimilate translocation using Positron-Emitting Tracer Imaging System (PETIS) data. *Journal of Experimental Botany* **56**:1419-1425.
- Kikuchi, K., S. Ishii, S. Fujimaki, N. Suzui, S. Matsushashi, I. Honda, Y. Shishido, and N. Kawachi. 2008. Real-time analysis of photoassimilate translocation in intact eggplant fruit using ¹¹CO₂ and a positron-emitting tracer imaging system. *Journal of the Japanese Society for Horticultural Science* **77**:199-205.
- Kim, E. E., M. C. Lee, T. Inoue, and W.-H. Wong. 2013. *Clinical PET and PET/CT: principles and applications*. Springer.
- King, G., P. Fonti, D. Nievergelt, U. Büntgen, and D. Frank. 2013. Climatic drivers of hourly to yearly tree radius variations along a 6 °C natural warming gradient. *Agricultural and Forest Meteorology* **168**:36-46.
- Kiser, M. R., C. D. Reid, A. S. Crowell, R. P. Phillips, and C. R. Howell. 2008. Exploring the transport of plant metabolites using positron emitting radiotracers. *HFSP Journal* **2**:189-204.

- Kiyomiya, S., H. Nakanishi, H. Uchida, S. Nishiyama, H. Tsukada, N. S. Ishioka, S. Watanabe, A. Osa, C. Mizuniwa, and T. Ito. 2001. Light activates H₂¹⁵O flow in rice: Detailed monitoring using a positron-emitting tracer imaging system (PETIS). *Physiologia Plantarum* **113**:359-367.
- Klein, T., M. K. F. Bader, S. Leuzinger, M. Mildner, P. Schleppi, R. T. W. Siegwolf, and C. Körner. 2016. Growth and carbon relations of mature *Picea abies* trees under 5 years of free-air CO₂ enrichment. *Journal of Ecology* **104**:1720-1733.
- Knoblauch, M. and W. S. Peters. 2010. Münch, morphology, microfluidics – our structural problem with the phloem. *Plant, Cell & Environment* **33**:1439-1452.
- Komor, E. 2000. Source physiology and assimilate transport: the interaction of sucrose metabolism, starch storage and phloem export in source leaves and the effects on sugar status in phloem. *Functional Plant Biology* **27**:497-505.
- Körner, C. 2003. Carbon limitation in trees. *Journal of Ecology* **91**:4-17.
- Körner, C. H., S. Pelaez-Riedl, and A. J. E. Van Bel. 1995. CO₂ responsiveness of plants: a possible link to phloem loading. *Plant, Cell & Environment* **18**:595-600.
- Kramer, P. J. and J. S. Boyer. 1995. *Water relations of plants and soils*. Academic Press, San Diego, CA, USA.
- Krijger, G. C., T. G. Verburg, W. Den Hollander, P. M. J. A. Hermans, J. J. M. De Goeij, and H. Wolterbeek. 1999. Approaches for nondestructive spatial distribution measurements in whole plants using radionuclides. *Journal of Plant Physiology* **155**:165-172.
- Kume, T., H. Takizawa, N. Yoshifuji, K. Tanaka, C. Tantasirin, N. Tanaka, and M. Suzuki. 2007. Impact of soil drought on sap flow and water status of evergreen trees in a tropical monsoon forest in northern Thailand. *Forest Ecology and Management* **238**:220-230.
- Kutta, W. 1901. Beitrag zur näherungsweise Integration totaler Differentialgleichungen. *Zeitschrift für angewandte Mathematik und Physik* **46**:435-453.
- Ladjal, M., R. Huc, and M. Ducrey. 2005. Drought effects on hydraulic conductivity and xylem vulnerability to embolism in diverse species and provenances of Mediterranean cedars. *Tree Physiology* **25**:1109-1117.
- Lalonde, S., M. Tegeder, M. Throne-Holst, W. B. Frommer, and J. W. Patrick. 2003. Phloem loading and unloading of sugars and amino acids. *Plant, Cell & Environment* **26**:37-56.
- Leakey, A. D. B., E. A. Ainsworth, C. J. Bernacchi, A. Rogers, S. P. Long, and D. R. Ort. 2009. Elevated CO₂ effects on plant carbon, nitrogen, and water relations: six important lessons from FACE. *Journal of Experimental Botany* **60**:2859-2876.
- Lechaudel, M., G. Vercambre, F. Lescourret, F. Normand, and M. Génard. 2007. An analysis of elastic and plastic fruit growth of mango in response to various assimilate supplies. *Tree Physiology* **27**:219-230.

- Lefcheck, J. S. 2016. piecewiseSEM: Piecewise structural equation modelling in r for ecology, evolution, and systematics. *Methods in Ecology and Evolution* **7**:573-579.
- Lemoine, R. 2000. Sucrose transporters in plants: update on function and structure. *Biochimica et Biophysica Acta (BBA) - Biomembranes* **1465**:246-262.
- Lemoine, R., S. L. Camera, R. Atanassova, F. Dédaldéchamp, T. Allario, N. Pourtau, J.-L. Bonnemain, M. Laloi, P. Coutos-Thévenot, L. Maurousset, M. Faucher, C. Girousse, P. Lemonnier, J. Parrilla, and M. Durand. 2013. Source-to-sink transport of sugar and regulation by environmental factors. *Frontiers in Plant Science* **4**:272.
- Lenoir, J. and J. C. Svenning. 2015. Climate-related range shifts – a global multidimensional synthesis and new research directions. *Ecography* **38**:15-28.
- Lens, F., C. Picon-Cochard, C. E. L. Delmas, C. Signarbieux, A. Buttler, H. Cochard, S. Jansen, T. Chauvin, L. C. Doria, M. del Arco, and S. Delzon. 2016. Herbaceous angiosperms are not more vulnerable to drought-induced embolism than angiosperm trees. *Plant Physiology* **172**:661-667.
- Leuning, R., A. Tuzet, and A. Perrier. 2004. Stomata as Part of the Soil-Plant-Atmosphere Continuum. Page 21 *in* M. Mencuccini, J. Grace, J. Moncrieff, and K. G. McNaughton, editors. *Forests at the land-atmosphere interface*. CABI Publishing, Wallingford, UK.
- Leuzinger, S. and M. K. F. Bader. 2012. Experimental vs. modeled water use in mature Norway spruce (*Picea abies*) exposed to elevated CO₂. *Frontiers in Plant Science* **3**:229.
- Leuzinger, S. and C. Körner. 2007. Water savings in mature deciduous forest trees under elevated CO₂. *Global Change Biology* **13**:2498-2508.
- Levin, C. S. and E. J. Hoffman. 1999. Calculation of positron range and its effect on the fundamental limit of positron emission tomography system spatial resolution. *Physics in Medicine and Biology* **44**:781.
- Li, G., V. Santoni, and C. Maurel. 2014. Plant aquaporins: roles in plant physiology. *Biochimica et Biophysica Acta (BBA) - General Subjects* **1840**:1574-1582.
- Liesche, J., C. Windt, T. Bohr, A. Schulz, and K. H. Jensen. 2015. Slower phloem transport in gymnosperm trees can be attributed to higher sieve element resistance. *Tree Physiology* **35**:376-386.
- Lo Gullo, M. A. and S. Salleo. 1992. Water storage in the wood and xylem cavitation in 1-year-old twigs of *Populus deltoides* Bartr. *Plant, Cell & Environment* **15**:431-438.
- Lockhart, J. A. 1965. An analysis of irreversible plant cell elongation. *Journal of Theoretical Biology* **8**:264-275.
- Long, S. P., E. A. Ainsworth, A. Rogers, and D. R. Ort. 2004. Rising atmospheric carbon dioxide: plants FACE the future. *Annual Review of Plant Biology* **55**:591-628.
- Lumen. 2004. *Boundless Biology: Plant Form and Physiology*.

- Lüthi, D., M. Le Floch, B. Bereiter, T. Blunier, J.-M. Barnola, U. Siegenthaler, D. Raynaud, J. Jouzel, H. Fischer, and K. Kawamura. 2008. High-resolution carbon dioxide concentration record 650,000–800,000 years before present. *Nature* **453**:379.
- Maherali, H., W. T. Pockman, and R. B. Jackson. 2004. Adaptive variation in the vulnerability of woody plants to xylem cavitation. *Ecology* **85**:2184-2199.
- Manderscheid, R., M. Erbs, S. Burkart, K. P. Wittich, F. J. Löpmeier, and H. J. Weigel. 2016. Effects of free-air carbon dioxide enrichment on sap flow and canopy microclimate of maize grown under different water supply. *Journal of Agronomy and Crop Science* **202**:255-268.
- Martínez-Vilalta, J., A. Sala, D. Asensio, L. Galiano, G. Hoch, S. Palacio, F. I. Piper, and F. Lloret. 2016. Dynamics of non-structural carbohydrates in terrestrial plants: a global synthesis. *Ecological Monographs* **86**:495-516.
- Martínez, J. P., H. Silva, J. F. Ledent, and M. Pinto. 2007. Effect of drought stress on the osmotic adjustment, cell wall elasticity and cell volume of six cultivars of common beans (*Phaseolus vulgaris* L.). *European Journal of Agronomy* **26**:30-38.
- Masschaele, B., M. Dierick, D. Van Loo, M. N. Boone, L. Brabant, E. Pauwels, V. Cnudde, and L. Van Hoorebeke. 2013. HECTOR: A 240kV micro-CT setup optimized for research. *Journal of Physics: Conference Series* **463**:012012.
- Matsushashi, S., S. Fujimaki, N. Kawachi, K. Sakamoto, N. S. Ishioka, and T. Kume. 2005. Quantitative modeling of photoassimilate flow in an intact plant using the Positron Emitting Tracer Imaging System (PETIS). *Soil Science and Plant Nutrition* **51**:417-423.
- Mayr, S., S. Rosner, and F. Meinzer. 2011. Cavitation in dehydrating xylem of *Picea abies*: energy properties of ultrasonic emissions reflect tracheid dimensions. *Tree Physiology* **31**:59-67.
- McCauley, M. M. and R. F. Evert. 1988a. The Anatomy of the Leaf of Potato, *Solanum tuberosum* L. 'Russet Burbank'. *Botanical Gazette* **149**:179-195.
- McCauley, M. M. and R. F. Evert. 1988b. Morphology and Vasculature of the Leaf of Potato (*Solanum tuberosum*). *American Journal of Botany* **75**:377-390.
- McDowell, N. G. 2011. Mechanisms linking drought, hydraulics, carbon metabolism, and vegetation mortality. *Plant Physiology* **155**:1051.
- McDowell, N. G., D. J. Beerling, D. D. Breshears, R. A. Fisher, K. F. Raffa, and M. Stitt. 2011. The interdependence of mechanisms underlying climate-driven vegetation mortality. *Trends in Ecology & Evolution* **26**:523-532.
- McDowell, N. G., W. T. Pockman, C. D. Allen, D. D. Breshears, N. Cobb, T. Kolb, J. Plaut, J. Sperry, A. West, D. G. Williams, and E. A. Yezpez. 2008. Mechanisms of plant survival and mortality during drought: why do some plants survive while others succumb to drought? *New Phytologist* **178**:719-739.
- McDowell, N. G. and S. Sevanto. 2010. The mechanisms of carbon starvation: how, when, or does it even occur at all? *New Phytologist* **186**:264-266.

- Meinzer, F. C., M. J. Clearwater, and G. Goldstein. 2001. Water transport in trees: current perspectives, new insights and some controversies. *Environmental and Experimental Botany* **45**:239-262.
- Meinzer, F. C., D. M. Johnson, B. Lachenbruch, K. A. McCulloh, and D. R. Woodruff. 2009. Xylem hydraulic safety margins in woody plants: coordination of stomatal control of xylem tension with hydraulic capacitance. *Functional Ecology* **23**:922-930.
- Meinzer, F. C. and K. A. McCulloh. 2013. Xylem recovery from drought-induced embolism: where is the hydraulic point of no return? *Tree Physiology* **33**:331-334.
- Mencuccini, M. and T. Hölttä. 2010. The significance of phloem transport for the speed with which canopy photosynthesis and belowground respiration are linked. *New Phytologist* **185**:189-203.
- Minchin, P. E. H. 2007. Mechanistic modelling of carbon partitioning. Pages 113-122 *in* J. Vos., L. F. M. Marcelis, P. H. B. de Visser, P. C. Struik, and J. B. Evers, editors. *Functional-Structural Plant Modelling in Crop Production*. Springer, Dordrecht, The Netherlands.
- Minchin, P. E. H. 2012. Input-output analysis of phloem partitioning within higher plants. Pages 519-532 *in* L. Wang and H. Garnier, editors. *System Identification, Environmental Modelling, and Control System Design*. Springer, London, UK.
- Minchin, P. E. H. and M. R. Thorpe. 1987. Measurement of unloading and reloading of photo-assimilate within the stem of bean. *Journal of Experimental Botany* **38**:211-220.
- Minchin, P. E. H. and M. R. Thorpe. 2003. Using the short-lived isotope ^{11}C in mechanistic studies of photosynthate transport. *Functional Plant Biology* **30**:831-841.
- Mitchell, P. J., A. P. O'Grady, D. T. Tissue, D. Worledge, and E. A. Pinkard. 2014. Coordination of growth, gas exchange and hydraulics define the carbon safety margin in tree species with contrasting drought strategies. *Tree Physiology* **34**:443-458.
- Moreno, F., W. Conejero, M. J. Martín-Palomo, I. F. Girón, and A. Torrecillas. 2006. Maximum daily trunk shrinkage reference values for irrigation scheduling in olive trees. *Agricultural Water Management* **84**:290-294.
- Mori, S., S. Kiyomiya, H. Nakanishi, N. S. Ishioka, S. Watanabe, A. Osa, S. Matsushashi, S. Hashimoto, T. Sekine, H. Uchida, S. Nishiyama, H. Tsukada, and A. Tsuji. 2000. Visualization of ^{15}O -water flow in tomato and rice in the light and dark using a positron-emitting tracer imaging system (PETIS). *Soil Science and Plant Nutrition* **46**:975-979.
- Moses, W. W. 2011. Fundamental limits of spatial resolution in PET. *Nuclear Instruments and Methods in Physics Research Section A: Accelerators, Spectrometers, Detectors and Associated Equipment* **648**, **Supplement 1**:S236-S240.
- Muggeo, V. M. R. 2008. Segmented: an R package to fit regression models with broken-line relationships. *R news* **8**:20-25.

- Münch, E. 1930. Stoffbewegungen in der Pflanze.
- Murata, Y., I. C. Mori, and S. Munemasa. 2015. Diverse Stomatal Signaling and the Signal Integration Mechanism. *Annual Review of Plant Biology* **66**:369-392.
- Myking, T., F. Bøhler, G. Austrheim, and E. J. Solberg. 2011. Life history strategies of aspen (*Populus tremula* L.) and browsing effects: a literature review. *Forestry* **84**:61-71.
- Nakanishi, H., S. Kiyomiya, T. Tsukamoto, H. Tsukada, H. Uchida, and S. Mori. 2002. Water ($H_2^{15}O$) flow in rice is regulated by the concentration of nutrients as monitored by positron multi-probe system (PMPS). *Soil Science and Plant Nutrition* **48**:759-762.
- Nikinmaa, E., T. Hölttä, P. Hari, P. Kolari, A. Mäkelä, S. Sevanto, and T. Vesala. 2013. Assimilate transport in phloem sets conditions for leaf gas exchange. *Plant, Cell & Environment* **36**:655-669.
- Norby, R. J., E. H. DeLucia, B. Gielen, C. Calfapietra, C. P. Giardina, J. S. King, J. Ledford, H. R. McCarthy, D. J. P. Moore, R. Ceulemans, P. De Angelis, A. C. Finzi, D. F. Karnosky, M. E. Kubiske, M. Lukac, K. S. Pregitzer, G. E. Scarascia-Mugnozza, W. H. Schlesinger, and R. Oren. 2005. Forest response to elevated CO_2 is conserved across a broad range of productivity. *Proceedings of the National Academy of Sciences of the United States of America* **102**:18052-18056.
- Norby, R. J., S. D. Wullschleger, C. A. Gunderson, D. W. Johnson, and R. Ceulemans. 1999. Tree responses to rising CO_2 in field experiments: implications for the future forest. *Plant, Cell & Environment* **22**:683-714.
- Norby, R. J. and D. R. Zak. 2011. Ecological lessons from Free-Air CO_2 Enrichment (FACE) Experiments. *Annual Review of Ecology, Evolution, and Systematics* **42**:181-203.
- Oguntunde, P. G. and A. M. Oguntuase. 2007. Influence of environmental factors on the sap flux density of mango trees under rain-fed cropping systems in West Africa. *International Journal of Plant Production* **1**:179-188.
- Ohya, T., K. Tanoi, Y. Hamada, H. Okabe, H. Rai, J. Hojo, K. Suzuki, and T. M. Nakanishi. 2008. An analysis of long-distance water transport in the soybean stem using $H_2^{15}O$. *Plant and Cell Physiology* **49**:718-729.
- Ortuño, M. F., W. Conejero, F. Moreno, A. Moriana, D. S. Intrigliolo, C. Biel, C. D. Mellisho, A. Pérez-Pastor, R. Domingo, M. C. Ruiz-Sánchez, J. Casadesus, J. Bonany, and A. Torrecillas. 2010. Could trunk diameter sensors be used in woody crops for irrigation scheduling? A review of current knowledge and future perspectives. *Agricultural Water Management* **97**:1-11.
- Ortuño, M. F., Y. García-Orellana, W. Conejero, M. C. Ruiz-Sánchez, O. Mounzer, J. J. Alarcón, and A. Torrecillas. 2006. Relationships between climatic variables and sap flow, stem water potential and maximum daily trunk shrinkage in lemon trees. *Plant and Soil* **279**:229-242.
- Paoletti, E., H. Pfanz, and A. Raschi. 2005. Pros and cons of CO_2 springs as experimental sites. Pages 195-202 in K. Omasa, I. Nouchi, and L. J. De Kok,

- editors. *Plant Responses to Air Pollution and Global Change*. Springer Japan, Tokyo.
- Park, S. J., W. L. Rogers, and N. H. Clinthorne. 2007. Effects of positron range and annihilation photon acollinearity on image resolution of a Compton PET. *IEEE Transactions on Nuclear Science* **54**:1543-1552.
- Partelová, D., M. Horník, J. Lesný, P. Rajec, P. Kováč, and S. Hostin. 2016. Imaging and analysis of thin structures using positron emission tomography: Thin phantoms and *in vivo* tobacco leaves study. *Applied Radiation and Isotopes* **115**:87-96.
- Patakas, A. and B. Noitsakis. 1997. Cell wall elasticity as a mechanism to maintain favorable water relations during leaf ontogeny in grapevines. *American Journal of Enology and Viticulture* **48**:352.
- Pearcy, R. W., E. D. Schulze, and R. Zimmermann. 2000. Measurement of transpiration and leaf conductance. Pages 137-160 *in* R. W. Pearcy, J. R. Ehleringer, H. A. Mooney, and P. W. Rundel, editors. *Plant physiological ecology*. Springer, Dordrecht, The Netherlands.
- Pearson, R. G. and T. P. Dawson. 2003. Predicting the impacts of climate change on the distribution of species: are bioclimate envelope models useful? *Global Ecology and Biogeography* **12**:361-371.
- Pereira, A. R., S. Green, and N. A. Villa Nova. 2006. Penman–Monteith reference evapotranspiration adapted to estimate irrigated tree transpiration. *Agricultural Water Management* **83**:153-161.
- Pereira, H. M., P. W. Leadley, V. Proença, R. Alkemade, J. P. W. Scharlemann, J. F. Fernandez-Manjarrés, M. B. Araújo, P. Balvanera, R. Biggs, W. W. L. Cheung, L. Chini, H. D. Cooper, E. L. Gilman, S. Guénette, G. C. Hurtt, H. P. Huntington, G. M. Mace, T. Oberdorff, C. Revenga, P. Rodrigues, R. J. Scholes, U. R. Sumaila, and M. Walpole. 2010. Scenarios for global biodiversity in the 21st century. *Science* **330**:1496.
- Pfautsch, S., J. Renard, M. G. Tjoelker, and A. Salih. 2015. Phloem as capacitor: radial transfer of water into xylem of tree stems occurs via symplastic transport in ray parenchyma. *Plant Physiology* **167**:963-971.
- Phelps, M. E., E. J. Hoffman, S.-C. Huang, and M. M. Ter-Pogossian. 1975. Effect of positron range on spatial resolution. *Journal of Nuclear Medicine* **16**:649-652.
- Phillips, N. G., R. D. Attard, O. Ghannoum, J. D. Lewis, B. A. Logan, and D. T. Tissue. 2011. Impact of variable [CO₂] and temperature on water transport structure–function relationships in *Eucalyptus*. *Tree Physiology* **31**:945-952.
- Pickard, W. F., P. E. H. Minchin, and M. R. Thorpe. 1993. Leaf export and partitioning changes induced by short-term inhibition of phloem transport. *Journal of Experimental Botany* **44**:1491-1496.
- Pinheiro, C. and M. M. Chaves. 2011. Photosynthesis and drought: can we make metabolic connections from available data? *Journal of Experimental Botany* **62**:869-882.

- Pinheiro, J., D. Bates, S. DebRoy, and D. Sarkar. 2014. R Core Team (2014) nlme: linear and nonlinear mixed effects models. R package version 3.1-117. <http://CRAN.R-project.org/package=nlme>.
- Poorter, H. and O. Nagel. 2000. The role of biomass allocation in the growth response of plants to different levels of light, CO₂, nutrients and water: a quantitative review. *Functional Plant Biology* **27**:1191-1191.
- Porporato, A., F. Laio, L. Ridolfi, and I. Rodriguez-Iturbe. 2001. Plants in water-controlled ecosystems: active role in hydrologic processes and response to water stress: III. Vegetation water stress. *Advances in Water Resources* **24**:725-744.
- Possen, B. J. H. M., E. Oksanen, M. Rousi, H. Ruhanen, V. Ahonen, A. Tervahauta, J. Heinonen, J. Heiskanen, S. Kärenlampi, and E. Vapaavuori. 2011. Adaptability of birch (*Betula pendula* Roth) and aspen (*Populus tremula* L.) genotypes to different soil moisture conditions. *Forest Ecology and Management* **262**:1387-1399.
- Rahmim, A. and H. Zaidi. 2008. PET versus SPECT: strengths, limitations and challenges. *Nuclear Medicine Communications* **29**:193-207.
- Raichle, M. E. 2009. A brief history of human brain mapping. *Trends in Neurosciences* **32**:118-126.
- Ramsfield, T. D., B. J. Bentz, M. Faccoli, H. Jactel, and E. G. Brockerhoff. 2016. Forest health in a changing world: effects of globalization and climate change on forest insect and pathogen impacts. *Forestry: An International Journal of Forest Research* **89**:245-252.
- Reidel, E. J., E. A. Rennie, V. Amiard, L. Cheng, and R. Turgeon. 2009. Phloem loading strategies in three plant species that transport sugar alcohols. *Plant Physiology* **149**:1601-1608.
- Rennie, E. A. and R. Turgeon. 2009. A comprehensive picture of phloem loading strategies. *Proceedings of the National Academy of Sciences of the United States of America* **106**:14162-14167.
- Ripple, W. J., C. Wolf, T. M. Newsome, M. Galetti, M. Alamgir, E. Crist, M. I. Mahmoud, and W. F. Laurance. 2017. World Scientists' Warning to Humanity: A Second Notice. *Bioscience* **67**:1026-1028.
- Rohli, R. V., T. A. Joyner, S. J. Reynolds, and T. J. Ballinger. 2015. Overlap of global Köppen–Geiger climates, biomes, and soil orders. *Physical Geography* **36**:158-175.
- Ruehr, N. K., C. A. Offermann, A. Gessler, J. B. Winkler, J. P. Ferrio, N. Buchmann, and R. L. Barnard. 2009. Drought effects on allocation of recent carbon: from beech leaves to soil CO₂ efflux. *New Phytologist* **184**:950-961.
- Runge, C. 1895. Über die numerische Auflösung von Differentialgleichungen. *Mathematische Annalen* **46**:167-178.
- Ryan, M. G. 2013. Three decades of research at Flakaliden advancing whole-tree physiology, forest ecosystem and global change research. *Tree Physiology* **33**:1123-1131.

- Ryan, M. G. and S. Asao. 2014. Phloem transport in trees. *Tree Physiology* **34**:1-4.
- Sack, L. and C. Scoffoni. 2013. Leaf venation: structure, function, development, evolution, ecology and applications in the past, present and future. *New Phytologist* **198**:983-1000.
- Sade, N., A. Gebremedhin, and M. Moshelion. 2012. Risk-taking plants. *Plant Signaling & Behavior* **7**:767-770.
- Sala, A., F. Piper, and G. Hoch. 2010. Physiological mechanisms of drought-induced tree mortality are far from being resolved. *New Phytologist* **186**:274-281.
- Sala, A., D. R. Woodruff, and F. C. Meinzer. 2012. Carbon dynamics in trees: feast or famine? *Tree Physiology* **32**:764-775.
- Salleo, S., M. A. Lo Gullo, P. Trifilò, and A. Nardini. 2004. New evidence for a role of vessel-associated cells and phloem in the rapid xylem refilling of cavitated stems of *Laurus nobilis* L. *Plant, Cell & Environment* **27**:1065-1076.
- Sardans, J., J. Peñuelas, and S. Lope-Piedrafita. 2010. Changes in water content and distribution in *Quercus ilex* leaves during progressive drought assessed by *in vivo* ^1H magnetic resonance imaging. *BMC Plant Biology* **10**:188.
- Sause, M. G. R. 2011. Investigation of pencil-lead breaks as acoustic emission sources. *Journal of Acoustic Emission* **29**:184-196.
- Savage, J. A., S. D. Beecher, L. Clerx, J. T. Gersony, J. Knoblauch, J. M. Losada, K. H. Jensen, M. Knoblauch, and N. M. Holbrook. 2017. Maintenance of carbohydrate transport in tall trees. *Nature Plants* **3**:965-972.
- Savage, J. A., M. J. Clearwater, D. F. Haines, T. Klein, M. Mencuccini, S. Sevanto, R. Turgeon, and C. Zhang. 2016. Allocation, stress tolerance and carbon transport in plants: how does phloem physiology affect plant ecology? *Plant, Cell & Environment* **39**:709-725.
- Scheffer, M., M. Holmgren, V. Brovkin, and M. Claussen. 2005. Synergy between small- and large-scale feedbacks of vegetation on the water cycle. *Global Change Biology* **11**:1003-1012.
- Schenk, H. J., S. Espino, D. M. Romo, N. Nima, A. Y. T. Do, J. M. Michaud, B. Papahadjopoulos-Sternberg, J. Yang, Y. Y. Zuo, K. Steppe, and S. Jansen. 2017. Xylem Surfactants Introduce a New Element to the Cohesion-Tension Theory. *Plant Physiology* **173**:1177.
- Schenk, H. J., K. Steppe, and S. Jansen. 2015. Nanobubbles: a new paradigm for air-seeding in xylem. *Trends in Plant Science* **20**:199-205.
- Schindelin, J., I. Arganda-Carreras, E. Frise, V. Kaynig, M. Longair, T. Pietzsch, S. Preibisch, C. Rueden, S. Saalfeld, B. Schmid, J.-Y. Tinevez, D. J. White, V. Hartenstein, K. Eliceiri, P. Tomancak, and A. Cardona. 2012. Fiji: an open-source platform for biological-image analysis. *Nature Methods* **9**:676-682.
- Schulz, D., S. Southeikal, S. S. Junnarkar, J.-F. Pratte, M. L. Purschke, S. P. Stoll, B. Ravindranath, S. H. Maramraju, S. Krishnamoorthy, F. A. Henn, P. O'Connor, C. L. Woody, D. J. Schlyer, and P. Vaska. 2011. Simultaneous assessment of

- rodent behavior and neurochemistry using a miniature positron emission tomograph. *Nature Methods* **8**:347-352.
- SCRIPPS. 2018. History of CO₂ concentrations in the atmosphere. <https://scripps.ucsd.edu/programs/keelingcurve/>.
- Secchi, F. and M. A. Zwieniecki. 2011. Sensing embolism in xylem vessels: the role of sucrose as a trigger for refilling. *Plant, Cell & Environment* **34**:514-524.
- Sevanto, S. 2014. Phloem transport and drought. *Journal of Experimental Botany* **65**:1751-1759.
- Sevanto, S., T. Hölttä, and N. M. Holbrook. 2011. Effects of the hydraulic coupling between xylem and phloem on diurnal phloem diameter variation. *Plant, Cell & Environment* **34**:690-703.
- Sevanto, S., N. G. McDowell, L. T. Dickman, R. Pangle, and W. T. Pockman. 2014. How do trees die? A test of the hydraulic failure and carbon starvation hypotheses. *Plant, Cell & Environment* **37**:153-161.
- Shimazaki, K.-i., M. Doi, S. M. Assmann, and T. Kinoshita. 2007. Light regulation of stomatal movement. *Annual Review of Plant Biology* **58**:219-247.
- Shugaeva, N. A., E. I. Vyskrebentseva, S. O. Orekhova, and A. G. Shugaev. 2007. Effect of water deficit on respiration of conducting bundles in leaf petioles of sugar beet. *Russian Journal of Plant Physiology* **54**:329-335.
- Silim, S., R. Nash, D. Reynard, B. White, and W. Schroeder. 2009. Leaf gas exchange and water potential responses to drought in nine poplar (*Populus* spp.) clones with contrasting drought tolerance. *Trees* **23**:959-969.
- Silva, L. C. R. and M. Anand. 2013. Probing for the influence of atmospheric CO₂ and climate change on forest ecosystems across biomes. *Global Ecology and Biogeography* **22**:83-92.
- Slewisinski, T. L. and D. M. Braun. 2010. Current perspectives on the regulation of whole-plant carbohydrate partitioning. *Plant Science* **178**:341-349.
- Slewisinski, T. L., C. Zhang, and R. Turgeon. 2013. Structural and functional heterogeneity in phloem loading and transport. *Frontiers in Plant Science* **4**:244.
- Smith, D. M. and S. J. Allen. 1996. Measurement of sap flow in plant stems. *Journal of Experimental Botany* **47**:1833-1844.
- Sperry, J. 2013. Cutting-edge research or cutting-edge artefact? An overdue control experiment complicates the xylem refilling story. *Plant, Cell & Environment* **36**:1916-1918.
- Sperry, J. S., M. A. Christman, J. M. Torres-Ruiz, H. Taneda, and D. D. Smith. 2012. Vulnerability curves by centrifugation: is there an open vessel artefact, and are 'r' shaped curves necessarily invalid? *Plant, Cell & Environment* **35**:601-610.
- Sperry, J. S., J. R. Donnelly, and M. T. Tyree. 1988. A method for measuring hydraulic conductivity and embolism in xylem. *Plant, Cell & Environment* **11**:35-40.

- Sperry, J. S. and D. M. Love. 2015. What plant hydraulics can tell us about responses to climate-change droughts. *New Phytologist* **207**:14-27.
- Sperry, J. S. and M. T. Tyree. 1988. Mechanism of water stress-induced xylem embolism. *Plant Physiology* **88**:581.
- Steppe, K., H. Cochard, A. Lacointe, and T. Améglio. 2012. Could rapid diameter changes be facilitated by a variable hydraulic conductance? *Plant, Cell & Environment* **35**:150-157.
- Steppe, K., D. J. W. De Pauw, R. Lemeur, and P. A. Vanrolleghem. 2006. A mathematical model linking tree sap flow dynamics to daily stem diameter fluctuations and radial stem growth. *Tree Physiology* **26**:257-273.
- Steppe, K., D. W. De Pauw, and R. Lemeur. 2008. A step towards new irrigation scheduling strategies using plant-based measurements and mathematical modelling. *Irrigation Science* **26**:505-517.
- Steppe, K., F. Sterck, and A. Deslauriers. 2015. Diel growth dynamics in tree stems: linking anatomy and ecophysiology. *Trends in Plant Science* **20**:335-343.
- Stedle, E., U. Zimmermann, and U. Lüttge. 1977. Effect of turgor pressure and cell size on the wall elasticity of plant cells. *Plant Physiology* **59**:285.
- Stiller, V. 2009. Soil salinity and drought alter wood density and vulnerability to xylem cavitation of baldcypress (*Taxodium distichum* (L.) Rich.) seedlings. *Environmental and Experimental Botany* **67**:164-171.
- Sultan, S. E. 2000. Phenotypic plasticity for plant development, function and life history. *Trends in Plant Science* **5**:537-542.
- Taiz, L. and E. Zeiger. 2010. *Plant physiology*. 5th edition. Sinauer Associates, Sunderland, MA, USA.
- Teskey, R., T. Wertin, I. Bauweraerts, M. Ameye, M. A. McGuire, and K. Steppe. 2014. Responses of tree species to heat waves and extreme heat events. *Plant, Cell & Environment*.
- Teskey, R., T. Wertin, I. Bauweraerts, M. Ameye, M. A. McGuire, and K. Steppe. 2015. Responses of tree species to heat waves and extreme heat events. *Plant, Cell & Environment* **38**:1699-1712.
- Thompson, M. V. 2006. Phloem: the long and the short of it. *Trends in Plant Science* **11**:26-32.
- Thompson, M. V. and N. M. Holbrook. 2003. Scaling phloem transport: water potential equilibrium and osmoregulatory flow. *Plant, Cell & Environment* **26**:1561-1577.
- Thoms, R., M. Köhler, A. Gessler, and G. Gleixner. 2017. Above and below ground carbohydrate allocation differs between ash (*Fraxinus excelsior* L.) and beech (*Fagus sylvatica* L.). *PLOS ONE* **12**:e0184247.
- Thorpe, M. R., A. P. Ferrieri, M. M. Herth, and R. A. Ferrieri. 2007. ¹¹C-imaging: methyl jasmonate moves in both phloem and xylem, promotes transport of jasmonate,

and of photoassimilate even after proton transport is decoupled. *Planta* **226**:541-551.

Thorpe, M. R., P. E. H. Minchin, N. Gould, J. McQueen, N. M. Holbrook, and M. A. Zwieniecki. 2005. *The stem apoplast: a potential communication channel in plant growth regulation*. Elsevier Academic Press, Amsterdam, The Netherlands.

Thuiller, W., D. M. Richardson, P. Pyšek, G. F. Midgley, G. O. Hughes, and M. Rouget. 2005. Niche-based modelling as a tool for predicting the risk of alien plant invasions at a global scale. *Global Change Biology* **11**:2234-2250.

Tognetti, R., A. Longobucco, and A. Raschi. 1999. Seasonal embolism and xylem vulnerability in deciduous and evergreen Mediterranean trees influenced by proximity to a carbon dioxide spring. *Tree Physiology* **19**:271-277.

Tognetti, R., A. Longobucco, A. Raschi, and M. B. Jones. 2001. Stem hydraulic properties and xylem vulnerability to embolism in three co-occurring Mediterranean shrubs at a natural CO₂ spring. *Functional Plant Biology* **28**:257-268.

Tollefson, J. 2015. Is the 2° C world a fantasy? . *Nature News* **527**:436-438.

Trifilò, P., F. Raimondo, M. A. Lo Gullo, P. M. Barbera, S. Salleo, and A. Nardini. 2014. Relax and refill: xylem rehydration prior to hydraulic measurements favours embolism repair in stems and generates artificially low PLC values. *Plant, Cell & Environment* **37**:2491-2499.

Tschaplinski, T. J., G. A. Tuskan, G. M. Gebre, and D. E. Todd. 1998. Drought resistance of two hybrid *Populus* clones grown in a large-scale plantation. *Tree Physiology* **18**:653-658.

Turgeon, R. 1996. Phloem loading and plasmodesmata. *Trends in Plant Science* **1**:418-423.

Turgeon, R. 2010. The role of phloem loading reconsidered. *Plant Physiology* **152**:1817-1823.

Turgeon, R. and R. Medville. 1998. The absence of phloem loading in willow leaves. *Proceedings of the National Academy of Sciences* **95**:12055-12060.

Turgeon, R. and L. E. Wimmers. 1988. Different patterns of vein loading of exogenous [¹⁴C]sucrose in leaves of *Pisum sativum* and *Coleus blumei*. *Plant Physiology* **87**:179-182.

Turgeon, R. and S. Wolf. 2009. Phloem transport: cellular pathways and molecular trafficking. *Annual Review of Plant Biology* **60**:207-221.

Tyree, M. T. and J. D. Alexander. 1993. Plant water relations and the effects of elevated CO₂: a review and suggestions for future research. *Vegetatio* **104**:47-62.

Tyree, M. T. and F. W. Ewers. 1991. The hydraulic architecture of trees and other woody plants. *New Phytologist* **119**:345-360.

Tyree, M. T. and J. S. Sperry. 1989. Vulnerability of xylem to cavitation and embolism. *Annual Review of Plant Physiology and Plant Molecular Biology* **40**:19-36.

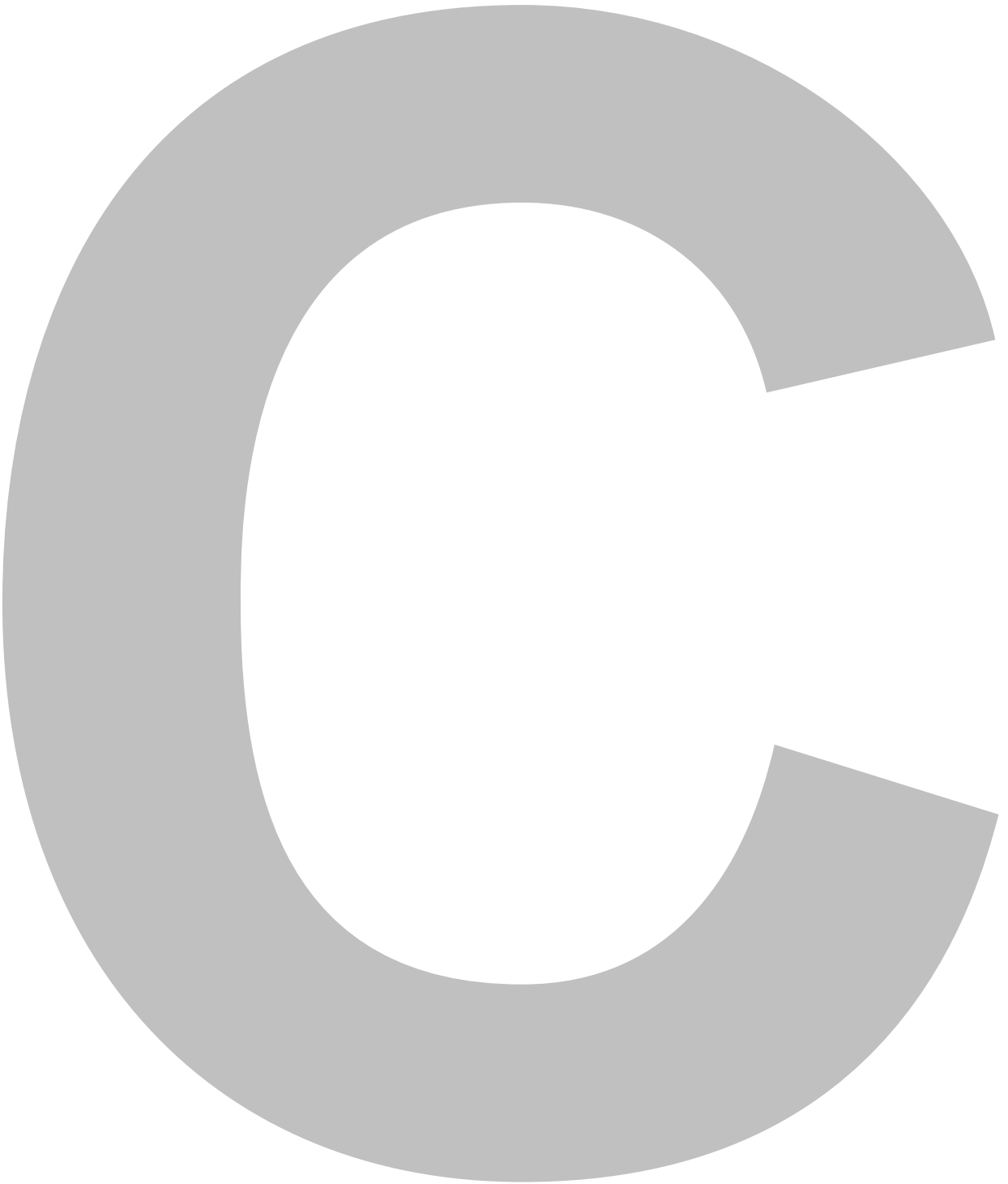
- Tyree, M. T. and S. Yang. 1990. Water-storage capacity of Thuja, Tsuga and Acer stems measured by dehydration isotherms. *Planta* **182**:420-426.
- Uchida, H., T. Okamoto, T. Ohmura, K. Shimizu, N. Satoh, T. Koike, and T. Yamashita. 2004. A compact planar positron imaging system. *Nuclear Instruments and Methods in Physics Research Section A: Accelerators, Spectrometers, Detectors and Associated Equipment* **516**:564-574.
- Urban, J., E. Bednárová, R. Plichta, V. Gryc, H. Vavrčík, J. Hacura, M. Fajstavr, and J. Kučera. 2014. Links between phenology and ecophysiology in a European beech forest. *iForest - Biogeosciences and Forestry* **8**:438-447.
- Urban, M. C. 2015. Accelerating extinction risk from climate change. *Science* **348**:571-573.
- Vallabhajosula, S., L. Solnes, and B. Vallabhajosula. 2011. A broad overview of positron emission tomography radiopharmaceuticals and clinical applications: what is new? *Seminars in Nuclear Medicine* **41**:246-264.
- Valladares, F., S. Matesanz, F. Guilhaumon, M. B. Araújo, L. Balaguer, M. Benito-Garzón, W. Cornwell, E. Gianoli, M. van Kleunen, D. E. Naya, A. B. Nicotra, H. Poorter, and M. A. Zavala. 2014. The effects of phenotypic plasticity and local adaptation on forecasts of species range shifts under climate change. *Ecology Letters* **17**:1351-1364.
- Van Bavel, M. G. and C. H. M. Van Bavel. 2005. Dynagage installation and operation manual. Dynamax Inc., Houston, TX, USA.
- Van Bel, A. J. E. 2003. The phloem, a miracle of ingenuity. *Plant, Cell & Environment* **26**:125-149.
- Van Bel, A. J. E. and J. B. Hafke. 2005. Physiochemical determinants of phloem transport. Pages 19-44 *in* N. M. Holbrook and M. A. Zwieniecki, editors. *Vascular transport in plants*. Elsevier Academic Press Amsterdam, The Netherlands.
- Van Camp, J., M. Hubeau, J. Van den Bulcke, J. Van Acker, and K. Steppe. 2018. Cambial pinning relates wood anatomy to ecophysiology in the African tropical tree *Maesopsis eminii*. *Tree Physiology* **38**:232-242.
- Van de Wal, B. A. E., C. W. Windt, O. Leroux, and K. Steppe. 2017. Heat girdling does not affect xylem integrity: an in vivo magnetic resonance imaging study in the tomato peduncle. *New Phytologist* **215**:558-568.
- Vandegheuchte, M. W. and K. Steppe. 2013. Sap-flux density measurement methods: working principles and applicability. *Functional Plant Biology* **40**:213-223.
- Verel, I., G. W. M. Visser, and G. A. van Dongen. 2005. The promise of immuno-PET in radioimmunotherapy. *Journal of Nuclear Medicine* **46**:164S-171S.
- Vergeynst, L. L., M. Dierick, J. A. N. Bogaerts, V. Cnudde, and K. Steppe. 2015a. Cavitation: a blessing in disguise? New method to establish vulnerability curves and assess hydraulic capacitance of woody tissues. *Tree Physiology* **35**:400-409.

- Vergeynst, L. L., M. G. R. Sause, N. J. F. De Baerdemaeker, L. De Roo, and K. Steppe. 2016. Clustering reveals cavitation-related acoustic emission signals from dehydrating branches. *Tree Physiology* **36**:786-796.
- Vergeynst, L. L., M. G. R. Sause, M. A. Hamstad, and K. Steppe. 2015b. Deciphering acoustic emission signals in drought stressed branches: the missing link between source and sensor. *Frontiers in Plant Science* **6**:494.
- Vertessy, R. A., T. J. Hatton, P. Reece, S. K. O'Sullivan, and R. G. Benyon. 1997. Estimating stand water use of large mountain ash trees and validation of the sap flow measurement technique. *Tree Physiology* **17**:747-756.
- Vilagrosa, A., E. Chirino, J. J. Peguero-Pina, T. S. Barigah, H. Cochard, and E. Gil-Pelegrin. 2012. Xylem cavitation and embolism in plants living in water-limited ecosystems. Pages 63-109 in R. Aroca, editor. *Plant responses to drought stress: from morphological to molecular features*. Springer Berlin, Germany.
- Vlassenbroeck, J., M. Dierick, B. Masschaele, V. Cnudde, L. Van Hoorebeke, and P. Jacobs. 2007. Software tools for quantification of X-ray microtomography at the UGCT. *Nuclear Instruments and Methods in Physics Research Section A: Accelerators, Spectrometers, Detectors and Associated Equipment* **580**:442-445.
- von Arx, G., E. Graf Pannatier, A. Thimonier, and M. Rebetez. 2013. Microclimate in forests with varying leaf area index and soil moisture: potential implications for seedling establishment in a changing climate. *Journal of Ecology* **101**:1201-1213.
- Walker, K. L., M. S. Judenhofer, S. R. Cherry, and G. S. Mitchell. 2015. Un-collimated single-photon imaging system for high-sensitivity small animal and plant imaging. *Physics in Medicine and Biology* **60**:403.
- Wang, Q., A. J. Mathews, K. Li, J. Wen, S. Komarov, J. A. O'Sullivan, and Y.-C. Tai. 2014. A dedicated high-resolution PET imager for plant sciences. *Physics in Medicine and Biology* **59**:5613.
- Waring, R. H., W. G. Thies, and D. Muscato. 1980. Stem growth per unit of leaf area: a measure of tree vigor. *Forest Science* **26**:112-117.
- Warren, J. M., R. J. Norby, and S. D. Wullschlegel. 2011. Elevated CO₂ enhances leaf senescence during extreme drought in a temperate forest. *Tree Physiology* **31**:117-130.
- Way, D. A. 2013. Will rising CO₂ and temperatures exacerbate the vulnerability of trees to drought? *Tree Physiology* **33**:775-778.
- Way, D. A., R. A. M. Oren, and Y. Kroner. 2015. The space-time continuum: the effects of elevated CO₂ and temperature on trees and the importance of scaling. *Plant, Cell & Environment* **38**:991-1007.
- Wehrl, H. F., M. Hossain, K. Lankes, C.-C. Liu, I. Bezrukov, P. Martirosian, F. Schick, G. Reischl, and B. J. Pichler. 2013. Simultaneous PET-MRI reveals brain function in activated and resting state on metabolic, hemodynamic and multiple temporal scales. *Nature Medicine* **19**:1184-1189.

- Weir, Q., B. Leblon, and A. La Rocque. 2011. On the use of X-ray computed tomography for determining wood properties: a review. *Canadian Journal of Forest Research* **41**:2120-2140.
- Weisenberger, A. G., B. Kross, S. J. Lee, J. McKisson, J. E. McKisson, W. Xi, C. Zorn, C. R. Howell, A. S. Crowell, C. D. Reid, and M. Smith. 2013. Nuclear physics detector technology applied to plant biology research. *Nuclear Instruments and Methods in Physics Research Section A: Accelerators, Spectrometers, Detectors and Associated Equipment* **718**:157-159.
- Wertin, T. M., M. A. McGuire, and R. O. Teskey. 2010. The influence of elevated temperature, elevated atmospheric CO₂ concentration and water stress on net photosynthesis of loblolly pine (*Pinus taeda* L.) at northern, central and southern sites in its native range. *Global Change Biology* **16**:2089-2103.
- Wheeler, J. K., J. S. Sperry, U. G. Hacke, and N. Hoang. 2005. Inter-vessel pitting and cavitation in woody Rosaceae and other vesselled plants: a basis for a safety versus efficiency trade-off in xylem transport. *Plant, Cell & Environment* **28**:800-812.
- Wickham, H. 2016. *ggplot2: elegant graphics for data analysis*. Springer, New York, NY, USA.
- Wiley, E. and B. Helliker. 2012. A re-evaluation of carbon storage in trees lends greater support for carbon limitation to growth. *New Phytologist* **195**:285-289.
- Williams, L. E., R. Lemoine, and N. Sauer. 2000. Sugar transporters in higher plants – a diversity of roles and complex regulation. *Trends in Plant Science* **5**:283-290.
- Willis, K. J. and R. J. Whittaker. 2002. Species diversity - scale matters. *Science* **295**:1245.
- Windt, C. W. and P. Blümler. 2015. A portable NMR sensor to measure dynamic changes in the amount of water in living stems or fruit and its potential to measure sap flow. *Tree Physiology* **35**:366-375.
- Windt, C. W., H. Soltner, D. van Dusschoten, and P. Blümler. 2011. A portable Halbach magnet that can be opened and closed without force: The NMR-CUFF. *Journal of Magnetic Resonance* **208**:27-33.
- Windt, C. W., F. J. Vergeldt, P. A. De Jager, and H. Van As. 2006. MRI of long-distance water transport: a comparison of the phloem and xylem flow characteristics and dynamics in poplar, castor bean, tomato and tobacco. *Plant, Cell & Environment* **29**:1715-1729.
- WMO. 2017. 2017 is set to be in top three hottest years, with record-breaking extreme weather.
- Woodruff, D. R. 2014. The impacts of water stress on phloem transport in Douglas-fir trees. *Tree Physiology* **34**:5-14.
- Woodruff, D. R. and F. C. Meinzer. 2011. Water stress, shoot growth and storage of non-structural carbohydrates along a tree height gradient in a tall conifer. *Plant, Cell & Environment* **34**:1920-1930.

- Wullschleger, S. D. and R. J. Norby. 2001. Sap velocity and canopy transpiration in a sweetgum stand exposed to free-air CO₂ enrichment (FACE). *New Phytologist* **150**:489-498.
- Wullschleger, S. D., T. J. Tschaplinski, and R. J. Norby. 2002. Plant water relations at elevated CO₂ – implications for water-limited environments. *Plant, Cell & Environment* **25**:319-331.
- Xu, Z., Y. Jiang, B. Jia, and G. Zhou. 2016. Elevated-CO₂ response of stomata and its dependence on environmental factors. *Frontiers in Plant Science* **7**:657.
- Xu, Z., H. Shimizu, Y. Yagasaki, S. Ito, Y. Zheng, and G. Zhou. 2013. Interactive effects of elevated CO₂, drought, and warming on plants. *Journal of Plant Growth Regulation* **32**:692-707.
- Xu, Z., G. Zhou, and H. Shimizu. 2010. Plant responses to drought and rewatering. *Plant Signaling & Behavior* **5**:649-654.
- Yamamoto, S., M. Honda, T. Oohashi, K. Shimizu, and M. Senda. 2011. Development of a brain PET system, PET-Hat: a wearable PET system for brain research. *IEEE Transactions on Nuclear Science* **58**:668-673.
- Yamori, W., K. Hikosaka, and D. A. Way. 2014. Temperature response of photosynthesis in C₃, C₄, and CAM plants: temperature acclimation and temperature adaptation. *Photosynthesis Research* **119**:101-117.
- Yao, R., R. Lecomte, and E. S. Crawford. 2012. Small-Animal PET: what is it, and why do we need it? *Journal of Nuclear Medicine Technology* **40**:157-165.
- Zavaliev, R., G. Sagi, A. Gera, and B. L. Epel. 2010. The constitutive expression of Arabidopsis plasmodesmal-associated class 1 reversibly glycosylated polypeptide impairs plant development and virus spread. *Journal of Experimental Botany* **61**:131-142.
- Zeiger, E. 1983. The biology of stomatal guard cells. *Annual Review of Plant Physiology* **34**:441-474.
- Zhang, C., L. Han, T. L. Slewinski, J. Sun, J. Zhang, Z.-Y. Wang, and R. Turgeon. 2014. Symplastic phloem loading in poplar. *Plant Physiology* **166**:306-313.
- Zhang, Y.-J., F. C. Meinzer, J.-H. Qi, G. Goldstein, and K.-F. Cao. 2013. Midday stomatal conductance is more related to stem rather than leaf water status in subtropical deciduous and evergreen broadleaf trees. *Plant, Cell & Environment* **36**:149-158.
- Zweifel, R., W. Eugster, S. Etzold, M. Dobbertin, N. Buchmann, and R. Häsler. 2010. Link between continuous stem radius changes and net ecosystem productivity of a subalpine Norway spruce forest in the Swiss Alps. *New Phytologist* **187**:819-830.
- Zweifel, R. and R. Häsler. 2001. Dynamics of water storage in mature subalpine *Picea abies*: temporal and spatial patterns of change in stem radius. *Tree Physiology* **21**:561-569.

- Zweifel, R., L. Zimmermann, and D. M. Newbery. 2005. Modeling tree water deficit from microclimate: an approach to quantifying drought stress. *Tree Physiology* **25**:147-156.
- Zweifel, R., L. Zimmermann, F. Zeugin, and D. M. Newbery. 2006. Intra-annual radial growth and water relations of trees: implications towards a growth mechanism. *Journal of Experimental Botany* **57**:1445-1459.
- Zwieniecki, M. A. and N. M. Holbrook. 2009. Confronting Maxwell's demon: biophysics of xylem embolism repair. *Trends in Plant Science* **14**:530-534.
- Zwieniecki, M. A., P. J. Melcher, and E. T. Ahrens. 2013. Analysis of spatial and temporal dynamics of xylem refilling in *Acer rubrum* L. using magnetic resonance imaging. *Frontiers in Plant Science* **4**:265.



CURRICULUM VITAE

Personalia

Name: Michiel Hubeau
 Date of birth: 14 June 1990
 Place of birth: Antwerp (Belgium)
 Nationality: Belgian
 Address: Kerkstraat 58, 2640 Mortsel
 Telephone: +32 476 41 76 22
 E-mail: Michiel.Hubeau@UGent.be

Education

2013-2018 PhD in Bioscience Engineering: Xylem and phloem functioning of *Populus tremula* trees under drought, and elevated CO₂ concentration and temperature.
 Promoter: Prof. dr. ir. Kathy Steppe

2011-2013 Master of Science in Bioscience Engineering: Environmental Technology, Ghent University
 Thesis: Plant-water relations of the mangrove species *Rhizophora stylosa*: a unique story
 Promoter: Prof. dr. ir. Kathy Steppe

2008-2011 Bachelor of Bioscience Engineering: Environmental Technology, University of Antwerp

2002-2008 Secondary school: Latin-mathematics, Sint-Gabriëlcollege Boechout

Additional education

2013-2018 Doctoral Schools Ghent University

2014 COST-action STReESS training school: Modelling of plant responses to stress conditions

2016 Anatomie van planten

Plant-water relations in the soil-plant-atmosphere continuum

Effective graphical displays

Communication skills

Job market for young researchers

Grants

- Sep 2017 Outstanding Graduate Student Presentation in session “Phloem function and dysfunction under drought” organised by Tree Physiology awarded by the International Union of Forest Research Organizations (IUFRO) at 125th Anniversary Congress
- Sep 2015 Grant from the Scientific Research Committee (CWO, Faculty of Bioscience Engineering, Ghent University) for participating in Xylem International Meeting 2015, Bordeaux
- Jan 2015 PhD grant for strategic Basic Research from the Agency for Innovation by Science and Technology in Flanders (IWT) for project “Onthulling van het suikertransport met behulp van radioactieve tracers en medische beeldvormingstechnieken”
- May 2014 COST grant for participation in the training school: “Modelling of plant responses to stress conditions”
- Sep 2013 Nomination Bayer Award for thesis “Plant-water relations of the mangrove species *Rhizophora stylosa*: a unique story”
- Aug 2012 Grant from the Scientific Research Committee (CWO, Faculty of Bioscience Engineering, Ghent University) for travel grant to Queensland, Australia for master thesis research

Research stays abroad

Aug-Oct 2012 Research stay at Moreton Bay Research station in North Stradbroke Island, Queensland, Australia for mangrove research in context of master thesis

Teaching and tutor activities

2014-2017 Teaching of a technical note (stomatal characteristics and porometer), special topic (phloem) and excursion (use of ecophysiological instruments) of the course Ecofysiologie

2014-2015 Tutor of master thesis of Jonathan Vermeiren: Ontwikkelen van een screeningstechniek naar de ladingsstrategieën van suikers in de bladeren van planten

2016-2017 Tutor of master thesis of Quincy Dekempe: Invloed van bladverwijdering op de source-sink relaties en trosontwikkeling bij tomaat

Tutor of master thesis of Alphonsine Byukusenge: Exploring the carbon supply chain of tomatoes: how are tomatoes connected with the leaves that provide them with photoassimilates?

Tutor of master thesis of Dheepashri Kannan: Investigation of stem photosynthesis by tracing internal ¹¹C-labelled CO₂ in tomato plants

2014-2017 Member of reading committee for five master theses

Publications

International publications with peer review (A1)

Epila, J.*, M. Hubeau* and K. Steppe. 2018. Drought effects on photosynthesis and implications of photoassimilate distribution in ¹¹C-labeled leaves in the African tropical tree species *Maesopsis eminii* Engl. *Forests* **9**:109.

Van Camp, J.*, M. Hubeau*, J. Van den Bulcke, J. Van Acker, and K. Steppe. 2018. Cambial pinning relates wood anatomy to ecophysiology in the African tropical tree *Maesopsis eminii*. *Tree Physiology* **38**:232-242.

Hubeau, M., and K. Steppe. 2015. Plant-PET Scans: *In Vivo* Mapping of Xylem and Phloem Functioning. *Trends in Plant Science* **20**:676-685.

Vandegehuchte, M. W., A. Guyot, M. Hubeau, S. R. E. De Groot, N. J. F. De Baerdemaeker, M. Hayes, N. Welte, C. E. Lovelock, D. A. Lockington, and K. Steppe. 2014. Long-term versus daily stem diameter variation in co-occurring mangrove species: Environmental versus ecophysiological drivers. *Agricultural and Forest Meteorology* **192–193**:51-58.

Vandegehuchte, M. W., A. Guyot, M. Hubeau, T. De Swaef, D. A. Lockington, and K. Steppe. 2014. Modelling reveals endogenous osmotic adaptation of storage tissue water potential as an important driver determining different stem diameter variation patterns in the mangrove species *Avicennia marina* and *Rhizophora stylosa*. *Annals of Botany* **114**:667-676.

*Equally contributing first authors

International proceedings with peer review (P1)

Mincke, J., M. Hubeau, J. Cortyn, B. Brans, C. Vanhove, S. Vandenberghe and K. Steppe. Normalization of ¹¹C-autoradiographic images for semi-quantitative analysis of woody tissue photosynthesis. *Acta Horticulturae* (under revision).

Hubeau, M., I. Passaris, G. Rogiers, M. Bollaerts, A. Brems, L. Appels, R. Dewil and G. Potters. 2012. Applications for biomass out of bamboo: pyrolysis oil,

activated carbon, pretreatments for digestion. Proceedings of the World Bamboo Congress **9**:361-374.

National proceedings without peer review

Hubeau, M., M. W. Vandegehuchte, A. Guyot, C. E. Lovelock, D. A. Lockington, and K. Steppe. 2014. Plant-water relations of the mangrove species *Rhizophora stylosa*: a unique story. Communications in Agricultural and Applied Biological Sciences **79**:57-63.

Oral Presentations

Hubeau, M. and K. Steppe. 2017. Tree response to drought under changing climate regimes: mitigation or amelioration? 125th Anniversary Congress of the International Union of Forest Research Organizations (IUFRO) – Session T5-205 Phloem function and dysfunction under drought. Freiburg, Germany, 18-22 September 2017.

Hubeau M. and Steppe K. 2015. *In vivo* visualisation of carbon transport in a changing climate. Xylem International Meeting. Bordeaux, France, 7-9 September 2015.

Hubeau, M., M. W. Vandegehuchte, A. Guyot, C. E. Lovelock, D. A. Lockington, and K. Steppe. 2014. Plant-water relations of the mangrove species *Rhizophora stylosa*: a unique story. 19th National Symposium on Applied Biological Sciences, Gembloux, Belgium, 7 February 2014.

Hubeau, M., I. Passaris, G. Rogiers, M. Bollaerts, A. Brems, L. Appels, R. Dewil and G. Potters. 2012. Applications for biomass out of bamboo: pyrolysis oil, activated carbon, pretreatments for digestion. 9th World Bamboo Congress. Antwerp, Belgium, 10-15 April 2012

Posters

Epila, J., M. Hubeau, N. De Baerdemaeker, H. Verbeeck, J.B.L. Okullo and K. Steppe. 2015. The non-food-tree-crop *Maesopsis eminii* Engl. investigated with PET and AE: A case of technology transfer. 9th Belgian Plant Biotechnology Association symposium. Brussels, Belgium, 13 November 2015.

Epila, J., N. De Baerdemaeker, M. Hubeau, H. Beeckman, H. Verbeeck, J.B.L. Okullo and K. Steppe. 2015. Combining AE, PET and wood anatomy to understand drought-stress responses of Africa's tropical forests: A case study of Ugandan *Maesopsis eminii* Engl. seedlings. 9th symposium of the Ghent Africa Platform. Ghent, Belgium, 17 December 2015.